DEVELOPMENT OF AN ANTENNA SYSTEM FOR A RELAY-BASED WIRELESS NETWORK

Ioannis Petropoulos

PhD

University of Bradford

— 2012 —

DEVELOPMENT OF AN ANTENNA SYSTEM FOR A RELAY-BASED WIRELESS NETWORK

Simulation and Measurement of Antenna Systems for Relay-Based Wireless Network, Covering the Backhaul and Access Links and Applying Beam Forming Technology

Ioannis Petropoulos
B.Sc, M.Sc.

Submitted for the degree of
Doctor of Philosophy

School of Engineering, Design and Technology
University of Bradford

— 2012 —

Abstract

DEVELOPMENT OF AN ANTENNA SYSTEM FOR A RELAY-BASED WIRELESS NETWORK

Simulation and Measurement of Antenna Systems for Relay-Based Wireless Network, Covering the Backhaul and Access Links and Applying Beam Forming Technology

Ioannis Petropoulos

Keywords

Relay Station, WiMAX, Long Term Evolution (LTE), Antenna Array, IEEE802.16j, Mutual Coupling, Beam Forming, Least Mean Square, Radiation Pattern

The proliferation of modern wireless networks increases demand for high capacity and throughput in order to provide faster, more robust, efficient and broadband services to end users. Mobile WiMAX and LTE are examples of such networks in which for some cases they have exposed limited connectivity due to harsh environment. Relay stations are preferred to overcome problems of weak or no access for such network devices, that are placed in specific positions to maintain high quality of data transfer at low cost and provide the required connectivity anywhere anytime. These stations should be equipped with an antenna system capable of establishing communication between base station (backhaul link) and end users (access link).

This thesis focuses on the design and development of a new antenna system that is suitable for a relay-based wireless network. Planar geometries of microstrip patch antennas are utilized. The antenna system comprises two antenna modules: a new design of a single antenna for access link and a new design of an antenna array for backhaul link realization. Both antenna specifications are compatible with the IEEE802.16j protocol standard. Hence, relay station should be capable of pointing its radiation pattern to the base station antenna, thus to achieve the desired radiation pattern of the relay station, a new beam-forming module is proposed, designed and developed to generate the proper radiation pattern. The beam-forming module incorporating digital phase shifters and attenuator chips is fabricated and tested. The optimization process using the Least Mean Square (LMS) algorithm is considered in this study to assign the proper phase and amplitude that is necessary to each radiation element excitation current, to produce the desired steered radiation pattern.

A comprehensive study on the coupling effects for several relative positions between two new backhaul and access link antenna elements is performed. Two new antenna configurations for coupling reduction are tested and the simulated and measured results in terms of antenna radiation performances were compared and commented.

Acknowledgements

I would like to express my deep gratitude and appreciation to my supervisors, Prof. Raed A. Abd-Alhameed, Dr. Steve Jones and Prof. Konstantinos Voudouris. I am grateful for their support, advice and encouragement during the difficult period of my PhD research.

I would like also to thank post-doctoral researcher Dr. Nikos Athanasopoulos for his significant help and advice regarding fabrication issues. His co-operation was very important to resolve critical problems that were raised through my research.

Furthermore I want to express my thanks to the REWIND project consortium for the meaningful and effective collaboration in which I gained useful experience for my PhD thesis.

I also wish to express my acknowledgements to my parents for their support and encouragement.

Table of Contents

CHAPTER 1 INTRODUCTION

1.1 BACKGROUND AND OBJECTIVES ..... -1-
1.2 MICROSTRIP ANTENNA FUNDAMENTALS ..... - 3 -
1.2.1 Basic concepts of microstrip antennas ..... - 3 -
1.2.2 Advantages and disadvantages ..... - 5 -
1.2.3 Feeding techniques ..... - 6 -
1.2.4 Impedance matching ..... - 10 -
1.2.5 Models of analysis ..... - 12 -
1.2.5.1 Transmission line model ..... - 12 -
1.2.5.2 Cavity model ..... - 14 -
1.2.6 Field modes ..... - 16 -
1.2.7 Microstrip antenna: Operation in tunable frequency ..... - 20 -
1.2.8 Advances in microstrip antennas ..... - 22 -
1.3 MICROSTRIP ARRAY FUNDAMENTALS ..... - 42-
1.3.1 Basic parameters of arrays ..... - 43-
1.3.2 Array architecture ..... - 48 -
1.3.3 Phase shifters ..... - 50 -
1.3.4 Received signal - Array factor ..... - 50 -
1.3.5 Grating lobes ..... - 52 -
1.3.6 Power dividers ..... - 53 -
1.3.7 Advances in planar antenna arrays ..... - 56 -
1.3.8 Array factor and electric field of a planar uniform array ..... - 66 -
1.4 SCOPE OF THIS WORK ..... - 74 -
1.5 REFERENCES ..... - 76 -

CHAPTER 2 RELAY STATIONS

2.1 INTRODUCTION ..... - 82 -
2.2 RELAY STATION OVERVIEW ..... - 82 -
2.3 RELAY STATION APPLICATIONS ..... - 84 -
2.3.1 Gap Filler ..... - 84 -
2.3.2 Coverage increase ..... - 84 -
2.3.3 Capacity and Throughput increase ..... - 85 -
2.3.4 In-building Relay usage ..... - 86 -
2.4 RELAYS IN CASE OF MOBILITY ..... - 87 -
2.5 TYPES OF RS ..... - 89 -
2.5.1 Transparent Relay ..... - 89 -
2.5.2 Non Transparent Relay ..... - 90 -
2.5.3 Time domain relay operation ..... - 91 -
2.6 RELAY DESCRIPTION ..... - 94 -
2.6.1 Hardware Subsystem ..... - 94 -
2.6.2 Relay Front End ..... - 96 -
2.7 CONCLUSIONS ..... - 107 -

2.8 REFERENCES……-107-

CHAPTER 3 BEAM-FORMING

3.1 INTRODUCTION ..... -109-
3.2 POWER DIVIDER CIRCUIT DESIGN..... - 111 -
3.3 BEAM-FORMING ARCHITECTURES AND TECHNIQUES..... - 114 -
3.4 BEAM-FORMING ALGORITHMS ..... - 116 -
3.5 CONCLUSIONS..... - 123 -
3.6 REFERENCES……...- 123 -

CHAPTER 4 ANTENNA SYSTEM DESIGN AND EVALUATION MEASUREMENTS

4.1 INTRODUCTION ..... - 125 -
4.2 ANTENNA SYSTEM DESIGN ..... - 126 -
4.3 ACCESS AND BACKHAUL ANTENNA DESIGN..... - 127 -
4.3.1 Access antenna design..... - 127 -
4.3.2 Access antenna simulation and fabrication ..... - 132 -
4.4 BEAMFORMING MODULE..... - 139 -
4.4.1 Beamforming circuit ..... - 139 -
4.4.2 LMS Algorithm..... - 147 -
4.5 BEAMFORMING ANTENNA TESTING..... - 150 -
4.6 FIELD MEASUREMENTS..... - 154 -
4.7 CONCLUSIONS..... - 160 -
4.8 REFERENCES……...- 160 -

CHAPTER 5 COUPLING EFFECTS AND MEASUREMENTS

5.1 INTRODUCTION ..... - 162 -
5.2 BASIC TERMS OF COUPLING ..... - 162 -
5.3 MUTUAL COUPLING ESTIMATION AND REDUCTION METHODS... - 170 -
5.4 COUPLING MEASUREMENTS..... - 179 -
5.4.1 Access antenna ..... - 181 -
5.4.2 Backhaul antenna ..... - 184 -
5.5 COUPLING EFFECTS STUDY..... - 189 -
5.5.1 Configuration 1 ..... - 190 -
5.5.2 Configuration 2 ..... - 192 -
5.6 RESULTS ..... - 194 -
5.7 CONCLUSIONS..... - 198 -
5.8 REFERENCES……- 198 -

CHAPTER 6 CONCLUSIONS AND SUGGESTIONS FOR FURTHER WORK

6.1 CONCLUSIONS..... - 203 -
6.2 SUGGESTIONS FOR FURTHER WORK ..... - 210 -
6.3 REFERENCES..... - 213 -

LIST OF AUTHOR'S PUBLICATIONS ..... - 216 -
SAMPLES OF AUTHOR'S PUBLICATIONS ..... - 217 -

List of Figures

Figure 1.1: Basic structure of a microstrip patch antenna…… -4-
Figure1.2: Different shapes of patch elements……..….-4-
Figure 1.3: Feeding technique using a microstrip line……... -6-
Figure 1.4: Coaxial cable fed patch antenna. ……-7-
Figure 1.5: Aperture coupled feed; (a) Cross section (b) Top view…….. -8-
Figure 1.6: Proximity coupled feed……-9-
Figure 1.7: Source load circuit……. -11-
Figure 1.8: Transmission line model; (a) Microstrip line structure (b) Field lines of strip conductor……-12-
Figure 1.9: Top view of microstrip antenna. …….-13-
Figure 1.10: Charge distribution on radiating elements and ground plane……..-15-
Figure 1.11: System coordination of a rectangular patch placed on dielectric substrate……....-16-
Figure 1.12: Patch antenna plus diodes……-21-
Figure 1.13: Patch antenna plus shorting pins……..-21-
Figure 1.14: Patch with air gap. ..... - 22 -
Figure 1.15: Experimental setup……...-23-
Figure 1.16: Proposed setup…….-24-
Figure 1.17: Patch Antenna; (a) with zero (b) first (c) second iteration…….-24-
Figure 1.18: Return loss as a function of frequency for antenna; (a) with zero and (b) one iteration..... - 25 -
Figure 1.19: Sierpinski gasket model..... - 26 -
Figure 1.20: The proposed antenna; (a) upper (b) sidelong view (c) serration of fed and coupled patch. ..... - 27 -
Figure 1.21: Proposed design and operation of two coupled patches; (a) Setup (b)VSWR diagram of two coupled radiators..... - 29 -

Figure 1.22: View of proposed antenna. ..... - 30 -
Figure 1.23: MOS capacitor configuration. ..... - 30 -
Figure 1.24: RLC equivalent circuit. ..... - 31 -
Figure 1.25: H shaped antenna. ..... - 32 -
Figure 1.26: RLC equivalent circuit. ..... - 32 -
Figure 1.27: Equivalent circuit of H shaped patch antenna. ..... - 33 -
Figure 1.28: Return loss diagrams with varying d. ..... - 34 -
Figure 1.29: Frequency vs. w dimension diagram. ..... - 35 -
Figure 1.30: Proposed antenna; (a) top view (b) side view. ..... - 35 -
Figure 1.31: PIFA antenna with slots. ..... - 36 -
Figure 1.32: U slot antenna; (a) side view (b) top view. ..... - 36 -
Figure 1.33: Efficiency for the three investigated cases of slot antenna. ..... - 37 -
Figure 1.34: Bowtie patch antenna. ..... - 37 -
Figure1.35: Designed prototype; (a) top view (b) side view. ..... - 38 -
Figure 1.36: Antenna for circular polarization. ..... - 39 -
Figure 1.37: Truncated patch antenna; (a) top view (b) side view. ..... - 40 -
Figure 1.38: The proposed wideband antenna; (a) top view (b) side view (c) S_{11} of the proposed patch antenna.. ..... - 41 -
Figure 1.39: Slotted patch with shorting pins; (a) top view (b) side view. ..... - 42 -
Figure 1.40: Linear Array with coordinate system. ..... -43-
Figure 1.41: Antenna array. ..... - 47 -
Figure 1.42: Phased Array configuration. ..... - 48 -
Figure 1.43: T/R and TDU configuration. ..... - 49 -
Figure 1.44: Array configuration incorporating a switch and a power divider. ..... - 49 -
Figure 1.45: Array configuration; (a) an array connected to an aggregation network (b) an array receives a waveform. ..... - 51 -
Figure 1.46: Power divider schematic. ..... - 53 -
Figure 1.47: A power divider connected to two patch antennas. ..... -54-
Figure 1.48: Equivalent circuit of power divider. ..... - 54 -
Figure 1.49: Power divider with transmission length l denoted. ..... - 55 -
Figure 1.50: Schematic view of patch array. ..... - 56 -
Figure 1.51: Hexagonal and circular array. ..... - 57 -

Figure 1.52: Description of array system with beam forming activity. ..... - 58 -
Figure 1.53: S_{11} vs. frequency; (a) hexagonal patch (b) circular patch (continuous line: measurement, dotted line: simulation). ..... - 58 -
Figure 1.54: Proposed phased array: W=35mm, L=28.3mm, Ws=3.8mm, S=6.0mm, d=41mm, l=6mm, y0=10mm. ..... - 59 -
Figure 1.55: Return Loss diagram with experimental and simulated results. ..... - 60 -
Figure 1.56: Radiation pattern of proposed array. ..... - 61 -
Figure 1.57: 2 patch antenna array with reflector. ..... - 61 -
Figure 1.58: An array of two radiation elements (a) Reflector of 2 patches (b) Reflector of one patch. ..... - 62 -
Figure 1.59: Four element antenna array……-63-
Figure 1.60: EBG structure for patch array; (a) circle shaped EBG (b) split ring resonator EBG. ..... - 63 -
Figure 1.61: Proposed configuration; (a) T Junction Power Divider (b) modified Wilkinson Power Divider. ..... - 64 -
Figure 1.62: Block diagram of RF PIN switch. ..... - 65 -
Figure 1.63: Radiation pattern; (a) 4 element array (b) 8 element array ..... - 65 -
Figure 1.64: Return loss of the designed array. ..... - 66 -
Figure 1.65: Electric field evaluation on P(r,θ,φ) using Cartesian coordinate system. ..... …….- 67 -
Figure 1.66: Planar array of M×L identical elements. ..... - 70 -

Figure 2.1: Overview of Relay Station use. ..... - 83 -
Figure 2.2: Use of RS as gap filler. ..... - 84 -
Figure 2.3: Cases of coverage increase. ..... - 85 -
Figure 2.4: RS for throughput increase. ..... - 86 -
Figure 2.5: Path Loss between in building and outdoor MS. ..... - 87 -
Figure 2.6: Possible configuration for sufficient indoor coverage. ..... - 87 -
Figure 2.7: RS usage in case of end user mobility. ..... - 88 -
Figure 2.8: RS usage in case of tunnels. ..... - 88 -
Figure 2.9: RS mobility scenario. ..... - 89 -

Figure 2.10: Transparent Relay topology. ..... - 89 -
Figure 2.11: Non transparent Relay configuration. ..... - 90 -
Figure 2.12: Relay based network operating in TTR mode. ..... - 91 -
Figure 2.13: TTR deployment. ..... - 92 -
Figure 2.14: Relay based network operating in STR mode. ..... - 93 -
Figure 2.15: STR deployment. ..... - 93 -
Figure 2.16: Relay prototype. ..... - 94 -
Figure 2.17: Relay top level architecture. ..... - 95 -
Figure 2.18: Relay hardware. ..... - 96 -
Figure 2.19: RF transmission and reception chain. ..... - 97 -
Figure 2.20: Transmission RF chain. ..... - 97 -
Figure 2.21: 1st block of transmission RF chain. ..... - 97 -
Figure 2.22: 2nd block of transmission RF chain. ..... - 98 -
Figure 2.23: 2nd block of transmission RF chain. ..... - 99 -
Figure 2.24: MGA amplifier properties. ..... - 99 -
Figure 2.25: 3rd block of transmission chain. ..... - 100 -
Figure 2.26: Performance of power amplifier; (a) gain and (b) reflection coefficient.
Figure 2.27: 2×2 switch matrix. ..... - 101 -
Figure 2.28: Switch matrix architecture. ..... - 102 -
Figure 2.29: Performance of 2×2 switch matrix in (a) transfer mode (b) isolation mode.
Figure 2.30: Spectrum transmitted from Relay to end user. ..... - 103 -
Figure 2.31: WiMAX transmitted signal. ..... - 104 -
Figure 2.32: RF chain in receiver. ..... - 104 -
Figure 2.33: First block of RF receiver. ..... - 104 -
Figure 2.34: 2nd RF receiver block. ..... - 105 -

Figure 3.1: Beam forming topology. ..... -109-
Figure 3.2: Power divider configuration. ..... - 111 -
Figure 3.3: 3 port Power divider. ..... - 112 -
Figure 3.4: T junction power divider types. ..... - 113 -
Figure 3.5: Wilkinson power divider. ..... - 113 -
Figure 3.6: Schematic of beam forming network. ..... - 114 -
Figure 3.7: Types of errors; (a) angle and (b) amplitude deviation. ..... - 115 -

Figure 3.8: Simulation and measurement for $\theta=0^0$ and $\theta= 30^0$. ..... - 116 -
Figure 3.9: LMS beamforming network. ..... - 117 -
Figure 3.10: LMS application to a linear array; (a) 5 elements (N=5) and (b) 10 elements (N=10). ..... - 119 -
Figure 3.11: Effects of varying spacing between the array elements; (a) $d=0.2\lambda$ (b) $d=0.5\lambda$ ..... - 120 -
Figure 3.12: MUSIC algorithm implementation. The angles in azimuth of signal reception are: $\varphi=13.40^0$, 100.180^0 and 160.360^0 ..... - 120 -
Figure 3.13: ESPRIT algorithm implementation. The angles in azimuth of signal reception are: $\varphi=74.260^0$, 140.460^0, 158.420^0 and 10.940^0. ..... - 121 -

Figure 4.1: Antenna system setup. ..... - 126 -
Figure 4.2: Patch antennas with equivalent circuits; (a) rectangle patch antenna (b) LC equivalent circuit of rectangle patch antenna (c) E shaped patch antenna (d) LC equivalent circuit of E shaped patch antenna. ..... - 130 -
Figure 4.3: Input impedance evaluation. ..... - 131 -
Figure 4.4: Access antenna; (a) simulation design (b) constructed design (c) cross section view. ..... - 133 -
Figure 4.5: Dimensions of e shape antenna. ..... - 133 -
Figure 4.6: S_{11} vs. frequency. ..... - 134 -
Figure 4.7: Radiation pattern of E shaped antenna; (a) xz plane (b) yz plane (c) 3D radiation pattern. ..... - 135 -
Figure 4.8: 16 element backhaul antenna array; (a) simulation design (b) fabrication design. ..... - 136 -
Figure 4.9: Inter element space. ..... - 136 -
Figure 4.10: Radiation pattern of 16 element array; (a) yz plane (b) xz plane (c) 3D radiation pattern. ..... - 138 -
Figure 4.11: Proposed Relay Station with antenna setup. ..... - 139 -
Figure 4.12: Side view of the beam forming circuit. ..... - 140 -
Figure 4.13: Beam forming circuit. ..... - 141 -
Figure 4.14: Length and width dimensions of microstrip lines of the 1:8 Wilkinson power divider. ..... - 143 -
Figure 4.15: Microstrip power divider circuit. ..... - 143 -

Figure 4.16: 1:8 Wilkinson Power Divider. - 144 -
Figure 4.17: S_{11} vs. frequency. - 145 -
Figure 4.18: Total experimental setup of beam forming circuit with the array. - 146 -
Figure 4.19: 16 element array and coordinate system. - 147 -
Figure 4.20: Reference signal for maximum in (40^o, 0^o), minimum in (30^0, 0^0), SLL< 10dB. - 149 -
Figure 4.21: Radiation pattern of 4×4 array with reference signal. - 150 -
Figure 4.22: Simulated and experimental radiation pattern of 16 element array for scenario (a). - 151 -
Figure 4.23: Simulated and experimental radiation pattern of 16 element array for scenario (b). - 152 -
Figure 4.24: Simulated and experimental radiation pattern of 16 element array for scenario (c). - 153 -
Figure 4.25: 16 element array with coordination system. - 155 -
Figure 4.26: Side view of field measurements configuration. - 156 -
Figure 4.27: Top view of field measurements configuration. - 156 -
Figure 4.28: Amplitude/Phase control unit. - 157 -
Figure 4.29: Configuration of Amplitude/Phase control unit. - 157 -
Figure 4.30: Amplitude/Phase control unit together with beam forming circuit. - 158 -

Figure 5.1: Planar array of M×N identical elements. - 164 -
Figure 5.2: Two patches excited by currents J_i and J_s. - 165 -
Figure 5.3: Linear array with coupling effect. - 167 -
Figure 5.4: Surface and reflected waves between two patches. - 169 -
Figure 5.5: Two patches separated by EBG construction. - 171 -
Figure 5.6: S_{21} parameter as a function of frequency. - 171 -
Figure 5.7: EBG and antenna configuration. - 172 -
Figure 5.8: M_1 and M_2 is patch antenna separated by a three row EBG structure... - 173 -
Figure 5.9: EBG structure. - 173 -
Figure 5.10: Proposed patches with EBG structure; (a) Experimental setup (b) EBG structure. - 175 -

Figure 5.11: Scattering parameters of patch elements; (a) S_{12} with and without EBG structure (b) S_{11} with and without EBG structure. ..... - 175 -
Figure 5.12: Two patches separated by a DGS configuration. ..... - 176 -
Figure 5.13: Two patch elements; (a) separated by EBG structure (b) with removed substrate (c) with cavity back..... - 176 -
Figure 5.14: S_{21} in terms of frequency. ..... - 177 -
Figure 5.15: Coupling as a function of distance between radiating elements..... - 179 -
Figure 5.16: Relay Station operation. ..... - 180 -
Figure 5.17: Antenna geometry and measurements; (a) antenna design, (b) antenna prototype. ..... - 182 -
Figure 5.18: S_{11} parameter for simulated and fabricated antenna. ..... - 182 -
Figure 5.19: Radiation pattern of access antenna for 3.5GHz; (a) yz plane (b) xz plane (c) 3D radiation pattern. ..... - 184 -
Figure 5.20: Backhaul antenna geometry and measurements; (a) backhaul antenna model (b) backhaul antenna prototype. ..... - 185 -
Figure 5.21: S_{11} parameter for backhaul antenna. ..... - 185 -
Figure 5.22: Radiation pattern of the backhaul antenna for 3.5GHz; (a) yz plane (b) xz plane (c) 3D radiation pattern. ..... - 187 -
Figure 5.23: Antenna arrangements under test; (a) configuration 1 (b) configuration 2… ..... - 189 -
Figure 5.24: Access and backhaul antenna setup during coupling measurements. . - 189 -
Figure 5.25: The investigated setup. ..... - 190 -
Figure 5.26: S_{21} for $\omega=180^0$; (a) simulation design (b) simulation and measurement. ..... …….- 190 -
Figure 5.27: S_{21} for $\omega=190^0$; (a) simulation design (b) simulation and measurement. ..... ……..- 191 -
Figure 5.28: S_{21} for $\omega=190^0$; (a) simulation design (b) simulation and measurement. ..... ……..- 191 -
Figure 5.29: Field lines that cause coupling effect. ..... - 192 -
Figure 5.30: The investigated setup. ..... - 192 -
Figure 5.31: S_{21} for $\omega=180^0$; (a) simulation design (b) simulation and measurement…….- 193 -

Figure 5.32: S_{21} for $\omega=190^0$; (a) simulation design (b) simulation and measurement. ..... ……..- 193 -
Figure 5.33: S_{21} for $\omega=200^0$; (a) simulation design (b) simulation and measurement…… ..... - 194 -
Figure 5.34: S_{21} as a function of angle ω for configuration 1. ..... - 195 -
Figure 5.35: S_{21} as a function of angle ω for configuration 2. ..... - 196 -
Figure 5.36: Relay Station with the proposed antennas. ..... - 197 -
Figure 5.37: Coupling comparison. ..... - 197 -

List of Tables

Table 1.1: Comparison of feeding methods. ..... - 9 -

Table 1.2: Features of joined and not joined patch antennas. ..... - 62 -

Table 2.1: Simulated parameters for different modulation…….-106-

Table 4.1: Features of access antenna and comparison with the desired specifications….

..... - 135 -

Table 4.2: Features of backhaul antenna and comparison with the desired specifications.…….- 139 -

Table 5.1: Patch antenna operating frequency. ..... - 172 -

Table 5.2: Coupling reduction method comparison. ..... - 177 -

Table 5.3: Access and backhaul antenna features. ..... - 187 -

Table 5.4: S_{21} variation for configuration 1. ..... - 194 -

Table 5.5: S_{21} variation for configuration 2. ..... - 195 -

List of Abbreviations

BF	Beam Forming
BPF	Band Pass Filter
BS	Base Station
CMA	Constant Modulus Algorithm
CPE	Customer Premises Equipment
DGS	Defect Ground Structure
DOA	Direction of Arrival
EBG	Electromagnetic Band Gap
ESPRIT	Estimation of Signal Parameters via Rotational Invariance Techniques
HPBW	Half Power Beam Width
LMS	Least Mean Algorithm
LPF	Low Pass Filter
LTE	Long Term Evolution
MIMO	Multiple Input Multiple Output
MoM	Method of Moments
MSA	Microstrip Antenna
MS	Mobile Station
MUSIC	Multiple Signal Classification
NTR	Non Transparent Relay
PCB	Printed Circuit Board
RLS	Recursive Least Square

RS Relay Station

RSS Received Signal Strength

SLL Side Lobe Level

SNR Signal to Noise Ratio

STR Simultaneously Transit Receive

TTR Time Division Transmit Receive

VSWR Voltage Standing Wave Ratio

WiFi Wireless Fidelity

WiMAX Wireless Interoperability for Microwave Access

CHAPTER 1

INTRODUCTION

1.1 BACKGROUND AND OBJECTIVES

Modern wireless networks, such as mobile WiMAX (Worldwide Interoperability for Microwave Access) and LTE (Long Term Evolution), offer high capacity and throughput in order to provide efficient and broadband services to end users. In cases of limited connectivity, due to environmental circumstances, Relay Stations are chosen to overcome problems of weak or no access. Relay Stations are network devices put in specific positions to maintain high quality of data transfer at low cost and provide connectivity anywhere anytime. Such devices should be equipped with an antenna system capable of establishing communication with Base Station (backhaul link) and with end users (access link).

In this thesis an antenna system suitable for a Relay based wireless network is designed and developed. The antenna system comprises two radiation modules: a single antenna for access link realization and an antenna array for backhaul link realization. Both antenna specifications are compatible with IEEE802.16j protocol. In addition the Relay Station should be capable of pointing its main lobe of radiation pattern to the Base Station antenna. In order to achieve the desired radiation pattern shape, a beam forming module is designed and developed to define proper radiation pattern. The beam forming

module incorporates digital phase shifters and attenuator chips. Least Mean Square (LMS) algorithm is generated and assigned proper phase and amplitude to each radiation element excitation current, to produce a pattern that points at Base Station.

Another point of interest of this thesis is the coupling between access and backhaul antenna. Coupling is a phenomenon that degrades the performance of a radiating element due to the presence and interaction of another one in the close environment. Two new antennas for access and backhaul link are designed and developed in this thesis. Two antenna configurations are examined and coupling is measured in terms of frequency. Results are depicted and commented.

To conclude, the main contributions of the present work can be summarized as follows:

- New design of a single antenna element operating at 3.5GHz frequency band with average gain of 9dB for access link realization
- New design of a beam steering antenna array for backhaul link realization
- New design of the feeding network for the beam steering antenna array
- New method for coupling reduction between the access antenna and the backhaul antenna

Let us mention here that both access and backhaul antennas operate in the same frequency band thus making their utilization beneficial for network operators and that both antennas have been designed based on the air interface of IEEE802.16j standard in terms of gain and bandwidth. Standard's specifications include 9dB gain and 500MHz bandwidth for access antenna and 18dB gain and 500MHz bandwidth for the backhaul antenna. The proposed antenna system aims to be incorporated with a Relay Station providing a flexible and easy to install network device.

1.2 MICROSTRIP ANTENNA FUNDAMENTALS

In this chapter the basic structure and features of microstrip antennas together with some advantages and drawbacks are outlined. Feeding techniques of such antennas are described and a comparison is performed among them. The issue of matching between the antenna and the transmission line is also mentioned providing mathematical equations. Transmission line and cavity model are denoted for more accurate calculations of dielectric constant and antenna's dimensions. Furthermore expressions of electric and magnetic field excited from a microstrip antenna are proved and outlined. In addition the radiating behavior of some basic antenna shapes and variations are depicted and commented. Methods of frequency tuning and circular polarization excitation are stated. Moreover chapter 1 includes advances in microstrip antennas in terms of bandwidth enhancement using stacked and fractal geometries. Patch shapes are also extensively investigated to provide broadband behavior. In addition mathematical formulas are provided where necessary to better support and prove the outlined results.

Microstrip technology has been investigated in order to define possible shapes and configurations for the design and development of the new access and backhaul antennas.

1.2.1 Basic concepts of microstrip antennas

A microstrip patch antenna is consisted of a radiating element of arbitrary shape which is placed on a dielectric substrate. The last is mounted on a ground plane. Fig. 1.1 shows the case of a rectangle microstrip patch antenna.

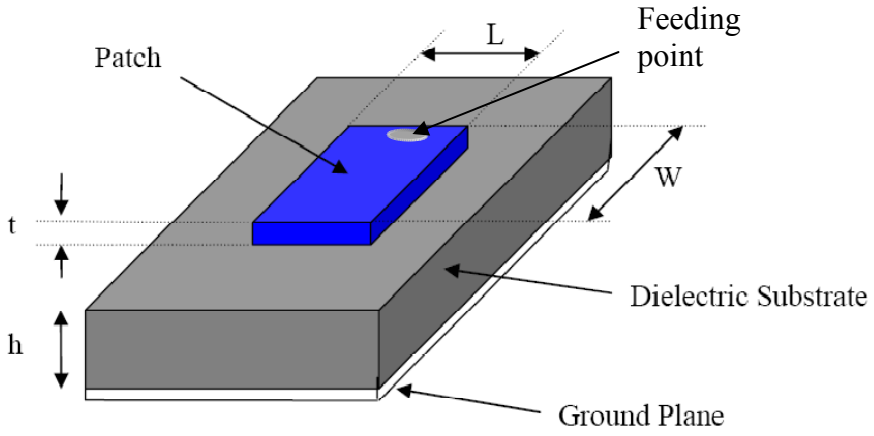

Figure 1.1: Basic structure of a microstrip patch antenna.

There is a specific relation between the patch's dimensions and the wavelength in free space: If L is the length of the patch then $0.3333\lambda_o < L < 0.5\lambda_0$ where λ_o is the free space wavelength [1]. Also it is selected t<<λ_o (t is the patch thickness). The height h of the dielectric substrate takes values: $0.003\lambda_0 \le h \le 0.05\lambda_0$ and the dielectric constant varies between: $2.2 \le \varepsilon_r \le 12$.

A patch antenna can take many shapes such as rectangular, triangular, circular, and elliptical as shown in Fig. 1.2.

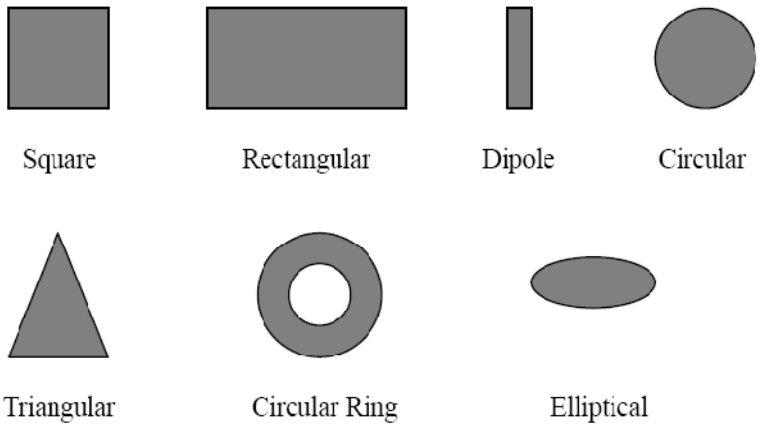

Figure 1.2: Different shapes of patch elements.

It is known that an antenna performs better if it is characterized by a thick dielectric substrate with low dielectric constant. Under these conditions the antenna has better efficiency and radiation but greater size. In order to reduce the size, materials with higher dielectric constant are used [2]. This leads to less efficiency and narrower bandwidth. So a compromise must be established between the antenna dimensions and operation performance.

1.2.2 Advantages and disadvantages

Microstrip antennas are widely used in wireless and satellite communications because they provide some excellent characteristics such as [2], [3]:

- Light weight.
- Planar configuration.
- Low cost of fabrication. They can be produced in large quantities.
- Support different types of polarization
- They can be easily connected to microwave circuits.
- Ability to operate in a variety of frequencies.

However patch antennas endure from some drawbacks which can be summarized as [3], [4]:

- Narrow bandwidth
- Low gain and efficiency

- Surface wave excitation

1.2.3 Feeding techniques

Several feeding techniques have been introduced to provide effective antenna operation. A feeding technique is a method of supplying the antenna with power in order to efficiently radiate [2]. Discontinuities and mismatched elements provide high losses and should be taken into consideration. The most popular techniques are presented in the text that follows.

I) MICROSTRIP LINE

As it is shown in Fig. 1.3, a conducting microstrip line is designed on the substrate and connected to the radiating element providing a planar structure. The width of the line is smaller than that of the patch.

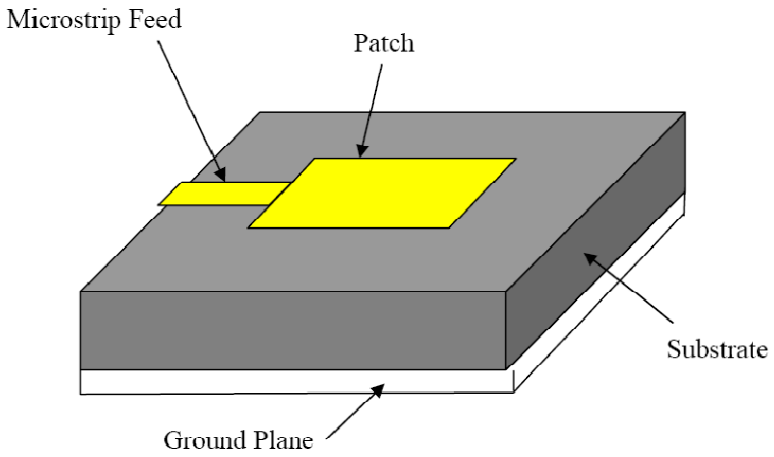

Figure 1.3 Feeding technique using a microstrip line.

In the point of connection between the microstrip line and the patch antenna, good matching should be provided in order to reduce losses.

II) COAXIAL FEED

In this case a coaxial cable is joined to the antenna. A coaxial cable is consisted of an inner conductor which is surrounded by a dielectric material. The last is covered by an outer conductor. The inner conductor is connected to the radiating element while the outer one is wrapped by an insulating material. The described feeding technique is depicted in Fig. 1.4.

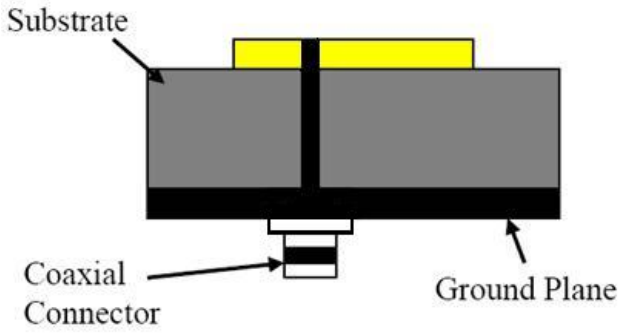

Figure 1.4: Coaxial cable fed patch antenna.

An advantage of the aforementioned technique is that we can choose the point of connection between the cable and the antenna in order to succeed the best matching. On the other hand the above configuration appears difficulties in simulation and provides narrow bandwidth [3].

Another category of feeding techniques comprises non contacting methods. In this case the feeding process is achieved by electromagnetic coupling. These methods are described below.

III) APERTURE COUPLED FEED

The scheme below shows the configuration of an aperture coupled feed microstrip antenna. The characteristic point here is the use of two substrates which are separated by a ground plane (Fig. 1.5). A microstrip line is placed on the bottom side of the lower substrate, while the upper substrate carries the radiating element. A slot is opened in the ground plane through which electromagnetic coupling is achieved.

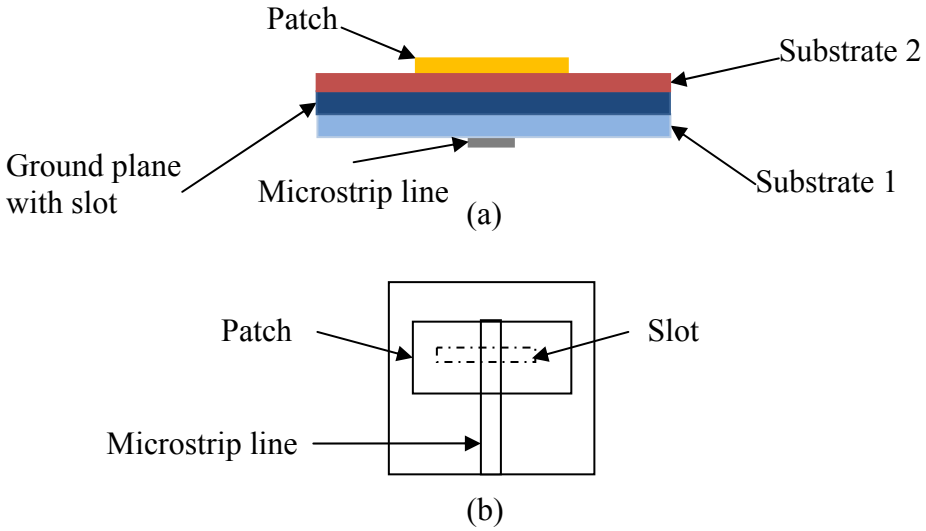

Figure 1.5: Aperture coupled feed; (a) Cross section (b) Top view.

The size, location and shape of the slot, specifies the amount of coupling. This setup leads to increased thickness of antenna. According to the theory [2], better antenna operation is performed when the lower substrate has a high dielectric constant and the upper one is thicker and has a lower dielectric constant.

IV) PROXIMITY COUPLED FEED

This method appears similarities with the previous one except that now the ground plane is missing. A microstrip line is designed on the lower substrate and the antenna element is mounted on the upper substrate (Fig. 1.6).

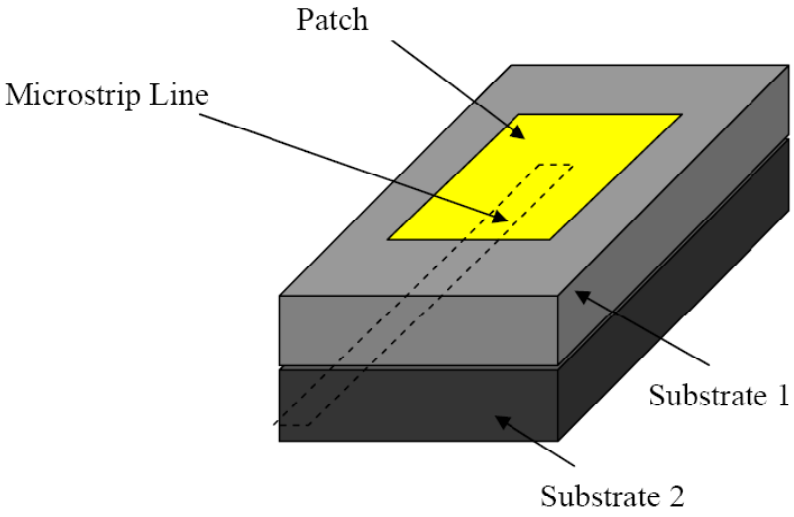

Figure 1.6: Proximity coupled feed.

The above methods are summarized in the table that follows [1]:

Table 1.1: Comparison of feeding methods.

Characteristics	**Microstrip Line Feed**	**Coaxial Feed**	**Aperture coupled Feed**	**Proximity coupled Feed**
Spurious feed radiation	More	More	Less	Minimum
Reliability	Better	Poor due to soldering	Good	Good
Ease of fabrication	Easy	Soldering and drilling needed	Alignment required	Alignment required
Impedance Matching	Easy	Easy	Easy	Easy
Bandwidth (achieved with impedance matching)	2-5%	2-5%	2-5%	13%

1.2.4 Impedance matching

The point where the antenna is connected to the feeding cable introduces losses which degrade the amplitude of power that arrives at the antenna. The efficient power transportation to the antenna element means that these discontinuity losses are minimized. When losses are at a low level, the circuit and the antenna are well matched [5]. Below follows the condition of antenna matching.

Let us consider that the antenna is equivalent to complex impedance Z_A where:

$$Z_A = R_A + jX_A \qquad 1.1$$

R_A is the resistive part of antenna impedance.

X_A is the reactive part of antenna impedance. It represents the energy stored at the near field region of the antenna.

$$R_A = R_r + R_L \qquad 1.2$$

where R_r is the radiation losses (wanted) and R_L is the ohmic losses.

For simplicity reasons let us assume that the antenna is lossless (R_L=0) and X_A=0. The antenna is fed by a source V_g which has real impedance R_g as shown in Fig. 1.7:

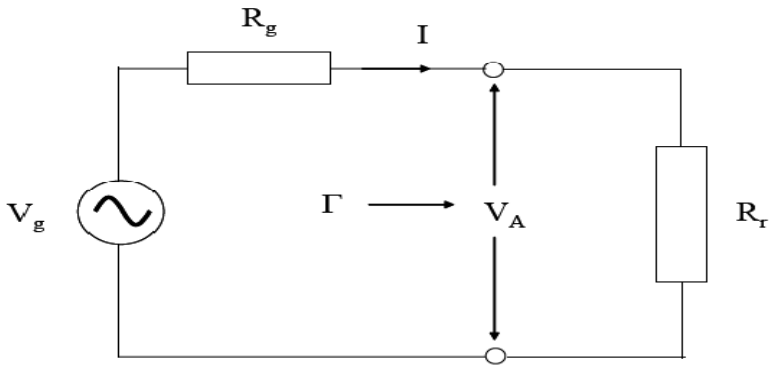

Figure 1.7: Source load circuit.

The power absorbed by resistance R_r (antenna) is:

$$P = \frac{1}{2}\mathrm{Re}(V_A \cdot I^*) \qquad 1.3$$

It is: $$V_A = \frac{R_g}{R_g + R_r} V_g \text{ and } I = I^* = \frac{V_A}{R_r}$$

Thus the power would be:

$$P = \frac{1}{2} V_g^2 \left(\frac{R_g}{R_g + R_r}\right)^2 \frac{1}{R_r} \qquad 1.4$$

The transferred power would be maximum if:

$$\frac{\partial P}{\partial R_r} = 0 \qquad 1.5$$

After calculations it is derived that: $R_r = R_g$.

Generally if the source and the antenna have complex form, the equation for impedance matching is:

$$Z_A = Z_g^* \qquad 1.6$$

1.2.5 Models of analysis

There are some methods to analyze patch antennas in order to define useful parameters. The most popular of them are: The transmission line model and the Cavity model.

1.2.5.1 Transmission line model

The antenna is depicted as a transmission line of length L and width W, with two slots at its edges as shown in the Fig. 1.8. The slots abstain distance L.

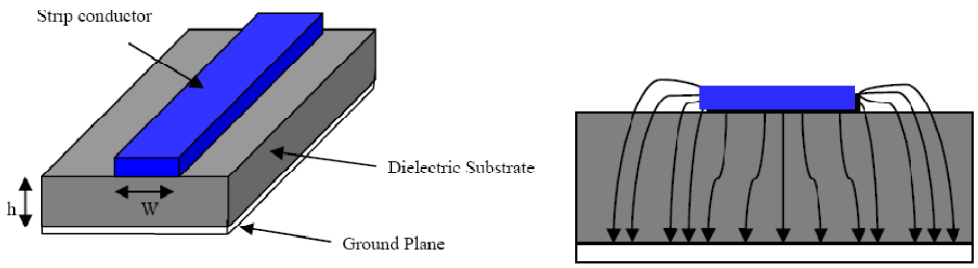

(a) (b)

Figure 1.8: Transmission line model; (a) Microstrip line structure (b) Field lines of strip conductor.

Around the antenna is developed a fringing field because of the finite dimensions of the transmission line. This field presents the antenna to be electrically greater than it is. Fringing field is low if h/L <<1 but should be taken into consideration for the evaluation of the resonant frequency. The transmission line model leads to a more accurate expression for the dielectric constant that contains the fringing fields. The effective dielectric constant is defined as [2]:

$$\varepsilon_{reff} = \frac{\varepsilon_r + 1}{2} + \frac{\varepsilon_r - 1}{2}\left(1 + 12\frac{h}{W}\right)^{-\frac{1}{2}} \qquad 1.7$$

Where ε_{reff} is the effective dielectric constant

ε_r is the dielectric constant of substrate

h is the height of dielectric substrate

W is the width of the patch

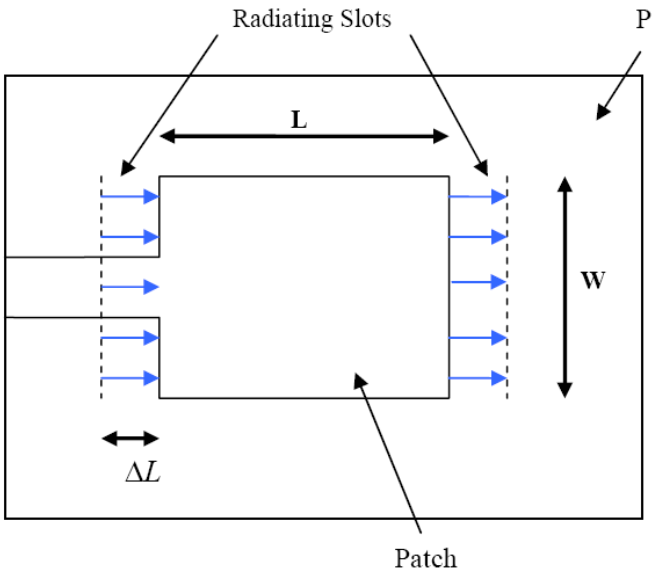

Figure 1.9: Top view of microstrip antenna.

Due to fringing fields, the patch antenna looks electrically larger by 2×ΔL as can be seen in Fig. 1.9. This length extension can be evaluated by the equation [6]:

$$\Delta L = 0.412h\frac{(\varepsilon_{reff} + 0.3)(\frac{W}{h} + 0.264)}{(\varepsilon_{reff} - 0.258)(\frac{W}{h} + 0.8)} \qquad 1.8$$

So the effective length of the patch would be:

$$L_{eff} = L + 2\Delta L \tag{1.9}$$

The resonant frequency is connected to the effective length by [3]:

$$L_{eff} = \frac{c}{2 f_0 \sqrt{\varepsilon_{reff}}} \tag{1.10}$$

James and Hall [7] gave an expression for the resonance frequency for a rectangular patch antenna for any mode.

$$f_0 = \frac{c}{2\sqrt{\varepsilon_{reff}}} \left[\left(\frac{m}{L}\right)^2 + \left(\frac{n}{W}\right)^2 \right]^{1/2} \tag{1.11}$$

where m and n are mode indicators.

1.2.5.2 Cavity model

In cavity model the area between the patch and the ground plane is represented as a cavity. The upper and lower sides are perfect electric walls which mean that no transverse component of magnetic field exists there. This assumption stands for thin substrates [4].

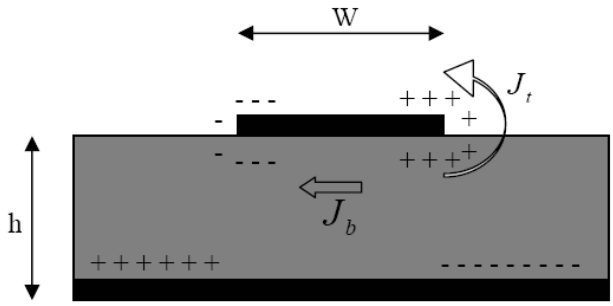

Figure 1.10: Charge distribution on radiating elements and ground plane.

As it is seen in Fig. 1.10, a charge distribution is formed on the upper and lower side of the radiating element and the ground plane. The charge movement is defined by the well known attractive and repulsive mechanisms [8]. A high concentration of charge is centered at the bottom surface of the patch while less charge is flowing on the top side. As result no magnetic field component is formed at the patch edges. Thus the region beneath the patch can be modeled as a cavity with its four sidewalls as perfect magnetic surfaces. The field lines are mostly concentrated in the area between the patch element and the ground plane.

The effective loss tangent is defined as:

$$\delta_{eff} = \frac{1}{Q_T} \tag{1.12}$$

where Q_T is the antenna quality factor expressed as:

$$\frac{1}{Q_T} = \frac{1}{Q_d} + \frac{1}{Q_c} + \frac{1}{Q_r} \tag{1.13}$$

where Q_d is the quality factor of the dielectric, Q_c is the quality factor of the conductor, and Q_r is the factor for radiation. The total effective loss tangent would be:

$$\delta_{eff} = \tan\delta + \frac{\Delta}{h} + \frac{P_r}{\omega_r W_T} \qquad 1.14$$

where $\tan\delta = \frac{1}{Q_d}$, $\frac{\Delta}{h} = \frac{1}{Q_c}$, $\frac{P_r}{\omega_r W_T} = \frac{1}{Q_r}$

Δ is the skin depth of the conductor , P_r is the power radiated from the patch, W_T is the energy stored in the patch and $\omega_r=2\pi f_r$ where f_r the resonant frequency.

1.2.6 Field modes

In this section the electric and magnetic fields excited in the area below a patch antenna are presented [2]. Fig. 1.11 represents a rectangle patch antenna of dimensions L and W placed upon a substrate of thickness h.

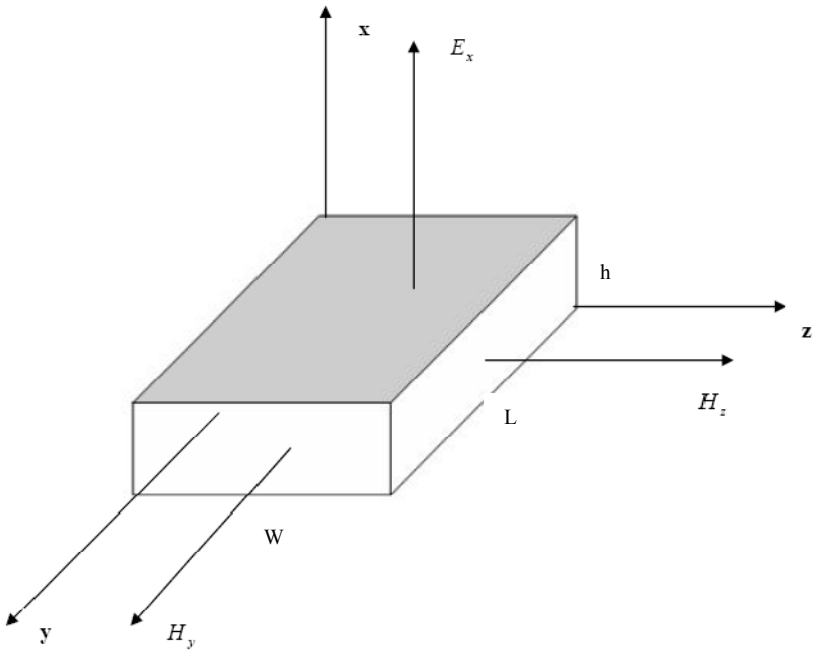

Figure 1.11 System coordination of a rectangular patch placed on dielectric substrate.

The height of substrate is very small, so the electric field is perpendicular to the patch's surface. Thus only TM modes are considered inside the substrate.

In order to define the form of electromagnetic field in the region below patch antenna, the magnetic potential "**A**" needs to be evaluated. The evaluation will be considered at x axis.

"**A**" satisfies the homogenous wave equation:

$$\nabla^2 A_x + k^2 A_x = 0 \qquad 1.15$$

The solution of the above equation has the form of:

$$A_x = [A_1\cos(k_x x) + B_1\sin(k_x x)][A_2\cos(k_y y) + B_2\sin(k_y y)][A_3\cos(k_z z) + B_3\sin(k_z z)] \quad 1.16$$

k_x, k_y, k_z are wave numbers. Electric and magnetic field are related to A_x through the following equations:

$$E_x = -j\frac{1}{\omega\mu\varepsilon}(\frac{\partial^2}{\partial x^2} + k^2)A_x \qquad H_x = 0 \qquad 1.17a$$

$$E_y = -j\frac{1}{\omega\mu\varepsilon}\frac{\partial^2 A_x}{\partial x\partial y} \qquad H_y = \frac{1}{\mu}\frac{\partial A_x}{\partial z} \qquad 1.17b$$

$$E_z = -j\frac{1}{\omega\mu\varepsilon}\frac{\partial^2 \mathrm{A}_x}{\partial x\partial y} \qquad H_z = -\frac{1}{\mu}\frac{\partial A_x}{\partial y} \qquad 1.17c$$

The boundary conditions would be:

$$\begin{aligned} &E_y(x=0, 0\le y\le L, 0\le z\le W) = E_y(x=h, 0\le y\le L, 0\le z\le W) = 0 \\ &H_y(0\le x\le h, 0\le y\le L, z=0) = H_y(0\le x\le h, 0\le y\le L, z=W) = 0 \\ &H_z(0\le x\le h, y=0, 0\le z\le W) = H_z(0\le x\le h, y=L, 0\le z\le W) = 0 \end{aligned} \quad 1.18$$

Applying the boundary conditions into field equations it is derived that:

$B_1 = 0$ and $k_x = \frac{m\pi}{h}$, m=0,1,2,…

$B_2 = 0$ and $k_y = \frac{n\pi}{L}$, n=0,1,2,…

$B_3 = 0$ and $k_z = \frac{p\pi}{W}$, p=0,1,2,…

Thus the magnetic field equation would be:

$$A_x = A_{mnp}\cos(k_x x)\cos(k_y y)\cos(k_z z) \qquad 1.19$$

It is derived that k_x, k_y, k_z satisfy the equation:

$$k_x^2 + k_y^2 + k_z^2 = (\frac{m\pi}{h})^2 + (\frac{n\pi}{L})^2 + (\frac{p\pi}{W})^2 = \omega^2\mu\varepsilon \qquad 1.20$$

where: ε is the dielectric constant of substrate and μ the permeability of the material.

It is known that $\lambda = \frac{2\pi}{k}$, $k = \sqrt{k_x^2 + k_y^2 + k_z^2}$, $f = \frac{c}{\lambda}$ where c is the speed of light, f the resonant frequency and λ the wavelength.

The resonant frequency of the mnp mode would be:

$$f_{mnp} = \frac{1}{2\pi\sqrt{\mu\varepsilon}}\sqrt{(\frac{m\pi}{h})^2 + (\frac{n\pi}{L})^2 + (\frac{p\pi}{W})^2} \qquad 1.21$$

The electric and magnetic fields inside dielectric would then be:

$$E_x = -j\frac{(k^2 - k_x^2)}{\omega\mu\varepsilon} A_{nmp} \cos(k_x x)\cos(k_y y)\cos(k_z z) \quad 1.22a$$

$$E_y = -j\frac{(k_x k_y)}{\omega\mu\varepsilon} A_{nmp} \sin(k_x x)\sin(k_y y)\cos(k_z z) \quad 1.22b$$

$$E_z = -j\frac{k_x k_z}{\omega\mu\varepsilon} A_{nmp} \sin(k_x x)\cos(k_y y)\sin(k_z z) \quad 1.22c$$

$$H_x = 0 \quad 1.22d$$

$$H_y = -\frac{k_z}{\mu} A_{nmp} \cos(k_x x)\cos(k_y y)\sin(k_z z) \quad 1.22e$$

$$H_z = \frac{k_y}{\mu} A_{nmp} \cos(k_x x)\sin(k_y y)\cos(k_z z) \quad 1.22f$$

1.2.7 Microstrip antenna: Operation in tunable frequency

Patch antennas have the ability to emit at a range of frequencies by adding some special features to the configuration. The operation frequency of a patch antenna can be varied using the following methods:

- Varactor diodes: It is a type of diode where its capacitance is dependent of the voltage applied to its edges. When voltage is increased, the capacitance is also enlarged and so the resonant frequency. It appears that voltage alteration affects the dielectric constant of substrate. Fig. 1.12 depicts a patch configuration together with diodes. Diodes are put in a way that connect patch and ground plane.

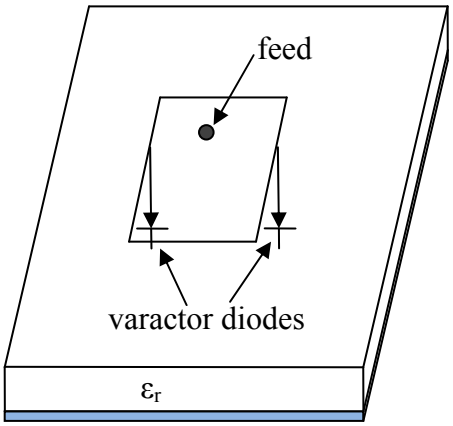

Figure 1.12: Patch antenna plus diodes.

- Shorting pins: They connect patch and ground plane. They appear inductance affecting the effective dielectric constant. Fig. 1.13 below shows the format:

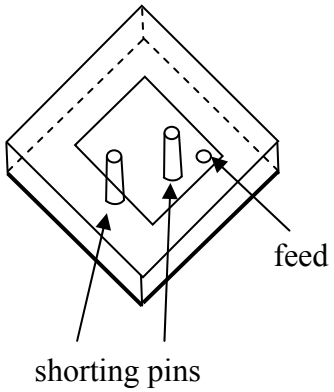

Figure 1.13: Patch antenna plus shorting pins.

- Air gap: The introduction of a air gap between the substrate and the ground plane, will change the effective dielectric constant. The main configuration is depicted in Fig. 1.14:

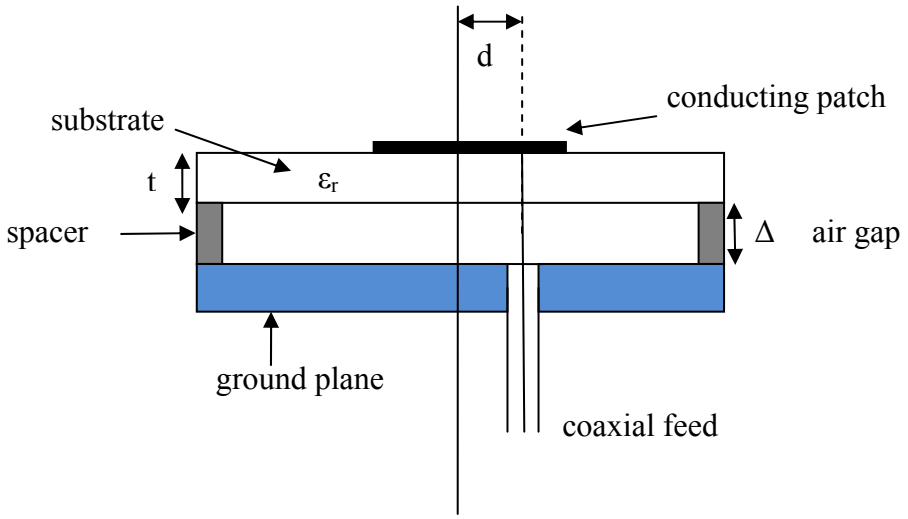

Figure 1.14: Patch with air gap.

ε_{eff} decreases as Δ increases. So resonant frequency can be set to a desired value by varying air gap [7].

From theory it is derived that: $f_{nm}(\Delta) = f(0)\sqrt{\frac{\varepsilon_r}{\varepsilon_{eff}}}$ 1.23

where: $$\varepsilon_{eff} = \frac{\varepsilon_r (t+\Delta)}{(t+\Delta\varepsilon_r)}$$ 1.24

and $f_{nm}(0)$ is the resonant frequency when Δ=0.

It is shown that when Δ increases, ε_{eff} lowers and f_{nm} is raised.

1.2.8 Advances in microstrip antennas

Microstrip antennas suffer from narrow bandwidth which limits the ability for broadband emission. D. Yoharaaj, Raja Syamsul Azmir and Alyani Ismail proposed an antenna configuration in order to overcome the problem [9]. The configuration is shown in Fig. 1.15:

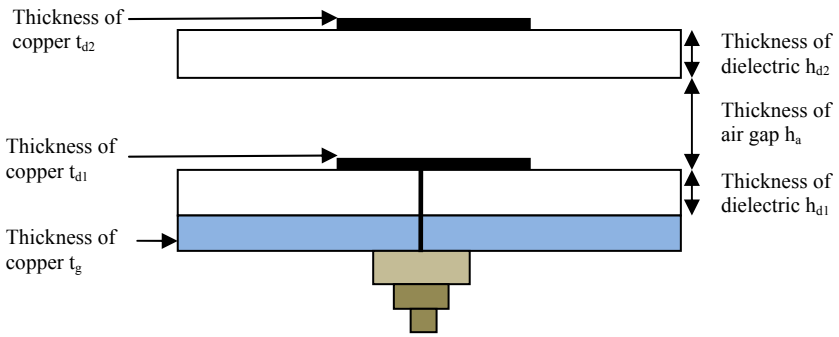

Figure 1.15: Experimental setup.

A stacked geometry including two patches and two substrates is designed. Coaxial cable is used for the excitation.

The dielectric constant as a function of thickness is:

$$\varepsilon_{av} = \frac{\varepsilon_r h_{d1} + \varepsilon_r h_a + \varepsilon_r h_{d2}}{\frac{h_t}{3}} \qquad 1.25$$

Where $h_t = h_{d1} + h_a + h_{d2}$ and a_2= 0.16605, a_4=0.00761, b_2= 0.09142 and $k_0=2\pi/\lambda$

The bandwidth would be:

$$BW = \frac{\sqrt{2}p}{45\pi}(1 - \frac{1}{\varepsilon_{av}} + \frac{2}{5\varepsilon_{av}^2})(\frac{1}{\varepsilon_{av}})(\frac{h_t}{\lambda})(\frac{W}{L}) \qquad 1.26$$

Where: $p = 1 + \frac{a_2}{20}(k_0 w)^2 + a_4 \frac{3}{560}(k_0 w)^4 + b_2 \frac{1}{10}(k_0 L)^2$

Simulations have shown that using an antenna of multiple substrates (Fig. 1.15), bandwidth is enhanced and the antenna acquires broadband features.

Fairus, Yusof, Pohan and Chuan worked on fractal antenna and stacked configuration in order to provide a functional scheme with wide bandwidth [10]. This configuration is depicted in Fig. 1.16. An increase in thickness leads to unwanted surface waves, spurious radiation and cross polarization. Thus substrate's thickness should be limited so that the antenna would operate efficiently.

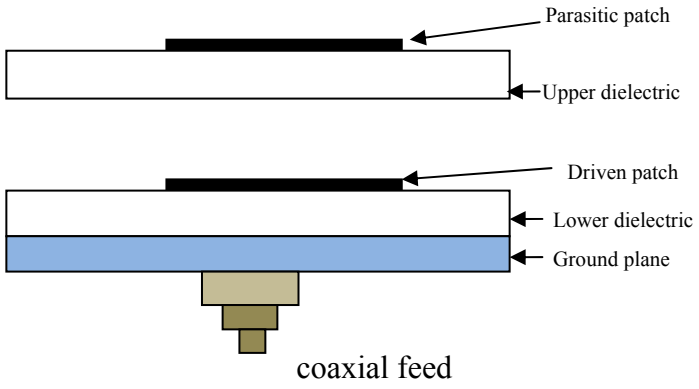

Figure 1.16: Proposed setup.

Low cross polarization can be achieved by using a lower dielectric of high constant and an upper dielectric of low constant. Such a configuration leads to low level of cross polarization. Driven and parasitic patches have fractal geometry. A fractal object is constructed of subunits and sub subunits that look like the whole object. Fig. 1.17 shows fractal geometry.

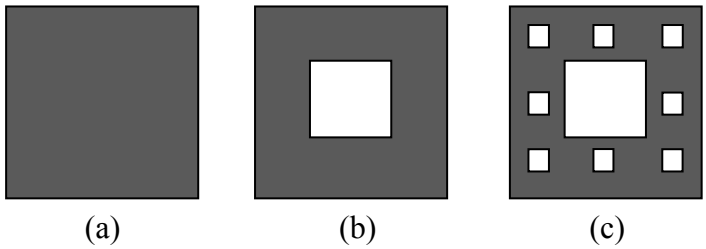

Figure 1.17: Patch Antenna; (a) with zero (b) first (c) second iteration.

Feed of parasitic patch is achieved by electromagnetic coupling. Fig. 1.18a and 1.18b below demonstrates the antenna performance with zero and one iteration. An increase in the number of iterations causes bandwidth increase.

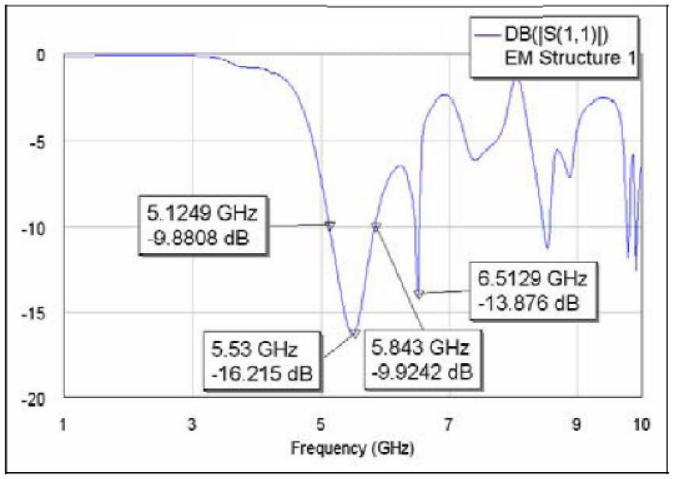

(a)

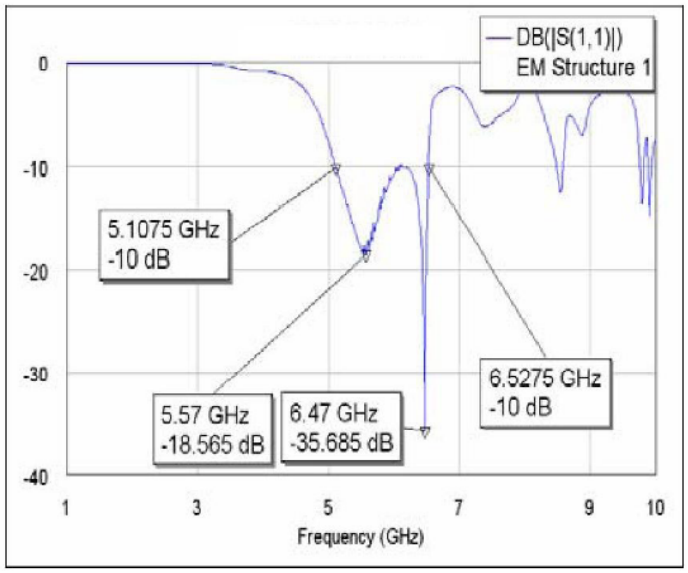

(b)

Figure 1.18: Return loss as a function of frequency for antenna; (a) with zero and (b) one iteration.

Microstrip antennas have the inherent drawback of narrow bandwidth [11]. Some methods to overcome this unwanted feature are:

1) Using a higher dielectric constant.
2) Meandering of the ground plane.
3) Inserting suitable slots in the radiating patch.
4) Using shorting stacked patches.

Elkamchouchi and Abouelseoud [12] focused their research on fractal geometry of patch antenna and how it could provide larger bandwidth.

Two types of antenna were simulated using FDTD method (Finite Difference Time Domain). A triangular patch and a Sierpinski patch were modelled (Fig. 1.19).

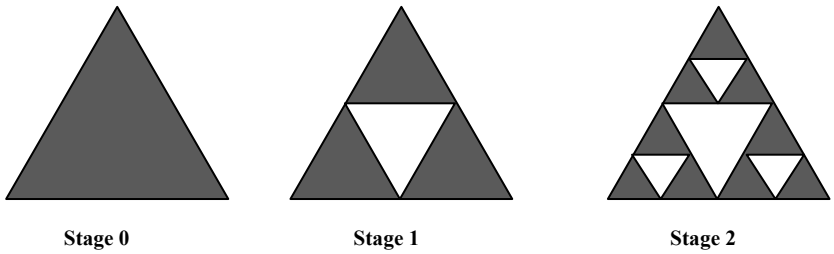

Figure 1.19: Sierpinski gasket model.

S_{11} parameter is derived for both cases (single triangular patch and Sierpinski gasket). A clear bandwidth enhancement is noticed proving that fractal geometry can increase bandwidth. S_{11} is -10dB at 23GHz for the case of the single patch antenna while the Sierpinski gasket model (stage 2) reaches -65dB.

Saksiri and Krairiksh proposed a serrated antenna in order to achieve a better quality of matching [13]. The experimental configuration is shown in Fig. 1.20.

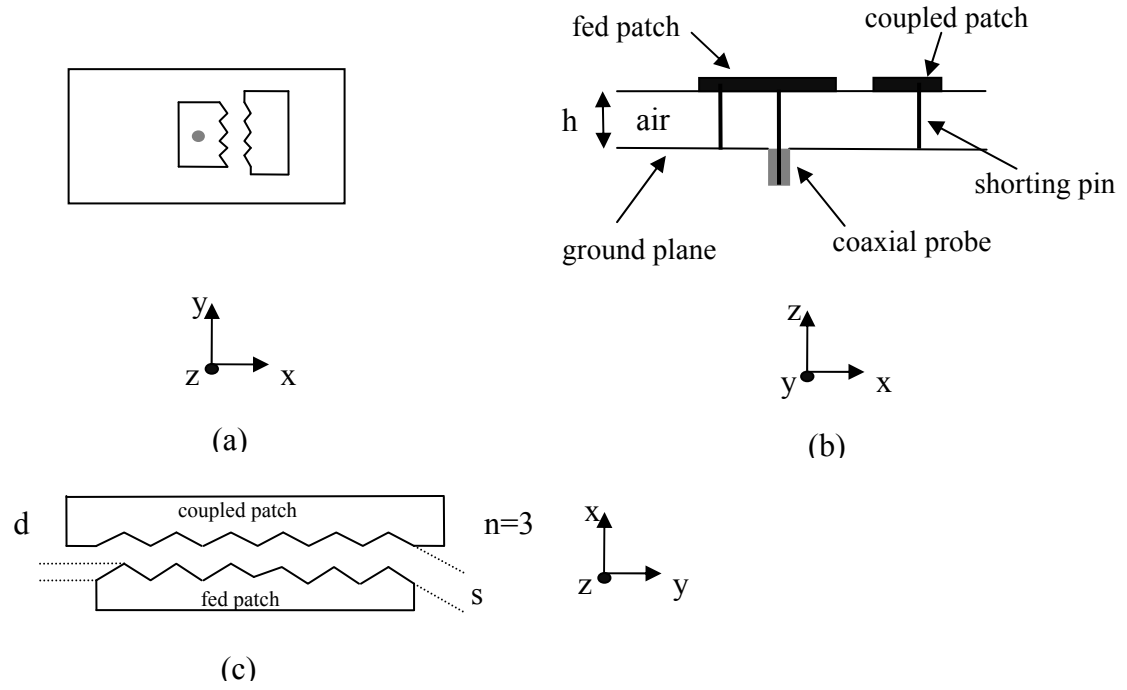

Figure 1.20: The proposed antenna; (a) upper (b) sidelong view (c) serration of fed and coupled patch.

As it is clear from Fig. 1.20, there are two patches, the fed and the coupled one. The feeding is succeeded by electromagnetic coupling. The matching between the fed and coupled patch depends on the serration depth, number of serrations (n) and distance between serrations. Results have shown that by increasing the number of serrations; return loss reaches lower values which lead to better matching conditions. Moreover bigger distance between the patches leads to decreased return loss.

Kumar and Bhooshan [14] focused their research on techniques to widen the bandwidth of a patch antenna. They used two antennas a driven and a parasitic one. The driven patch was fed and the parasitic one was stimulated by electromagnetic coupling.

The bandwidth of the antenna is given by the form:

$$\mathrm{BW} = \frac{\mathrm{VSWR} - 1}{\mathrm{Q}\sqrt{\mathrm{VSWR}}} \tag{1.27}$$

where Q is the quality factor and:

$$VSWR = \frac{1 + |\Gamma|}{1 - |\Gamma|} \tag{1.28}$$

where Γ is the reflection coefficient which is defined as the measure of the reflected waves at the feeding point of the antenna.

Γ equals to:

$$\Gamma = \frac{Z_{in} - Z_0}{Z_{in} + Z_0} \tag{1.29}$$

where Z_0 is the characteristic impedance of the feed line and Z_{in} the input impedance at the feeding point.

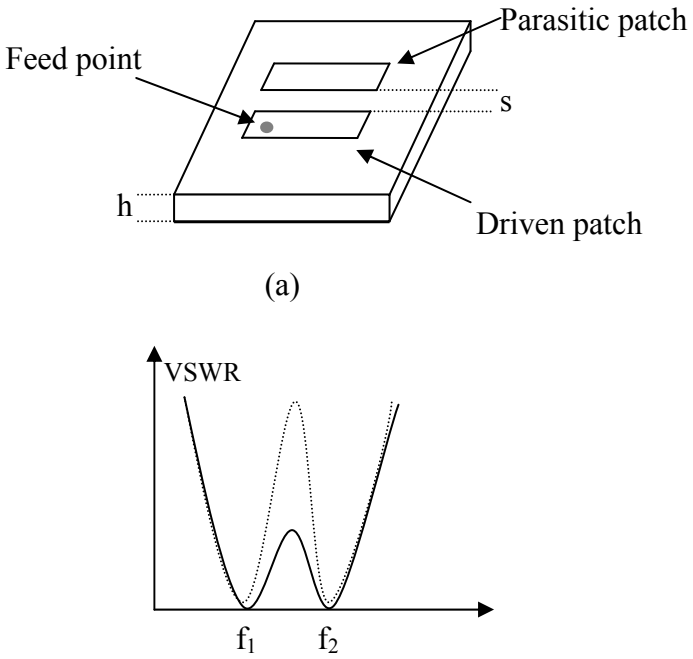

Figure 1.21: Proposed design and operation of two coupled patches; (a) Setup (b)VSWR diagram of two coupled radiators.

Fig. 1.21a represents the experimental disposition and Fig. 1.21b shows the results for individual and coupled resonators. It is clear that coupling provides larger bandwidth. An increase in substrate's thickness could also lead to wider bandwidth but also to the development of unwanted surface waves and spurious radiation.

A. K. Gautam and B. R. Vishvakarma, investigated a narrow band but frequency tuneable antenna. The microstrip antenna includes two MOS capacitors at its radiating edges [15]. The experimental disposition is described in Fig. 1.22:

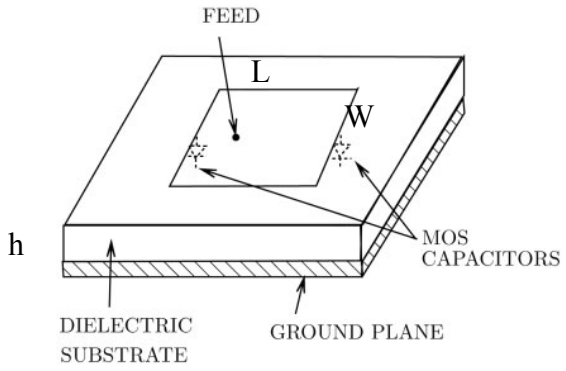

Figure 1.22: View of proposed antenna.

A MOS capacitor is consisted of a metal surface placed on an insulator which is mounted on a semiconductor as shown in Fig. 1.23:

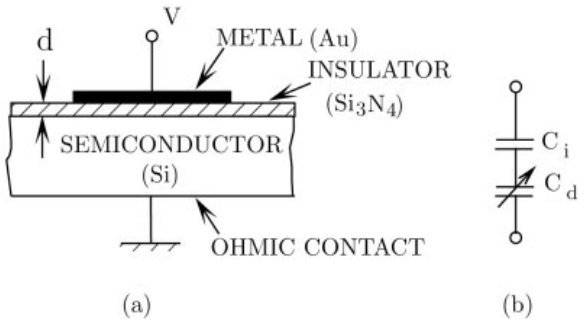

Figure 1.23: MOS capacitor configuration.

It is proved that a change in voltage of the capacitor, differs the electrical length of the patch and hence the resonant frequency.

From theory it is known that the capacity of a MOS capacitor equals to:

$$C_{mos} = \frac{C_i}{[1 + (\frac{2V_g C_i^2}{\varepsilon q N_\alpha})]^{1/2}} \qquad 1.30$$

where C_i is the insulator capacitance, ε is the permittivity of the semiconductor, N_A is the accepter concentration and q is the charge of electron.

Microstrip antenna has an equivalent RLC circuit described in Fig. 1.24:

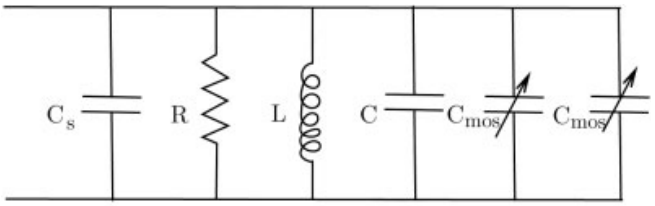

Figure 1.24: RLC equivalent circuit.

where R,L,C describes the patch antenna and C_s is the fringing capacitance.

$$C_s = \frac{0.01668}{\omega}\left(\frac{\Delta L}{h}\right)\left(\frac{W}{\lambda}\right)\varepsilon_e \qquad 1.31$$

where W, L and h are dimensions denoted in Fig. 1.22, ΔL is the length extension due to fringing fields, ε_e is the effective dielectric constant.

The total capacitance of the patch antenna plus the MOS capacitors would be:

$$C_{total} = 2C_{mos} + C_s + C \qquad 1.32$$

The resonance frequency is:

$$f_r = \frac{1}{2\pi\sqrt{L(2C_{mos} + C_s + C)}} \qquad 1.33$$

which clearly indicates the dependency of frequency from capacitance and thus voltage.

J. A. Ansari, Satya Kesh Dubey, Prabhakar Singh, R. U. Khan, and Babau R. Vishvakarma suggested an H shaped microstrip antenna with dual frequency operation [16]. Fig. 1.25 shows the scheme of the antenna.

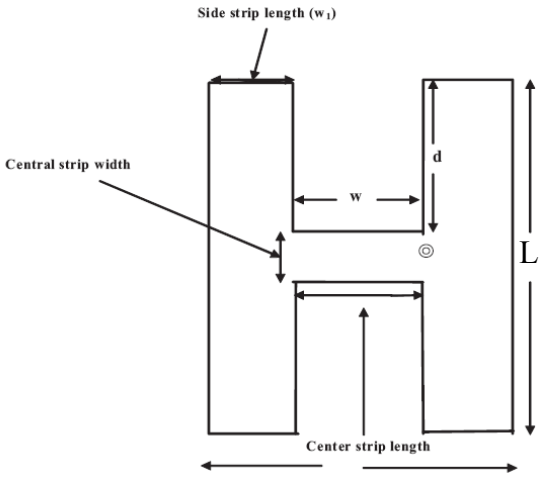

Figure 1.25: H shaped antenna.

It is clear that the two non radiating edges are cut creating notches. Thus a change to surface current density occurs leading to variation in electric and magnetic fields along dimensions w and d.

A rectangular patch corresponds to a parallel RLC circuit depicted in Fig. 1.26:

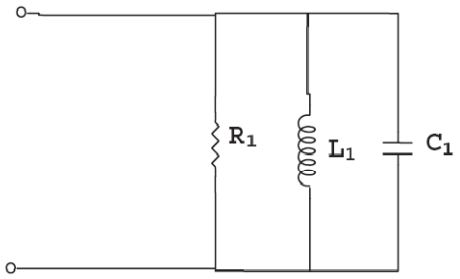

Figure 1.26: RLC equivalent circuit.

where

$$C_1 = \frac{\varepsilon_0 \varepsilon_e LW}{2h} \cos^{-2}\left(\frac{\pi y_0}{L}\right) \qquad 1.34a$$

$$L_1 = \frac{1}{\omega^2 C_1} \qquad 1.34b$$

$$R_1 = \frac{Q_r}{\omega C_1} \qquad 1.34c$$

$$Q_r = \frac{c\sqrt{\varepsilon_e}}{4fh} \qquad 1.34d$$

$$\varepsilon_e = \frac{\varepsilon_r + 1}{2} + \frac{\varepsilon_r - 1}{2}\left(1 + \frac{10h}{W}\right)^{-1/2} \qquad 1.34e$$

and y_o is the feed location, Q_r is the quality factor, ε_e is the effective dielectric constant h the substrate's thickness and L, W the dimensions of the patch element.

The input impedance of the above RLC circuit equals to:

$$Z_p = \frac{1}{\frac{1}{R_1} + \frac{1}{j\omega L_1} + j\omega C_1} \qquad 1.35$$

The appearance of the notches, adds an inductance ΔL and a capacitance ΔC to the equivalent circuit as shown in Fig. 1.27.

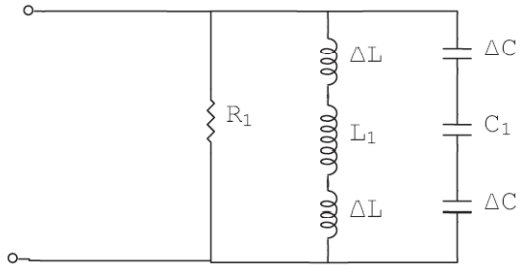

Figure 1.27: Equivalent circuit of H shaped patch antenna.

$$\Delta L = \frac{Z_1}{16 f \cos^{-2}\left(\frac{\pi y_0}{L}\right)} \tan\left(\frac{\pi f d}{c}\right), \qquad 1.36a$$

$$\Delta C = \left(\frac{d}{w}\right) C_s \qquad 1.36b$$

where C_s is the gap capacitance between two side strips and Z_1 is the characteristic impedance of a microstrip line of width w_1.

The new values of inductance and capacitance due to the introduction of notches would be:

$$L_2 = L_1 + 2\Delta L \tag{1.37}$$

$$C_2 = \frac{C_1 \Delta C}{2C_1 + \Delta C} \tag{1.38}$$

And the input impedance:

$$Z_H = \frac{1}{\frac{1}{R_1} + \frac{1}{j\omega L_2} + j\omega C_2} \tag{1.39}$$

From the above forms VSWR, Γ, and Return Loss are calculated. Return Loss diagram is carried out with d varying between 5 and 12mm. Diagrams depicted in Fig. 1.28, prove dual frequency operation.

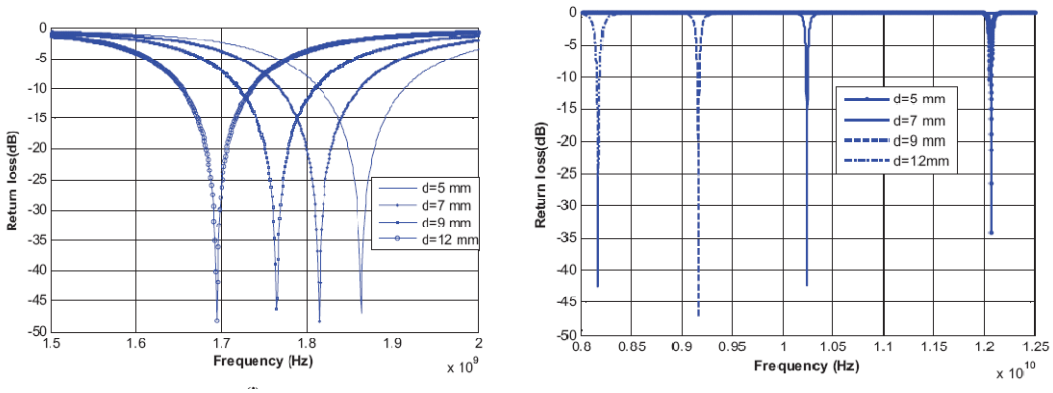

Figure 1.28: Return loss diagrams with varying d.

An increase in w affects the resonance frequency leading it to lower values as can be noticed in Fig. 1.29.

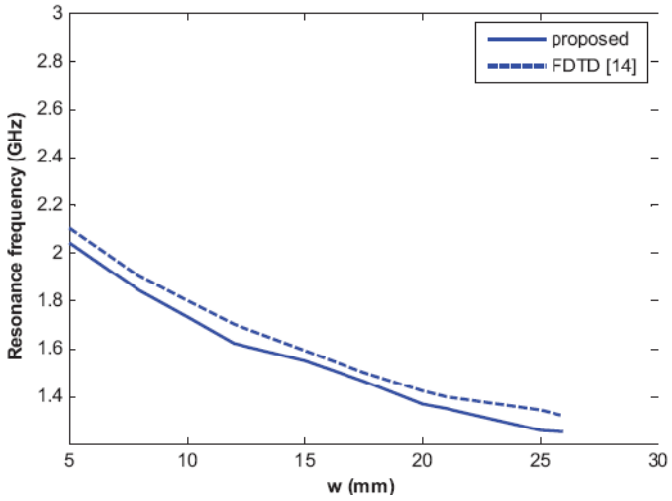

Figure 1.29: Frequency vs. w dimension diagram.

Many feeding mechanisms have been proposed in the literature in order to succeed wideband antenna properties [17], [18]. An L shaped microstrip feeding line, combined with a patch antenna has been investigated and can be seen in Fig. 1.30.

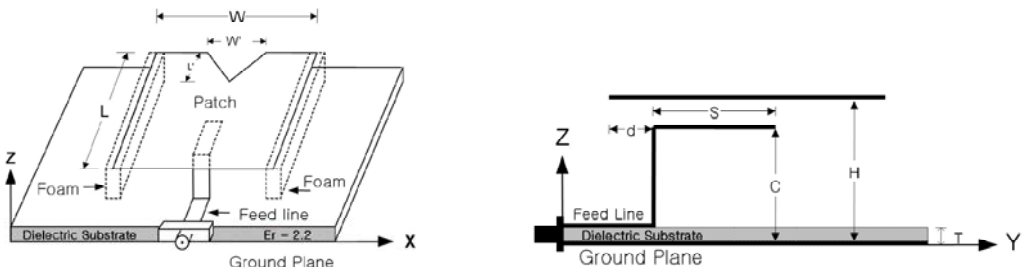

(a) (b)

Figure 1.30: Proposed antenna; (a) top view (b) side view.

Antenna excitation is made by electromagnetic coupling since no contact occurs between antenna and feeding line [19]. Measurements and simulations of the

investigated setup showed 31% impedance bandwidth while gain appears to be 7dBi for operation frequency (615 MHz).

Another antenna category that has gained special attention due to its broadband radiation capabilities, is the Planar Inverted F Antenna (PIFA) [20], [21]. A case of PIFA antenna can be seen in Fig. 1.31.

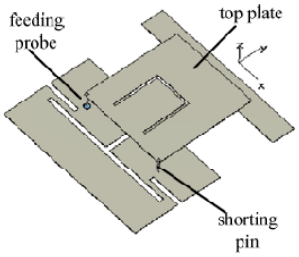

Figure 1.31: PIFA antenna with slots.

The specialty of this configuration is that it introduces slots in the radiating element and in the ground plane. These slots are responsible for multiband behavior and bandwidth enhancement. The slot variation on ground plane and patch element, makes the antenna radiate at different frequency bands [22]. A different case of U slot antenna is seen in Fig. 1.32(a) and (b).

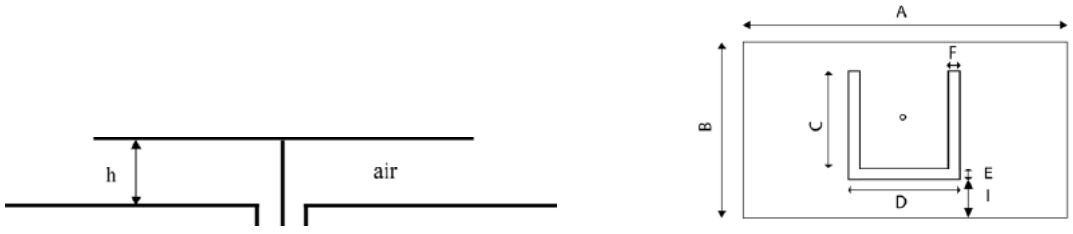

(a) (b)

Figure 1.32: U slot antenna; (a) side view (b) top view.

This type was investigated by putting a shorting pin connecting the radiating element with the ground plane and then FR4 substrate. For these cases different matching conditions and antenna efficiency were derived [23] and presented in Fig. 1.33.

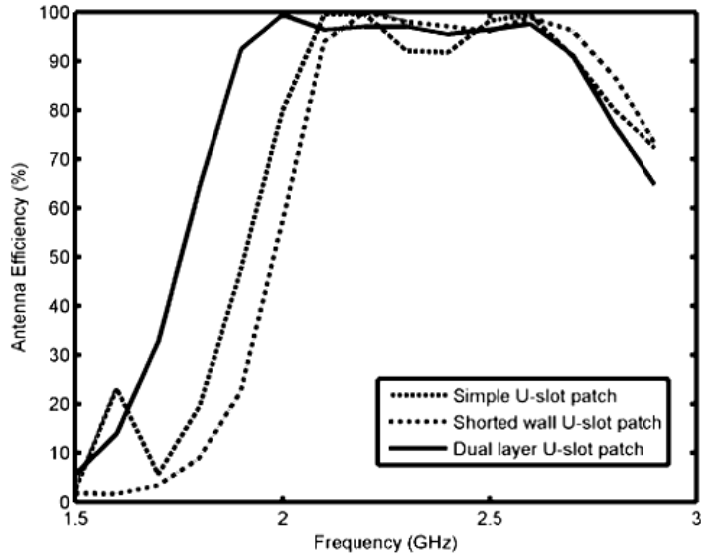

Figure 1.33: Efficiency for the three investigated cases of slot antenna.

In this case efficiency is estimated to be more than 90% for the frequency band of IEEE 802.11b/g/n proving that the designed antenna is suitable for Wi-Fi applications.

Bowtie patches have also been chosen for bandwidth increase. A typical bowtie antenna can be seen in Fig. 1.34.

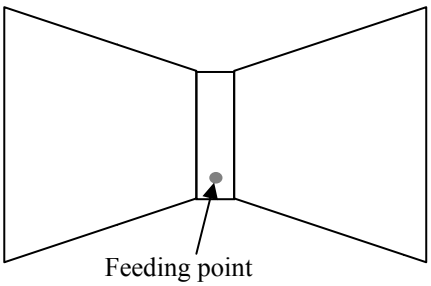

Figure 1.34: Bowtie patch antenna.

Different versions of such antennas have been appeared in literature [24], [25], [26]. The typical value of impedance bandwidth they succeed is 27%.

Pramod Kumar [27] presented a method for developing wideband patch antennas following a set of steps in order to succeed the desired antenna characteristics. These steps include the initial patch design, the introduction of slots and the introduction of an air substrate. Each step is combined with optimization procedures so that the patch would acquire the desired features in terms of operation frequency, bandwidth and gain. A prototype was designed, fabricated and depicted in Fig. 1.35:

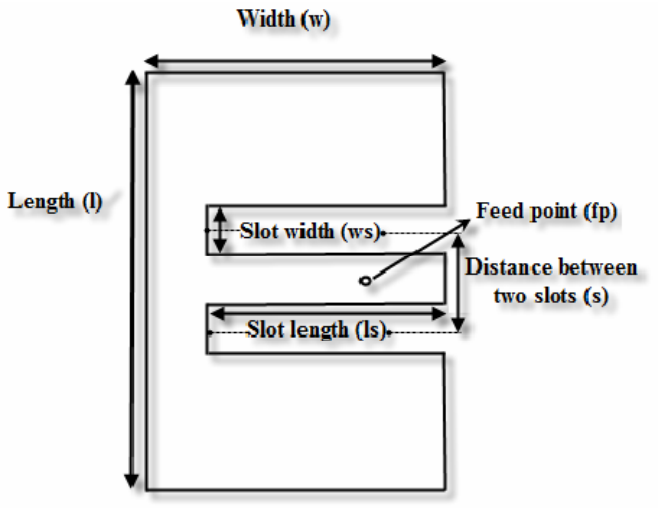

(a)

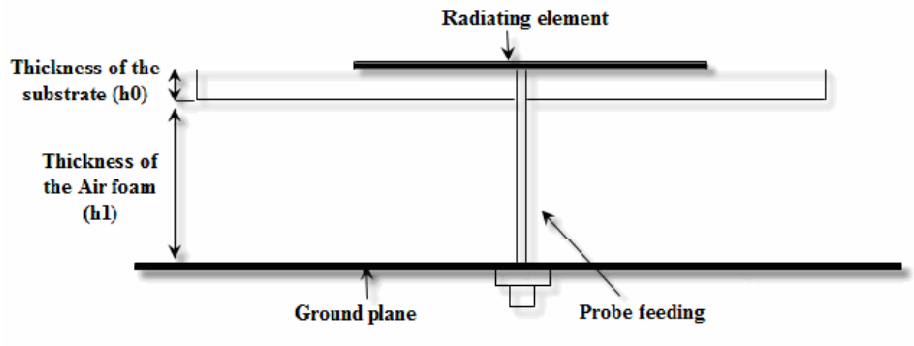

(b)

Figure1.35: Designed prototype; (a) top view (b) side view.

Simulations and measurements showed that gain is 6.3dB, bandwidth 18% and the range of operation is between 2 to 2.3GHz.

Many microstrip antennas have been designed to produce circularly polarized radiation for satellite and radar applications. These studies include special feeding methods and antenna geometries [28] [32]. C Z. Zhou, G. Fu and Q.Chen suggested a complex design to achieve high axial ratio bandwidth. The proposed configuration includes FR4, foam substrate, an L shaped microstrip line and a parasitic patch [33] and is depicted in Fig. 1.36.

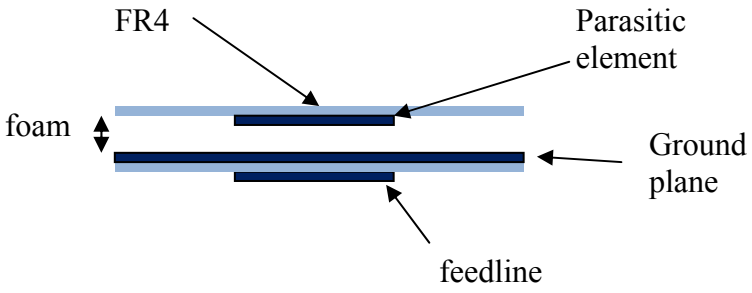

Figure 1.36: Antenna for circular polarization.

The antenna depicted in Fig. 1.36 was simulated and fabricated achieving 44.4% of bandwidth and 3dB axial ratio bandwidth 44.9% at operation frequency 2.4GHz. A similar microstrip antenna was designed and fabricated by Ali K. Aswad, Lway Faisal Abdulrazak and Tharek Abd. Rahman [34]. This prototype has composite structure, with two truncated edges for circular polarization support (Fig. 1.37).

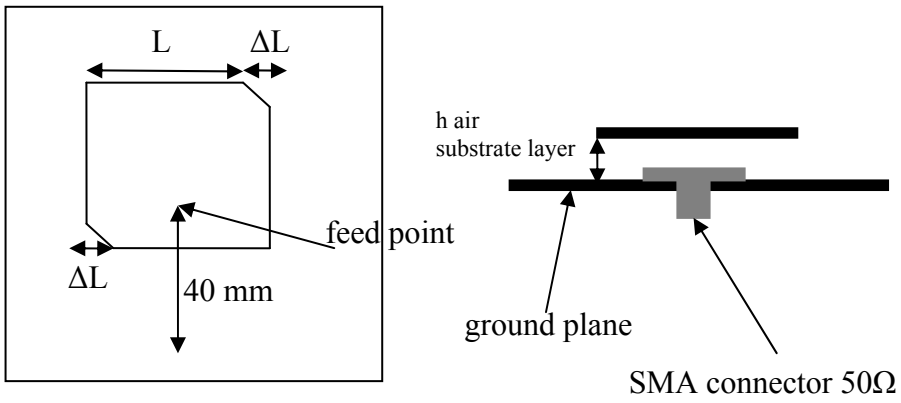

(a) (b)

Figure 1.37: Truncated patch antenna; (a) top view (b) side view

Another case of wide bandwidth is achieved by introducing slots to ground plane combined with an U shaped antenna [35]. Such a configuration can be seen in Fig. 1.38. A U shaped patch is fed by a coaxial cable and separated by an air gap. Ground plane involves slots for bandwidth increase.

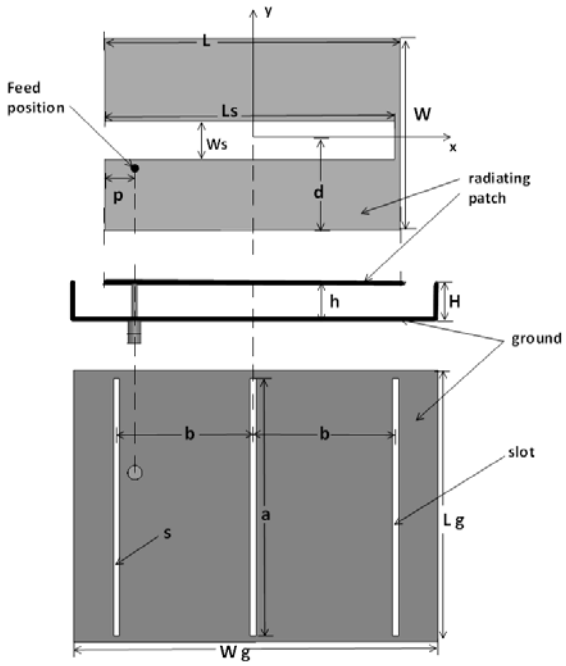

(a)

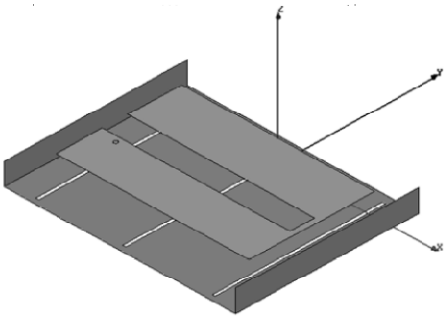

(b)

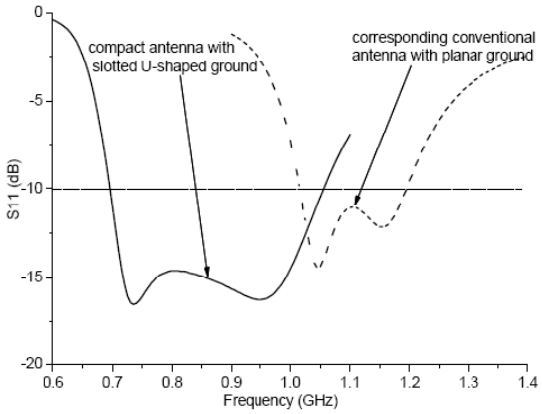

(c)

Figure 1.38: The proposed wideband antenna; (a) top view (b) side view (c)S_{11} of the proposed patch antenna.

S_{11} is derived for the antenna depicted in Fig. 1.38c and compared with the case were a planar ground plane without slots is introduced. Bandwidth is enhanced and shifted to lower frequencies.

A similar design as the above was introduced by S. Vikan and J. A. Aas [36] to achieve broadband characteristics by adding slots in the radiation element and shorting pins connecting the patch element with ground plane. The suggested setup can be seen in Fig. 1.39:

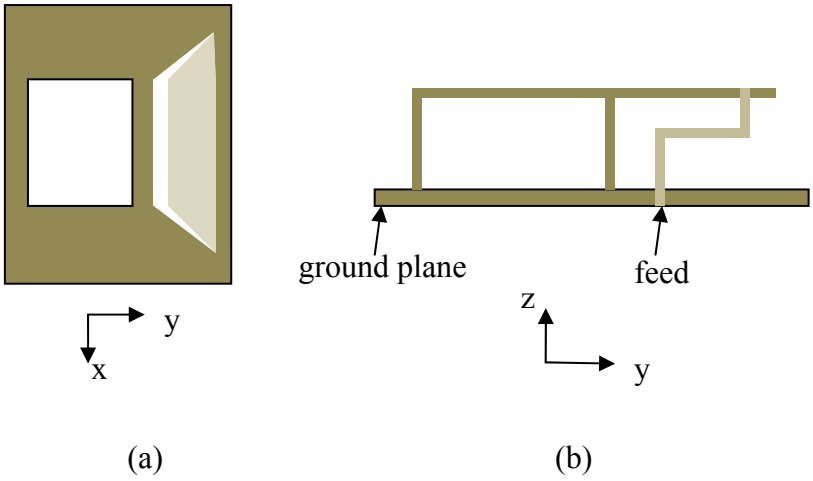

Figure 1.39: Slotted patch with shorting pins; (a) top view (b) side view.

The proposed setup was simulated and fabricated showing 88% bandwidth from 1.94GHz to 5.01GHz frequency band.

Beside the ability of the patch antenna to radiate over a wide range of frequencies, beam steering features using MEMS switches; have also been investigated through literature [37],[40].

1.3 MICROSTRIP ARRAY FUNDAMENTALS

An array is a set of radiating elements placed in proper position to produce a radiation pattern of increased gain and directivity. The direction of beam can be adjusted by phase shifter mechanisms. Below follows a description of the main characteristics of arrays together with mathematical equations that show the antenna's attributes. Terms such as mutual coupling, array factor, grating lobes are mentioned and analyzed. Furthermore several types of arrays are presented including stacked, circular and conformal geometries, adaptive and dual band operation arrays. In addition a variety of

feeding networks is described including T junction and Wilkinson power dividers. Let us mention that recent advances in wireless networks require an antenna array of high functionality that is able to transmit and receive through any circumstance.

1.3.1 Basic parameters of arrays

Power density of an antenna S(θ,φ) is defined as [41]:

$$S(\theta,\phi) = \frac{P_{rad} D(\theta,\phi)}{4\pi R^2} \qquad 1.40$$

where D(θ,φ) is the antenna's directivity, P_{rad} is the total radiated power and R is the distance.

Fig. 1.40 depicts a linear array plus the coordinate system.

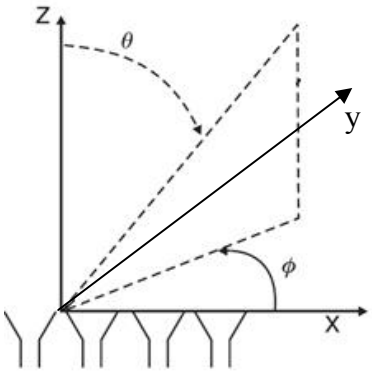

Figure 1.40: Linear Array with coordinate system.

From Equation 1.40, the directivity D(θ,φ) would be:

$$D(\theta,\phi) = \frac{4\pi R^2 S(\theta,\phi)}{P_{rad}} \qquad 1.41$$

It is known that:

$$P_{rad} = \int_{\Omega} S(\theta,\phi)d\Omega = \int_{\Omega} S(\theta,\phi)R^2 \sin\theta d\theta d\phi = R^2 \int_0^{\pi} S(\theta,\phi)\sin\theta d\theta \int_0^{2\pi} d\phi$$

and $\frac{P_{rad}}{R^2} = \int_0^{\pi} S(\theta,\phi)\sin\theta d\theta \int_0^{2\pi} d\phi$

So Equation 1.41 becomes:

$$D(\theta,\phi) = \frac{4\pi S(\theta,\phi)}{\int_{\Omega} S(\theta,\phi)d\Omega} \qquad 1.42$$

Regarding Equation 1.42, both polarizations (co polarization and cross polarization) are taken into account in the evaluation of power density.

Let us mention here that the radiated power P_{rad} is less than the input one because of antenna losses and reflected signal.

$$P_{rad} = \varepsilon_L P_{in}(1-|\Gamma|^2) \qquad 1.43$$

where ε_L is the efficiency factor and is related to circuit losses (feed network, phase shifters) and Γ is the reflection coefficient.

Another important antenna parameter is the Gain G(θ,φ). It is defined as follows:

$$G(\theta,\phi) = \varepsilon_L(1-|\Gamma|^2)D(\theta,\phi) \qquad 1.44$$

Actually gain is equal to directivity decreased by efficiency factor and reflection coefficient. For Γ=0 (perfect matching) and ε_L=100% gain and directivity coincide.

The multiplication of gain and input power gives the EIRP (Effective Isotropic Radiated Power), which expresses the amount of power radiated by an isotropic antenna to produce the peak power observed in the direction of maximum antenna gain.

EIRP is defined as:

$$EIRP = P_T - L_C + G_a \tag{1.45}$$

where P_T is the transmit power in dBm, L_c is the cable losses in dB and G_a is the gain in dBi.

For a planar array of M×N elements, the EIRP would be:

$$EIRP = N\varepsilon_L P_{in} D_{cell}(1 - |\Gamma|^2) \tag{1.46}$$

where: N is the number of elements, ε_L is the efficiency factor, D_{cell} is the element directivity, Γ is the reflection coefficient.

The above expression shows clearly the relation between EIRP, gain and directivity. The combination of Equations 1.44 and 1.46 gives:

$$EIRP = G(\theta, \phi) P_{in} \tag{1.47}$$

In order to evaluate the far field radiation pattern of a linear array of N identical elements depicted in Fig. 1.41, the following equation is used:

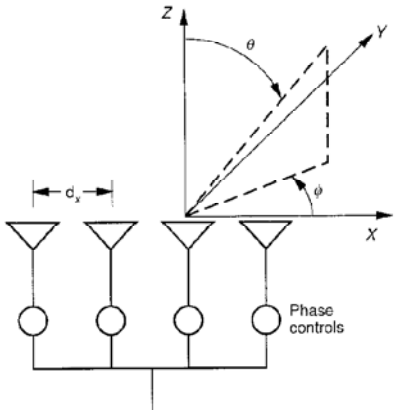

Figure 1.41: Antenna array.

$$\vec{E}(\theta,\phi) = \vec{f}(\theta,\phi)\sum_{n=1}^{N}\alpha_n \exp[jk_0(nd_x u)] \qquad 1.48$$

where u=sin(θ) cos(φ).

a_n are weights given to each element, f(θ,φ) is the pattern of one element.

Let's evaluate the total field for φ=0. The weight a_n is chosen to be: $a_n = |a_n|\exp(-jk_0 nd_x u_0)$ and $u_0 = \sin\theta_0$. So the total field would be:

$$\vec{E}(\theta,\phi) = \vec{f}(\theta,\phi)\sum_{n=1}^{N}|\alpha_n|\exp[jk_0 nd_x(u-u_0)] \qquad 1.49$$

The phase of each element changes by assigning weights to each of them. So there must exist a phase shifting mechanism.

1.3.2 Array architecture

The basic array architecture combined with a mechanism of amplitude/phase control (phased array) is depicted in the following scheme:

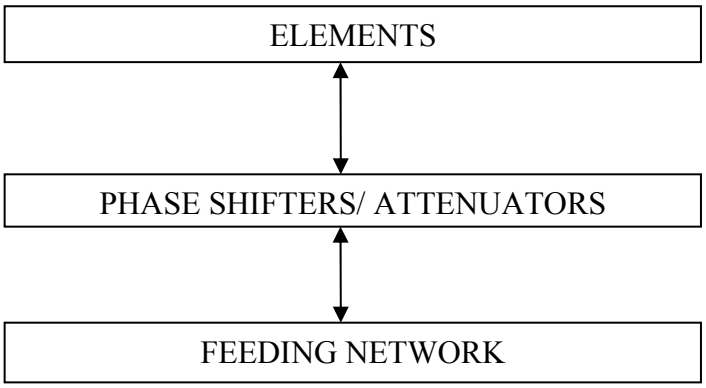

Figure 1.42: Phased Array configuration.

As it is seen in Fig. 1.42 the antenna elements are first connected to a unit which performs phase shifting/amplitude adjustments. After that, the feeding network is included that performs proper power division.

Phase shifters/attenuator modules, act as a beam forming system when a radiation pattern with specific attributes is needed. Beam forming system can assign each port an explicit beam to provide a desired radiation pattern.

Array architecture involves T/R (Transmit/Receive) and TDU (Time Delay Unit) modules, such as phase shifters, to achieve a certain desired radiation shape. A T/R module performs the following activities:

I) Separation of transmit and receive channel

II) Low noise amplification of received signals

III) Variable gain setting

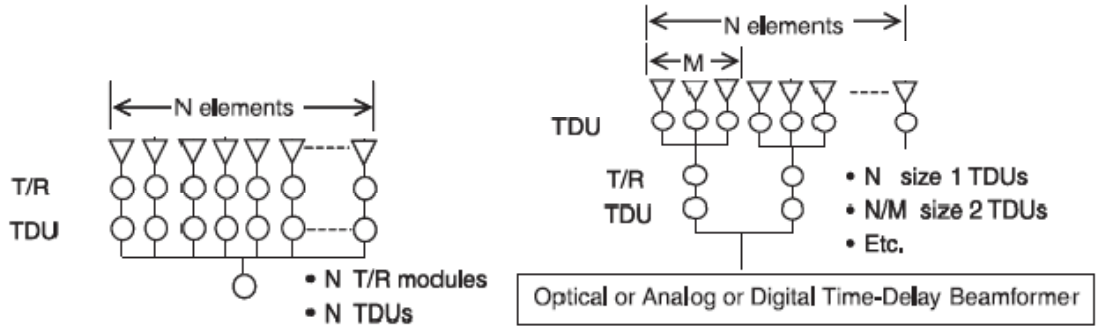

Figure 1.43: T/R and TDU configuration.

Fig. 1.43a shows that each radiation element can be connected to a different T/R and TDU module fed by a central point [41]. In Fig. 1.43b, elements are grouped and then each group is assigned a T/R and TDU module. Losses can be detected in the T/R module, the power divider and the phase shifting devices.

Fig. 1.44 describes the case of an array architecture including a switch that aims to separate transmit and receive channel. The switch connects the transmitter/receiver to the power divider which performs power division/union [41].

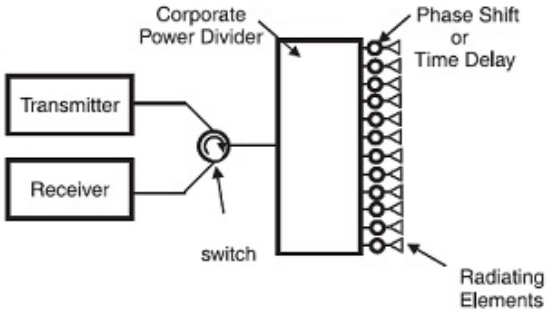

Figure 1.44: Array configuration incorporating a switch and a power divider.

1.3.3 Phase shifters

A phase shifter is the most significant part of an phased array providing changes to the transmission phase angle [41]. They can be grouped into analog devices and digital ones. Analog devices produce a change in phase by altering the value of an analog parameter such as voltage. Digital devices include a number of binary states where each one corresponds to a specific phase change. Examples of phase shifters are mentioned below:

i) Ferrite phase shifters.

ii) Diode phase shifters.

iii) MMIC and MEMS shifters.

iv) Ferroelectric phase shifters.

1.3.4 Received signal Array factor

For a linear array of K elements depicted in Fig. 1.45a and 1.45b, assuming that:

i) Equal distances of all elements to network

ii) No additional phase shifting

iii) No mutual coupling between elements

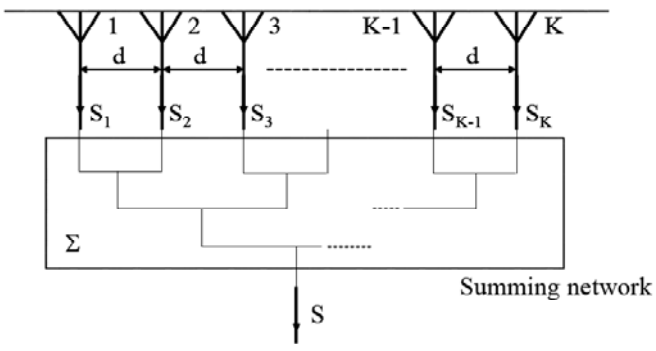

(a)

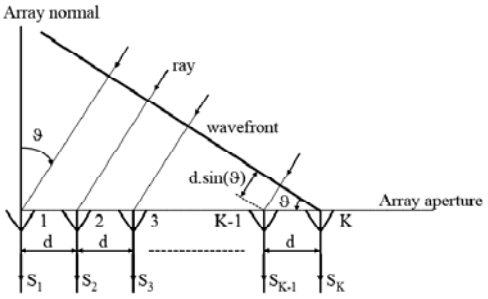

(b)

Figure 1.45: Array configuration; (a) an array connected to an aggregation network (b) an array receives a waveform.

The total received signal is [42]:

$$S(\theta) = S_e(\theta) S_a(\theta) \tag{1.50}$$

where: $S_e(\theta)$ is known as "element factor" and $S_a(\theta)$ is called "array factor".

$$S_a(\theta) = \sum_{i=1}^{K} e^{jk_0(K-i)d\sin\theta} \tag{1.51}$$

k_0 is the wavelength $k_0=2\pi/\lambda_0$ and λ_0 the free space wavelength.

The element factor expresses the radiation pattern of one radiator. The array factor states the radiation pattern of K isotropic radiators.

In Equation 1.51, i denotes the i^{th} radiator of the array depicted in Fig. 1.48a and 1.48b. Another form of array factor is:

$$\left|S_a(\theta)\right| = \left|\frac{\sin(\pi \frac{kd}{\lambda_0}\sin(\theta))}{\sin(\pi \frac{d}{\lambda_0}\sin(\theta))}\right| \qquad 1.52$$

1.3.5 Grating lobes

Equation 1.52 takes its maximum value when $\pi \frac{d}{\lambda_0}\sin(\theta)$ becomes zero [42].

Thus: $$\pi \frac{d}{\lambda_0}\sin(\theta) = m\pi \qquad 1.53$$

where m is an integer.

If we want just one maximum and not a second one then:

$$\pi \frac{d}{\lambda_0}\sin(\theta_{\max}) \le \pi$$

For $\theta_{\max} = \pi/2$ finally it is derived that:

$$\frac{d}{\lambda_0} \le 1 \qquad 1.54$$

The appearance of a second, third etc. maximum peak in the radiation pattern of an array is an unwanted phenomenon. These lobes are called grating lobes and they be eliminated by defining the element's distances to be less than one wavelength as Equation 1.54 implies.

1.3.6 Power dividers

The power from a main source is divided in order to feed the elements of an array. A power divider has a form shown in Fig. 1.46.

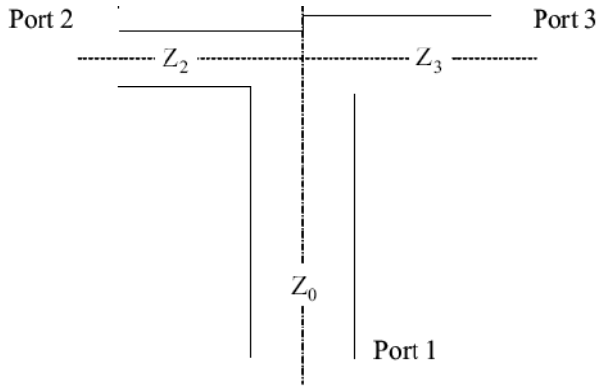

Figure 1.46: Power divider schematic.

If P_1 is the power that enters Port 1 and P_2 and P_3 the power that exits Ports 2 and 3 respectively then P_2 and P_3 are related through the equation:

$$P_3 = K^2 P_2 \qquad 1.55$$

where K is defined by the designer.

And $P_1 = P_2 + P_3$. 1.56

Thus: $$P_2 = \frac{1}{1+K^2} P_1 \text{ and } P_3 = \frac{K}{1+K^2} P_1 \qquad 1.57$$

In the simple case where a power divider feeds two patch antennas (Fig. 1.47) the equivalent circuit is shown in Fig. 1.48.

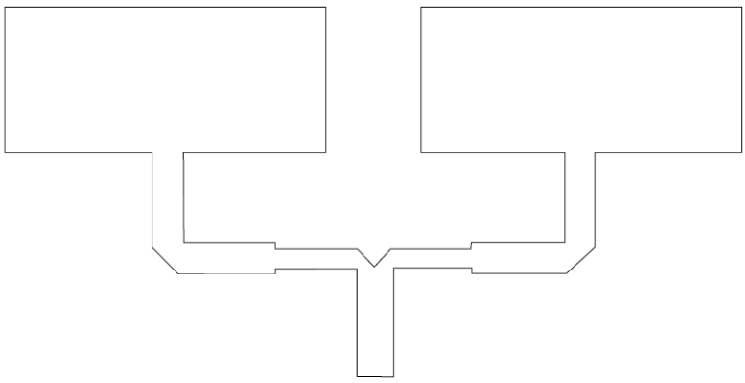

Figure 1.47: A power divider connected to two patch antennas.

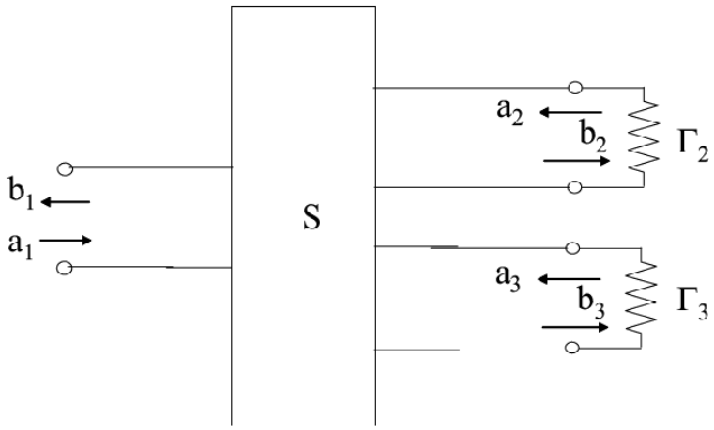

Figure 1.48: Equivalent circuit of power divider.

The scattering matrix from the circuit depicted in Fig. 1.48 would have the form:

$$\begin{bmatrix} b_1 \\ b_2 \\ b_3 \end{bmatrix} = \begin{bmatrix} S_{11} & S_{12} & S_{13} \\ S_{21} & S_{22} & S_{23} \\ S_{31} & S_{32} & S_{33} \end{bmatrix} \begin{bmatrix} a_1 \\ a_2 \\ a_3 \end{bmatrix} \qquad 1.58$$

where a_1, a_2, a_3, b_1, b_2, b_3 are complex voltage wave amplitudes and Γ_2 and Γ_3 are the reflection coefficients at the input of the antenna elements.

The amplitudes of the incoming and out coming signals are related to the reflection coefficient through the form:

$$a_2 = \Gamma_2 b_2 \text{ and } a_3 = \Gamma_3 b_3 \qquad 1.59$$

By substitution of Equation 2.27 in 2.26 the following expressions for b_1, b_2 and b_3 are derived:

$$b_2 = \frac{(1 - S_{33}\Gamma_3)S_{21} + S_{23}\Gamma_3 S_{31}}{(1 - S_{22}\Gamma_2)(1 - S_{33}\Gamma_3) - S_{23}S_{32}\Gamma_2\Gamma_3}\alpha_1 \qquad 1.60a$$

$$b_3 = \frac{(1 - S_{22}\Gamma_2)S_{31} + S_{32}\Gamma_2 S_{21}}{(1 - S_{22}\Gamma_2)(1 - S_{33}\Gamma_3) - S_{23}S_{32}\Gamma_2\Gamma_3}\alpha_1 \qquad 1.60b$$

$$b_1 = S_{11}a_1 + S_{12}\Gamma_2 b_2 + S_{13}\Gamma_3 b_3 \qquad 1.60c$$

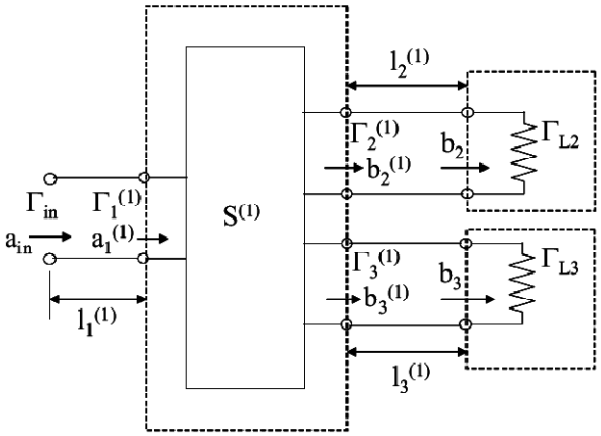

Figure 1.49: Power divider with transmission length l denoted.

If we take into consideration the transmission line's length (Fig. 1.49), the input and output signals take the form:

$$a_1 = a_{in}e^{-\gamma l_1^{(1)}} \qquad 1.61a$$

$$b_2 = b_2^{(1)}e^{-\gamma l_2^{(1)}} \qquad 1.61b$$

$$b_3 = b_3^{(1)} e^{-\gamma l_3^{(1)}} \qquad 1.61c$$

The reflection coefficients will vary as:

$$\Gamma_{in} = \Gamma_1^{(1)} e^{-2\gamma l_1^{(1)}} \qquad 1.62a$$

$$\Gamma_2^{(1)} = \Gamma_{L2} e^{-2\gamma l_2^{(1)}} \qquad 1.62b$$

$$\Gamma_3^{(1)} = \Gamma_{L3} e^{-2\gamma l_3^{(1)}} \qquad 1.62c$$

where γ is the attenuation factor

1.3.7 Advances in planar antenna arrays

Min Shi, Junwei Lu, and David J. Ireland introduced an adaptive patch antenna array for indoor mobile wireless network [43]. They investigated the use of hexagonal and circular shaped antennas.

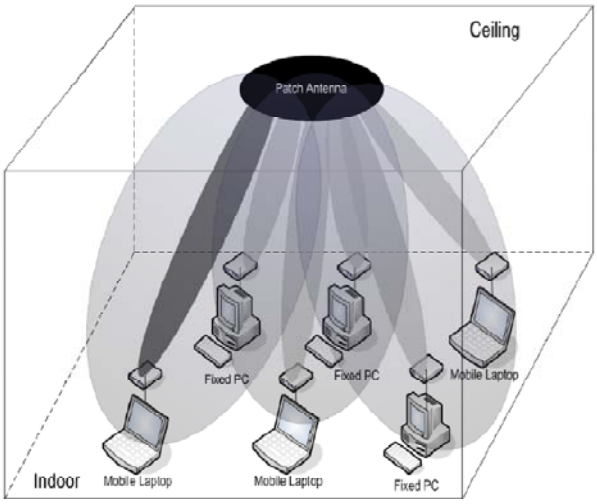

Figure 1.50: Schematic view of patch array.

The array of Fig. 1.50 can be used in WLAN networks to produce beam forming increasing the security level of the system.

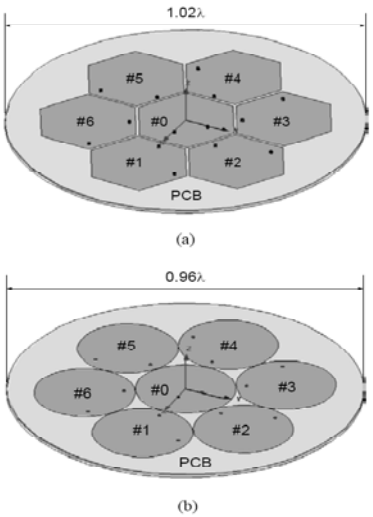

Figure 1.51: Hexagonal and circular array.

The array is consisted of a main patch antenna denoted as “0” (Fig. 1.51) and a number of parasitic elements. Beam steering can be achieved by adjusting switches connected to the parasitic elements. A more precise view of the suggested configuration can be seen in Fig. 1.52 where each element is connected to a specific circuit to provide the desired behavior.

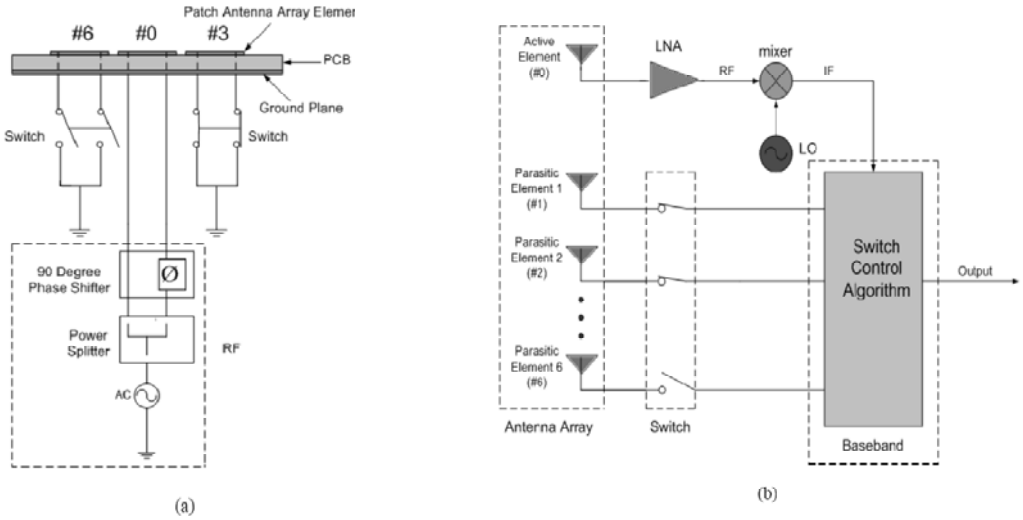

Figure 1.52: Description of array system with beam forming activity.

In Fig. 1.53, S_{11} parameter can be viewed for the case of hexagonal patch elements and circular patch elements.

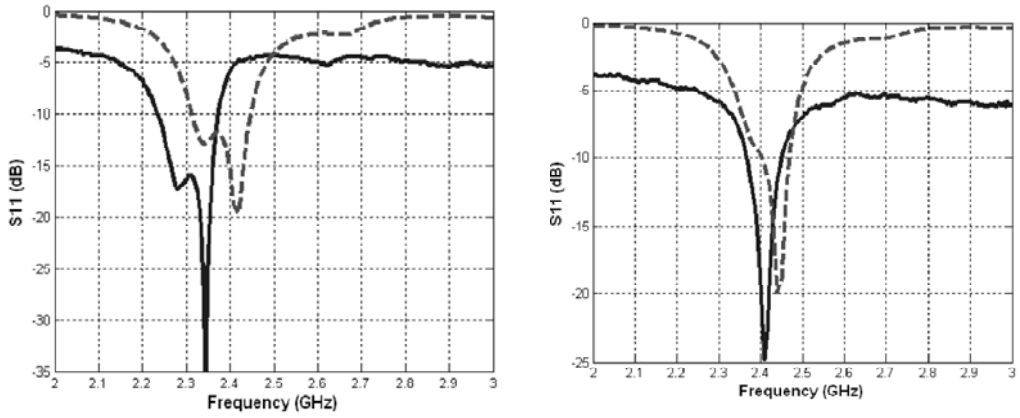

(a) (b)

Figure 1.53: S_{11} vs. frequency; (a) hexagonal patch (b) circular patch (continuous line: measurement, dotted line: simulation).

As it is seen from the above schemes a slight difference of measured and simulated curve is occurred, probably because of errors in antenna fabrication.

Yazid Yusuf, and Xun Gong designed a planar phased array with a driven and two parasitic elements fed by mutual coupling [44] as can be seen in Fig. 1.54. An array system uses phase shifters to achieve beam steering and focus the radiation on the desired directions. These phase shifters have a high cost. The proposed configuration introduces a different and low cost, way of beam steering using capacitors to control phase.

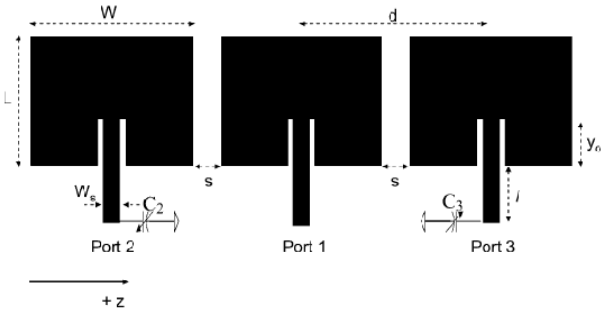

Figure 1.54: Proposed phased array: W=35mm, L=28.3mm, Ws=3.8mm, S=6.0mm, d=41mm, l=6mm, y0=10mm.

A change in reactive loads (C_2 and C_3), produce a change in phase. Patches 2 and 3 are fed by mutual coupling.

Let us consider the array of Fig. 1.54 as a 3 port network. The voltages are related to the currents through Z matrix as follows:

$$\begin{bmatrix} V_1 \\ V_2 \\ V_3 \end{bmatrix} = \begin{bmatrix} Z_{11} & Z_{12} & Z_{13} \\ Z_{21} & Z_{22} & Z_{23} \\ Z_{31} & Z_{32} & Z_{33} \end{bmatrix} \begin{bmatrix} I_1 \\ I_2 \\ I_3 \end{bmatrix} \qquad 1.63$$

The complex impedances of C_2 and C_3 are $Z_{C2} = 1/j\omega C_2$ and $Z_{C3} = 1/j\omega C_3$ respectively. Voltages at ports 2 and 3 are described by the equations:

$V_2 = -Z_{C2} I_2$ and $V_3 = -Z_{C3} I_3$.

Thus Equation 1.63 becomes:

$$\begin{bmatrix} \frac{I_2}{I_1} \\ \frac{I_3}{I_1} \end{bmatrix} = \begin{bmatrix} Z_{22} + Z_{C2} & Z_{23} \\ Z_{32} & Z_{33} + Z_{C3} \end{bmatrix}^{-1} \begin{bmatrix} -Z_{21} \\ -Z_{31} \end{bmatrix} \qquad 1.64$$

The radiation pattern of the array is the multiplication of the pattern of a single element by the array factor.

The array factor of the three elements of Fig. 1.54 is:

$$AF = 1 + \frac{I_2}{I_1} e^{-jkd\cos\theta} + \frac{I_3}{I_1} e^{jkd\cos\theta} \qquad 1.65$$

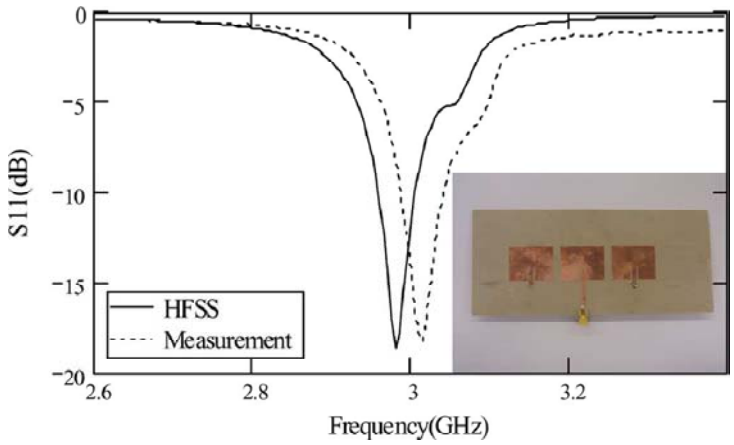

Figure 1.55: Return Loss diagram with experimental and simulated results.

Fig. 1.55 reveals a slight difference between the two curves due to fabrication errors. Fig. 1.56 depicts the radiation pattern of the proposed three element array.

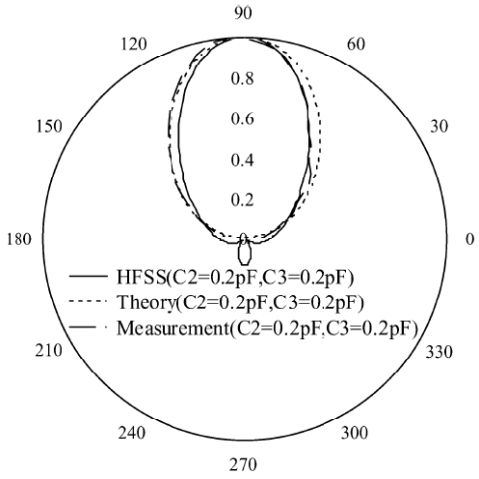

Figure 1.56: Radiation pattern of proposed array.

Anitzine, Argota and Pérez proposed an array configuration including a reflector to increase bandwidth and achieve better matching conditions decreasing return loss [45]. The suggested setup has the form depicted in Fig. 1.57:

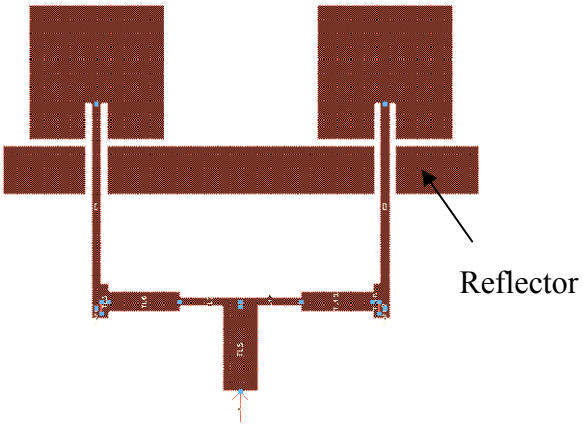

Figure 1.57: 2 patch antenna array with reflector.

Two radiation elements are fed by microstrip lines. A horizontal orthogonal patch lies on the same substrate and as simulations show, decreases S_{11}. Two cases were investigated. In the first the reflector is made of two discrete patches and in the second, of one patch. These cases are shown if Fig. 1.58.

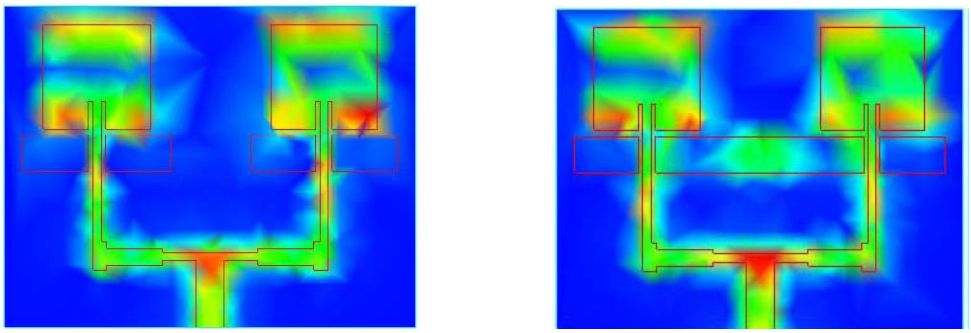

(a) (b)

Figure 1.58: An array of two radiation elements (a) Reflector of 2 patches (b) Reflector of one patch.

The characteristics of each case are presented in the table that follows:

Table 1.2: Features of joined and not joined patch antennas.

Joined	BW (MHz)	BW (%)	Efficiency (%)	S_{11} (dB)
No	290	5.5	94.41	-40.06
Yes	397	7.48	91.62	-42.16

The condition presented in Fig. 1.58b has wider bandwidth and better matching conditions are obtained.

Cui WeiDong proposed a four element patch antenna with a taper microstrip feeding line for bandwidth enhancement [46]. The antenna is depicted below:

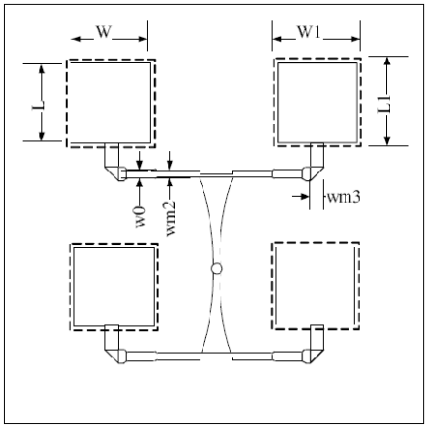

Figure 1.59: Four element antenna array.

The above array uses tapers with dimensions found using the formulas defined in [47]. The achieved impedance bandwidth is 10% for S_{11}<-20dB. In addition the configuration appeared in Fig. 1.59 was modified to include Electromagnetic Band Gap (EBG) ground structures. These forms are characterized by periodical compositions in ground plane that minimize surface waves and thus degrade cross polarization. EBG structures add complexity to the configuration but reduce mutual coupling and enhance gain [48 51]. A ground plane of periodic circles and split ring resonators were introduced in the array of Fig. 1.59 and the results can be viewed in Fig. 1.60a and 1.60b respectively.

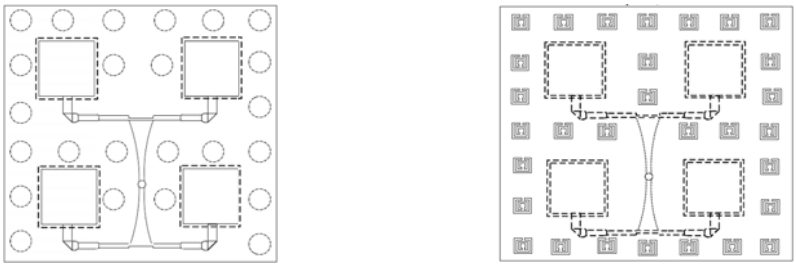

(a) (b)

Figure 1.60: EBG structure for patch array; (a) circle shaped EBG (b) split ring resonator EBG.

In both cases the cross polarization level is decreased compared with the case of the simple array, thus proving that EBG formation can effectively cause surface wave suppression.

The case where an array is combined with proper modules in order to steer radiation pattern to desired direction has been widely investigated and presented in literature. MEMS switches [52] and RF PIN diodes [53] have been used in order to adjust main lobe of radiation to specific direction. A linear 8 element array comprising RF PIN diodes has been designed, presenting adjustable pattern and tunable operation frequency [54]. The proposed configuration can be seen in Fig. 1.61.

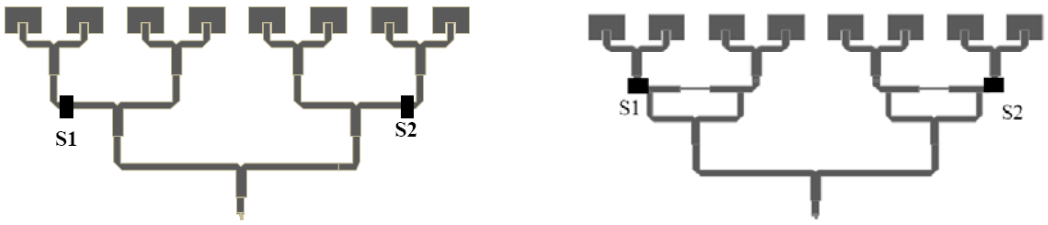

(a) (b)

Figure 1.61: Proposed configuration; (a) T Junction Power Divider (b) modified Wilkinson Power Divider.

Power is equally distributed to the radiation elements by the use of T junction (Fig. 1.61a) or modified Wilkinson Power Divider (Fig. 1.61b). The designs and full features of these power dividers can be found in [55]. S1 and S2 are the RF PIN diode switches that are controlled by an external dc voltage. The state of these switches (ON/OFF) affect the radiation pattern emitted by the array. The block diagram of the switch used in this study can be seen below.

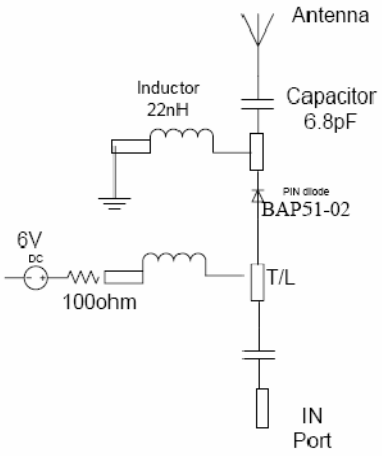

Figure 1.62: Block diagram of RF PIN switch.

The proposed array comprises FR4 glass epoxy (εr=4.6, tanδ=0.03). The ON state of the switches activates 8 elements while the OFF state excites 4 elements. The radiation pattern of 4 and 8 element array is Fig. 1.63a and 1.63b respectively.

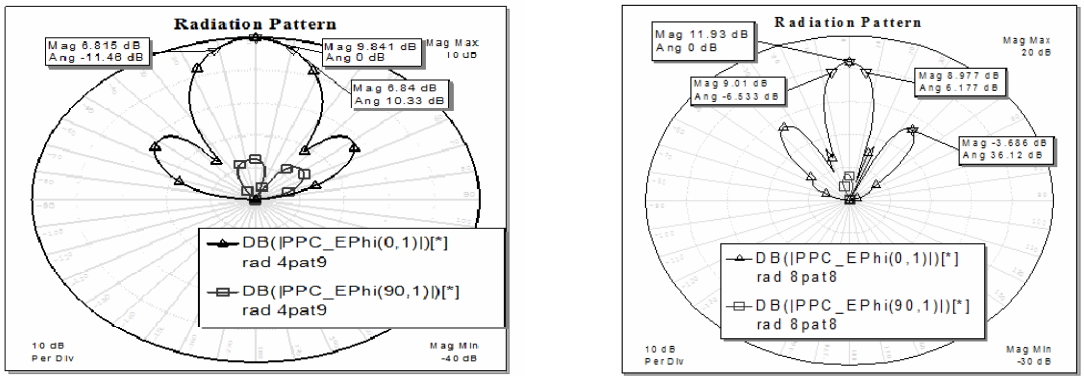

(a) (b)

Figure 1.63: Radiation pattern; (a) 4 element array (b) 8 element array.

The increase in the number of elements increases gain and reduces Half Power Beamwidth as expected. Let us mention here that the state of the PIN diodes affect the operation frequency as can be seen in Fig. 1.64.

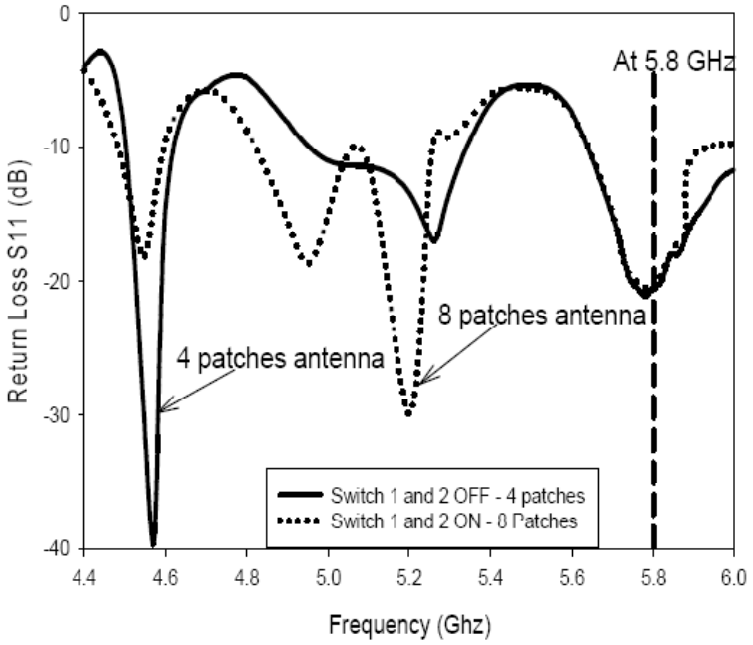

Figure 1.64: Return loss of the designed array.

4 patch array seems to operate at 4.58GHz, 5.25GHz and 5.8GHz while the 8 patch array resonates at 4.58Ghz, 4.9Ghz, 5.2GHz and 5.8 GHz.

1.3.8 Array factor and electric field of a planar uniform array

In this section the case of the array factor of a planar uniform array is derived and investigated. Electric field and directivity formulas are expressed in terms of the excitation amplitude and phase of each radiation element [56], [57].

Let us assume n elements lying on xy plane as can be seen in Fig. 1.65. The total electric field on P(r,θ,φ) would be:

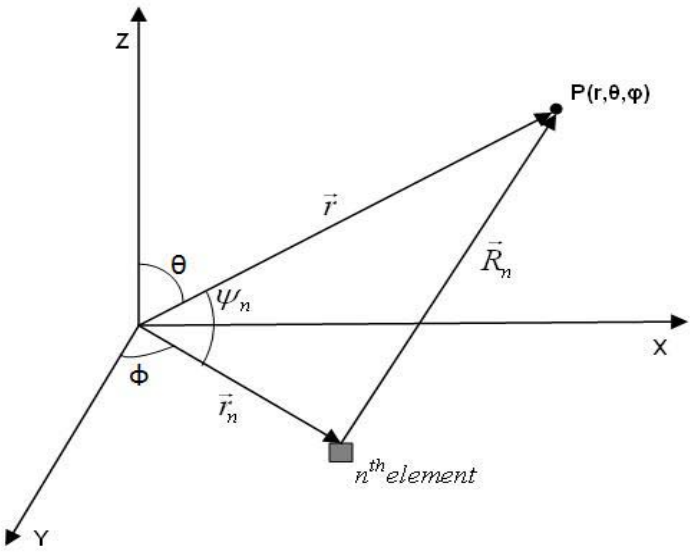

Figure 1.65: Electric field evaluation on P(r,θ,φ) using Cartesian coordinate system.

$$\vec{E}(\vec{r}) = \sum_{n}^{N} \vec{f}_n(\vec{r})\alpha_n \frac{e^{-jkR_n}}{R_n} \qquad 1.66$$

where:

$\vec{f}_n(\vec{r})$ is the radiation pattern function of the nth element,

a_n is the excitation of the nth element. a_n has amplitude and phase components.

$$R_n = \left|\vec{R}_n\right| = \left|\vec{r} - \vec{r}_n\right| = (\left|\vec{r}\right|^2 + \left|\vec{r}_n\right|^2 - 2\left|\vec{r}\right|\left|\vec{r}_n\right|\cos\psi_n)^{1/2} \qquad 1.67$$

It is

$$R_n = \left|\vec{r}\right|(1 + \frac{\left|\vec{r}_n\right|^2}{\left|\vec{r}\right|^2} - 2\frac{\left|\vec{r}_n\right|^2}{\left|\vec{r}\right|^2}\cos\psi_n)^{1/2} \qquad 1.68$$

$$\cos\psi_n = \frac{\hat{r}_n\hat{r}}{\left|\hat{r}_n\right|\left|\hat{r}\right|} = \hat{r}_n\hat{r}$$

So Equation 1.68 becomes:

$$R_n = \left|\vec{r}\right|(1 + \frac{\left|\vec{r}_n\right|^2}{\left|\vec{r}\right|^2} - 2\frac{\left|\vec{r}_n\right|^2}{\left|\vec{r}\right|^2}\hat{r}_n\hat{r})^{1/2} \cong \left|\vec{r}\right|(1 - \frac{\left|\vec{r}_n\right|}{\left|\vec{r}\right|}\hat{r}_n\hat{r}) = \left|\vec{r}\right| - \left|\vec{r}_n\right|\hat{r}_n\hat{r} \qquad 1.69$$

By substitution of Equation 1.69 to Equation 1.66 it is derived:

$$\vec{E}(\vec{r}) = \frac{e^{-jk|\vec{r}|}}{|\vec{r}|} \sum_{n}^{N} \vec{f}_n(\vec{r}) \alpha_n \exp(jk|\vec{r}_n|\hat{r}_n\hat{r}) \qquad 1.70$$

The excitation of each element is described by the form:

$$a_n = |a_n| e^{-j(\tau_n \omega + \phi_n)} \qquad 1.71$$

where $|a_n|$ is the amplitude of excitation,

τ_n is the time delay,

φ_n is the phase shift

Strong directivity is achieved when Equation 1.70 is maximized for a specific $\vec{r}_0$ and frequency ω_0. $\vec{E}(\vec{r})$ is maximum when:

$$\alpha_n \exp(jk|\vec{r}_n|\hat{r}_n\hat{r}_0) = |a_n|$$

$$|\alpha_n| e^{-j(\tau_n\omega_0 + \phi_n)} e^{jk_0|\vec{r}_n|\hat{r}_n\hat{r}_0} = |a_n|$$

$$e^{-j(\tau_n\omega_0 + \phi_n)} e^{jk_0|\vec{r}_n|\hat{r}_n\hat{r}_0} = 1$$

$$k_0|\vec{r}_n|\hat{r}_n\hat{r}_0 - \tau_n\omega_0 - \phi = \pm 2m\pi \qquad 1.72$$

The field expression for the maximum $\vec{E}(\vec{r})$ is:

$$\vec{E}(\vec{r}_0) = A\frac{e^{-jk|\vec{r}_0|}}{|\vec{r}_0|} \sum_{n}^{N} \vec{f}_n(\vec{r}_0)|\alpha_n| \qquad 1.73$$

For m=0 and $\tau_n=\tau$=constant, Equation 1.72 becomes:

$$\phi_n = k_0|\vec{r}_n|\hat{r}_n\hat{r}_0 - \tau\omega_0 \qquad 1.74$$

If Equation 1.71 is substituted to Equation 1.70 for τ=0 and the antenna elements are identical then the field equation becomes:

$$\vec{E}(\vec{r}) = \frac{e^{-jk|\vec{r}|}}{|\vec{r}|}\vec{f}(\vec{r})\sum_{n}^{N} |\alpha_n| \exp[\, j(k|\vec{r}_n|\hat{r}_n\hat{r} - \phi_n)]$$

1.75

By substitution of Equation 1.74 to Equation 1.75, we have:

$$\vec{E}(\vec{r}_0) = \frac{e^{-jk|\vec{r}_0|}}{|\vec{r}_0|}\vec{f}(\vec{r}_0)\sum_{n}^{N} |\alpha_n| \exp[\, j(\frac{\omega-\omega_0}{c})|\vec{r}_n|\hat{r}_n\hat{r}_0] \qquad 1.76$$

If $\omega=\omega_0$ and $\vec{r} \neq \vec{r}_0$ the total electric field take the following form:

$$\vec{E}(\vec{r}_0) = \frac{e^{-jk|\vec{r}_0|}}{|\vec{r}_0|}\vec{f}(\vec{r}_0)\sum_{n}^{N} |\alpha_n| \exp[\, jk|\vec{r}_n|(\hat{r}_n\hat{r} - \hat{r}_n\hat{r}_0)] \qquad 1.77$$

where r_0 is the direction of maximization of E field.

The radiation intensity at a direction $\vec{r}$ is given by the form:

$$\vec{U}(\vec{r}) = \frac{r^2}{2\eta}\left|\vec{\mathrm{E}}(\vec{r})\right|^2 \qquad 1.78$$

where η is the free space impedance and r the distance of the point of interest.

In logarithmic scale Equation 1.78 can be written as:

$$\vec{U}(\vec{r}) = 10\log B + 20\log(\left|\vec{E}(\vec{r})\right|) \quad 1.79$$

where B=$\frac{r^2}{2\eta}$.

The normalized value of radiation intensity is: $U_0(r) = \frac{U(r)}{U(r_0)}$

$U(r_0)$ is maximum radiation intensity at direction r_0.

Directivity is defined as:

$$D = \frac{4\pi}{\iint_{4\pi} U_0^2(\vec{r})dr} \quad 1.80$$

For the case of a planar array of M×L elements, the total electric field would be evaluated by the following procedure.

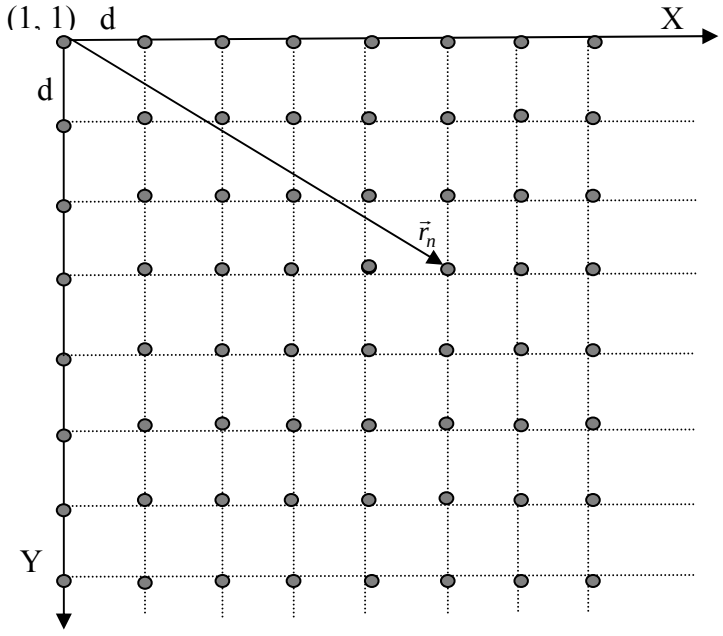

Figure 1.66: Planar array of M×L identical elements.

It is: $|\vec{r}_n|\hat{r}_n = \vec{r}_n$ and $\vec{r}_n = (m-1)d\hat{x} + (l-1)d\hat{y}$.

$$\hat{r} = \sin\theta\cos\phi\hat{x} + \sin\theta\sin\phi\hat{y} + \cos\theta\hat{z}$$

So $\vec{r}_n\hat{r} = (m-1)d\sin\theta\cos\phi + (l-1)d\sin\theta\sin\phi$

Assuming identical elements, Equation 1.75 becomes:

$$\vec{E}(\vec{r}) = A\frac{e^{-jk|\vec{r}|}}{|\vec{r}|}\vec{f}(\vec{r})\sum_{m=1}^{M}\sum_{l=1}^{L}|\alpha_{ml}|\exp\{j[k(m-1)d\sin\theta\cos\phi + k(l-1)d\sin\theta\sin\phi] - \phi_{ml}\} \quad 1.81$$

Equation 1.81 can be written in a different form as:

$$\vec{E}(\vec{r}) = A\frac{e^{-jk|\vec{r}|}}{|\vec{r}|}\vec{f}(\vec{r})AF_xAF_y \quad 1.82$$

where: $AF_x = \sum_{m=1}^{M}|a_m|e^{j[k(m-1)d\sin\theta\cos\phi-\phi_m]}$ and $AF_y = \sum_{l=1}^{L}|a_l|e^{j[k(l-1)d\sin\theta\sin\phi-\phi_l]}$ 1.83

AF_x and AF_y are known as array factors and $|a_{ml}| = |a_m||a_l| = 1$.

AF_x becomes maximum for specific values of θ and φ, when:

$$\begin{aligned} &k(m-1)d\sin\theta_0\cos\phi_0 - \phi_m = 0 \\ &and \\ &\phi_m = k(m-1)d\sin\theta_0\cos\phi_0 \end{aligned} \quad 1.84$$

For m=m+1, Equation 1.84 becomes:

$$\phi_{m+1} = kmd\sin\theta_0\cos\phi_0 \quad 1.85$$

The phase difference between two adjacent elements along x axis would be:

$$\phi_{m+1} - \phi_m = kmd\sin\theta_0\cos\phi_0 - kd(m-1)\sin\theta_0\cos\phi_0 = kd\sin\theta_0\cos\phi_0$$

$$\beta_m = kd\sin\theta_0\cos\phi_0 \quad 1.86$$

Following the same steps for the array factor AF_y it is derived that the phase difference between two adjacent elements along y axis would be:

$$\beta_l = kd\sin\theta_0\sin\phi_0 \tag{1.87}$$

Equations 1.83 can be written as a function of β_m and β_l as:

$$AF_x = \sum_{m=1}^{M} e^{j[(m-1)(kd\sin\theta\cos\phi-\beta_m]} \quad \text{and} \quad AF_y = \sum_{l=1}^{L} e^{j[(l-1)(kd\sin\theta\sin\phi-\beta_l]} \tag{1.88}$$

By setting $\psi=kd\sin\theta\cos\varphi\ \beta_m$ Equation 1.88 is now:

$$AF_x = \sum_{m=1}^{M} e^{j[(m-1)\psi]} \tag{1.89}$$

It is $\begin{aligned} AF_x &= 1 + e^{j\psi} + e^{j2\psi} + e^{j3\psi} + \ldots + e^{j(M-1)\psi} \\ AF_x e^{j\psi} &= e^{j\psi} + e^{j2\psi} + \ldots + e^{jM\psi} \end{aligned}$

By subtraction of the above equations we derive:

$$AF_x(e^{j\psi}-1) = e^{jM\psi}-1 \Leftrightarrow AF_x = \frac{e^{jM\psi}-1}{e^{j\psi}-1} \tag{1.90}$$

$$AF_x = \frac{e^{jM\psi}-1}{e^{j\psi}-1} = \frac{e^{j\frac{M}{2}\psi}}{e^{j\frac{\psi}{2}}}\frac{(e^{j\frac{M}{2}\psi}-e^{-j\frac{M}{2}\psi})}{(e^{j\frac{1}{2}\psi}-e^{-j\frac{1}{2}\psi})} = e^{j\frac{M-1}{2}\psi}\frac{\sin(\frac{M}{2}\psi)}{\sin(\frac{\psi}{2})}$$

For small values of ψ the above expression is approximated to:

$$AF_x = \frac{\sin(\frac{M}{2}\psi)}{\frac{\psi}{2}} \tag{1.91}$$

In a similar way it is proved that: $AF_y = \frac{\sin(\frac{L}{2}\psi)}{\frac{\psi}{2}}$ where in this case ψ= kdsinθsinφ β_l

Radiation pattern will appear nulls at the direction where:

$$AF_x = 0$$
$$\sin(\frac{M}{2}\psi) = 0$$
$$\mathrm{M}(kd\sin\theta_0\cos\phi_0 - \beta_x) = \pm 2\kappa\pi$$
$$\beta_m = kd\sin\theta_0\cos\phi_0 \pm \frac{2}{\mathrm{M}}\kappa\pi$$

κ is a physical number. In a similar manner it is proved that:

$$\beta_l = kd\sin\theta_0\sin\phi_0 \pm \frac{2}{L}\kappa\pi \qquad 1.92$$

So the conditions for null occurrence are:

$$\beta_m = kd\sin\theta_0\cos\phi_0 \pm \frac{2}{\mathrm{M}}\kappa\pi \qquad 1.93a$$

$$\beta_l = kd\sin\theta_0\sin\phi_0 \pm \frac{2}{L}\kappa\pi \qquad 1.93b$$

Maximum radiation will appear where:

$$\sin(\frac{1}{2}\psi) = 0$$

$$kd\sin\theta_0\cos\phi_0 - \beta_m = \pm 2\kappa\pi$$
$$\beta_m = kd\sin\theta_0\cos\phi_0 \pm 2\kappa\pi$$

In a similar way, it is proved that:

$$\beta_l = kd\sin\theta_0\sin\phi_0 \pm 2\kappa\pi \qquad 1.94$$

So the conditions for maximum occurrence are:

$$\beta_m = kd\sin\theta_0\cos\phi_0 \pm 2\kappa\pi \qquad 1.95a$$

$$\beta_l = kd\sin\theta_0\sin\phi_0 \pm 2\kappa\pi \qquad 1.95b$$

1.4 SCOPE OF THIS WORK

Summing up the preceding study in chapter 1, microstrip patch antennas were presented and described in terms of advantages/drawbacks and principles of operation. Microstrip antenna technology was chosen for the proposed antenna system because it provides planar geometry and ability to mount on surfaces. In this way, the proposed antenna system can be easily incorporated with a Relay Station to provide a configuration with reduced size and ease the installation procedure. A research regarding microstrip patch antennas recent advances was denoted and commented in order to identify patch shapes and substrate configurations for obtaining the IEEE802.16j air interface specifications in terms of gain and bandwidth.

Moreover chapter 1 investigated several array concepts such as directivity, radiation intensity, gain and EIRP. Phased array configurations have been investigated with a special reference on power dividers and phase shifting mechanisms. Studies regarding switched beam arrays were presented and a mathematical analysis of the Array Factor term has been carried out, obtaining expressions of the phase step between radiation elements for maximum or minimum occurrence at specific angle.

The analysis of chapter 1 has been performed in order to define possible shapes and configurations of the access and backhaul antenna in order to meet the gain and bandwidth specifications of the IEEE802.16j protocol.

In chapter 2, Relay Stations are presented as the devices that carry the proposed antennas system. Some scenarios of Relay Station application are analyzed and depicted where necessary. A simulation of Relay Station RF chain of transmission and reception is set up and generated. Results are depicted and commented.

In chapter 3, a review regarding beam forming systems is presented. Beam forming module comprises a proper circuit for power distribution and an algorithm for defining the required radiation pattern shape. Several such algorithms are denoted and commented. The analysis and literature review of chapter 3 will be considered as the basis for the design of the new beam forming feeding circuit.

In chapter 4, the proposed antenna system is fully described and analyzed. The single antenna for access link realization is designed and constructed. Its features are depicted and commented. Moreover the backhaul link array is designed and developed. Its characteristics are also outlined. In addition the new beam forming module in terms of circuit design and algorithm implementation is presented. Several scenarios of radiation pattern shapes are depicted and commented. Simulation and experimental curves show good agreement and are explained.

In chapter 5, the coupling phenomenon between antenna elements is discussed. Coupling is defined and expressed using mathematical formulas. Some studies regarding coupling evaluation are presented. Furthermore some antenna structures for reducing coupling are outlined. The chapter continues with the presentation and evaluation of two new antenna configurations for coupling reduction. Coupling measurements are denoted and commented proving the validity and efficiency of the proposed antenna setup.

Finally chapter 6 includes a synopsis of the work presented and identifies a few points for further study and research.

1.5 REFERENCES

[1] P. S. Nakar, "Design of a compact microstrip patch antenna for use in wireless/cellular devices", MSC thesis, Department of Electrical And Computer Engineering, Florida state university, 2004.

[2] C. A. Balanis, "Antenna Theory: Analysis and Design", John Wiley & Sons, Inc, 1997.

[3] G. Kumar, and K. P. Ray, "Broadband Microstrip Antennas", Artech House, Inc, 2003.

[4] R. Garg, P. Bhartia, I. Bahl, A. Ittipiboon, "Microstrip Antenna Design Handbook", Artech House, Inc, 2001.

[5] H. J. Visser, "Array and Phased Array Antenna Basics", John Wiley & Sons, Ltd, 2005.

[6] E. O. Hammerstad, "Equations for Microstrip Circuit Design," Proc. Fifth European Microwave Conf., pp. 268-272, September 1975.

[7] J. R. James, P.S. Hall, "Handbook of Microstrip Antennas, vol. 1, Peter Peregrinus, London, UK, 1989.

[8] W. F. Richards, "Antenna Handbook: Theory Applications and Design", (Y.T. Lo and S.W. Lee, eds.), Van Nostrand Reinhold Co., New York, 1988.

[9] D. Y. Azmir, R. Syamsul, I. Alyani, "A New Approach for Bandwidth Enhancement Technique in Microstrip Antenna for Wireless Applications", RF and Microwave Conference, pp. 205-209, September 2006.

[10] Y. M. Fairus, M. Pohan, I. Peranggi, E. Mazlina, M. N. Asniza, "Stacked Square Fractal Antenna with Improved Bandwidth for Wireless Local Area Network Access Point" RF and Microwave Conference, pp.228-232, September2006.

[11] J. Zurcher, "Broadband Patch Antennas", Artech Print on Demand, 1995.

[12] H. M. Elkamchouchi, G. Abouelseoud, "A compact broadband Sierpinski gasket patch microstrip antenna", Proceedings of the Twenty First National Radio Science Conference, pp. 1-8, 16 18 March 2004.

[13] W. Saksiri, M. Krairiksh, "A couple microstrip antenna employing serrated coupling", Microwave and Wireless Components Letters, IEEE , vol.15, no.2, pp. 77-79, February 2005.

[14] P. Kumar, G. Singh, S. Bhooshan, T. Chakravarty, "Gap Coupled Microstrip Antennas", International Conference on Computational Intelligence and Multimedia Applications, vol.4, no., pp.434-437, December 2007.

[15] A. K. Gautam, B. R. Vishvakarma, "Frequency agile active microstrip antenna", Microwave and Optical Technology Letters, vol. 49, pp. 431-434, 2007.

[16] J. A. Ansari, Satya Kesh Dubey, Prabhakar Singh, R. U. Khan, Babau R. Vishvakarma, "Analysis of compact H shaped microstrip antenna", Microwave and Optical Technology Letters, vol. 50, pp. 1779-1784, 2008.

[17] K. F. Lee, K. M. Luk, F. Tong, S. M. Shum, T. Huynh, and R. O. Lee, "Experimental and simulation studies of the coaxially fed U slot rectangular patch antenna", IEEE Proc, vol. 144, pp. 354-358, October 1997.

[18] C. L. Mak, K. M. Luk, K. F. Lee, and Y. L. Chow, "Experimental study of a microstrip patch antenna with an L shaped probe", IEEE Transactions On Antennas And Propagation, vol. 48, no. 5, May 2000.

[19] H. J. Lee, J. Y. Lee K. B. Lee, “Design of Wideband Microstrip Patch Antenna”, 2nd International Conference on Computer Science and its Applications, pp.1-3, 10-12 December 2009.

[20] C. R. Rowell and R.D. Murch, “A compact PIFA suitable for dual frequency 900/1800 MHz operation,” IEEE Transactions on Antennas and Propagation, vol. 46, pp. 596-598, 1998.

[21] F. Wang, Z. Du, Q. Wang, and K. Gong, “Enhanced bandwidth PIFA with T shaped ground plane”, Electronics letters, vol. 40, no. 23, pp. 1504-1505, 2004.

[22] W. X. Li, X. Liu, S. Li, “Design of a Broadband and Multiband Planar Inverted F Antenna”, Computing International Conference on Communications and Mobile, vol. 2, pp.90-93, April 2010.

[23] M. A. Matin, M. P. Saha, H. M. Hasan, “Design of broadband patch antenna for WiMAX and WLAN”, International Conference on Microwave and Millimeter Wave Technology, pp.1-3, 8-11 May 2010.

[24] J. Yuan, C. Gu, “Design of compact broadband circularly polarized bowtie patch antenna”, International Conference on Microwave and Millimeter Wave Technology, vol.3, pp.1070-1072, 21-24 April 2008.

[25] H. Wong, K. Mak, K. Luk, “Wideband Shorted Bowtie Patch Antenna With Electric Dipole”, IEEE Transactions on Antennas and Propagation, vol.56, no.7, pp.2098-2101, July 2008.

[26] S. Qu, J. Li, Q. Xue, C. H. Chan, S. Li, “Wideband and Unidirectional Cavity Backed Folded Triangular Bowtie Antenna”, IEEE Transactions on Antennas and Propagation, vol.57, no.4, pp.1259-1263, Apr. 2009.

[27] K. M. Pramod, R. Jyoti, S. S. Kumar, V. S. K. Reddy, “Simplified and efficient technique for designing of broadband patch antenna”, Applied Electromagnetics Conference, pp.1-4, December 2009.

[28] T. N. Chang, “A wideband coplanar waveguide fed circularly polarised antenna”, Microwaves, Antennas and Propagation, IET vol. 2, no. 4, June 2008.

[29] C. Y. Huang, J. Y. Wu and K. L. Wong, “Cross slot coupled microstrip antenna and dielectric resonator antenna for circular polarization”, IEEE Transactions on Antennas and Propagation, vol. 47, no. 4, April 1999.

[30] J. Row, “The design of a squarer ring slot antenna for circular polarization”, IEEE Transactions on Antennas and Propagation, vol. 53, no. 6, June 2005.

[31] N. Herscovici, Z. Sipus, and D. Bonefacic, “Circularly polarized single fed wide band microstrip patch,” IEEE Transactions on Antennas and Propagation, vol. 51, no. 6, pp. 1277-1280, 2003.

[32] W. Chen, C. Wu, K. Wong, “Single feed square ring microstrip antenna with truncated corners for compact circular polarization operation”, Electronics Letters, vol.34, no.11, pp.1045-1047, May 1998.

[33] C. Z. Zhou, G. Fu, Q. Chen, “Wideband circularly polarized square slot antenna with parasitic patch”, 8th International Symposium on Antennas, Propagation and EM Theory, pp.158-160, 2-5 November 2008.

[34] A. K. Aswad, L. F. Abdulrazak, T. A. Rahman, “Design and development of high gain wideband circularly polarized patch antenna”, IEEE International RF and Microwave Conference, pp.109-111, 2-4 December 2008.

[35] W. Hsu and K. Wong, “Broad Band Probe Fed Patch Antenna with a U Shaped Ground Plane for Cross Polarization Reduction”, IEEE Trans. Antennas Propagation, vol. 50, no. 3, March 2002.

[36] S. Vikan, J. A. Aas., “Broad Band Folded Patch Antenna with Shorts and Slots”, The Second European Conference on Antennas and Propagation, pp.1-5, 11-16 November 2007.

[37] A. Mehta, D. Syahkal, H. Nakano, “Beam adaptive single arm rectangular spiral antenna with switches”, Microwaves, Antennas and Propagation, IEE Proceedings, vol. 153, no. 1, pp. 13-18, February 2006.

[38] C. Won, M. Lee, G. P. Li and F. Flaviis, “Reconfigurable Beam Scan Single Arm Spiral Antenna With Integrated MEMS switches”, IEEE Transactions on Antenna and Propagation, vol. 54, no. 2, pp. 455-463, February 2006.

[39] G. H. Huff, J. T Bernhard, “Integration of packaged RF MEMS switches with radiation pattern reconfigurable square spiral microstrip antennas”, IEEE Transactions on Antenna and Propagation, vol. 54, no. 2, pp. 464-469, February 2006.

[40] A. Mehta, D. M. Syahkal, P. J. Massey, H. Nakano, “A switched beam star patch antenna”, IEEE International Symposium on Antennas and Propagation Society, pp.1-4, 5-11 July 2008.

[41] R. J. Mailloux, “Phased Array Antenna Handbook”, Artech House Publishers, 2nd edition, 2005.

[42] H. Visser, “Array and Phased Array Antenna Basics”, Wiley, September, 2005.

[43] M. Shi, J. Lu, D. J. Ireland, “Smart patch antenna for indoor mobile wireless computing”, Microwave Conference Proceedings, Asia Pacific Conference Proceedings , vol. 3, pp. 4, 4-7 December 2005.

[44] Y. Yusuf, X. Gong, “A Low Cost Patch Antenna Phased Array With Analog Beam Steering Using Mutual Coupling and Reactive Loading”, Antennas and Wireless Propagation Letters, IEEE , vol. 7, pp. 81-84, 2008.

[45] I. Fernandez, J. Antonio Romo, B. Anton, “Matching of microstrip patch array antennas with reflectors”, Proceedings of the Fourth European Conference on Antennas and Propagation, pp.1-4, 12-16 April 2010.

[46] C. WeiDong, “High gain linear polarization microstrip antenna with four element electromagnetically coupled patch”, 2nd Asian Pacific Conference on Synthetic Aperture Radar, pp.250-253, 26-30 October 2009.

[47] J. D. Kraus, J. Ronald, “Antenna for all application”, Third Edition, New York, 2002.

[48] B. Bhuvaneswari, K. Malathi, “Double layer patch antenna array using novel EBG structure for reducing mutual coupling losses”, IEEE Region 10 Conference , pp. 1225-1229, 21-24 November 2010.

[49] M. N. M. Tan., T. A. Rahman, S. K. A. Rahim, M. T. Ali, M. F. Jamlos, “Antenna array enhancement using mushroom like electromagnetic band gap (EBG)”, Proceedings of the Fourth European Conference on Antennas and Propagation, pp.1-5, 12-16 April 2010.

[50] E. Rajo Iglesias, O. Quevedo Teruel, L. Inclan Sanchez, “Mutual Coupling Reduction in Patch Antenna Arrays by Using a Planar EBG Structure and a Multilayer Dielectric Substrate”, IEEE Transactions on Antennas and Propagation, vol. 56, no. 6, pp. 1648-1655, June 2008.

[51] M. Coulombe, S. Farzaneh Koodiani, C. Caloz, “Compact Elongated Mushroom (EM) EBG Structure for Enhancement of Patch Antenna Array Performances”, IEEE Transactions on Antennas and Propagation, vol. 58, no. 4, pp. 1076-1086, April 2010.

[52] J. Kiriazi, H. Ghali, H. Ragaie, H. Haddara, "Reconfigurable dual band dipole antenna on silicon using series MEMS switches", Antennas and Propagation Society International Symposium, vol. 1, pp. 403-406, 2003.

[53] R. N. Simons, "Novel On Wafer Radiation Pattern Measurement Technique for MEMS Actuator Based Reconfigurable Patch Antennas", 24th Annual Antenna Measurement Techniques Association Meeting and Symposium, Glenn Research Center, Cleveland, Ohio, 2002.

[54] M. T. Ali, M.R. Kamarudin, M. Tan, T.A. Rahman, "Reconfigurable beam shaping antenna with Wilkinson Power Divider at 5.8GHz", IEEE International RF and Microwave Conference, pp. 436-440, December 2008.

[55] J. R. James, P.S. Hall, "Handbook of Microstrip Antennas", vol. 2, Peter Peregrinus Ltd., London, 1989.

[56] A. C. Balanis, "Antenna Theory: Analysis and design", John Wiley, 2005.

[57] N. C. Athanasopoulos, "Development of a conformal cylindrical microwave antenna with flexible and adaptive radiation pattern", PhD. thesis, National Technical University of Athens, Greece, 2006.

CHAPTER 2

RELAY STATIONS

2.1 INTRODUCTION

In this chapter Relay Stations are defined and described. Their advantages are denoted revealing that these devices can play a significant role improving the performance of a wireless network. Application scenarios are mentioned with corresponded schematic for better understanding. Furthermore types of Relay Stations depending on the usage scenarios are described. Moreover a presentation and description of the Relay Station Front End follows in terms of mixers, local oscillators, filters and power amplifiers utilized. Two types of simulations are performed and depicted: The transmission RF chain is presented and analyzed in terms of spectrum and time domain transmitted signal. The reception RF chain is also mentioned in terms of Signal to Ratio (SNR) and Receive Signal Strength (RSS). Major information outlined in this chapter has been taken from FP7 REWIND project deliverables.

2.2 RELAY STATION OVERVIEW

Relay Stations (RS) are network devices placed in between Base Station (BS) and Mobile Stations (MS) as intermediate links to ensure and enhance the quality of transmission. A Relay Station produces two links:

- The backhaul link for connecting RS with BS and

- The access link for connecting RS with MS

Relays can be used under a 4G wireless network such mobile WiMAX or LTE. Specifications about the air interface of a wireless network that incorporates Relays have been defined in IEEE 802.16j protocol [1], [2].

The introduction of RSs within a wireless network can be very profitable for the proper operation of the network as they present advantages which are summarized below:

- Increase coverage
- Increase throughput
- Operation in case of RS and MS mobility
- Low cost compared to BS installation

Fig. 2.1 gives a general view of Relay's applications which would be further investigated in this chapter.

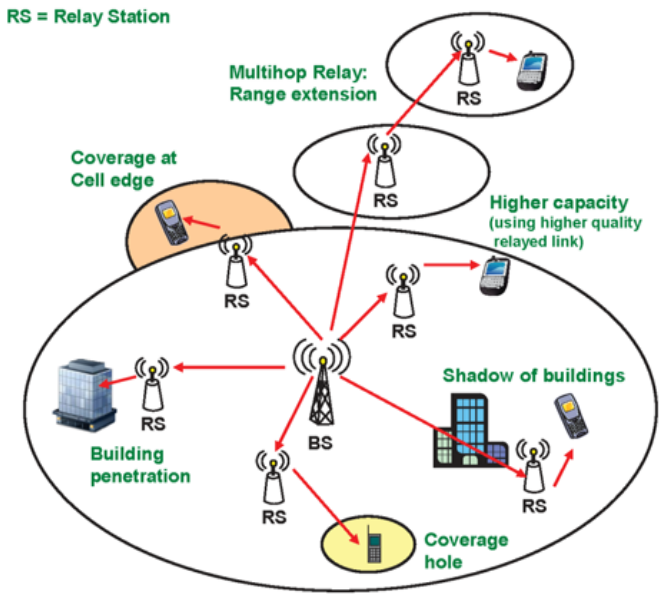

Figure 2.1: Overview of Relay Station use.

2.3 RELAY STATION APPLICATIONS

In this section, the basic usage scenarios of Relays are outlined. Each scenario describes a specific weakness of a wireless network and shows that the introduction of an RS can overcome this weakness.

2.3.1 Gap Filler

In an urban area there are some places that provide low link quality. That is because buildings, trees and obstacles are located in between BS and that places, degrading the transmission link. The establishment of RSs on the top of buildings or houses can enhance transmission to coverage holes and provide connectivity to end users placed anywhere as described in Fig. 2.2.

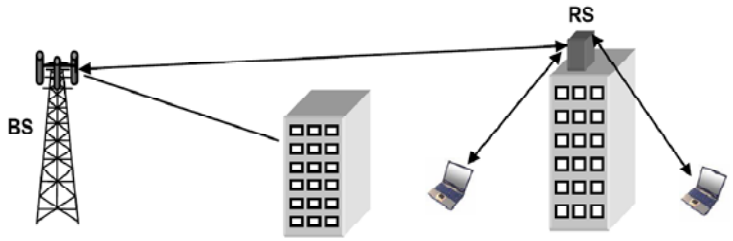

Figure 2.2: Use of RS as gap filler.

2.3.2 Coverage increase

Mobile users can be located in the area outside the range of a BS. Instead of installing a new BS, which is rather expensive, it would be more efficient to set up a RS in the limit of BS's range, to establish an effective link.

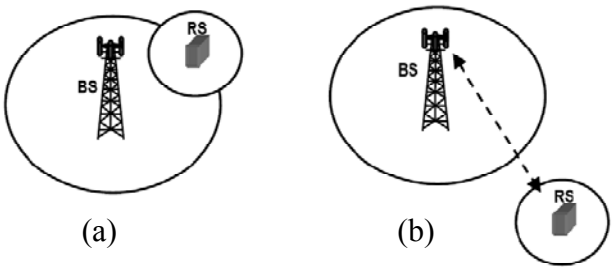

Figure 2.3: Cases of coverage increase.

An RS can also be put outside the coverage area of a BS extending the coverage capability of the network, as can be seen in Fig. 2.3b.

Another way to extend connectivity could be the increase in the power of the transmitter. Such a solution would require more expensive amplifiers and also demand an increase in the power of the end user's device. In that case the coverage of the network would be little extended. The use of RS would be much more efficient because it combines connectivity in remote areas at low cost.

2.3.3 Capacity and Throughput increase

Let us suppose that a Base Station transmits to a Mobile Station (User B) according to Fig. 2.4. The link quality is degraded due signal attenuation and interference. This degradation decreases the level of modulation and thus throughput. If a RS is placed between the BS and a MS (User A), then the level of modulation is maintained high, more data packets are successfully delivered to destination and so throughput is high.

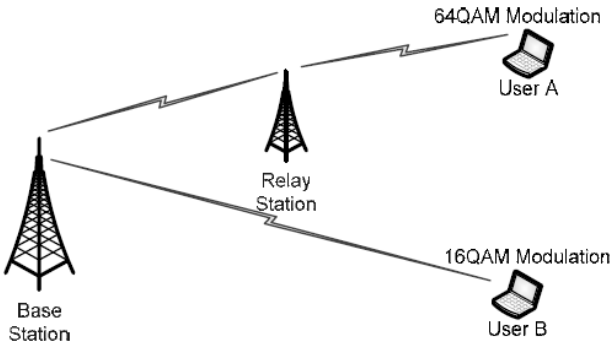

Figure 2.4: RS for throughput increase.

Capacity of a wireless channel is defined as [3]:

$$C = B\log_2(1+\frac{S}{N+I}) \qquad 2.1$$

where C is the capacity in bits/sec, B is the channel bandwidth, S is the signal power, N is the noise and I the interference.

The introduction of a RS creates a link of high SINR (Signal to Noise plus Interference ratio) which leads to increased channel capacity.

2.3.4 In building Relay usage

It has been found that an important percentage of the whole traffic generated by a wireless network takes place in the area inside buildings and houses. First and second walls or other obstacles cause serious signal attenuation. A BS should increase its level of power consumption in order to provide service to in building subscribers but only a few of them would be adequately served [4].

Fig. 2.5 shows that the difference in path loss between in and outdoor use is approximately 15dB. The introduction and placement of RSs in proper points could effectively solve the problem of indoor signal penetration.

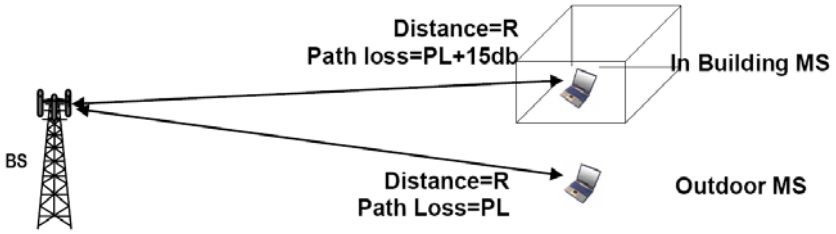

Figure 2.5: Path Loss between in building and outdoor MS.

Fig. 2.6 shows a possible solution for establishing high quality transmission links. A RS could be mounted on the top inside wall of a building to connect MSs to the external BS.

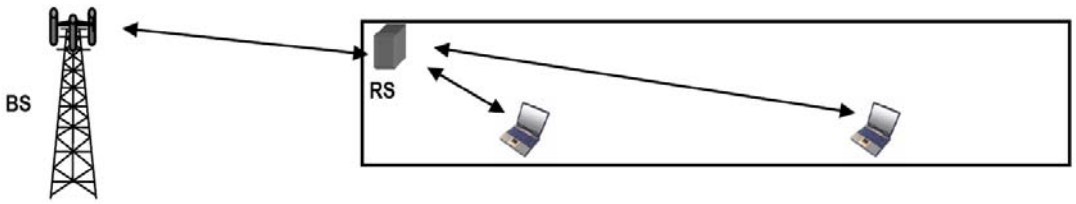

Figure 2.6: Possible configuration for sufficient indoor coverage.

2.4 RELAYS IN CASE OF MOBILITY

Relay has the ability to support end user mobility. In case of a car travelling, the connectivity can be ensured by placing many RSs along the streets and link one of them to the closest BS. Fig.2.7 depicts such a possible scenario [5].

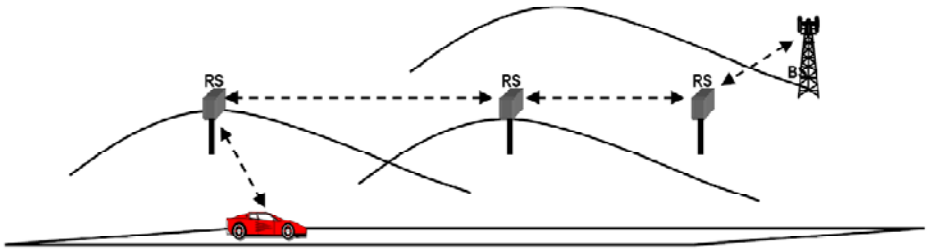

Figure 2.7: RS usage in case of end user mobility.

Another possible scenario is the placement of RSs in tunnels to maintain connectivity and link quality. This application is depicted below.

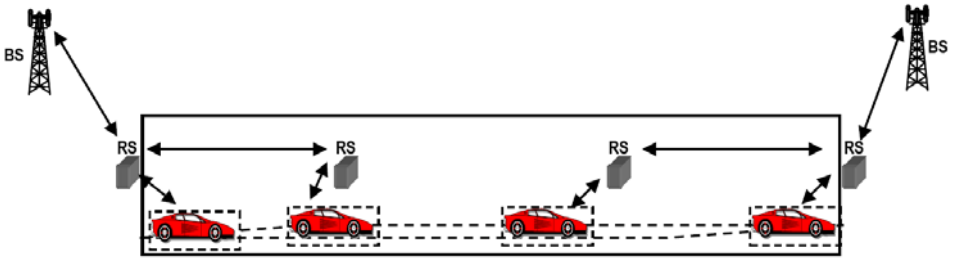

Figure 2.8: RS usage in case of tunnels.

Depending on the size of the tunnel a sufficient number of RSs can be mounted at the start, end and along the passage to ensure service to end user.

In case of high speed train, buses or boats, mobile Relays can be incorporated in the network to ensure connectivity under these circumstances. In such usage, RSs must be proper equipped to perform handover process, in order to find the closest BS, as can be seen in Fig. 2.9.

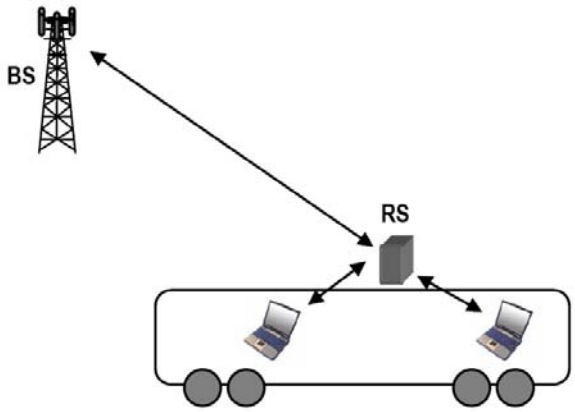

Figure 2.9: RS mobility scenario.

2.5 TYPES OF RS

In the text that follows Relays are categorized to some basic types whether they are used for channel capacity improvement or coverage extension. They are also divided whether the antennas of the Relay transmit/receive simultaneously or not.

2.5.1 Transparent Relay

In this case, MS is not aware of RS existence and receives all control data directly from the BS [6], [7]. Fig. 2.10 depicts a transparent Relay.

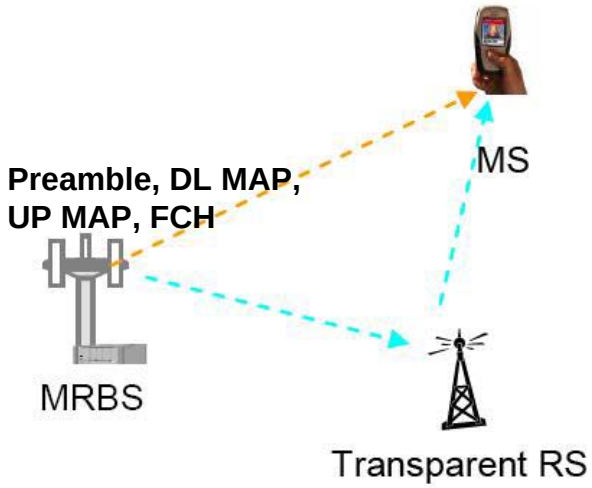

Figure 2.10: Transparent Relay topology.

In Fig. 2.10, the MRBS (Multi Relay Base Station) can be connected to MSs and RSs, establishing two links. MS receives the control data information from MRBS. That information include preamble, FCH, UP and DL MAP.

- Preamble – It is the 1st symbol. It allows MS to synchronize to the BS
- FCH – It is a burst that enables BS to advertize the configuration of the system
- UP and DL MAP – It is a burst that defines for the MS the location and size of the UP or DL subframe

A transparent Relay configuration improves channel quality, increases the link capacity but it does not extend the coverage of the network.

2.5.2 Non Transparent Relay

In this case, MS does not know about any relaying operation and considers the Relay Station as it serving BS. Fig.2.11 depicts the operation of a non transparent topology.

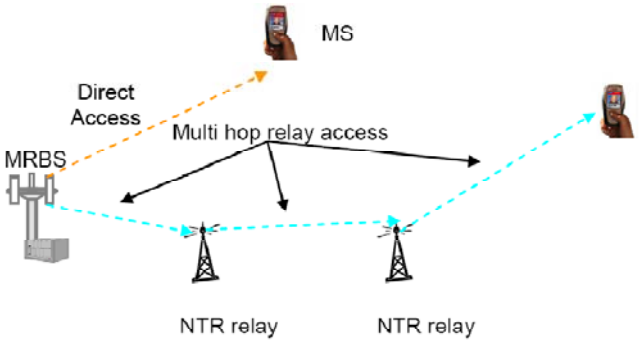

Figure 2.11: Non transparent Relay configuration.

NTR Relay delivers all control data information to the MSs. This case is ideal for coverage extension and improvement of channel quality.

2.5.3 Time domain Relay operation

The RS device can operate in two modes [6]:

- Time Division Transmit Receive mode (TTR)

  Relay is equipped with two kinds of antennas: One for communicating with the end user (access link) and the other for establishing communication with the Base Station (backhaul link). Part of the time, the access link only operates and the other part backhaul link is active.

In Fig. 2.12, MRBS creates communication with an RS and a CPE (Customer Premises Equipment) emitting in a frequency f_1 [8], [9]. At a second time, Relay communicates with CPE in frequency f_2.

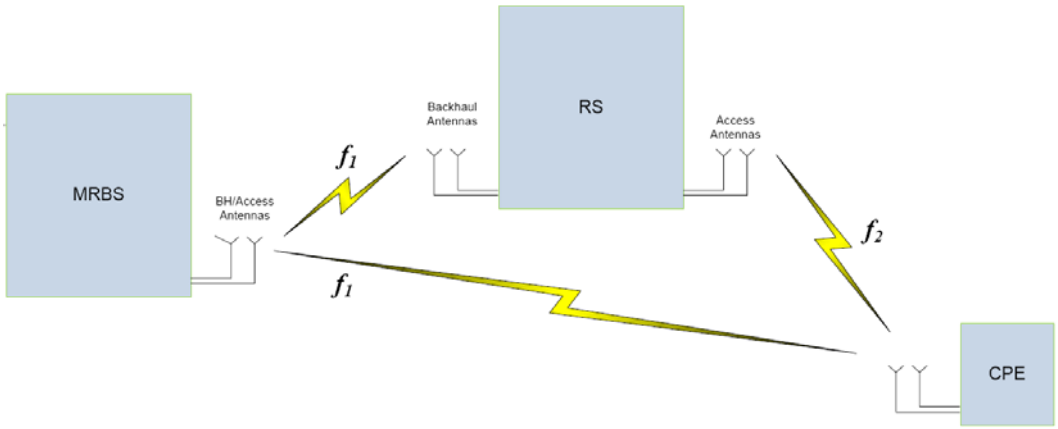

Figure 2.12: Relay based network operating in TTR mode.

"MRBS" stands for: Multi Relay Base Station and refers to the ability of Base Station to establish communication with Relays and end users. Fig. 2.13 clearly shows the TTR mode performance.

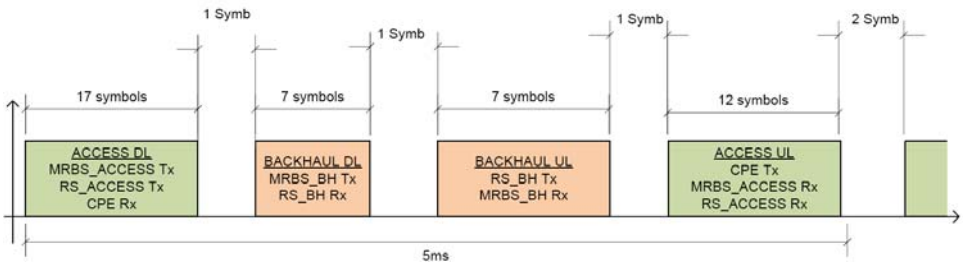

Figure 2.13: TTR deployment.

The above figure denotes the uplink and downlink communication in different time slots. The first time period, MRBS and RS transmit data at CPE, realizing the access downlink connection. The second time period, MRBS transmits information to RS at backhaul downlink connection. The third time period, RS transmits to MRBS, establishing the backhaul uplink communication. Finally in the fourth time period, CPE transmits and MRBS/RS receives data.

- Simultaneously Transmit Receive mode (STR)

  In this case two kinds of antennas are used by RS: One for the access and the other for the backhaul link as before. But now both antennas operate as the same time. Proper isolation between the antenna elements is required in this case.

In Fig. 2.14, the STR mode is active. In this case, MRBS simultaneously communicates with RS and CPE. Also RS enables access and backhaul links concurrently.

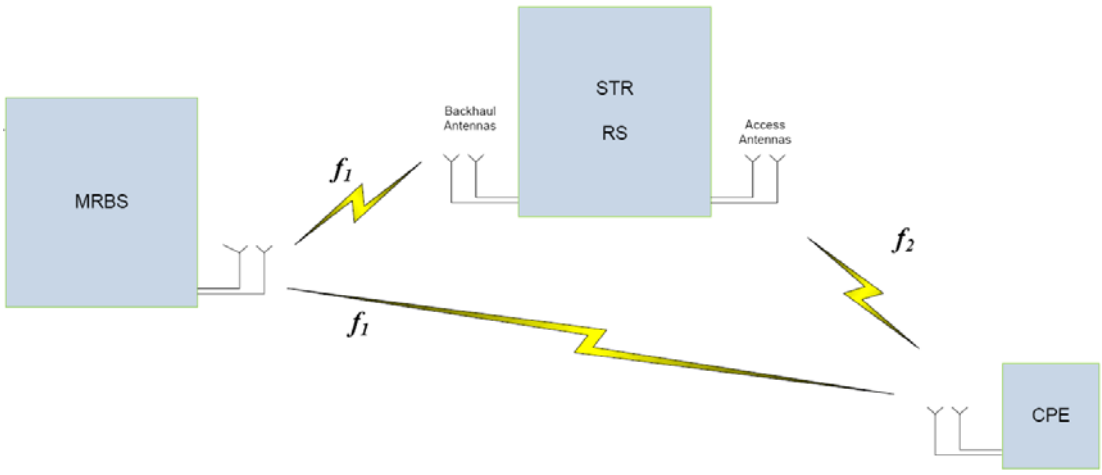

Figure 2.14: Relay based network operating in STR mode.

The exact performance of STR mode is described below:

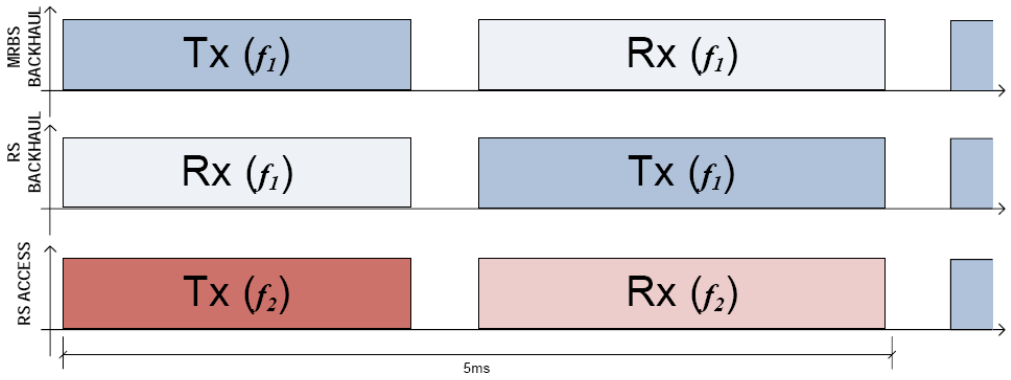

Figure 2.15: STR deployment.

Fig. 2.15 clearly shows that for the first time slot, RS transmits data to both CPE and MRBS. In the second time slot, the RS receives data from CPE and simultaneously transmits to the MRBS. In the case of STR mode the access and backhaul antennas of the RS should be well isolated in order to cause minimum interference to each other.

2.6 RELAY DESCRIPTION

2.6.1 Hardware Subsystem

Under the REWIND project (FP7, project number: 216751), a Non Transparent Relay prototype was fabricated, measured and is depicted in Fig. 2.16. In this chapter the Relay characteristics in terms of RF front End are outlined. The final Relay prototype, excluding the antennas has dimensions: 33cm×24.5cm×12cm [10].

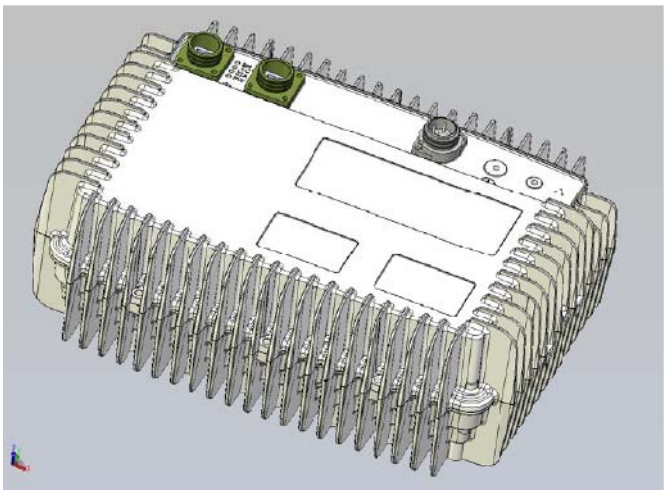

Figure 2.16: Relay prototype.

The top level architecture of the Relay prototype is shown in Fig. 2.17.

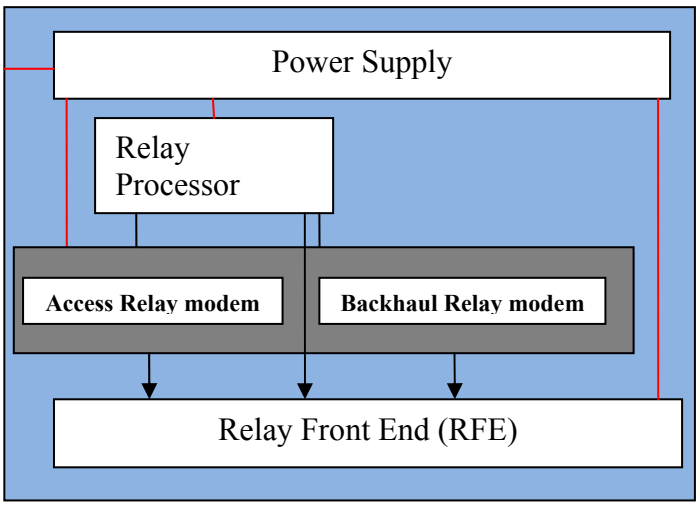

Figure 2.17: Relay top level architecture.

The parts of Relay architecture are explained below:

- The Relay processor is a unit that performs advanced routing processing used for management.
- The Access and Backhaul Relay modems perform operations defined by the IEEE802.16j MAC and PHY specifications.
- The Relay Front End unit executes switching, filtering and amplification process.
- The power supply module transforms AC power to DC and allocates power to the other modules.

The Relay architecture that was designed and tested under REWIND project has the following hardware structure. It comprises two modules: The Relay Front End and the RF processor. These two units are described in Fig. 2.18 [11], [12]:

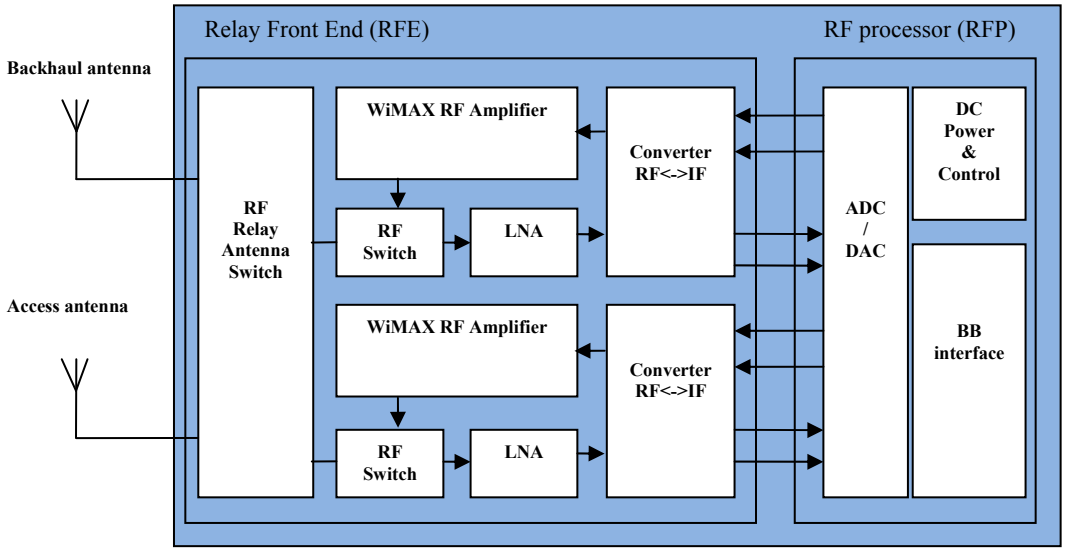

Figure 2.18: Relay hardware.

Fig. 2.18 shows that Relay architecture includes two sub units:

- The Relay Front End which executes amplifying, filtering and switching operations.
- The RF processor which performs analog to digital conversion and provides the interface to BB process.

2.6.2 Relay Front End

The Technological Educational Institute of Athens in collaboration with Ubiqam Company, as part of the REWIND consortium, designed and simulated the Relay Front End using the commercial software ADS2009. The design includes two RF chains. One that is connected to the access antenna and is used for transmission and the other RF chain is connected to the backhaul antenna and receives data. Fig. 2.19 describes the proposed configuration [13].

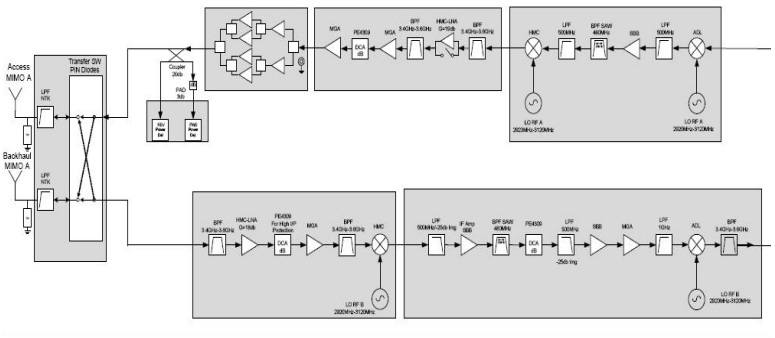

Figure 2.19: RF transmission and reception chain.

- **Transmission chain**

The transmission chain of the Relay Front End is depicted in Fig. 2.20. Chain is consisted of separate blocks each of them performing a specific operation.

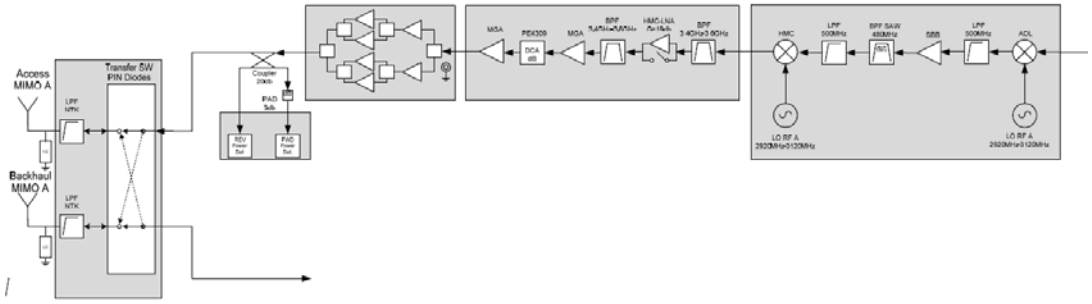

Figure 2.20: Transmission RF chain.

The first block of the transmission RF chain is depicted in Fig. 2.21.

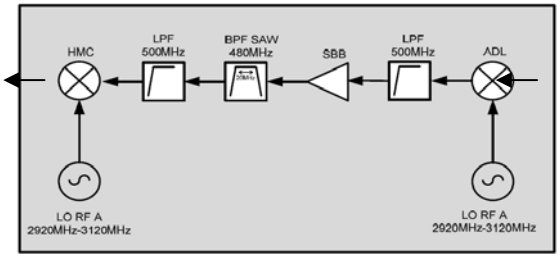

Figure 2.21: 1st block of transmission RF chain.

The 3.5GHz modulated WiMAX signal arrives and is down converted to 480MHz. It is then passed through a Low Pass Filter (LPF) and amplified using an SBB 1000 MMIC amplifier. The signal then passes through a BPF and a LPF filter for discarding unwanted harmonics and finally it is up converted to 3.5GHz.

The second block of transmission RF chain is depicted in Fig. 2.22. The signal subsists filtering and amplifying process.

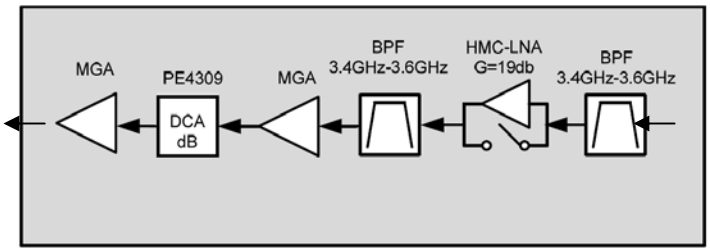

Figure 2.22: 2nd block of transmission RF chain.

The Band Pass Filter was simulated using microstrip coupled lines. Next a HMC716LP3 Low Noise Amplifier (LNA) enhances the signal. Gain (S_{21}) and reflection coefficient (S_{11}) of LNA was simulated providing results depicted in Fig. 2.23.

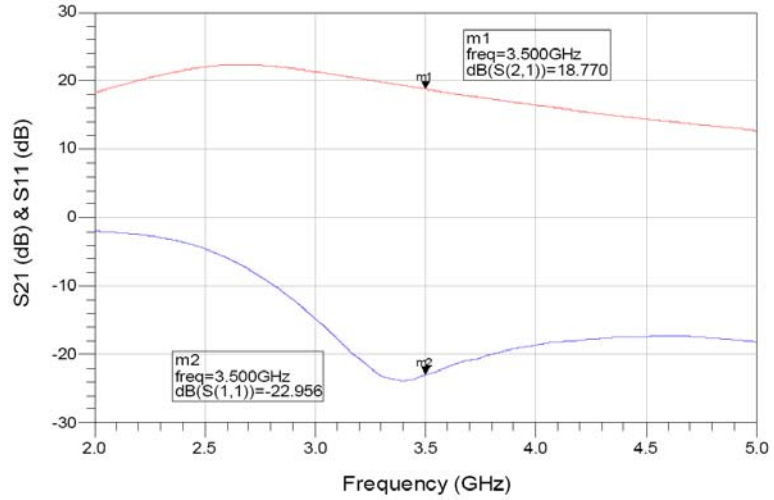

Figure 2.23: 2nd block of transmission RF chain.

Fig. 2.23 shows that S_{21} is 18.77dB and S_{11} is -22.956dB for 3.5GHz. Onwards signal passes through a second BPF and then through a high linearity amplifier MGA 30316. Gain and reflection coefficient of the amplifier are drawn in Fig. 2.24.

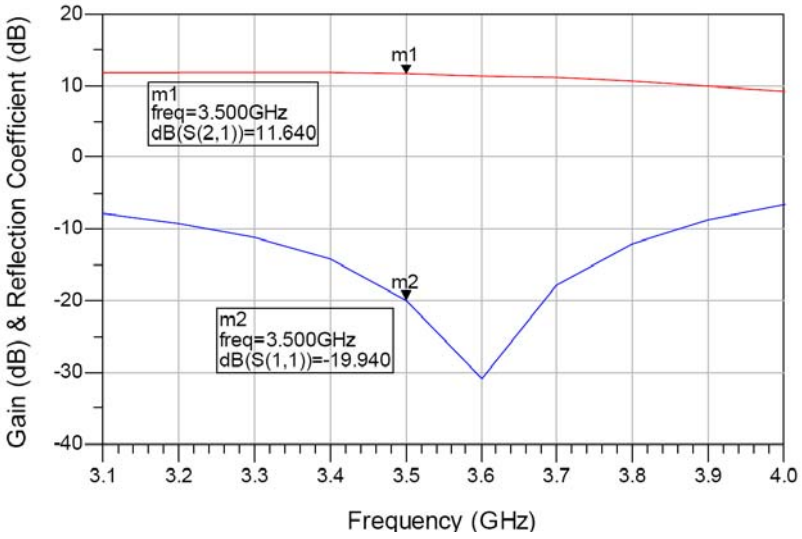

Figure 2.24: MGA amplifier properties.

S_{21} of the amplifier is estimated to be 11.64dB while S_{11} is -19.940dB. After MGA amplifier, a controllable attenuator PE4309 from Peregrine Semiconductor follows. This module covers a band from 0 to 31.5dB with a step of 0.5dB.

The final stage of RF transmitter chain involves a power amplification unit. This unit is depicted in Fig. 2.25.

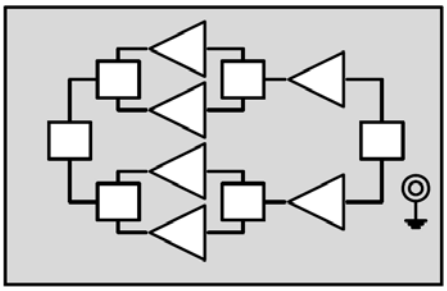

Figure 2.25: 3rd block of transmission chain.

AP562 amplifier of TriQuint Semiconductor was modeled in ADS2009. Power amplification unit comprises a power divider which splits input power in two half parts which are then amplified using the AP562 model. Then these two parts are further divided and amplified. Finally the four power signals are united using a Wilkinson power combiner. The performance of the proposed amplifier is depicted in Fig. 2.26.

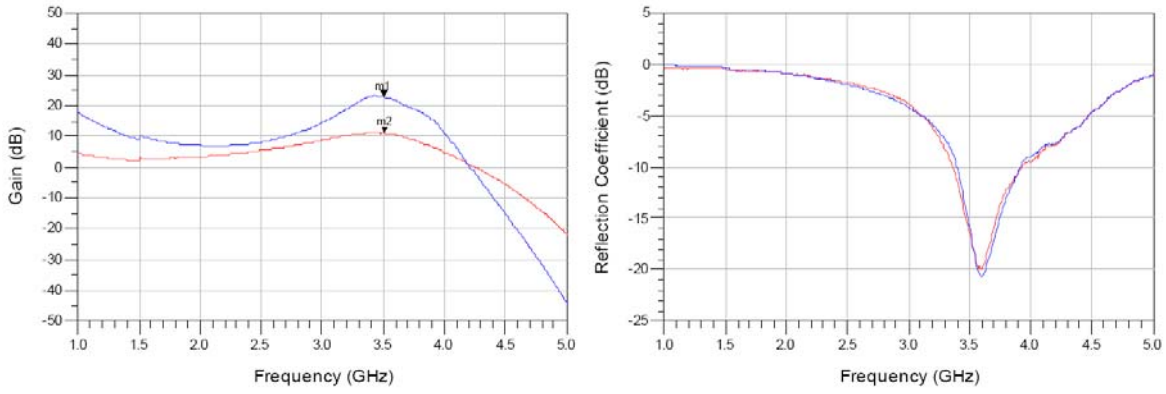

(a) (b)

Figure 2.26: Performance of power amplifier; (a) gain and (b) reflection coefficient. Blue line corresponds to the overall amplification performance of 3rd block of chain. Red line corresponds to the performance of the AP562 amplifier.

Fig. 2.26a shows that the gain that the 3rd block provides is 22dB while the gain of the AP562 is estimated 11dB. The use of a combination of AP562 model with power dividers and combiners increases gain at about 11dB.

Finally a 2×2 switch matrix [14] module is used that determines the active links. The designed matrix has the form of Fig. 2.27:

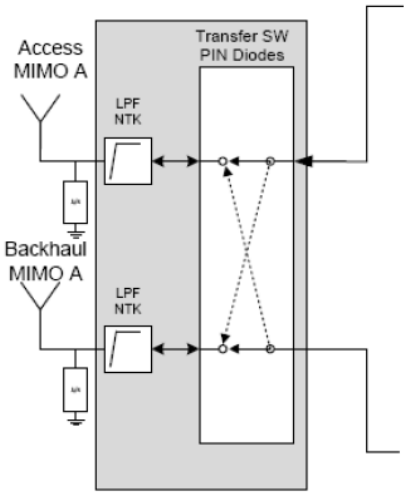

Figure 2.27: 2×2 switch matrix.

Switch matrix operates in two modes [14]. The first one refers to the solid black lines of Fig. 2.27. This state allows transmission of RS to MS and reception of RS from BS. The second mode is represented by the dot line in Fig. 2.27. In this state RS transmits to BS and RS receives data from MS. Switch matrix can operate in both TTR and STR mode. The switch matrix depicted in Fig. 2.28, uses PIN diodes and microstrip lines placed on Nelco N4350 13 substrate (ε_r=3.5, tanδ=0.0065, dielectric thickness d=0.508mm).

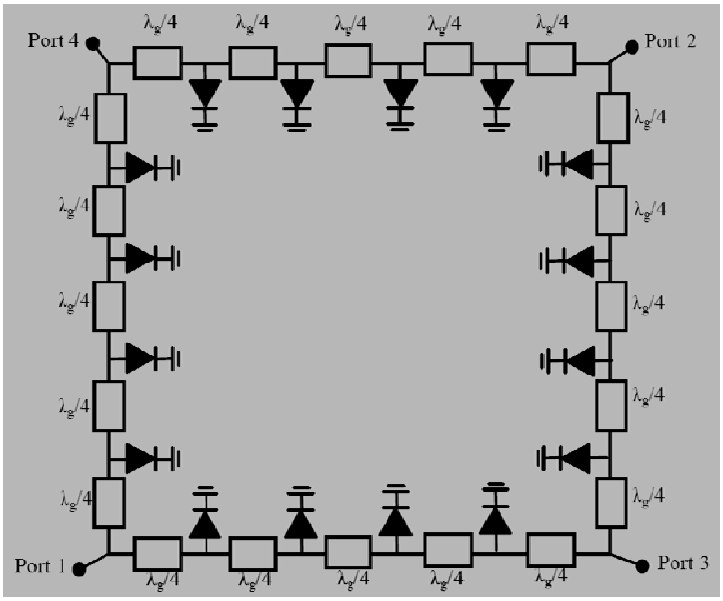

Figure 2.28: Switch matrix architecture.

The length of the microstrip lines is $\lambda_g/4$=11.45mm and width 1.13mm. If the number of PIN diodes is increased then isolation is also increased but this raises insertion loss. The number of PIN diodes should be kept balanced for maintaining isolation and insertion loss at acceptable levels.

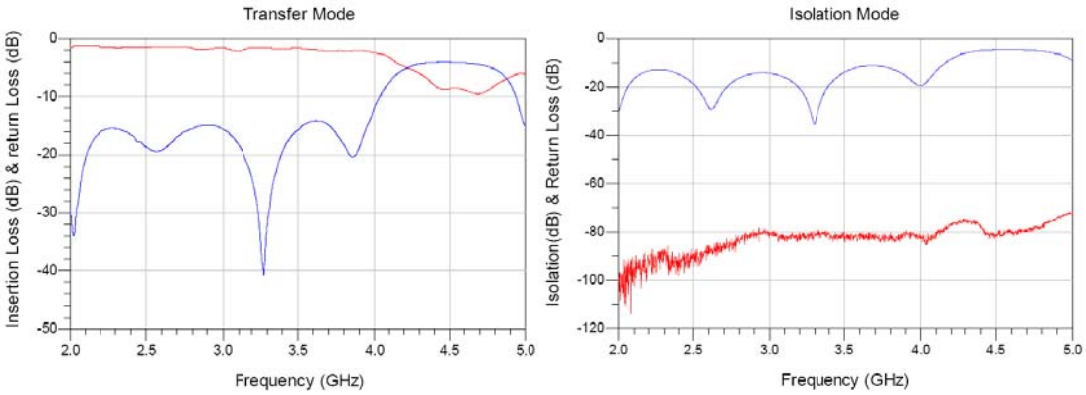

(a) (b)

Figure 2.29: Performance of 2×2 switch matrix in (a) transfer mode (b) isolation mode. The blue line corresponds to Return Loss while the red one to Insertion Loss.

Fig. 2.29a depicts the operation of the designed switch in transfer mode. Power is transferred from port 1 to port 3 while ports 2 and 4 are terminated. Return Loss varies below 14dB for the frequency range of 3.3 to 3.8GHz. Insertion Loss is approximately 2dB for the same frequency range. Regarding Fig. 2.29b, the isolation is presented between ports 1 and 4, while ports 2 and 3 are terminated. Return Loss is below 12dB for the frequency range of 3.3 to 3.5GHz while isolation is around 80dB for the same frequency range [15].

Using ADS2009 the RF chain previously presented is simulated. A WiMAX 802.16e RF signal enters the chain. This signal has the following characteristics: Carrier frequency is 3.5GHz and channel bandwidth is 10MHz. The input power is 10dBm and frame duration 5msec. The transmitted spectrum from RS to MS is depicted in Fig. 2.30 [16].

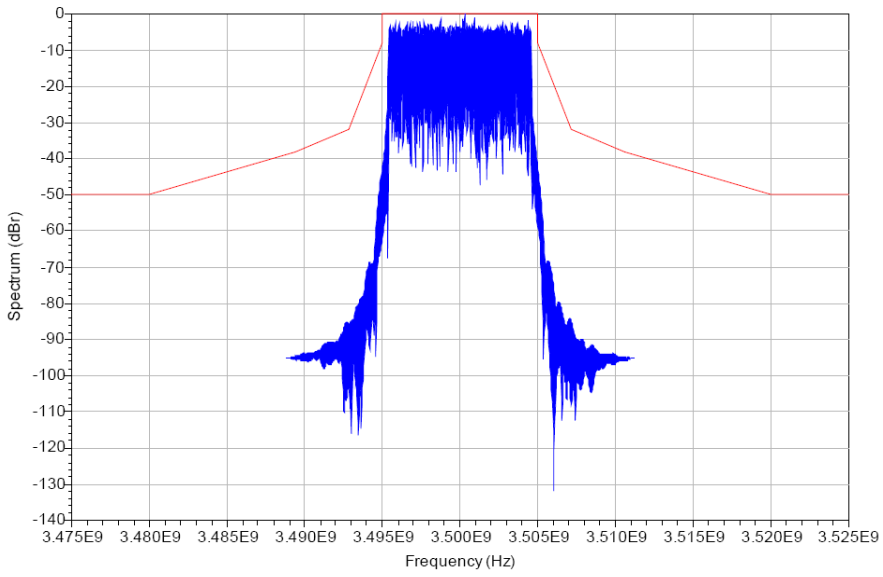

Figure 2.30: Spectrum transmitted from Relay to end user.

The transmitted spectrum falls within the defined WiMAX specifications. The emitted signal in time domain is presented in Fig. 2.31:

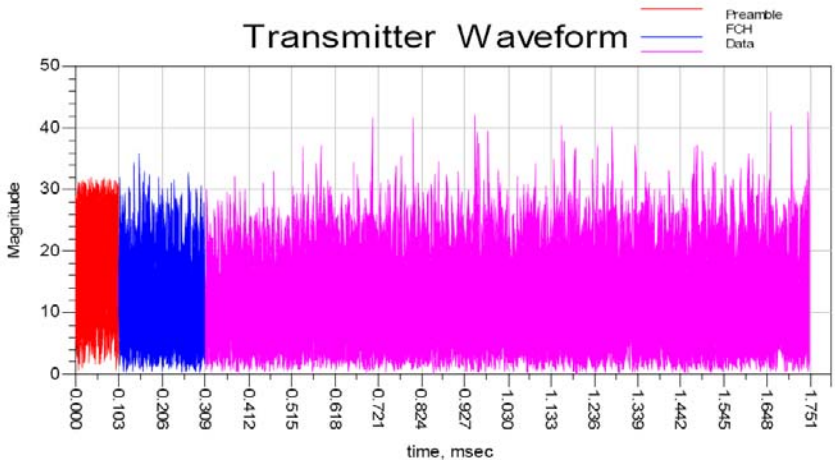

Figure 2.31: WiMAX transmitted signal.

Time domain obviously shows that signal power is approximately 32.2dBm. This clearly denotes a power amplification produced by the RF transmission chain as input power is 10dBm. The estimated power gain is 42dBm.

- **Reception chain**

The RF receiver chain is described in Fig. 2.32 [12]:

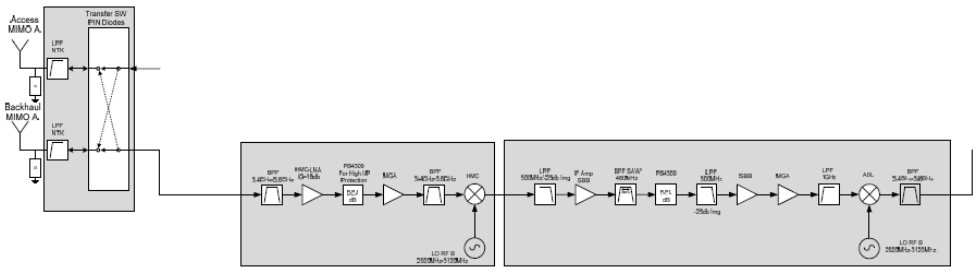

Figure 2.32: RF chain in receiver.

The first block in Fig. 2.32 is depicted below:

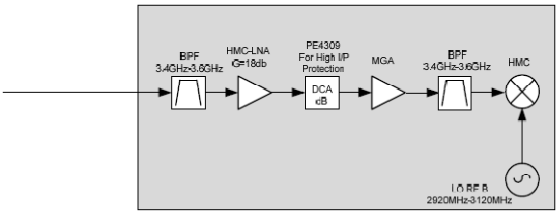

Figure 2.33: First block of RF receiver.

The first block of RF receiver includes the following components:

- A Band Pass Filter (BPF) in the frequency range of 3.4 to 3.6GHz.
- A Low Noise Amplifier providing 18dB Gain (LNA model HMC716LP3)
- A controllable attenuator that provides 0 to31.5dB magnitude with a step of 3dB (model PE4309)
- An MGA model amplifier (model MGA30316)

For the BPF filter, the mixer (HMC) and the Local Oscillator (LO), parts from ADS2009 library were used.

The second RF receiver block is depicted in Fig. 2.34.

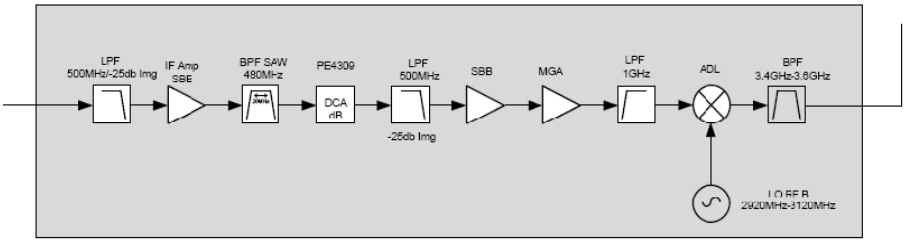

Figure 2.34: 2nd RF receiver block.

The block depicted in the previous figure includes:

- Low Pass Filter (LPF), Band Pass Filter (BPF), ADL (mixer) and LO (Local Oscillator) were chosen from ADS2009 libraries
- An IF SBB amplifier was used to enhance the intermediate frequency of 480MHz
- A SAW Band Pass Filter (BPF) was used to discard the unwanted received signals
- A controllable attenuator that provides 0 to31.5dB magnitude with a step of 3dB (model PE4309)

- SBB1000 MMIC amplifier was selected operating in 480MHz frequency
- An MGA amplifier was chosen (model MGA62563 chip)

The BS to RS link was simulated (backhaul link). The input data is outlined below:

i. Carrier frequency is 3.5GHz

ii. The Power of the received signal is 30dBm

iii. Channel bandwidth is 10MHz

iv. The frame duration was set to 5msec

Received signal strength (RSS), Signal to Noise ratio (SNR) were obtained for different modulation schemes. The results are depicted in the table that follows:

Table 2.1: Simulated parameters for different modulation.

Modulation	RSS(dBm)	SNR (dB)
QPSK	88	2.9
QPSK	84	6.3
16QAM	82	8.6
16QAM	78	12.7
64QAM	77	13.8
64QAM	74	16.9
64QAM	73	18
64QAM	71	19.9

The increase in the level of modulation causes raise to RSS and SNR.

2.7 CONCLUSIONS

Chapter 2 presented Relay Stations in terms of modes of operation and usage scenarios. These network devices provide capacity and throughput increase together with coverage

extension, improving the quality of the transmitted signal and the performance of the wireless network. Relay Station should be equipped with a highly operational and flexible antenna system, providing access and backhaul connectivity. This antenna system is developed and tested in chapter 4.

2.8 REFERENCES

[1] V. Genc, S. Murphy, Y. Yu, J. Murphy, "IEEE 802.16j Relay based Wireless Access Networks: An Overview", IEEE Wireless Communications Magazine Special Issue on Recent Advances and Evolution of WLAN and WMAN Standards, 2008.

[2] Y. Yu, S. Murphy, L. Murphy, "Planning Base Station and Relay Station Locations in IEEE 802.16j Multi hop Relay Networks", IEEE International Conference on Communications, pp. 2586–2591, IEEE Press, New York, 2008.

[3] J. D. Gibson, "The Communications Handbook (Electrical Engineering Handbook), CRC Press, 2nd edition, 2002.

[4] N. Athanasopoulos, P. Tsiakas, K. Voudouris, I. Georgas, and G. Agapiou, "Multi hop Relay in Next Generation Wireless Broadband Access Networks: An Overview" 2nd International ICST Conference on Mobile Lightweight Wireless Systems, Barcelona, Spain, 10-12 May 2010.

[5] N. Athanasopoulos, P. Tsiakas, K. Voudouris, D. Manor, A. Mor, G. Agapiou, "An IEEE802.16j Prototype Relay Station Architecture", IEEE MELECON Conference, Valetta, Malta, 26-29 April 2010.

[6] IEEE Standard for Local and metropolitan area networks, "Part 16: Air Interface for Broadband Wireless Access Systems. Amendment 1: Multiple Relay Specification", IEEE Std., June 2009.

[7] IEEE Standard for Local and Metropolitan Area Networks, "Part 16: Air Interface for Fixed and Mobile Broadband Wireless Access Systems. Amendment 2: Physical and Medium Access Control Layers for Combined Fixed and Mobile Operation in Licensed Bands and Corrigendum 1", IEEE Std., February 2006.

[8] IEEE 802.16 2004: IEEE Standard for Local and Metropolitan Area Networks. Part 16: Air Interface for Fixed and Mobile Broadband Wireless Access Systems 2004.

[9] H. Zeng, C. Zhu, "System Level Modeling and Performance Evaluation of 802.16j Multi Hop Relay Systems", Next Generation Mobile Networks Symposium, 2008.

[10] REWIND WP4: System Specifications, Architecture Definition, D4.1 Summary of Network Architecture Analysis and Selected Network Architecture.

[11] REWIND WP6: Development of Network Components and Prototype Products, D6.2.1 RS Sub system Design Report and Critical Design Review.

[12] REWIND WP6: Development of Network Components and Prototype Products, D6.2.2 Relay Prototype Sub system Test Report and System Integration Plan.

[13] REWIND WP6: Development of Network Components and Prototype Products, D6.3 Relay Prototype System Integration Report.

[14] K. Voudouris, N. Athanasopoulos, A. Meir, D. Manor, P. Tsiakas, I. Georgas, I. Petropoulos, G. Agapiou, "2×2 Switch Matrix for WiMAX Relay Station Applications", IEEE Microwave and Wireless Components Letters, vol. 21, no. 8, pp. 424-426, August 2011.

[15] N. Athanasopoulos, I. Petropoulos, K. Voudouris, "2x2 Switch Matrix for a prototype WiMAX Relay Station", International Conference on Electromagnetic in Advanced Applications, Torino, Italy, September 2011.

[16] REWIND WP6: Development of Network Components and Prototype Products D6.4 Final Integration and Relay Prototype System Test Report.

CHAPTER 3

BEAM FORMING

3.1 INTRODUCTION

Beam forming (BF) refers to the ability of an antenna system to steer the main lobe of radiation to a specific/desired direction, produce nulls in the directions of interference, cause side lobe suppression and in general shape radiation pattern based on some requirements. Such a system can be realized using a proper low loss circuit that includes transmission lines, power dividers, phase shifters and attenuators to distribute and process signal power to antenna elements. It also comprises a suitable algorithm for assigning appropriate phases and amplitudes to each antenna element.

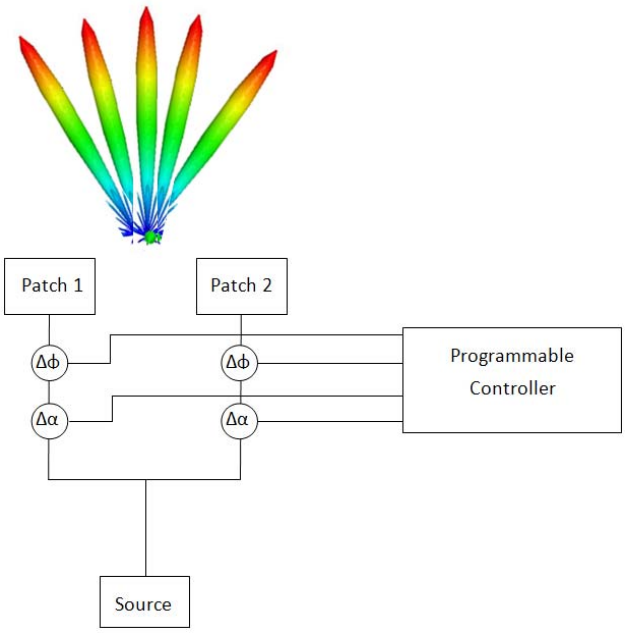

Figure 3.1: Beam forming topology.

Fig. 3.1 depicts a single case of a two element array. Each radiation element is connected to a phase shifter and an attenuator for assigning proper phase $\Delta\varphi$ and amplitude $\Delta\alpha$ respectively. The circuit also comprises a power divider for suitable power distribution. Phase shifters and attenuators are connected to a processor which incorporates algorithm for proper phase and amplitude assignment. From the above it is clear that a beamforming module includes the following:

- Power divider circuit design
- Beam steering algorithm

In this chapter two planar microstrip circuits for power division are presented and depicted. T junction and Wilkinson power divider are described and relevant mathematical equations that clarify their principles of operation are outlined and commented. Also a common beam forming architecture is depicted, giving special attention to the errors introduced by phase shifters and proposing a method for compensating these errors. In addition two beam forming algorithms, the Least Mean Square (LMS) and the Constant Modulus Algorithm (CMA) are presented for beam forming and pattern shaping. Their operation is denoted together with mathematical equations based on relevant references. In addition a second type of algorithms called Direction of Arrival Estimation (DOA) is outlined. This type performs estimations for identifying the direction of optimal signal reception. DOA and BF algorithm can be many times utilized together to provide an adaptive and smart antenna system.

3.2 POWER DIVIDER CIRCUIT DESIGN

A power divider circuit is used to distribute input power to all radiating elements. The schematic of a three port power divider [1] has the form depicted in Fig. 3.2:

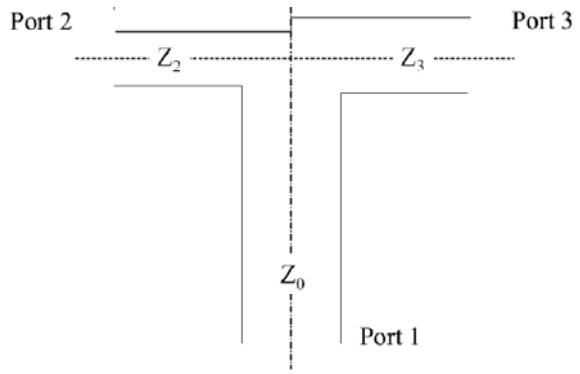

Figure 3.2: Power divider configuration.

Input power P_1 is divided into P_2 and P_3 extracted from ports 2 and 3 respectively. It is easily noticed that:

$$P_1=P_2+P_3 \qquad 3.1$$

The division of power is determined by the equation:

$$P_3=K^2P_2 \qquad 3.2$$

By combining Equations 3.1 and 3.2, the output power can be written as:

$$P_2 = \frac{1}{1+K^2}P_1 \quad \text{and} \quad P_3 = \frac{K^2}{1+K^2}P_1 \qquad 3.3$$

where K is a constant defined by the manufacturer.

The configuration depicted in Fig. 3.2 is called T junction power divider. Let us consider the case of the following 3 port planar circuit [2].

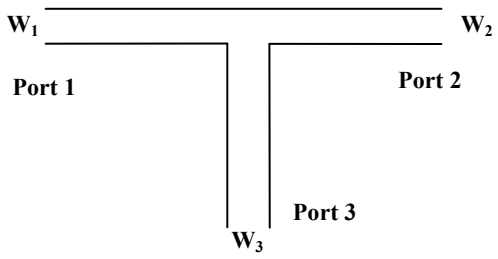

Figure 3.3: 3 port Power divider.

The S parameter of the 3 port divider is:

$$S = \begin{bmatrix} S_{11} & S_{12} & S_{13} \\ S_{21} & S_{22} & S_{23} \\ S_{31} & S_{32} & S_{33} \end{bmatrix} \text{ with } [S][S^*]^T = [I] \qquad 3.4$$

Regarding Fig.3.3, considering that ports 1 and 2 are symmetrical to port 3, the following equations are valid:

$$|S_{11}| = |S_{22}| \text{ and } |S_{31}| = |S_{32}| \qquad 3.5$$

Several types of T junctions have been investigated and presented. Some common types [3] are depicted in Fig. 3.4. The following shapes have been designed on substrate with ε_r=2.5 and thickness h=0.1524cm. In Fig. 3.4b and 3.4c, widths have been adjusted in order to achieve $|S_{31}| - |S_{21}| = 2.5\text{dB}$.

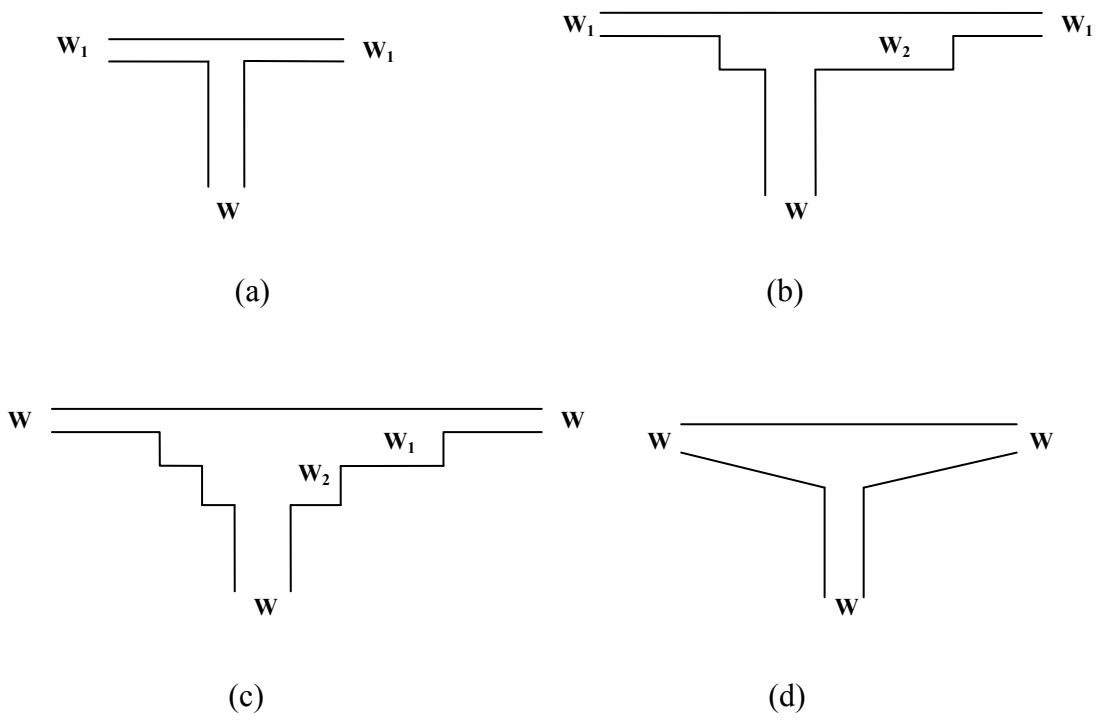

Figure 3.4: T junction power divider types.

A special case of power division configurations is the Wilkinson power divider [4] which is depicted in Fig. 3.5. Signals exited from ports 2 and 3 are of equal magnitude and phase. Quarter wave transformers are incorporated to match the common port to the split ones. The resistance also matches all three ports and isolates ports 2 and 3.

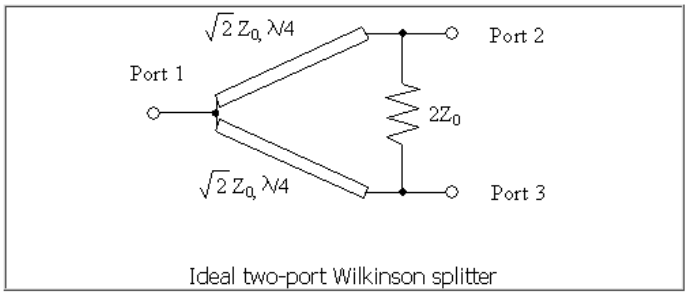

Figure 3.5: Wilkinson power divider.

Let us suppose that ports 1, 2 and 3 of Fig. 3.5 are terminated in Z_0=50Ω impedance. Total impedance at ports 2 and 3 is resulted by parallel addition of the relevant impedances:

$$\frac{1}{Z_t} = \frac{1}{Z_0} + \frac{1}{Z_0} \qquad 3.6$$

Equation 3.6 finally becomes:

$$Z_t = \frac{Z_0}{2} \qquad 3.7$$

A quarter wave transformer should be added between Z_0 of port 1 and Z_t of ports 2 and 3 to succeed matching:

$$2Z_q = 2\sqrt{Z_0 Z_t} = 2\frac{\sqrt{2}}{2} Z_0 = \sqrt{2} Z_0 \qquad 3.8$$

Several forms of Wilkinson power dividers that provide unequal power distribution have also been presented in the literature [5]-[8].

3.3 BEAM FORMING ARCHITECTURES AND TECHNIQUES

Many beam forming architectures have been presented and studied in literature incorporating different circuit styles and methods of beam steering. Y. H. Chen et al [9] presented a beam forming circuit connected to a linear 8 element array, operating at 2.6GHz. The proposed configuration is depicted in Fig. 3.6:

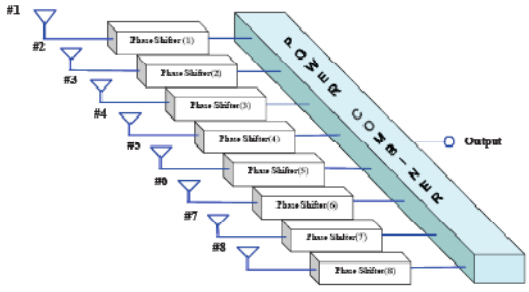

Figure 3.6: Schematic of beam forming network.

Each radiation element is connected to a phase shifter and then power is combined to the output. Phase shifters incorporate digital step attenuators, RF switches and 90^0 hybrid couplers. An error is introduced each time a phase and attenuation is assigned to the system. This error is caused by losses and inability of the system to adopt the specified values of amplitude and phase.

The attenuation and phase errors are depicted in Fig. 3.7:

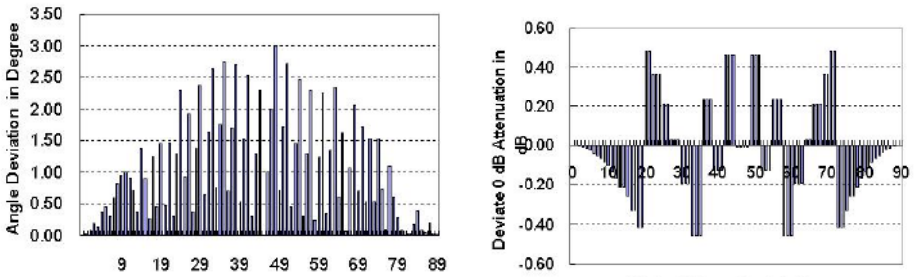

(a) **(b)**

Figure 3.7: Types of errors; (a) angle and (b) amplitude deviation.

The angle deviation can reach 3^0 at 49^0 and amplitude error varies from 0.5 to 0.5dB. Aliakbarian et al [10] presented a circularly polarized array with a digital beam forming unit. A calibration formula is described to overcome imbalance phenomena and RF impairments. Signal is processed by an FPGA module where I and Q component signals are distinguished. A matrix is assigned through calibration phase in order to remove all imbalances:

$$M = a_0 \begin{bmatrix} \cos(\theta) & \sin(\theta) \\ -\sin(\theta) & \cos(\theta \end{bmatrix} \times \begin{bmatrix} \beta & 0 \\ \beta \tan(\phi) & 1/\cos(\phi) \end{bmatrix} \qquad 3.9$$

where β and φ are amplitude and phase deviations between I and Q components of one element. a_0 and θ are the amplitude and phase deviations of the I component between antenna 1 and antenna 2.

Measured and simulated radiation pattern are depicted in Fig. 3.8 utilizing Equation 3.9 for imbalance compensation.

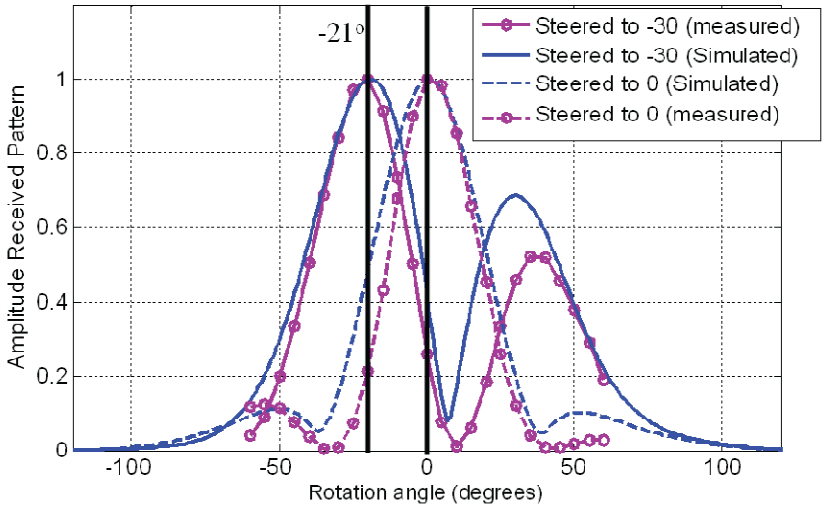

Figure 3.8: Simulation and measurement for $\theta=0^0$ and $\theta= 30^0$.

Even if Equation 3.9 is used for taking into consideration imbalances, steering main lobe to 30^0 leads to maximum at 21^0. This discrepancy is caused by mutual coupling effect between radiation elements.

3.4 BEAM FORMING ALGORITHMS

Beam forming refers to the production of a radiation pattern with specific desired characteristics. This is achieved by additive contribution of phases in the preferred direction and destructive contribution of phases in the direction of interferences. A

beam steering pattern is resulted by multiplying the signal emitted by each radiation element with a weight. For a linear array of N elements, the angular response for all angles ($90^0<\theta<90^0$) is [11], [12]:

$$R(\theta) = W^H(n)S(\theta) \qquad 3.10$$

where: $W^H(n)$ is the hermitian of the weight vector W and S is the steering vector.

The steering vector is equal to:

$$S(\theta) = [1, e^{-j\theta}, e^{-j2\theta}, ..., e^{-j(N-1)\theta}]^T \qquad 3.11$$

In this section the Least Mean Square (LMS) algorithm is described. It is used for the estimation of the phases and amplitudes of the signals that will enter the array giving the proper characteristics to radiation pattern. LMS algorithm was proposed by Widrow and Hoff in 1959 [13]. It evaluates the optimum value for the desired variable, trying to minimize the mean square error. This algorithm will be fully analyzed in the text that follows.

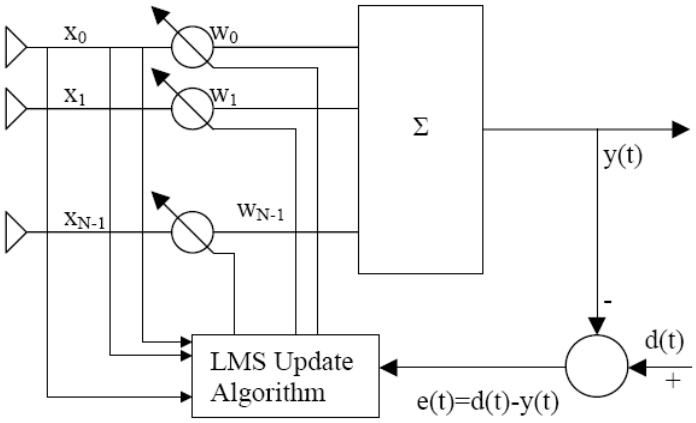

Figure 3.9: LMS beamforming network.

Fig. 3.9 describes a beamformer which through iterative process, it computes the optimum values of W in order to minimize the mean square error of e(t).

The weight vector equation described in [14] is:

$$w(n+1) = w(n) + \frac{1}{2}\mu[-\nabla_w\{E[e^2(n)]\}] \quad 3.12$$

where: μ represents the convergence of the algorithm, $e^2(n)$ denotes the mean square error between the reference signal d(n) and the beamformer output y(n) and is equal to:

$$e^2(n) = [d^*(n) - y(n)]^2 = [d^*(n) - w^H x(n)]^2 \quad 3.13$$

The gradient of the above equation is:

$$\nabla_w\{E[e^2(n)]\} = -2r + 2wR \quad 3.14$$

where: $r = E[d^*(n)x(n)]$ is called cross correlation matrix. It is a measure of how similar is x(n) and d(n). $R = E[x^T(n)x(n)]$ represents the auto correlation matrix.

Equation 3.12 can be written as:

$$\begin{aligned} w(n+1) &= w(n) + \mu x(n)[d^*(n) - x^H(n)w(n)] \\ w(n+1) &= w(n) + \mu x(n)e^*(n) \end{aligned} \quad 3.15$$

We set to the algorithm an initial arbitrary value, let us say w(0) and then through iterations the mean square error is minimized and the desired weight vector is obtained.

The μ parameter seen in Equation 5.12 expresses the level of convergence. According to the LMS theory, it takes values: $0<\mu<1/\lambda_{max}$. λ_{max} is the maximum value of correlation matrix R. If values of λ are widespread, the convergence is slow.

Many papers have been presented in literature, describing arrays and beam forming units that incorporate LMS algorithm to steer radiation lobe to desired directions. Guerreiro et al [15] have presented a planar array where the LMS algorithm is applied

to steer the main lobe of radiation to the desired direction and produce nulls in the interference directions. The paper investigates the efficiency of the beam steering algorithm for a varying number of iterations showing satisfactory results. Al Ardi et al [16] have studied the case of LMS application to a linear antenna array and varied parameters such as number of elements, spacing between the array elements etc. Some results are depicted in Fig. 3.10:

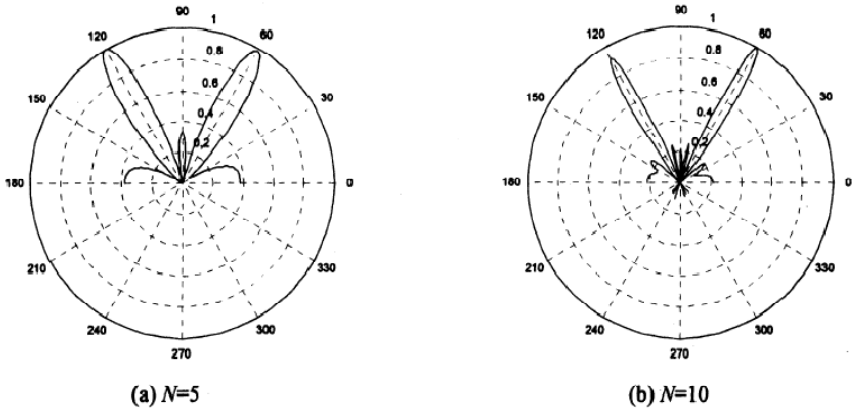

Figure 3.10: LMS application to a linear array; (a) 5 elements (N=5) and (b) 10 elements (N=10).

An element increase leads to Half Power Beam width (HPBW) decrease and gives rise to array directivity. It does not seem to affect the direction of radiation.

Element spacing is also studied, giving the following results shown in Fig. 3.11.

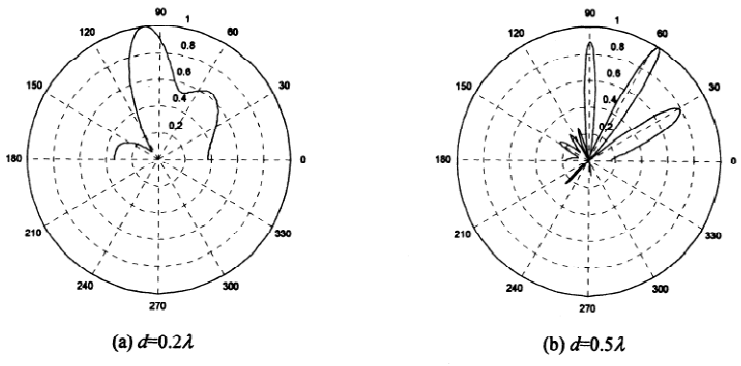

Figure 3.11: Effects of varying spacing between the array elements; (a) d=0.2λ (b) d=0.5λ.

By placing the array elements closely ($d<\lambda_0/2$) coupling become dominant and distorts radiation pattern. By increasing space at half of the wavelength, lobes of high directivity are appeared.

LMS algorithm is often combined to Direction of Arrival Estimation algorithms (DOA) [17]. These algorithms estimate the direction of a desired signal and then a beam forming algorithm is applied (LMS) to steer radiation to the specific direction. Many DOA algorithms can be found in literature. MUSIC (Multiple Signal Classification) is a widely used DOA algorithm [17], [18]. This algorithm provides information regarding the angle of arrival, the strengths and the number of signals. The application of MUSIC for the case of a planar 8×8 gives the following results depicted in Fig. 3.12:

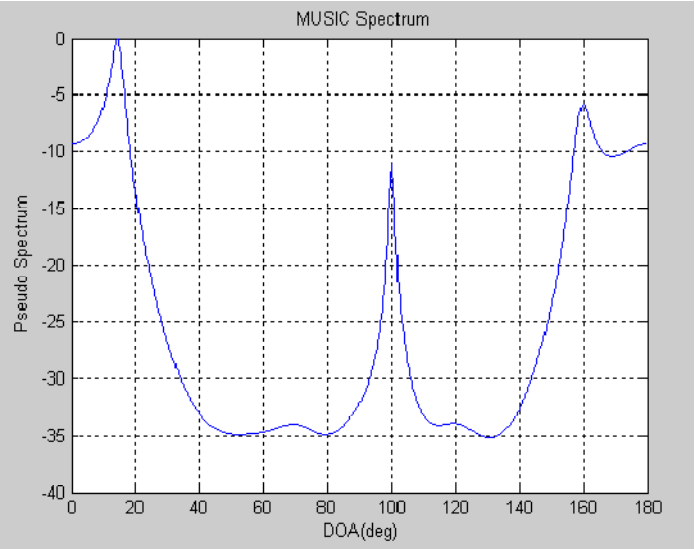

Figure 3.12: MUSIC algorithm implementation. The angles in azimuth of signal reception are: $\varphi=13.40^0$, 100.180^0 and 160.360^0.

A disadvantage of MUSIC is that if two or more signal sources are very close to each other then MUSIC cannot distinguish them.

A second commonly used DOA algorithm is ESPRIT (Estimation of Signal Parameters via Rotational Invariance Techniques). It requires less computational power and storage regarding MUSIC [19]. ESPRIT has been examined for the case of a linear array of 8 elements giving results depicted in Fig. 3.13:

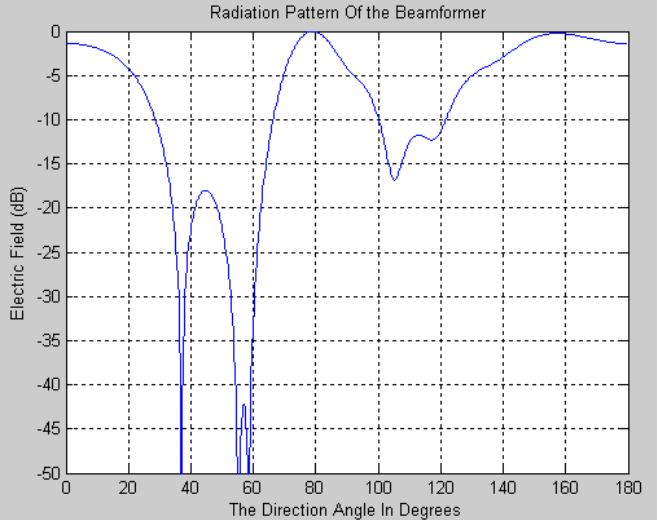

Figure 3.13: ESPRIT algorithm implementation. The angles in azimuth of signal reception are: φ=74.260^0, 140.460^0, 158.420^0 and 10.940^0.

Susmita Das has published a research in smart antennas where a comparison is performed between different beam forming algorithms [20]. Besides LMS algorithm, Constant Modulus Algorithm is described (CMA). It does not require reference signal and it needs time to converge. This property limits the efficiency of CMA algorithm in a rapidly changing environment.

Weight update is performed using the equation:

$$W(n+1) = W(n) + \mu X(n) e^{*}(n) \qquad 3.16$$

where: μ is the step size, X(n) represents the input vector,

$e(n) = Y(n)(R_2 - |Y(n)|^2)$ and $R_2 = E\left\{\frac{|X(n)|^4}{|X(n)|^2}\right\}$

Y(n) is the array output at the n^{th} iteration.

Another beam forming algorithm described in [20], is the Recursive Least Square algorithm, (RLS). In this case weight update is performed by the equation:

$$W(n) = W(n-1) + K(n)\xi^{*}(n) \qquad 3.17$$

where: K(n) is the gain vector and ξ(n) is an error estimation defined as:

$$\xi(n) = d(n) - W^{H}(n-1)U(n) \qquad 3.18$$

RLS algorithm converges faster than the simple LMS. The last is proved to be simple and provides ease of computation.

3.5 CONCLUSIONS

Chapter 3 handled the beam forming property in terms of array configuration and algorithm implementation. The presented literature review will be taken into consideration during the design procedure of the phased array for the backhaul link. The aforementioned survey will be used as the basis for the development of the phased array feeding circuit and the beam forming algorithm that is going to be applied.

3.6 REFERENCES

[1] H. J. Visser, Array and Phased Array Antenna Basics, Wiley, 2005.

[2] G. R. Branner, P. Kumar, D. G. Thomas, "Design of microstrip T junction power divider circuits for enhanced performance", Proceedings of the 38th Midwest Symposium on Circuits and Systems, vol. 2, no., pp.1213-1216, 13-16 August 1995.

[3] P. B. Kumar, Branner G. R., Razmafrouz, D. Brody, "Optimization of microwave T junction power divider circuits", Proceedings of the 37th Midwest Symposium on Circuits and Systems, vol. 2, no., pp.1235-1237, 3-5 August 1994.

[4] E. J. Wilkinson, "An N way hybrid power divider", IRE Transactions on Microwave Theory Technology, vol. 8, pp. 116-118, January 1960.

[5] J. S. Lim, G.Y. Lee, Y. C. Jeong, D. Ahn, and K. S. Choi, "A 1:6 Unequal Wilkinson Power Divider", 36th European Microwave Conference Proceedings, Manchester, , pp. 200-203, September 2006.

[6] S. Oh, J. Koo, M. S. Hwang, C. Park, Y. C. Jeong, J. S. Lim, K. S. Choi, D. Ahn, "An Unequal Wilkinson Power Divider with Variable Dividing Ratio", International Microwave Symposium, pp.411-414, 3-8 June 2007.

[7] L. Chen, H. Xie, Y. Jiao, F. Zhang, "A novel 4:1 unequal dual frequency Wilkinson power divider", International Conference on Microwave and Millimeter Wave Technology, pp.1290-1293, 8-11 May 2010.

[8] J. S. Lim, S. W. Lee, C. S. Kim, J. S. Park, D. Ahn, S. Nam, "A 4.1 unequal Wilkinson power divider", IEEE Microwave and Wireless Components Letters, vol.11, no.3, pp.124-126, March 2001.

[9] Y.H. Chen, J. Chen, P. C. Hsien, D. C. Chang, J. H. Huang, "Performance evaluation of mobile WiMAX beam forming network implemented by RF digital step attenuators", 14th European Wireless Conference, pp.1 6, 22-25 June 2008.

[10] H. Aliakbarian, V. Volskiy van der Westhuisen, E. Wolhuter, R. Vandenbosch, P.J. Soh, "Imbalance calibration of a digital beam forming array and the effect of mutual coupling on its steering", IEEE International Symposium on Antennas and Propagation, pp.2461-2464, 3-8 July 2011.

[11] L. Godara, “Application of Antenna Arrays to Mobile Communications,Part Π: beam forming and direction of arrival considerations”, Proceeding of the IEEE, vol. 85, no. 8, pp. 1195-1234, August 1997.

[12] S. Bellofiore, J. Foutz, C. A. Balanis, and A. S. Spanias, “Smart Antenna System for Mobile Communication Networks Part 2: Beamforming and Network Throughput” IEEE Antenna's and Propagation Magazine, vol. 44, no. 4, August 2002.

[13] B. Widrow and M.E. Hoff., “Adaptive Switch Circuits, IRE WESCOM, Conv. Rec., Part 4, 1960

[14] S. Haykin, “Introduction to Adaptive Filters”, Macmillan Publishing Company, New York, 1985.

[15] A.M.G. Guerreiro, A.D.D. Neto, F.A. Lisboa, “Beamforming applied to an adaptive planar array”, IEEE Radio and Wireless Conference, pp.209-212, 9-12 August 1998.

[16] A. Ardi, E. M. Shubair, R. M. Al Mualla, “Performance evaluation of the LMS adaptive beamforming algorithm used in smart antenna systems”, IEEE 46th Midwest Symposium on Circuits and Systems, vol.1, pp. 432-435, 27-30 December 2003.

[17] M. Alam, Md. Majharul, I. Rajib, S. J. Biswas, “Design and Performance Analysis of Smart Antenna System for DECT Radio Base Station in Wireless Local Loop”, Journal of Communications, vol. 5, no. 8, pp. 593-603, August 2010.

[18] C.A. Balanis, “Antenna Engineering”, Wiley, 3rd edition, 2005.

[19] F. Gross, “Smart Antenna for Wireless Communication with MATLAB” The McGraw Hill Companies, Inc. 2005.

[20] S. Das, “Smart antenna design for wireless communication using adaptive beam forming approach”, IEEE Region 10 Conference, pp.1-5, 19-21 November 2008.

CHAPTER 4

ANTENNA SYSTEM DESIGN AND EVALUATION

4.1 INTRODUCTION

An new antenna system for a Relay Station is designed, simulated and fabricated. It includes a single antenna element for connecting Relay Station to Mobile Station (access link) and an antenna array for communication between Relay Station and Base Station (backhaul link). Specifications of the antennas have been provided by the Air Interface of IEEE 802.16j protocol. The single antenna element has high gain, broad main lobe and wide bandwidth for end user access while the array provides high gain and low Half Power Beam width. Moreover the array is equipped with beam forming features so that Relay Station can point its main lobe to the Base Station, put nulls in direction of interference and suppress side lobes for gain enhancement. A Relay Station should be able of radiation pattern control so that it can communicate with Base Station regardless of the position in which it is placed. For this reason a new beam forming circuit is designed, simulated and constructed, including power dividers and chips for proper amplitude and phase assignments. Least Mean Square (LMS) algorithm is generated to evaluate the phase and amplitude excitation currents to steer radiation pattern to desired direction, where Base Station is positioned. Several beam forming scenarios of Base Station's position are considered. For each of these scenarios, experimental and simulated radiation pattern is extracted, depicted and results are commented.

4.2 ANTENNA SYSTEM DESIGN

An antenna system for a Relay based wireless network is presented. The proposed setup is depicted below:

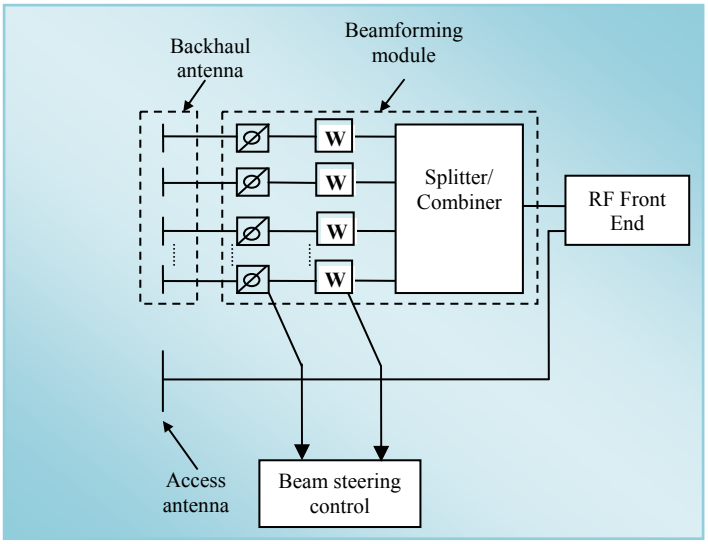

Figure 4.1: Antenna system setup.

It includes a backhaul antenna array for connecting Relay Station with Base Station (backhaul link) and an access antenna for connecting Relay Station with end users (access link). The configuration also comprises a beam forming module that splits power to a number of paths equal to the radiation elements. Each of these paths incorporates phase shifters and attenuators. Phase shifters and attenuators assign proper phases and amplitudes to the signals in order to steer the radiation emitted by the array to the desired direction. Phase and amplitudes are controlled by a beam steering control unit. A proper algorithm is embedded to this unit that give specific and desired characteristics to the radiation pattern of the array.

4.3 ACCESS AND BACKHAUL ANTENNA DESIGN

4.3.1 Access antenna design

The text that follows describes the configuration of a 2 substrate E-shaped patch antenna. The initial design of the antenna is a rectangle patch. The patch's dimensions are [1]:

$$L = L_{eff} - \Delta L \tag{4.1}$$

where: L_{eff} is the effective length of the antenna equal to:

$$L_{eff} = \frac{c}{2f_0\sqrt{\varepsilon_{reff}}} \tag{4.2a}$$

$$\Delta L = h \times 0.412 \frac{(\varepsilon_{reff} + 0.3)(\frac{W}{h} + 0.264)}{(\varepsilon_{reff} - 0.258)(\frac{W}{h} + 0.8)} \tag{4.2b}$$

$$\varepsilon_{reff} = \frac{\varepsilon_r + 1}{2} + \frac{\varepsilon_r - 1}{2}[1 + 12\frac{h}{W}]^{-1/2} \text{ for W/h>1} \tag{4.2c}$$

ε_{reff} is the effective dielectric constant of the substrate,

h is the substrate's thickness

W is the width of the patch

ε_r is the relative dielectric constant

f_0 is the resonant frequency

The width of the patch is equal to:

$$W = \frac{c}{2f_0}\sqrt{\frac{2}{\varepsilon_r + 1}} \tag{4.3}$$

An inherent drawback of patch antennas is their narrow bandwidth [2]. Limited bandwidth is caused because the space under the patch behaves like a resonant cavity with high quality factor. For this reason stacked geometry is preferred for bandwidth enhancement [3].

As described in [3], the bandwidth of a microstrip antenna is equal to:

$$B = \frac{(VSWR - 1)}{Q\sqrt{VSWR}} \bullet 100\% \qquad 4.4$$

where B represents bandwidth, VSWR is the Voltage Standing Wave Ratio and Q is the Quality factor.

Q is reduced when thicker or lower permittivity substrates are used. A reduction of Q gives raise to B as can be noticed in Equation 4.4. In [4] and [5] is also proved that a stacked geometry configuration can lead to wider bandwidth. Relevant equations are denoted below:

$$\varepsilon_t = \frac{\varepsilon_r (h_1 + h_2)}{h_1 + h_2 \varepsilon_r} \qquad 4.5$$

where $h_t = h_1 + h_2$. ε_t is the total dielectric permittivity of a structure comprising two substrates. h_1 and h_2 are the thickness of the utilized substrates.

Bandwidth of the stacked patch antenna would then be:

$$BW = \frac{\sqrt{2}p}{45\pi}(1 - \frac{1}{\varepsilon_t} + \frac{2}{5\varepsilon_t^2})(\frac{1}{\varepsilon_t})(\frac{h_t}{\lambda})(\frac{W}{L}) \qquad 4.6$$

where

$$p = 1 + \frac{\alpha_2}{20}(k_0 W)^2 + \alpha_4(\frac{3}{560})(k_0 W)^4 + b_2(\frac{1}{10})(k_0 L)^2$$

$\alpha_2 =$ 0.16605

$\alpha_4 =$ 0.00761

$b_2 =$ 0.09142

$k_o = 2\pi/\lambda$

L is the length and W the width of the patch element

An increase in substrate thickness leads to surface wave excitation which distorts radiation pattern and reduced radiation efficiency. Also higher order cavity modes with field dependency on z axis are excited and affect radiation pattern and impedance characteristics [2]. In conclusion a balance should be kept for bandwidth enhancement and substrate's thickness to provide a broadband antenna with low surface waves. Further bandwidth widening can be achieved using an E shaped patch antenna.

A rectangle patch antenna has the form depicted in Fig. 4.2a:

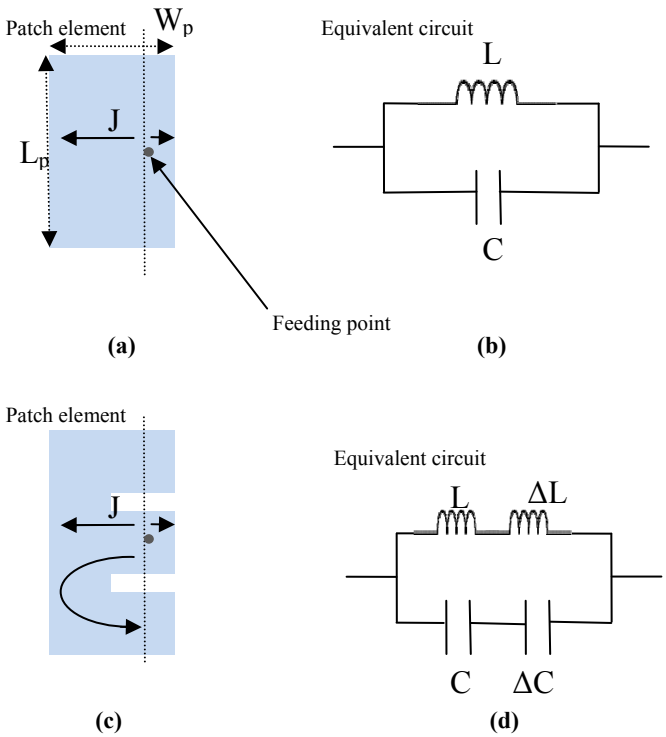

Figure 4.2: Patch antennas with equivalent circuits; (a) rectangle patch antenna (b) LC equivalent circuit of rectangle patch antenna (c) E shaped patch antenna (d) LC equivalent circuit of E shaped patch antenna.

A single rectangle patch element can be represented as an LC circuit depicted in Fig. 4.2b [6], [7]. The current entered the antenna by the feeding point is moved to the patch edges and resonates the element at a frequency. The introduction of slots makes part of the current to be moved at an additional path as depicted in Fig. 4.2c. The current that runs through the additional path makes the antenna resonate at a second lower frequency and adds a series inductance and capacitance to the equivalent LC circuit (Fig. 4.2d). The slots introduced in the patch element can be represented as a zero thickness transverse magnetic wall into the antenna [7].

The patch antenna is fed by a 50Ω coaxial cable. The feeding point has been investigated for obtaining 3.5GHz resonant frequency. From [8] the input impedance at the point (x_0, y_0) of a rectangular patch, shown in Fig. 4.3 can be written as:

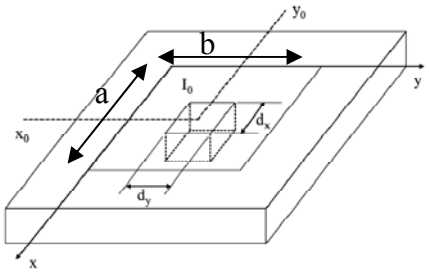

Figure 4.3: Input impedance evaluation.

$$Z_{in} = -jn_0k_0h \sum_{m=0}^{\infty} \sum_{n=0}^{\infty} \frac{\psi^2_{mn}(x_0, y_0)}{k_0^2 - k_{mn}^2} G_{mn} \tag{4.7}$$

where: n_0 is the free space impedance

$k_0=2\pi/\lambda_0$ is the wave number in free space

h is the substrate's thickness

$$\psi_{mn}(x,y) = \frac{\chi_{mn}}{\sqrt{ab}} \cos(\frac{m\pi}{a}x)\cos(\frac{n\pi}{b}y) \tag{4.8}$$

is the modal field with

$$\chi_{mn} = \begin{cases} 1 & if \quad m=0\_and\_n=0 \\ \sqrt{2} & if \quad m=0\_or\_n=0 \\ 2 & if \quad m\neq 0\_and\_n=0 \end{cases} \tag{4.9}$$

k_{mn} is the wave number of m, n mode

$$G_{mn} = \sin c(\frac{m\pi d_x}{2a}) \sin c(\frac{n\pi d_y}{2b}) \tag{4.10}$$

If $k_0=k_{mn}$ the denominator of Equation 4.7 becomes 0 and the Z_{in} is infinite. A loss mechanism should be introduced in Equation 4.7 so that the antenna could emit. This

loss mechanism is expressed in terms of the effective loss tangent. The expression for input impedance becomes:

$$Z_{in} = -jn_0k_0h\sum_{m=0}^{\infty}\sum_{n=0}^{\infty}\frac{\psi^2{}_{mn}(x_0,y_0)}{\varepsilon_r(1-j\delta_{eff})k_0{}^2-k_{mn}^2}G_{mn} \qquad 4.11$$

The final composite structure of the E shaped patch antenna has been optimized in terms of patch length, width, slot length and width and substrate thickness in order to present resonance at 3.5GHz and adequate bandwidth.

4.3.2 Access antenna simulation and fabrication

Starting from a rectangle patch antenna, the initial shape has been optimized with the introduction of a second substrate, slots and by varying the dimensions of the radiation element in order to achieve 500MHz bandwidth and 9dB gain based on the specifications of the IEEE802.16j standard.

The proposed antenna has been designed, simulated in HFSSv.11 and fabricated and has the following form:

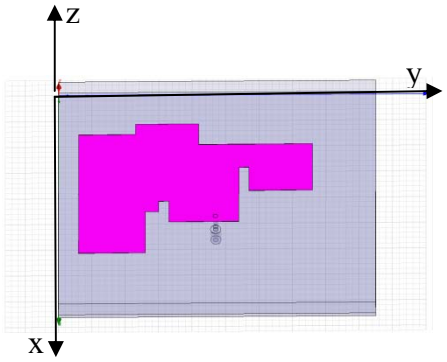

(a)

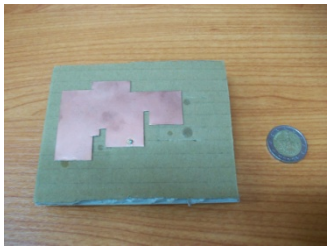

(b)

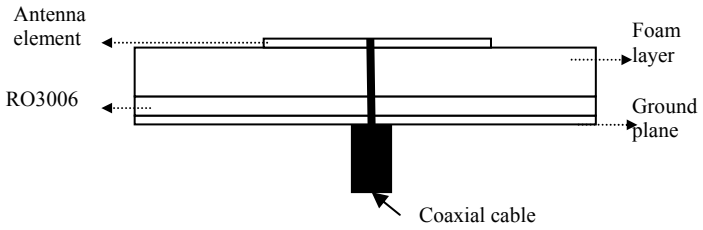

(c)

Figure 4.4: Access antenna; (a) simulation design (b) constructed design (c) cross section view.

The simulated antenna is depicted in Fig. 4.4a. The constructed one is shown in Fig. 4.4b. A cross section of the proposed antenna structure is viewed in Fig. 4.4c.

An E-shaped patch antenna is designed and mounted on foam substrate (ε_r=1, tanδ=0.0025, h=0.5cm). Foam substrate is placed on Rogers Ro 3006 (ε_r=6.15, tanδ=0.0025, h=1.28mm). Rogers Ro 3006 dielectric is then placed on ground plane (h=35μm). Dimensions of the E shape antenna are depicted in Fig. 4.5.

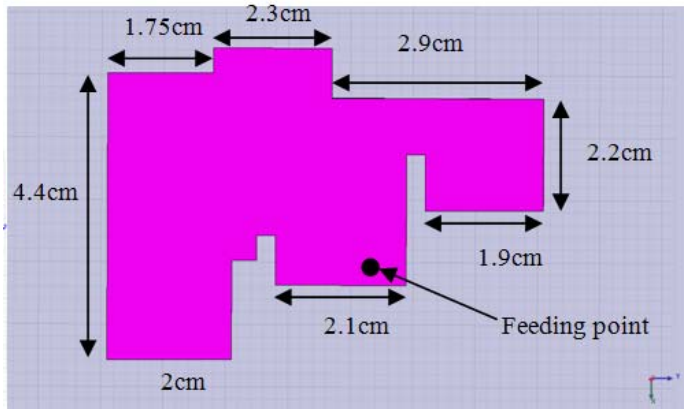

Figure 4.5: Dimensions of e shape antenna.

Measured and simulated S_{11} are depicted in Fig. 4.6. Measured S_{11} is estimated to be: S_{11}= -31.93 dB for 3.4GHz.

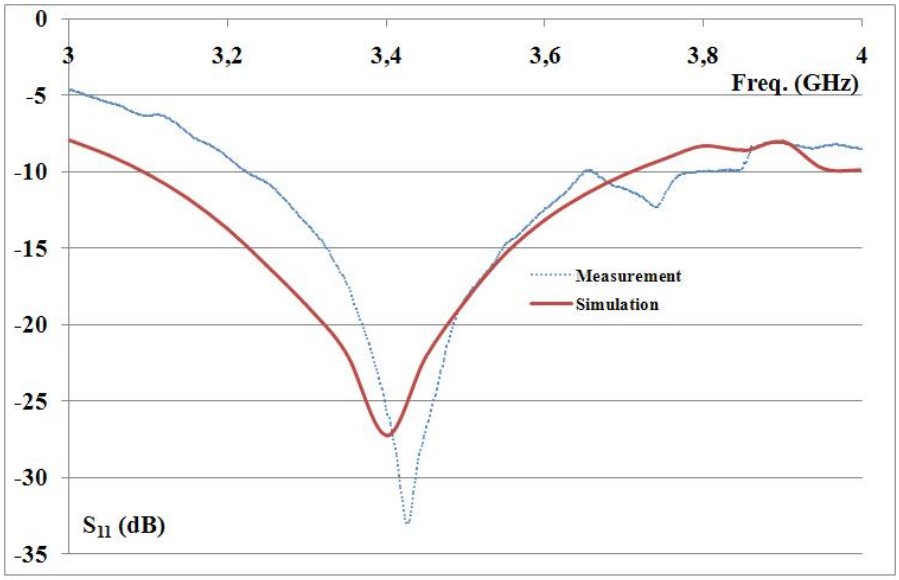

Figure 4.6: S_{11} vs. frequency.

Bandwidth of the proposed antenna is 520MHz or 15.2%. Radiation pattern in terms of norm. Power is depicted in Fig. 4.7a and 4.7b.

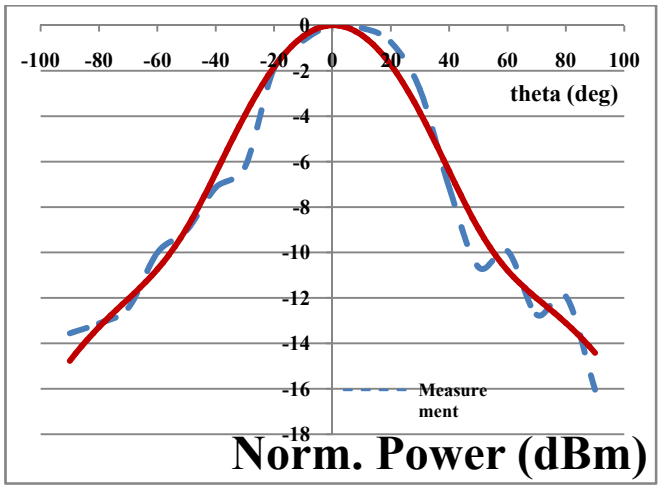

(a)

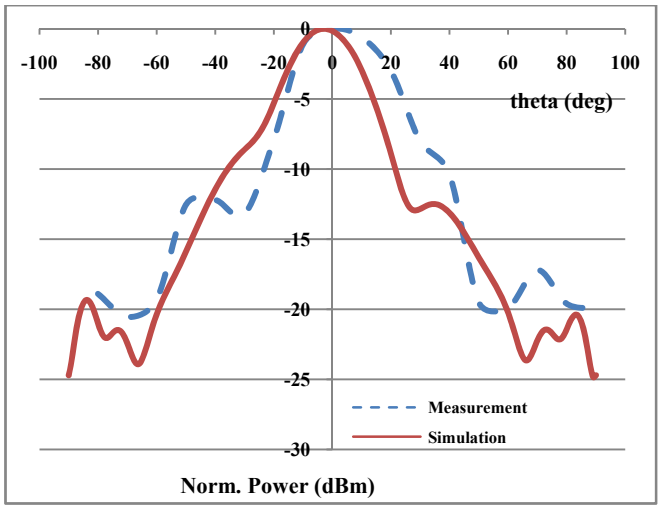

(b)

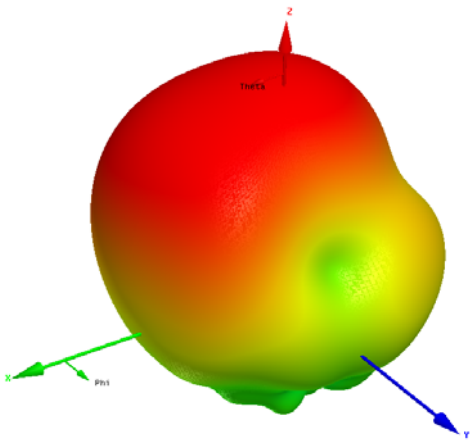

(c)

Figure 4.7: Radiation pattern of E shaped antenna; (a) xz plane (b) yz plane (c) 3D radiation pattern.

Radiation pattern features are denoted in Table 4.1, together with the air interface specifications of IEEE802.16j standard.

Table 4.1: Features of access antenna and comparison with the desired specifications.

	Gain (dB) for 3.4GHz	**HPBW xz plane (deg)**	**HPBW yz plane (deg)**	**Bandwidth (MHz)**
Access antenna	**10**	75	42	520
Specifications	**9**	(sectorial) 60	(sectorial) 50	500

4.3.3 Backhaul antenna

The antenna depicted in the previous section is used as radiation element in a 4×4 planar array. The distance between the antenna elements has been investigated and optimized in order to maintain low side lobe levels. The purpose in the case of the backhaul antenna is to achieve 500MHz bandwidth and 18dB gain. This array is designed, fabricated and can be seen in Fig. 4.8. The total size of array is 32.6×30cm.

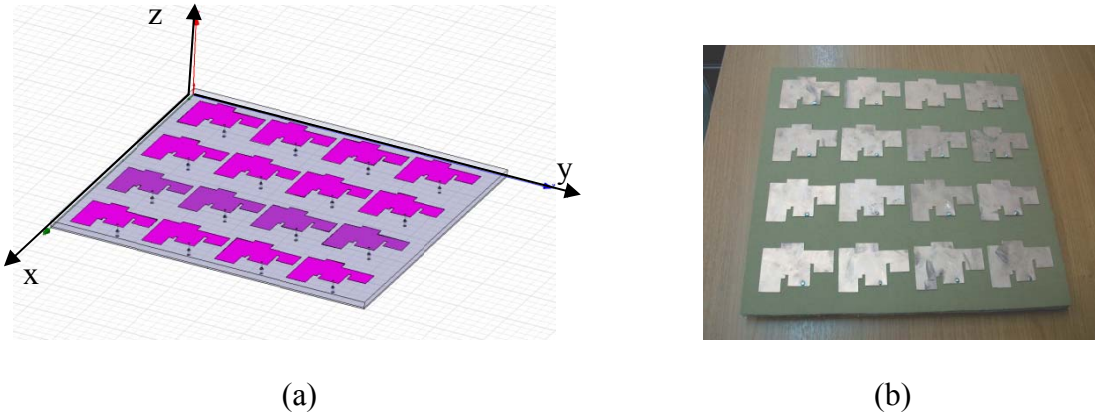

(a) (b)

Figure 4.8: 16 element backhaul antenna array; (a) simulation design (b) fabrication design.

The distance between two adjacent elements is denoted in Fig. 4.9.

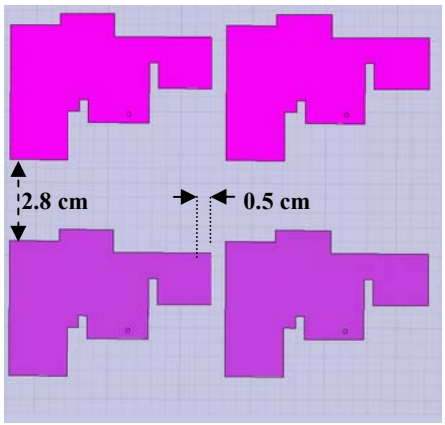

Figure 6.9: Inter element space.

Let us mention here that the inter element spacing (center to center) is $0.87\lambda_0$. The purpose is to place radiation elements in such a distance to prevent grating lobes and maintain mutual coupling and side lobe levels as low as possible. Grating lobes can be prevented by adjusting the inter element spacing to be smaller than λ_0. Strong mutual coupling can also be prevented by adjusting distance between patches to be more than $\lambda_0/2$ [8]. So the distance should be:

$$\frac{\lambda_0}{2} \leq d \leq \lambda_0 \qquad 4.12$$

After successive simulations it has been found that patches should abstain $0.87\lambda_0$. It has been found that this distance gives high gain, a broad main beam and low side lobe levels.

Radiation pattern in terms of power distribution can be seen below:

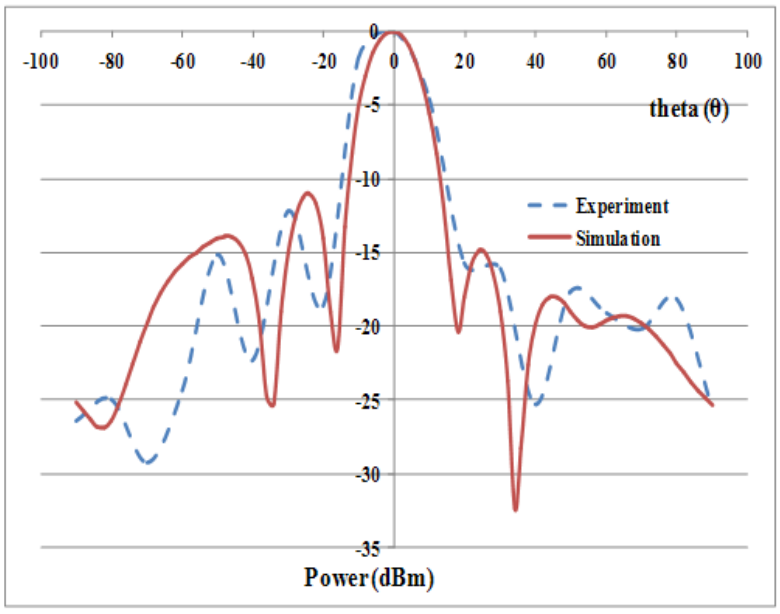

(a)

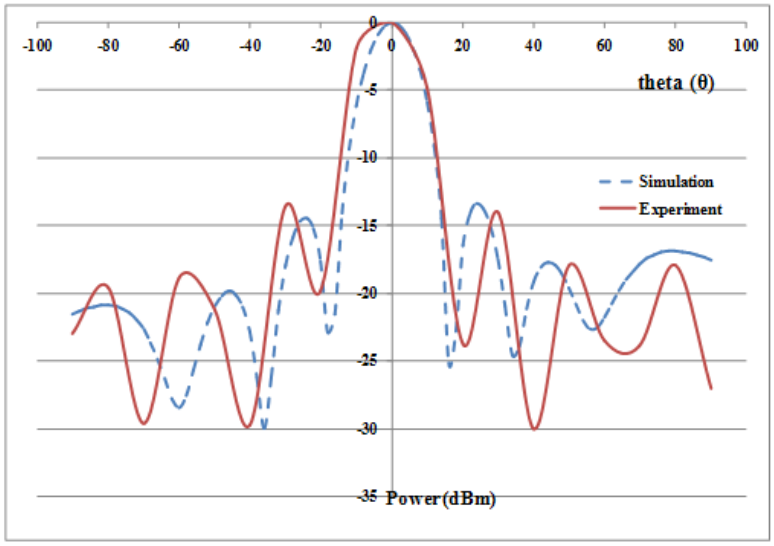

(b)

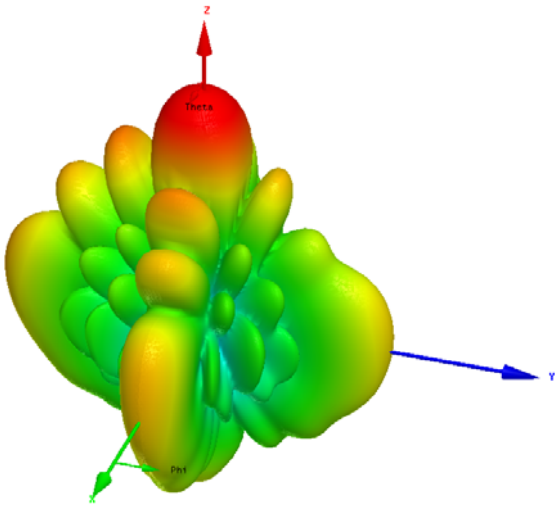

(c)

Figure 4.10: Radiation pattern of 16 element array; (a) yz plane (b) xz plane (c) 3D radiation pattern.

The features of the 16 element array together with air interface specifications of the IEEE802.16j standard.

Table 4.2: Features of backhaul antenna and comparison with the desired specifications.

	Size (cm)	**Gain (dBi) for 3.4GHz**	**HPBW xz plane (deg)**	**HPBW yz plane (deg)**	**Bandwidth (MHz)**
Backhaul antenna	32.6×30	21.2	14	14	424
Specifications		18	15	15	500

The proposed antenna presents higher gain and lower HPBW than the commercial one. Both access and backhaul antennas would be mounted on a Relay Station. A proposed setup could be the following:

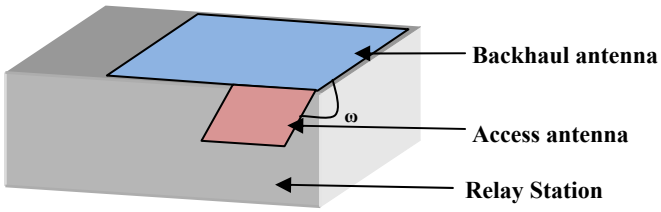

Figure 4.11: Proposed Relay Station with antenna setup.

Backhaul antenna is mounted on one side of the Relay while access antenna can rotate using a proper mechanism as can be seen in Fig. 4.11.

4.4 BEAMFORMING MODULE

4.4.1 Beamforming circuit

Beamforming circuit comprises the microstrip power dividers that split and distribute the signal power to each of the radiation elements. Phase shifters and attenuators have

been adjusted to microstrip lines for beam steering realization. Side view of the proposed beamforming circuit is depicted in Fig. 4.12.

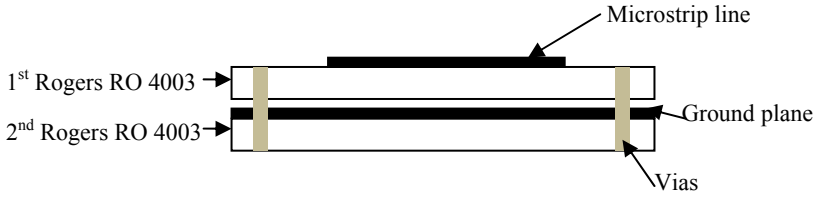

Figure 4.12: Side view of the beam forming circuit.

Microstrip lines of copper (h=35μm) are placed on Rogers Ro 4003 substrate (ε_r=3.55, h=0.508mm). A second Rogers Ro 4003 is mounted beneath the first, on the top of which ground plane of copper (35μm) is placed. On the bottom side of the 1st and 2nd Rogers Ro substrates, lines of digital information are designed. Both substrates are hold with vias. Microstrip lines are designed with length equal to [9]:

$$L = N\frac{\lambda_g}{2} \qquad 4.13$$

and

$$\lambda_g = \frac{\lambda_0}{\sqrt{\varepsilon_r}} \qquad 4.14$$

N is a physical number, λ_g is the wave length in substrate, λ_0 is the wave length in free space and ε_r is the relative dielectric constant of the substrate. Microstrip lines form a 1:8 Wilkinson power divider [10] for accurate power division and transfer to the radiation elements. A Wilkinson power divider splits an input signal into equal amplitude and phase output signals. It incorporates a 100Ω chip resistor that isolates and matches ports. The widths of the microstrip lines have been defined using the formulas [11]:

$$\frac{W}{h} = \frac{8}{\exp(A) - 2\exp(-A)} \text{ for } W/h \le 2 \qquad 4.15a$$

$$\frac{W}{h}=\frac{2}{\pi}\{B-1-\ln(2B-1)+\frac{\varepsilon_r-1}{2\varepsilon_r}[\ln(B-1)+0.39-\frac{0.61}{\varepsilon_r}] \text{ for } W/h\geq 2 \qquad 4.15b$$

where:

$$A=\frac{\pi}{\eta_0}\sqrt{2(\varepsilon_r+1)}Z+\frac{\varepsilon_r-1}{\varepsilon_r+1}(0.23+0.11/\varepsilon_r)$$

$$B=\frac{\pi\eta_0}{2\sqrt{\varepsilon_r}Z}$$

η_0=377Ω is the impedance of free space

Initial values for length L and width W are:

L=1.13cm for N=1

W=1.12mm for Z=50Ω characteristic impedance

The above values have been used for the initial beam former circuit design. Then optimization has been performed to improve circuit's dimensions to better operate at 3.3 to 3.8GHz frequency range. Layout of the final design is depicted in Fig. 4.13.

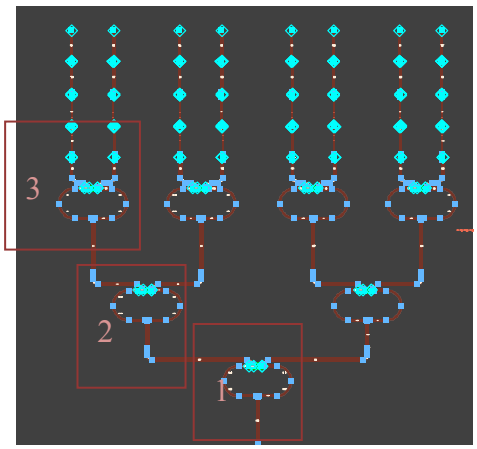

Figure 4.13: Beam forming circuit.

The size of microstrip lines in each bracket is denoted below:

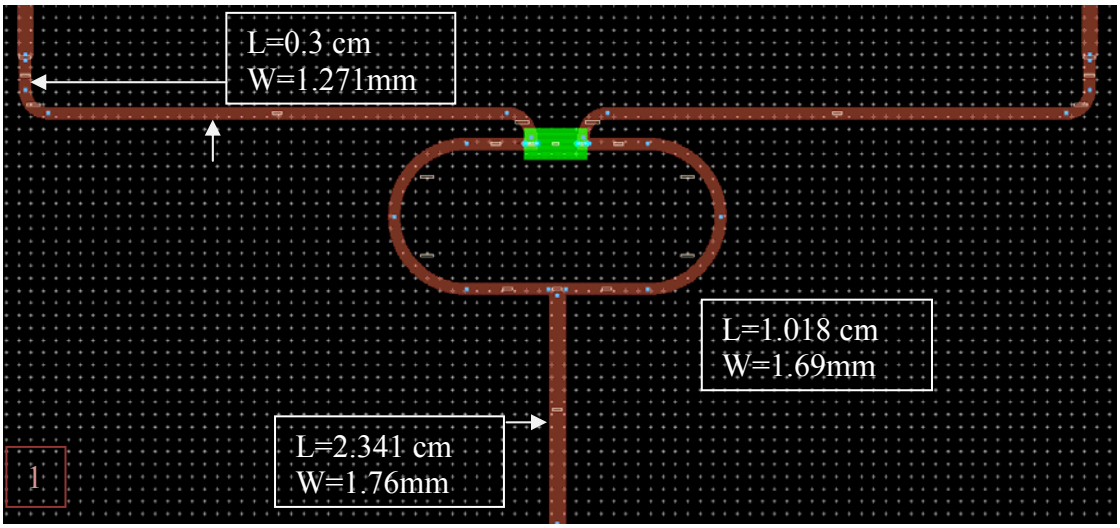
L=0.3 cm
W=1.271mm
L=1.018 cm
W=1.69mm
L=2.341 cm
W=1.76mm
1

(a)

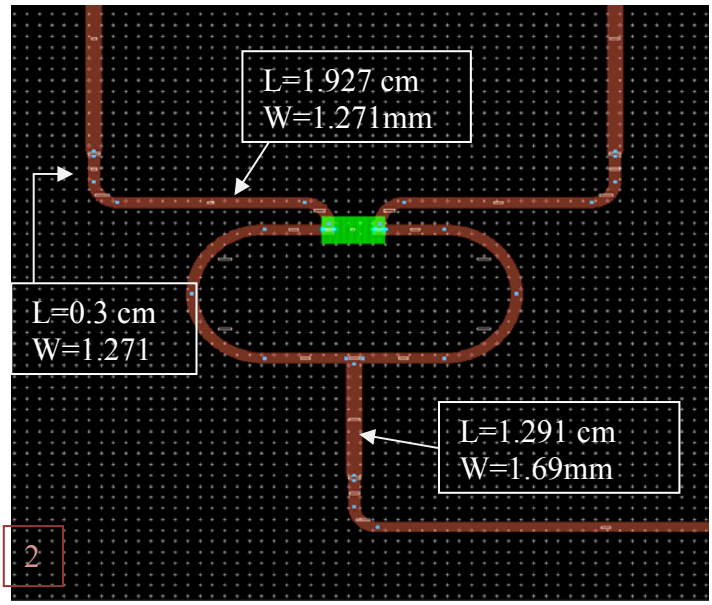
L=1.927 cm
W=1.271mm
L=0.3 cm
W=1.271
L=1.291 cm
W=1.69mm
2

(b)

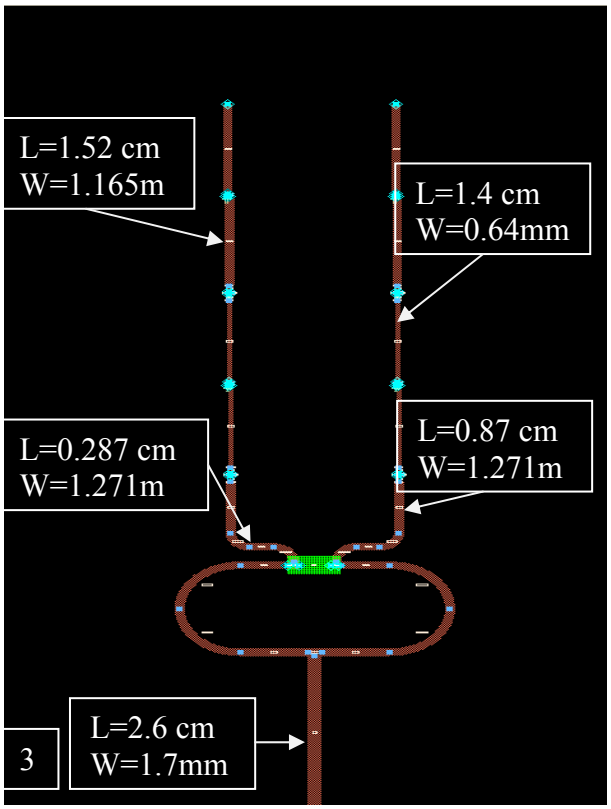

(c)

Figure 4.14: Length and width dimensions of microstrip lines of the 1:8 Wilkinson power divider.

In Fig. 4.15 the top side view of the designed circuit is drawn together with the phase shifters, attenuators and resistor chips.

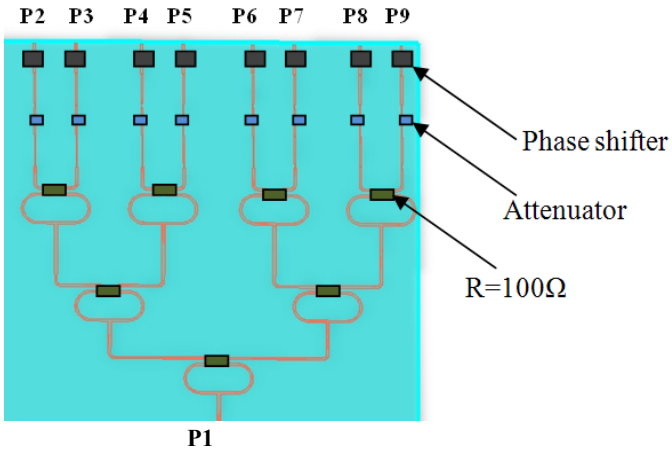

Figure 4.15: Microstrip power divider circuit.

The power divider designed and presented above is fabricated and depicted in Fig. 4.16:

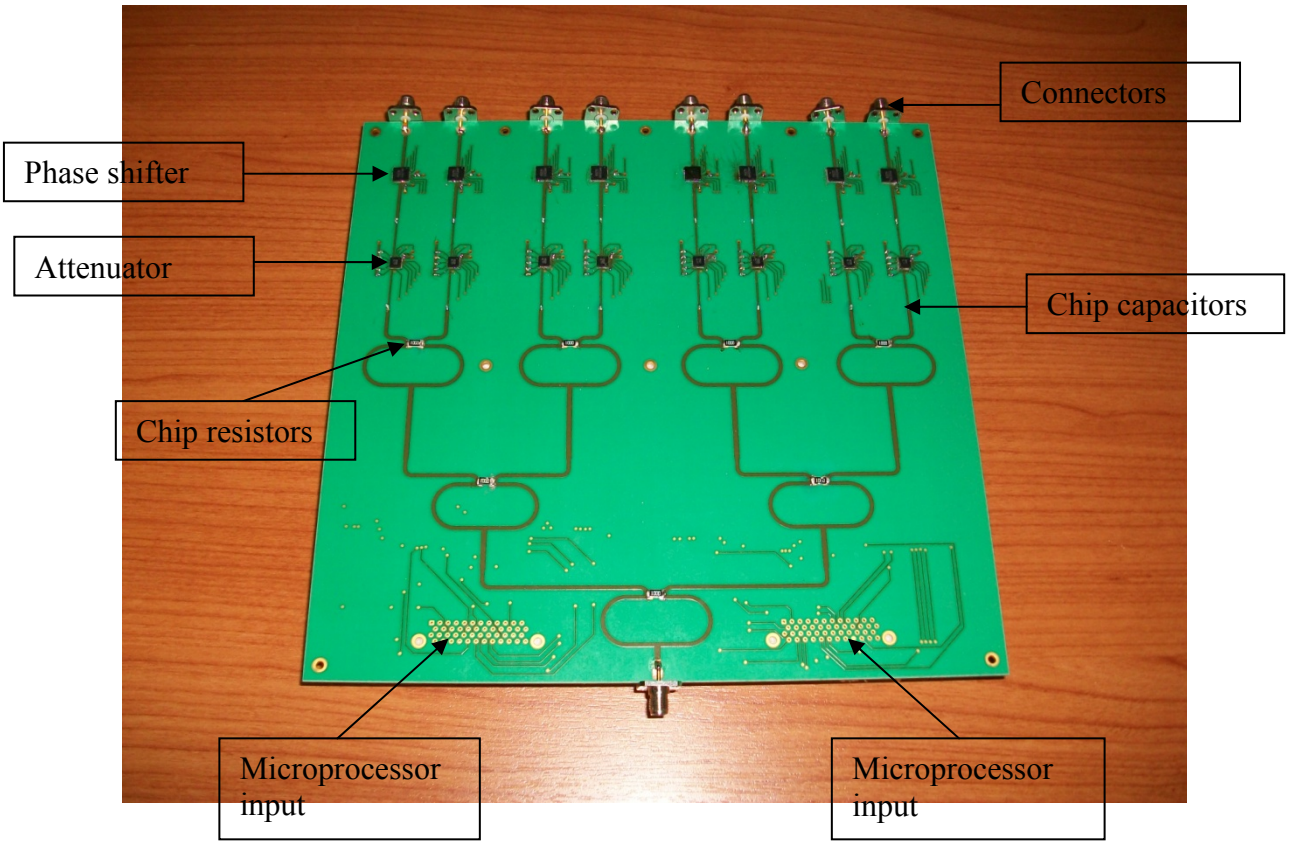

Figure 4.16: 1:8 Wilkinson Power Divider.

The above scheme shows a 1:8 Wilkinson power divider. Phase shifters [12], attenuators [13], capacitors, resistors [14] and connectors are mounted on the corresponded positions. Two such dividers are going to excite a 16 element array. This array will establish the backhaul link connecting Relay Station and Base Station.

The dimensions of the Wilkinson power divider (Fig. 4.16) are 21.2×21.8cm. Fig. 4.17 depicts the S_{11} at the input of the 1:8 power divider.

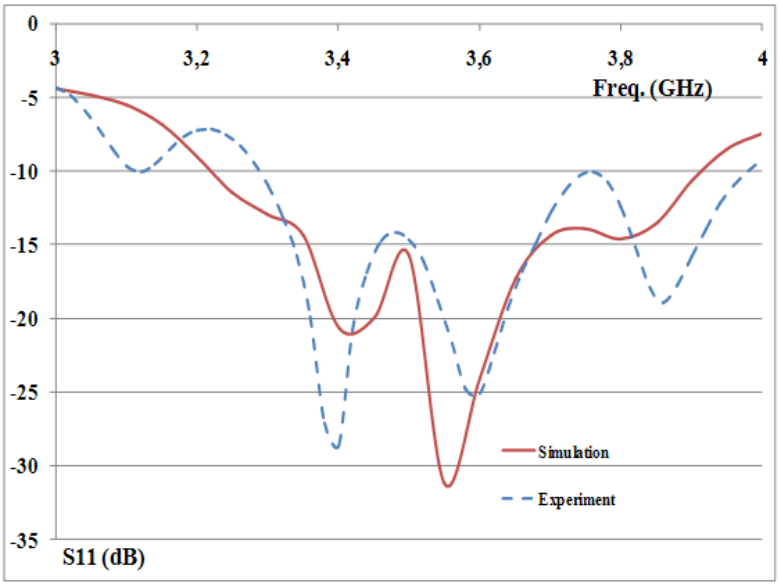

Figure 4.17: S_{11} vs. frequency.

Measurements of S_{11} parameter have been carried out using Anritsu MS6036A VNA. The designed beam forming circuit operates in 3.3GHz to 4GHz frequency range presenting 700MHz bandwidth (S_{11}< -10dB). The minimum value of S_{11} is -27,112dB for 3.38GHz. The simulated and experimental curves depicted in Fig. 4.17 are in good agreement. Their differences are caused due to ohmic, dielectric and conductor losses and microstrip line coupling. The designed beam forming circuit presents adequate bandwidth that covers the operation frequencies of the array presented in the previous section. Thus the array and the beam forming circuit can be efficiently combined.

Fig. 4.17 has been derived assigning 0 dB attenuation and 0^o phase shift at each attenuator and phase shift correspondingly.

The schematic that describes the total configuration of the beamforming circuit that feeds the 16 element array is depicted below:

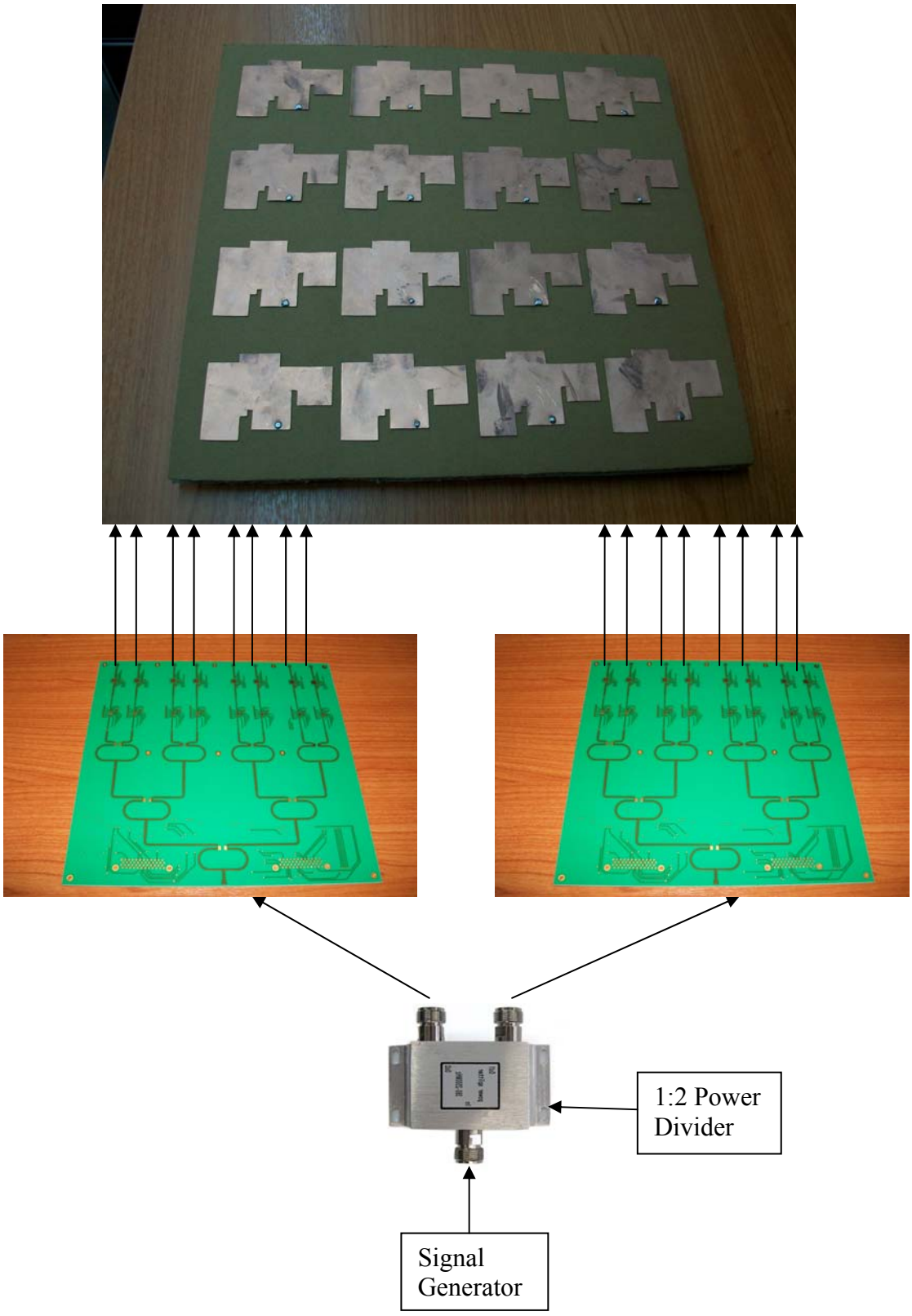

Figure 4.18: Total experimental setup of beam forming circuit with the array.

4.4.2 LMS Algorithm

Least Mean Square algorithm was applied by beam steering control unit (Fig. 4.1) to steer the main lobe of radiation to desired direction, put nulls and suppress side lobes. Using Mathcad v.14, a mask that represents the ideal radiation pattern with the desired characteristics is depicted. Then LMS is applied in order to derive the attenuation and phase of signals that enter each radiation element and produce an array pattern that approximates mask.

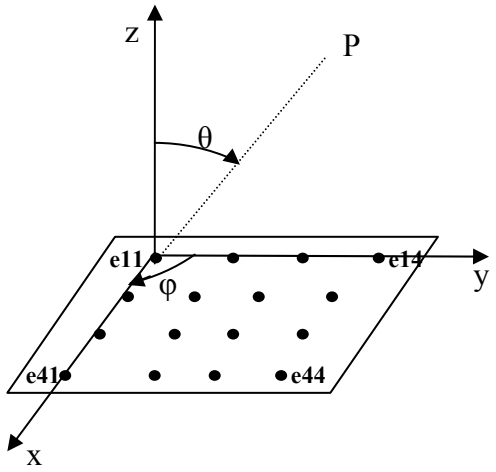

Figure 4.19: 16 element array and coordinate system.

Fig. 4.19 shows a planar array of 16 elements with a Cartesian coordinate system. Angles of interest (θ,φ) are also denoted.

The array factor used for the above planar array has the following form [15]:

$$AF(\theta,\varphi,a,b)=\sum_{m=1}^{4}\sum_{n=1}^{4}a_{mn}\exp\{i[(k(m-1)d\sin\theta\cos\varphi+k(n-1)d\sin\theta\sin\varphi-b_{mn}]\} \quad 4.16$$

where:

a_{mn} is a 4×4 matrix that represents the magnitude of the signal that enters mn radiation element

b_{mn} is a 4×4 matrix that represents the phase of the signal that enters mn radiation element

$k=2\pi/\lambda_0$ is the wave number equal to 73.3

m, n are physical numbers

d=7.45cm is the distance between two adjacent elements (center to center)

The radiation pattern of a rectangle patch element is approximately [15]:

$$E_e(\theta) = \frac{\sin(\frac{kh}{2}\cos\theta)}{\frac{kh}{2}\cos\theta}\cos(\frac{kL_e}{2}\sin\theta) \qquad 4.17$$

where $k=2\pi/\lambda_0$ is the wave number equal to 73.3

λ_0=8.57cm for 3.5GHz

h=8.47mm is the total substrate thickness of the array

L_e is the effective length of the patch

The total far field electric field produced by the array is:

$$E_t(\theta,\varphi) = \frac{e^{-jkr}}{r}AF(\theta,\varphi,a,b)E_e(\theta) \qquad 4.18$$

A reference signal is formed based on required radiation pattern characteristics. Requirements include specific angle of maximum, angle of null and side lobe level suppression. The studied scenario involves the following demands: Maximum at: (θ, φ)=(40, 0), Null at (θ, φ)=(30, 0) and side lobe SLL<-10dB. Angles are in degrees. The resulted reference signal has the form depicted in Fig. 4.20:

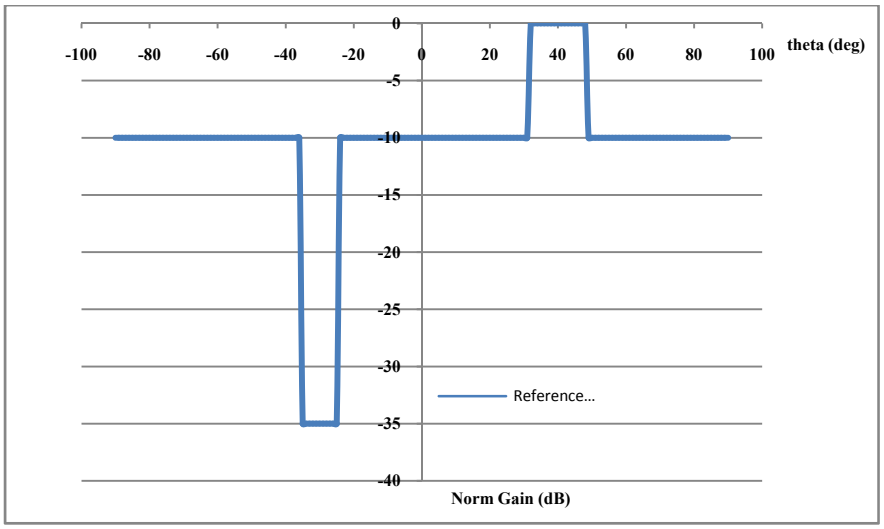

Figure 4.20: Reference signal for maximum in (40^o, 0^o), minimum in (-30^0, 0^0), SLL< -10dB.

After applying the algorithm, the amplitudes and phases of signals that excite radiation elements and produce a radiation pattern that approximates reference signal are calculated. Amplitude and phase matrices are:

$$a = \begin{bmatrix} a_{11} & a_{12} & a_{13} & a_{14} \\ a_{21} & a_{22} & a_{23} & a_{24} \\ a_{31} & a_{32} & a_{33} & a_{34} \\ a_{41} & a_{42} & a_{43} & a_{44} \end{bmatrix} = \begin{bmatrix} -15 & -3 & 0 & 0 \\ 0 & 0 & 0 & 0 \\ 0 & 0 & 0 & 0 \\ 0 & 0 & 0 & -12 \end{bmatrix} \text{ in dB} \qquad 4.19a$$

$$\text{and } b = \begin{bmatrix} b_{11} & b_{12} & b_{13} & b_{14} \\ b_{21} & b_{22} & b_{23} & b_{24} \\ b_{31} & b_{32} & b_{33} & b_{34} \\ b_{41} & b_{42} & b_{43} & b_{44} \end{bmatrix} = \begin{bmatrix} 348.88 & 202.53 & 219.44 & 90 \\ 22.50 & 95.65 & 236.35 & 22.50 \\ 331.96 & 286.62 & 264.44 & 0 \\ 101.28 & 146.23 & 180.06 & 337.59 \end{bmatrix} \text{ in deg} \qquad 4.19b$$

Let us mention here that attenuation matrices a and b have a quantized range of values which is: a=[0, -3, -6, -9, -12, -15, -18, -21, -24, -27, -30, -33, -36, -39, -42, -45] dB and b=[0, 0, 5.625, 11.250… 354.375] in deg with angle step of 5.625^0.

Matrices 4.19a and 4.19b are introduced in Equation 4.16 and 4.18 giving the total field depicted in Fig. 4.21:

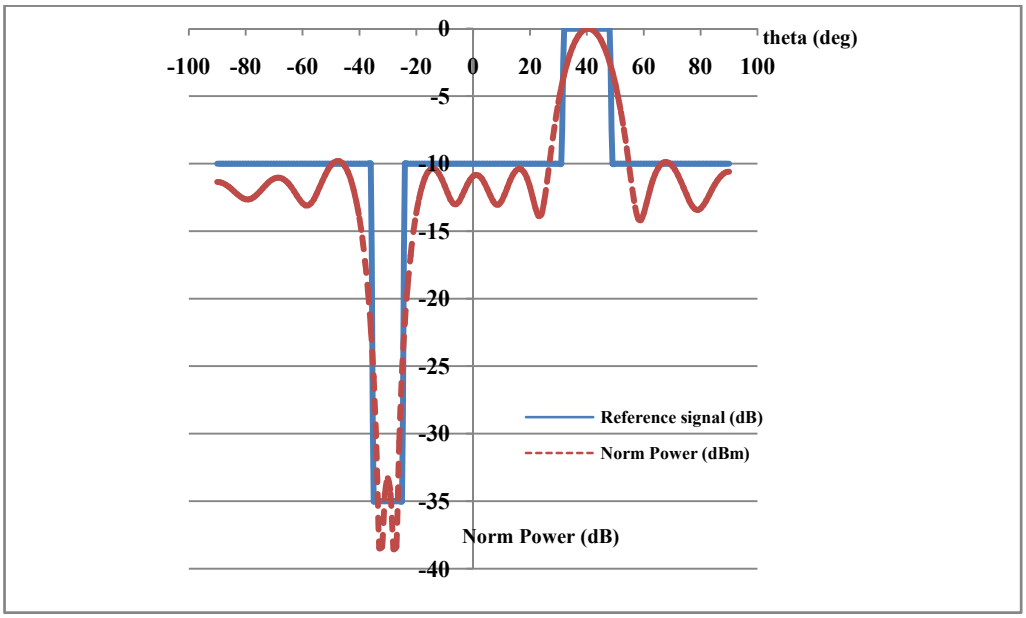

Figure 4.21: Radiation pattern of 4×4 array with reference signal.

Two patterns of Fig. 4.21 present 78.43% convergence and 31.1sec convergence time.

4.5 BEAMFORMING ANTENNA TESTING

The LMS algorithm presented in the previous section was applied in the testing board described in Fig. 4.18. Three scenarios of beam forming have been considered and presented below:

a. Maximum at (-18^0,0^0), null at (34^0, 0^0) and Side Lobe level SLL<-10dB.

The algorithm gives the following results in terms of amplitude and phase:

$$\alpha = \begin{bmatrix} -6 & 0 & 0 & 0 \\ -3 & -6 & -6 & -6 \\ -6 & -6 & -6 & -3 \\ 0 & 0 & 0 & -6 \end{bmatrix} \text{ in dB} \qquad 4.20a$$

$$\beta = \begin{bmatrix} 298.2 & 275.73 & 298.2 & 191.8 \\ 258.82 & 16.85 & 135 & 140.67 \\ 90 & 163.14 & 315.05 & 208.2 \\ 123.76 & 0 & 326.35 & 315.05 \end{bmatrix} \text{ in deg} \qquad 4.20b$$

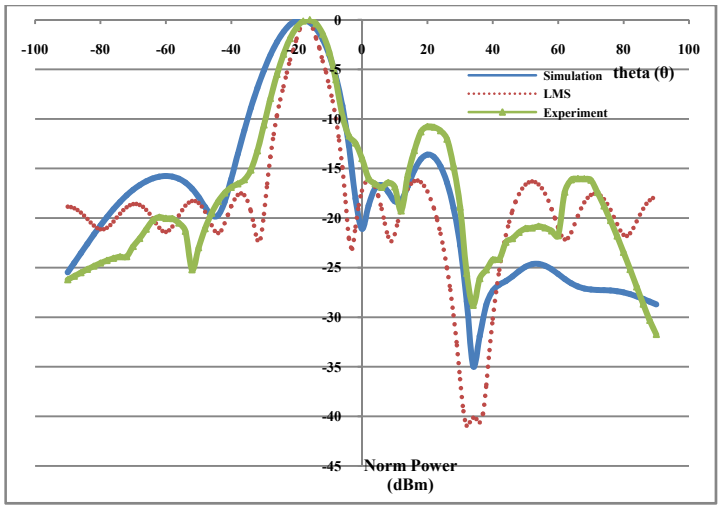

Figure 4.22: Simulated and experimental radiation pattern of 16 element array for scenario (a).

Fig. 4.22 shows that scenario requirements are met. Side lobe levels on all three curves are below -10dB. Angle of null is 34^0 while angle of maximum is -18^0. LMS algorithm considers an array of rectangle patches with no mutual coupling. On contraire in simulation curve, E-shaped radiation elements have been considered with mutual coupling. That is why these two curves do not coincide. The experiment curve comprises ohmic, dielectric and conductor losses, line coupling and imbalance phenomena of attenuators and phase shifters. Imbalance phenomena are relevant to the weakness of attenuator and phase shifter to adjust precise values of amplitude and phase. In spite of these imbalances and losses the radiation pattern has the desired form.

b. Maximum at $(22,0^0)$, null at $(80^0, 0^0)$ and Side Lobe level SLL<-10dB.

For scenario (b) the same procedure as above has been performed. LMS algorithm gives the following results:

$$\alpha = \begin{bmatrix} -3 & 0 & 0 & 0 \\ -6 & -6 & -6 & -3 \\ -6 & -6 & -6 & -6 \\ 0 & 0 & 0 & -3 \end{bmatrix} \text{ in dB} \qquad 4.21a$$

$$\beta = \begin{bmatrix} 236.2 & 264.3 & 179.9 & 118.0 \\ 33.7 & 168.7 & 112.4 & 354.3 \\ 112.4 & 337.4 & 309.3 & 78.7 \\ 0 & 286.4 & 213.7 & 241.7 \end{bmatrix} \text{ in deg} \qquad 4.21b$$

Relevant curves are depicted in Fig. 4.23.

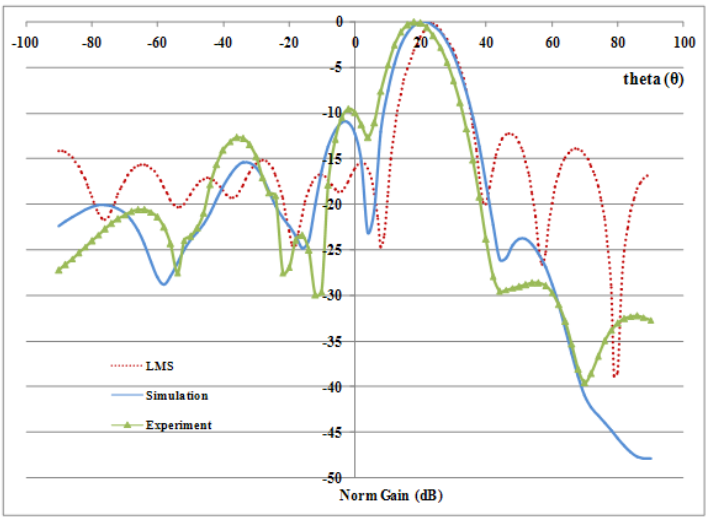

Figure 4.23: Simulated and experimental radiation pattern of 16 element array for scenario (b).

Blue line of Fig. 4.23 meets the specified requirements set by scenario (b) except from maximum of main lobe. The simulation curve presents $\theta_{max}=20^0$. This slight difference may be caused by E-shaped antenna elements and mutual coupling effects.

The experimental line presents maximum at $\theta_{max}=18^0$. This 4^0 deviation compared to the ideal radiation pattern (LMS curve) is caused by losses in power divider and imbalance phenomena.

c. Maximum at (-22,0^0), null at (20^0, 0^0) and Side Lobe level SLL<-10dB.

For scenario (c) the LMS algorithm gives the following results:

$$\alpha = \begin{bmatrix} -12 & 0 & 0 & 0 \\ -3 & 0 & 0 & 0 \\ 0 & 0 & 0 & -3 \\ 0 & 0 & 0 & -12 \end{bmatrix} \text{ in dB} \qquad 4.22a$$

$$\beta = \begin{bmatrix} 315.05 & 303.8 & 236.35 & 270.05 \\ 129.3 & 11.25 & 118.14 & 219.43 \\ 129.38 & 151.91 & 112.52 & 174.43 \\ 0 & 354.48 & 354.48 & 337.58 \end{bmatrix} \text{ in deg} \qquad 4.22b$$

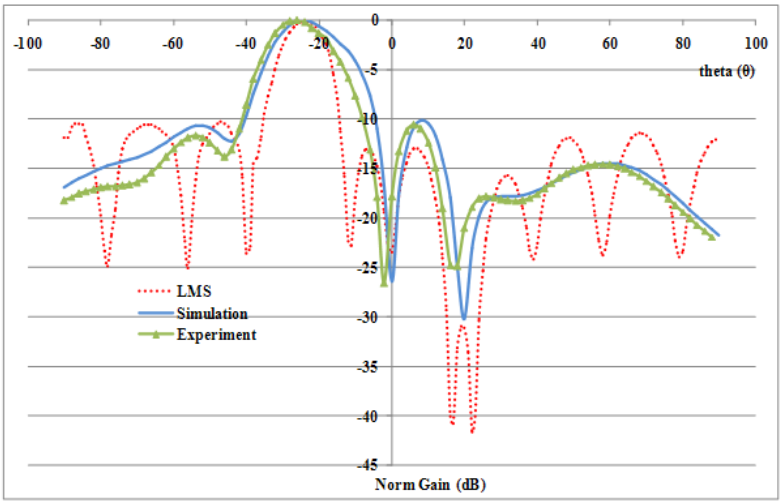

Figure 4.24: Simulated and experimental radiation pattern of 16 element array for scenario (c).

In this case simulation and experiment agree at high level and differ from the LMS curve. The last one presents maximum at -22 deg while the experiment curve seems to be maximized at -21 deg.

4.6 FIELD MEASUREMENTS

In order to examine the beam forming features of the designed array, the experimental setup depicted in Fig. 4.18 is realized. Experiments take placed inside anechoic chamber, where the investigated antenna is set to the opposite side of a receiver antenna. Radiation pattern of the array takes several forms dependent on the amplitude and phase definitions. Signal generator is set to emit a sinusoidal wave of 3.5GHz. For each radiation pattern case a spectrum analyzer connected to the receiver antenna records the received signal strength in terms of distance l. The l parameter is connected to angle θ (theta) through the expression:

$$\tan\theta = \frac{l}{s} \qquad 4.23$$

Finally the diagram of the normalized received power is expressed as a function of the angle θ (theta).

The orientation of the array inside anechoic chamber is depicted below. Figure clearly shows the angle of interest θ (theta).

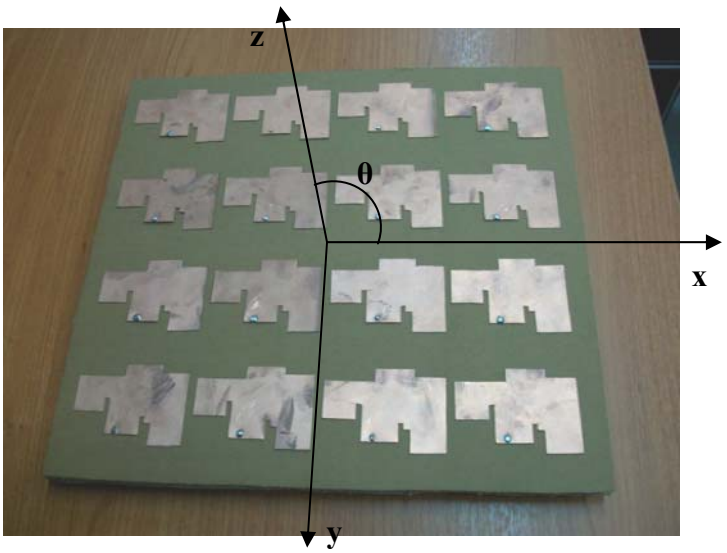

Figure 4.25: 16 element array with coordination system.

The experimental gain of the array is derived using the formula [1]:

$$Gt(dB) = 20\log(\frac{4\pi R}{\lambda}) + 10\log(\frac{Pr}{Pt}) - Gr(dB) \qquad 4.24$$

where Gt is the gain of the array, Gr is the gain of the antenna receiver, R is the distance between the two antennas, λ is the wavelength, Pr is the power transmitted by the array and Pt is the power accepted by the receiver antenna.

Fig. 4.26 and 4.27 describe the experimental setup during the procedure of evaluating the radiation pattern of the tested antenna for the scenarios denoted in section 4.5.

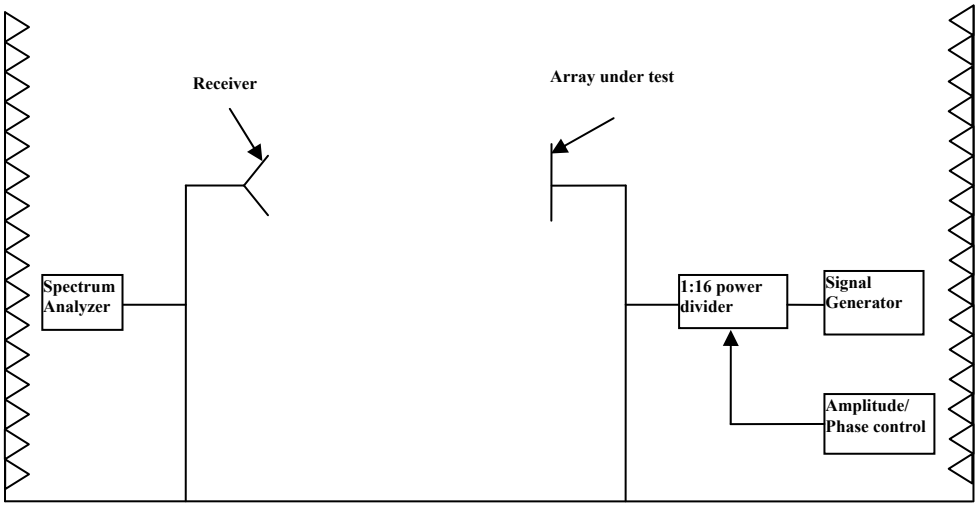

Figure 4.26: Side view of field measurements configuration.

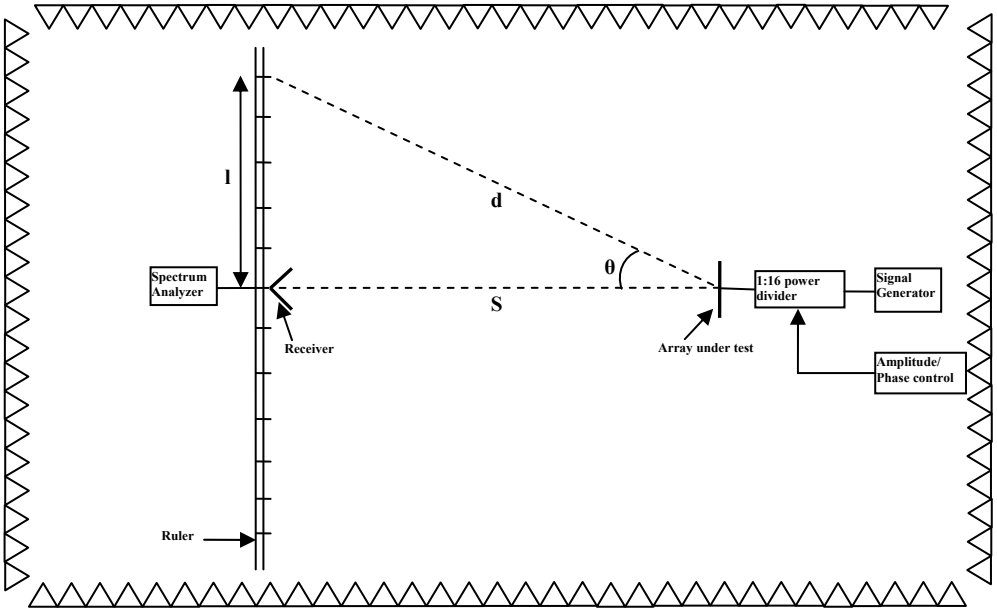

Figure 4.27: Top view of field measurements configuration.

The Amplitude/Phase control unit is described in Fig. 4.28. It includes the

- AVR EVK 1100 microcontroller of Atmel,
- 74HC154 chip (4 to 16 line decoder/demultiplexer),
- 74VHC139 chip (Dual 2 to 4 decoder/demultiplexer)
- 74LS164 chip (serial in parallel out shift register)

Both decoders are used for the addressing phase shifters and attenuators while shift register transforms a serial to parallel bit stream to forward it to the proper device.

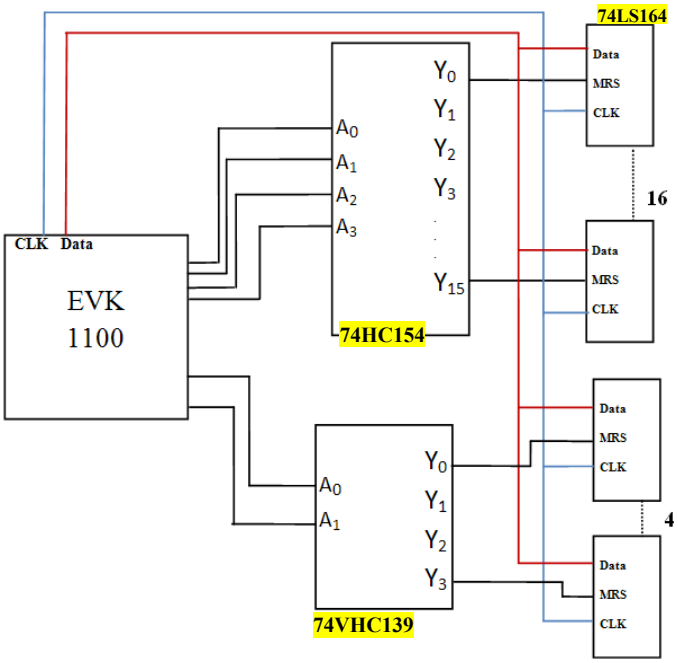

Figure 4.28: Amplitude/Phase control unit.

Shift registers depicted in Fig. 4.28 are further connected to phase shifters and attenuator chip as described in Fig. 4.29. Physical realization of Fig. 4.28 is depicted in Fig. 4.29.

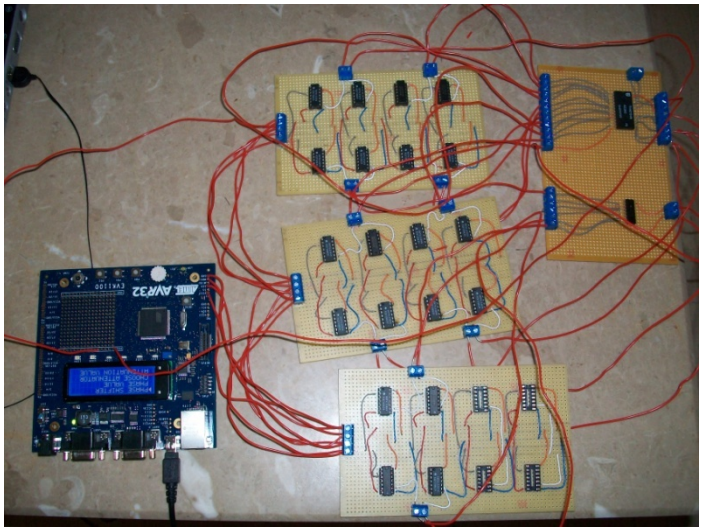

Figure 4.29: Configuration of Amplitude/Phase control unit.

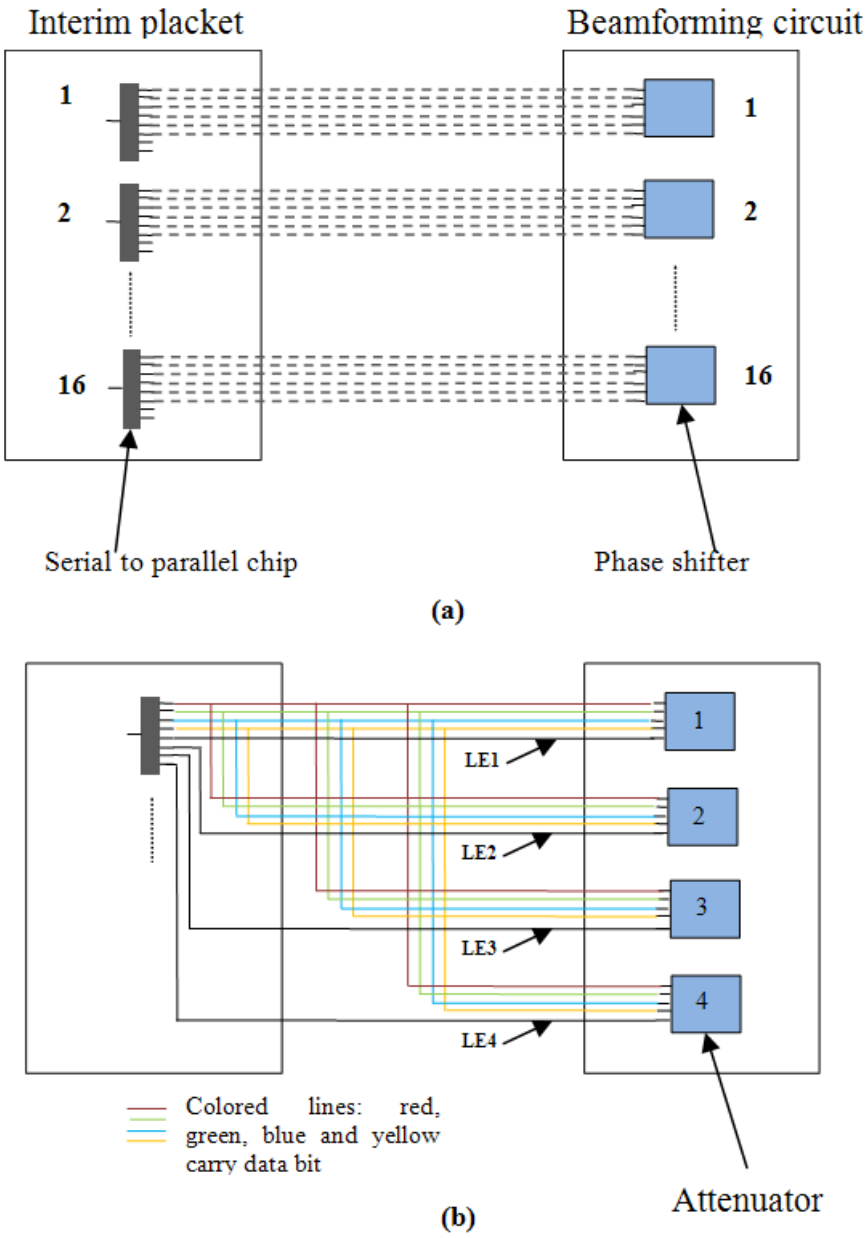

Figure 4.30: Amplitude/Phase control unit together with beam forming circuit.

Shift register (Serial to parallel chip) 74LS164 is used to provide the required information to the phase shifters and attenuators depicted above. Fig. 4.30 shows that each shift register is directly connected to each phase shifter individually. Digital bit information enters serial to parallel chip in serial form and then is transferred to phase shifter in parallel from.

Regarding attenuators, one shift register can serve four attenuators as can be seen in Fig. 4.30b. So four shift registers are needed to support 16 attenuators. The latter receive a four bit word to assign proper amplitude. The operation is similar to the previous one but now the attenuators are equipped with Latch Enable property (LE). When LE1 is HIGH (logic one), the corresponded attenuator is able to receive information. When LE1 is LOW (logic zero), the attenuator does not receive any data.

The state of the attenuator is controlled, besides LE feature, from Power Up 1 (PUP1) and Power Up 2 (PUP2) options. According to datasheet of the attenuator PUP1 and PUP2 should be kept at high state so that the device could provide the whole attenuation range.

4.7 CONCLUSIONS

Chapter 4 presented the design, simulation, fabrication and evaluation of a new access and backhaul antenna to be incorporated with a Relay Station. Both antennas are based on microstrip technology which provides advantages outlined in chapter 1. The access antenna provides gain 10dB and bandwidth 520MHz while the backhaul antenna provides gain 21dB and bandwidth 424MHz for the frequency band of 3.4GHz. These features are compliant with the air interface specifications of the IEEE802.16j protocol which is referred to the Relay based mobile WiMAX. Let us mention here that both antennas are operating in the same frequency band and thus making their utilization by network operators very advantageous. Regarding backhaul antenna, a new feeding network design was presented and tested, providing sufficient behavior in terms of the S parameters for the frequency range of interest. Moreover the backhaul antenna which is actually a phased array was tested regarding its beam forming features. Some radiation

pattern scenarios were considered where the experimental results were satisfactory and accepted. The work done in chapter 4, proved the proper operation of the access and backhaul antenna under a Relay based network.

4.8 REFERENCES

[1] C. Balanis, “Antenna Theory; Analysis and Design”, second edition, Wiley and Sons, New York, 1982.

[2] Y. Azmir, R. Syamsul, I. Alyani, “A New Approach for Bandwidth Enhancement Technique in Microstrip Antenna for Wireless Applications”, RF and Microwave Conference, pp. 205-209, September 2006.

[3] James R. James, Jim R. James, “Handbook of microstrip antennas”, Institution of Electrical Engineers, 1989.

[4] D.R. Jackson, N. G. Alexopoulos, “Simple formulas for the input impedance, bandwidth, and radiation efficiency of a rectangular patch”, Antennas and Propagation Society International Symposium, Digest, vol. 2, pp.1130-1133, 26 30, January 1989.

[5] F. Abboud, J. P. Damiano, A. Papiernik, "Accurate model for the input impedance of coax-fed rectangular microstrip antenna with and without air-gaps," Sixth International Conference on Antennas and Propagation, pp.102-106 vol.1, 4-7 Apr 1989.

[6] F. Yang, Xue Xia Zhang, Xiaoning Ye, Y. Rahmat Samii, “Wide band E shaped patch antennas for wireless communications”, IEEE Transactions on Antennas and Propagation, vol. 49, no. 7, pp. 1094-1100, July 2001.

[7] X. Zhang, F. Yang, “Study of a slit cut on a microstrip antenna and its applications”, Microwave Optical Technology Letters, John Wiley & Sons, Inc. pp. 297–300, 1998.

[8] H. J. Visser, “Array and Phased Array Antenna Basics”, Wiley, 2005.

[9] D. M. Pozar, “Microwave Engineering”, third edition, John Wiley & Sons, 2004.

[10] D. M. Pozar, “Microwave and RF Design of Wireless Systems”, John Wiley & Sons, 2000.

[11] E. O. Hammerstad, “Equations for Microstrip Circuit Design”, 5th European Microwave Conference, pp. 268-272, 1 4 September 1975.

[12] Hittite HMC648LP6, Hittite Microwave Corporation, Chelmsford, MA, 2008.
Link: http://www.hittite.com/content/documents/data_sheet/hmc648lp6.pdf

[13] Hittite HMC629LP4, Hittite Microwave Corporation, Chelmsford, MA, 2008.
Link: http://www.hittite.com/content/documents/data_sheet/hmc629lp4.pdf

[14] IMS024 Power Series single sided resistors, International Manufacturing Services, Portsmouth, Rhode Island.
Link: http://www.ims resistors.com/IMSpowersingleside.pdf

[15] C. A. Balanis, “Modern Antenna Handbook”, Wiley Interscience, 1st edition, 2008.

CHAPTER 5

COUPLING EFFECTS AND MEASUREMENTS

5.1 INTRODUCTION

A definition of coupling together with mathematical formulas is denoted in this chapter. Equation for mutual voltage and impedance are derived and methods of extracting coupling coefficient are stated and proved. In addition chapter 5 also mentions some studies regarding coupling estimation and reduction methods including Electromagnetic Band Gap (EBG) structures for surface wave and coupling degradation. Such structures are depicted and commented.

In chapter 5, two new designs of access and backhaul antenna are presented and their features are depicted and commented. Both antennas are based on low cost FR4 substrate and they operate in the same frequency. Two new antenna configurations are proposed and tested in terms of coupling. The purpose of these tests is to achieve low interaction between the antenna elements and combine the corresponding antenna configuration with the Relay Station.

5.2 BASIC TERMS OF COUPLING

The interaction between two or more antenna elements can be described by coupling coefficient. The latter can be defined in two ways dependent of whether the antenna

elements emit or receive power [1]. In the case of emission of two radiation elements placed closed to each other, coupling coefficient is described as:

$$C_e = \frac{P_2}{P_1} \tag{5.1}$$

where P_2 is the power accepted by antenna 2 and P_1 is the power carried by antenna 1. In the case of reception coupling coefficient is expressed as:

$$C_r = \frac{P_2}{P_1} \tag{5.2}$$

where P_2 is the power impinged on antenna 2 due to antenna 1 and P_1 is the power accepted by antenna 1 due to external field.

It is derived that C_e and C_r can be written in terms of scattering parameters.

$$C_e = \frac{|S_{21}|^2}{1-|S_{11}|^2} \tag{5.3}$$

$$C_r = \frac{|S_{21}|^2}{|1+S_{11}|^2} \tag{5.4}$$

The phenomenon of coupling can also be measured by the form [2]:

$$C = 20\log\left(\frac{2Z_{12}R_N}{(Z_r+R_N)^2 - Z_{12}^2}\right) \tag{5.5}$$

where Z_{12} refers to the mutual impedance interaction between the antennas 1 and 2, Z_r is the input impedance and R_N the normalization resistance.

Coupling affects the pattern of an array [3]. Let us consider the case of an M×N planar array of identical elements placed at equal distance between them (Fig. 5.1).

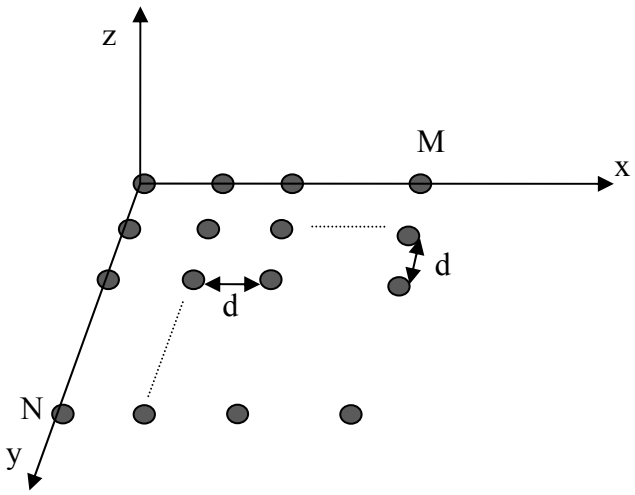

Figure 5.1: Planar array of M×N identical elements.

The voltage appeared in the mn^{th} element due to current in pq^{th} element is equal to:

$$V_{mn} = \sum_{p}\sum_{q} Z_{mn,pq} I_{pq} \qquad 5.6$$

where $Z_{mn,pq}$ is the impedance that presents the mn^{th} element due to the current in the pq element. I_{pq} is the current of the pq^{th} element. The impedance of the mn^{th} element would then be:

$$Z_{mn} = \frac{V_{mn}}{\mathrm{I}_{mn}} = \sum_{p}\sum_{q} Z_{mn,pq} \frac{I_{pq}}{I_{mn}} \qquad 5.7$$

Total impedance of an element would be the addition of the self impedance of the element (mn=pq) plus the mutual impedances ($mn \neq pq$).

A method of computation the mutual impedance has been proposed by Newman, Richmond and Kwan [4] using Method of Moments. Let us consider the case of two patch antennas placed nearby (Fig. 5.2). Both patches lie on a substrate of dielectric constant ε_r and thickness h. The one patch is excited through coaxial cable by current of density J_i. J_s is the current that rises on both patches.

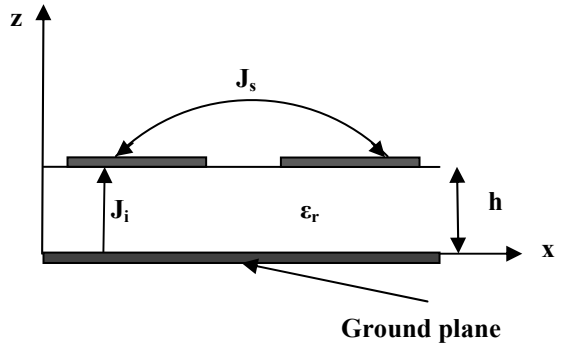

Figure 5.2: Two patches excited by currents J_i and J_s.

If N current shapes are developed on both patches, the integral equation that associates J_i and J_s is:

$$-\iint_S J_s E_m ds = \int_L J_i E_m dl\,, \qquad \text{m=1,2,…N} \qquad 5.8$$

where S is the surface of the patches and L the length of the feeding line.

Current density J_s can be written as:

$$J_s = \sum_{n=1}^{N} I_n J_{mn} \qquad 5.9$$

where I_n are unknown coefficients and J_{mn} are known current functions.

By substitution of Equation 5.9 to Equation 5.8 it is derived that:

$$V_m = \sum_{n=1}^{N} I_n Z_{mn} \qquad 5.10$$

where $V_m = \int_L J_i E_m dl$ and $Z_{mn} = -\iint_S J_s E_m ds$

As current density functions for the rectangle patch are chosen:

$$J_m = \frac{\sin[k(h-|x|)]\hat{x}}{w\sin(kh)} \qquad 5.11$$

where $k=2\pi/\lambda$, h is the thickness of substrate and w the width of the patch.

A way to evaluate and depict mutual coupling effect to radiation pattern was described by Steyskal and Herd [5]. For a linear array of receiving elements depicted in Fig. 5.3, the total array pattern would be:

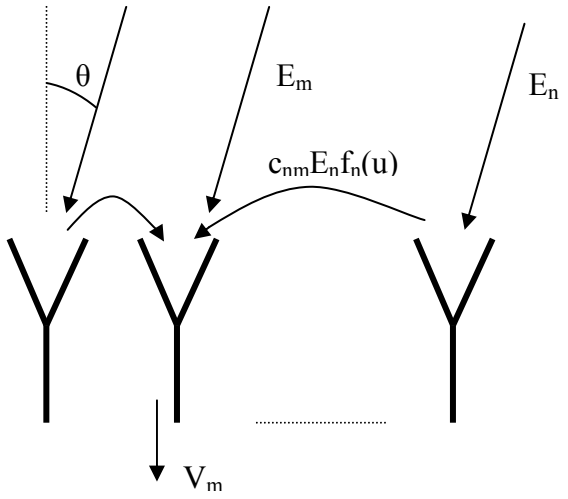

Figure 5.3: Linear array with coupling effect.

$$F(\theta) = \sum_n a_n f_n(\theta) e^{jnkd\sin(\theta)} = f^a(\theta) \sum_n a_n e^{jnkd\sin(\theta)} + \sum_n a_n \delta f_n(\theta) e^{jnkd\sin(\theta)} \qquad 5.12$$

where $\alpha_n = |a_n| e^{j\varphi_n}$ is the complex weight of the incident wave in terms of the excited amplitude and phase. $F_n(\theta)$ is the array pattern, $f^a(\theta)$ is the isolated element pattern, and $\delta f_n(\theta)$ is the element pattern due to coupling.

Total array pattern from a specific direction (θ) is the summation of the element pattern plus a term that expresses the coupling effect.

Total voltage induced at the m^{th} element can be written as:

$$u_m(\theta) = c_{mn} E_m f^i(\theta) \qquad 5.13$$

where c_{mn} is the coupling matrix that expresses the interaction of the m element from n. E_m expresses the field that impinges on the m^{th} element and $f^i(\theta)$ represents the isolated element pattern.

Equation 5.13 can be written in matrix form as:

$$\begin{bmatrix} u_1(\theta) \\ \vdots \\ u_N(\theta) \end{bmatrix} = c_{mn} \begin{bmatrix} u_1'(\theta) \\ \vdots \\ u_N'(\theta) \end{bmatrix} \qquad 5.14$$

where the matrix on the left represents the voltages at the output of the elements and the matrix on the right includes the voltages without mutual coupling consideration.

Coupling coefficient c_{mn} can be derived solving the equation:

$$g_m(\theta) = f^i(\theta) \sum_n c_{nm} e^{jnkd\sin(\theta)} \qquad 5.15$$

Equation 5.15 finally gives:

$$c_{nm} = \frac{1}{2\pi} \int_{-\frac{\pi}{kd}}^{\frac{\pi}{kd}} \frac{g_m(\theta)}{f^i(\theta)} e^{-jnkd\sin(\theta)} \qquad 5.16$$

where $g_m(\theta)$ is the voltage output from the m^{th} element, k is the wavelength and d is the distance between the elements.

Another way to evaluate the coupling coefficient is to write the field created by a linear array in the following form:

$$E_m = \sum_n u_n f^i(\theta) \frac{e^{-jkr}}{r} = f^i(\theta) \frac{e^{-jkr}}{r} \sum_n u_n \qquad 5.17$$

Element m is excited and all the others are terminated. The voltage appeared in the element n is:

$$u_n = (\delta_{nm} + s_{nm})a_m \qquad 5.18$$

where δ_{nm} is the delta of Kronecker defined as:

$\delta_{nm} = \begin{matrix} 1 \ldots n = m \\ 0 \ldots n \neq m \end{matrix}$ and s_{nm} is scattering matrix

By substitution of Equation 5.18 to Equation 5.17, the radiated field becomes:

$$\mathrm{E}_m = a_m f^i(\theta)\frac{e^{-jkr}}{r}\sum_n (\delta_{nm} + s_{nm})e^{jkn\sin(\theta)} \qquad 5.19$$

Or in matrix form: **C=I+S** 5.20

where **C** is the coupling matrix, **I** stands for the unitary matrix and **S** scattering matrix.

In [8] and [9], the relation between mutual coupling and the surface/reflected waves occurred in the substrate of a patch array, were investigated.

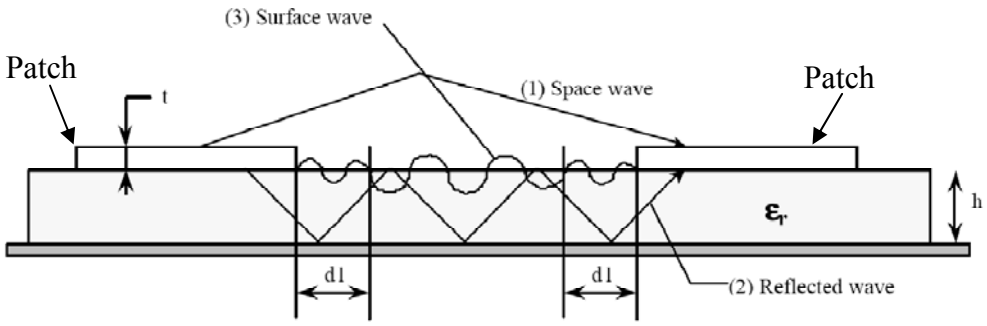

Figure 5.4: Surface and reflected waves between two patches.

In Fig. 5.4, the excitation of patch 1, leads to the creation of surface and reflected waves that travels from one patch to another through the substrate. It is claimed that:

- High values of dielectric constant ε_r, lead to enhanced reflected waves

- For small values of loss tangent tan(δ), the reflected waves have constant magnitude, regardless distance between patches and frequency
- If the distance between patches is: $d \geq \frac{5}{7}\lambda_g$, where λ_g is the wave length in the substrate, then surface wave occur. λ_g is dependent of dielectric constant and thickness of the substrate.

5.3 MUTUAL COUPLING ESTIMATION AND REDUCTION METHODS

Coupling between antenna elements is an unwanted phenomenon which degrades the performance of the system and needs to be reduced. One technique to achieve mutual coupling reduction is the introduction of electromagnetic band gap (EBG) structures among radiation elements. EBG configurations are periodic metallic constructions placed between antennas which introduce additional capacitance and inductance to the system and reduce the level of interaction among antenna elements. The shape of EBG structure varies and depends on substrate's thickness and operation frequency.

Pynttäri, Mäkinen, Heikkinen, Kivikoski [13] proposed a novel EBG configuration for reducing surface waves and mutual coupling (Fig.5.5).

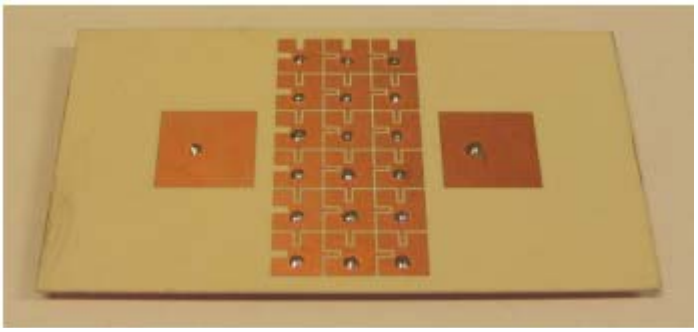

Figure 5.5: Two patches separated by EBG construction.

The construction depicted in Fig. 3.11 leads to a clear reduction of S_{21} parameter which implies a mutual coupling degradation. Fig. 5.6 shows that S_{21} is reduced because of the introduction of EBG structure.

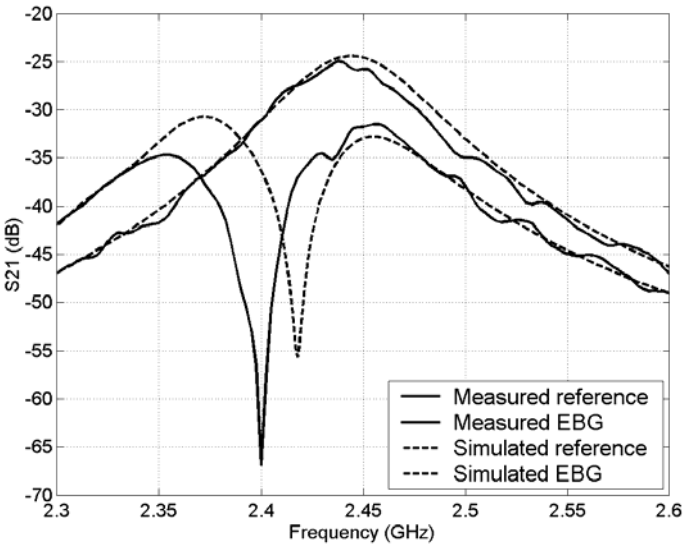

Figure 5.6: S_{21} parameter as a function of frequency.

Let us mention here that Jing Liang and Hung Yu David Yang [14] have investigated the EBG structure characteristics and shown that the resonant frequency of a patch antenna is affected by the presence of EBG structure.

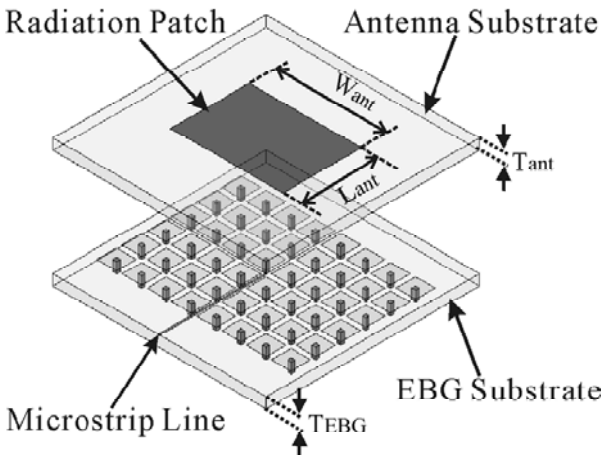

Figure 5.7: EBG and antenna configuration.

In Fig. 5.7 a first substrate includes the periodic metallic fabrication. Upon the first substrate is placed a microstrip line which feeds the configuration. A second substrate is then mounted above microstrip line, on the top of which lies the antenna. The table that follows includes the variations of operation frequency when EBG is used and when it is not used.

Table 5.1: Patch antenna operating frequency.

Patch Dimension (mm^2)	**Plain Antenna Resonant Freq (GHz)**	**EBGAntenna Resonant Freq (GHz)**
10×10	6.29	2.92
20×20	3.32	2.15
30×30	2.25	1.67
40×40	1.71	1.27
50×50	1.38	1.03
60×60	1.15	0.85

It is clear that the use of EBG structure alters the resonant frequency which takes lower values.

Fan Yang and Yahya Rahmat Samii [15] investigated the coupling effect between two patch antennas. First two patch antennas were placed close to each other in a thick and

high permittivity substrate. The latter broadens the bandwidth of the antenna system but also produces surface waves which lead to strong mutual coupling. The introduction of rows of mushroom like EBG structure between the antenna elements suppresses the coupling effect, by producing a frequency band gap. That gap forbids waves which fall within a certain frequency range to propagate. Fig. 5.8 shows the experimental configuration.

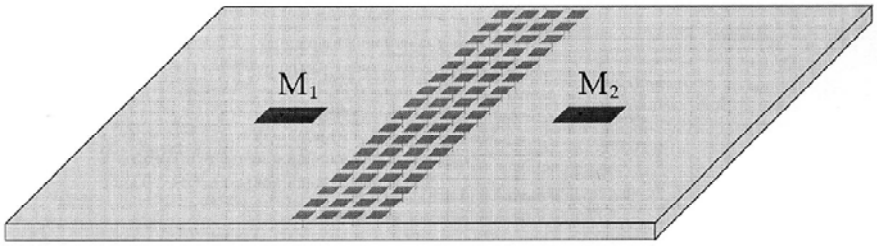

Figure 5.8: M_1 and M_2 is patch antenna separated by a three row EBG structure.

The EBG structure is depicted below and it is consisted of metallic plains placed on the substrate and connected with vias to the ground plane (Fig. 5.9).

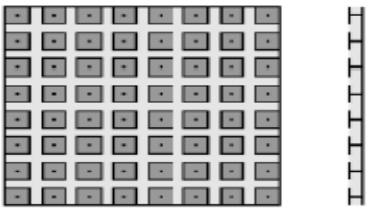

Figure 5.9: EBG structure.

The additional inductance and capacitance that the EBG structure introduces is:

$$L = \mu_0 h \qquad 5.21$$

$$C = \frac{W\varepsilon_0(1+\varepsilon_r)}{\pi} \coh^{-1}\left(\frac{2W+g}{g}\right) \qquad 5.22$$

where μ_0 is the free space permeability,

ε_r is the free space dielectric constant,

g is the width of the gap,

h the substrate's height,

W the patch width

The additional inductance comes from the current that flows through vias and the capacitance because of the adjacent patches. Finally the bandwidth of the gap is determined by the equation:

$$BW = \frac{1}{\eta}\sqrt{\frac{L}{C}} \qquad 5.23$$

where η is the impedance of free space equal to 120π.

Another work that proves the efficiency of EBG structure to reduce coupling has been published by F. Caminita et. all [18]. This study presents two patch elements separated by a "cactus" shaped EBG structure including stubs as can be seen in Fig. 5.10a and 5 .10b.

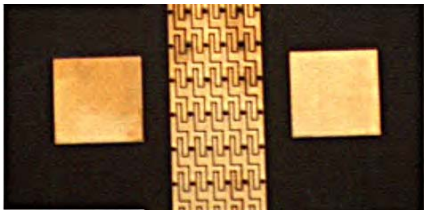

(a)

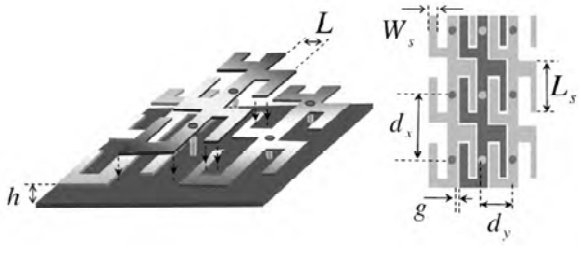

(b)

Figure 5. 10: Proposed patches with EBG structure; (a) Experimental setup (b) EBG structure.

All structure is placed on a substrate of ε_r=2.33 and height h=1.524mm.

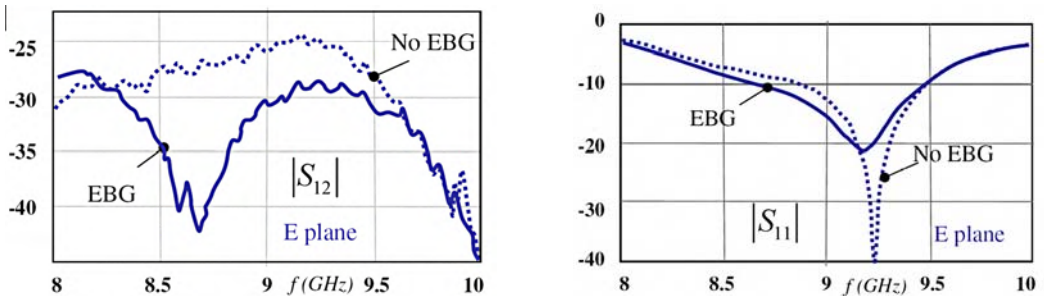

(a) **(b)**

Figure 5. 11: Scattering parameters of patch elements; (a) S_{12} with and without EBG structure (b) S_{11} with and without EBG structure.

The use of EBG structure clearly increases the value of S_{11} parameter for 9.2GHz but also reduces the level of coupling for about 5dB (Fig. 5.11).

Another method for mutual coupling reduction is the Defect Ground Structure (DGS). It is realized by etching shapes on ground plane. These shapes change the capacitance and inductance of ground plane, affecting the current distribution [19]. Salehi et. all [20] presented a DGS configuration and compared it with other methods of coupling reduction. The DGS setup they proposed can be seen in Fig. 5.12.

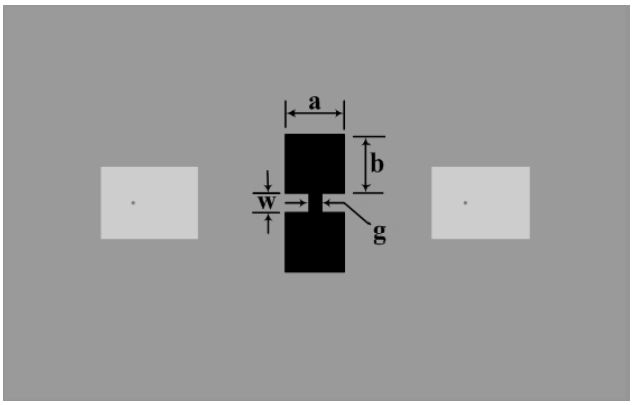

Figure 5.12: Two patches separated by a DGS configuration.

Fig. 5.12 depicts two patch antennas placed on a substrate with permittivity 10.2. The two patches are probe fed. In between the two patches, a dumbbell is etched on the ground plane. The above case is simulated in order to obtain coupling. Besides the configuration seen in Fig. 5.12, other setup are tested and depicted below.

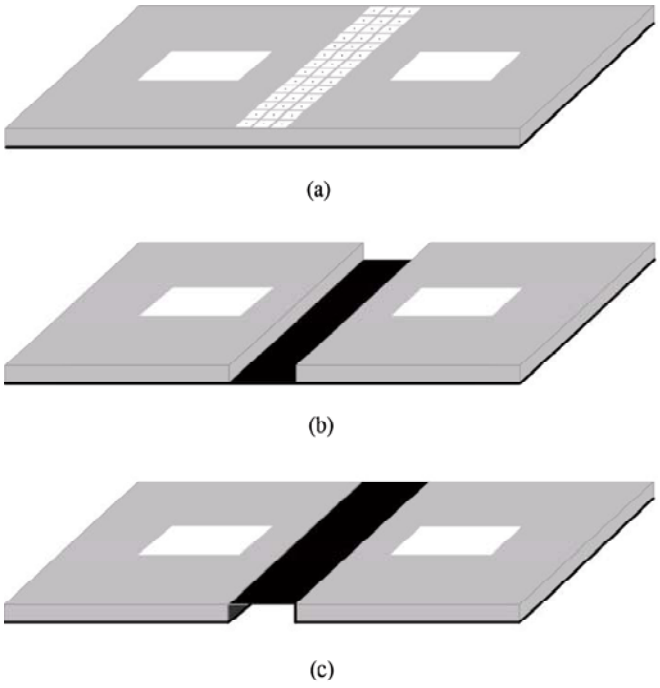

Figure 5.13: Two patch elements; (a) separated by EBG structure (b) with removed substrate (c) with cavity back.

Simulations are performed and S_{21} is derived and depicted.

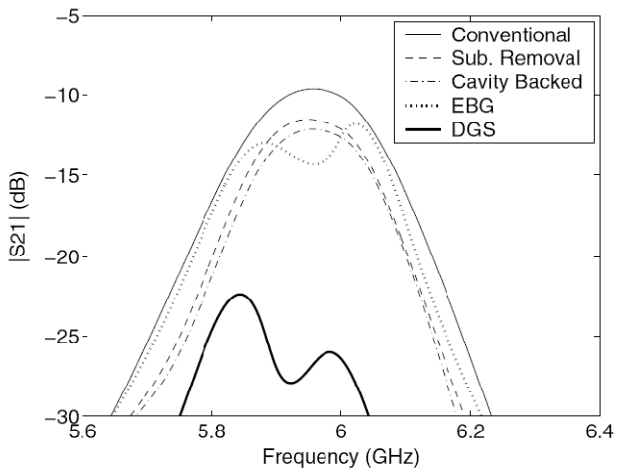

Figure 5.14: S_{21} in terms of frequency.

Table 5.2 includes all the S_{21} values for all coupling reduction methods at the frequency of 6GHz.

Table 5.2: Coupling reduction method comparison.

Method	**Substrate removal**	**Cavity back**	**EBG**	**DGS**	**Conventional**
Coupling reduction (dB)	12	12.5	12.8	26.3	10

The comparison of all methods of coupling reduction reveals that for the frequency of 6 GHz, the DGS methods performs better and proves to be the most efficient way of eliminating the mutual coupling.

Many methods of mutual coupling calculation and measurements have been presented in the litetature [21] [24]. Kara in [25] has made a comparison between some methods of coupling estimation. Let us consider an array of rectangular identical patches coaxially fed. According to Modified Volume Equivalence Theorem, coupling coefficient C_{pe} can be written as:

$$C_{pe} = 20\log\left\{\frac{25R_0\varepsilon_{eL}^2}{2\pi^5(\varepsilon_{eL}-1)}\frac{h\lambda_0^2}{SL_{ef}{}^2}\frac{1}{R_T}\times[1+\frac{1}{hS\varepsilon_{eL}}(\frac{\lambda_0}{2\pi})^2]\cos^2(\frac{\pi}{2\sqrt{\varepsilon_{eL}}})\right\} - 40\log[\frac{1}{2}(\sqrt{\frac{R_T}{50}}+\sqrt{\frac{50}{R_T}})]$$

5.24

where R_0 is the resistance of vacuum,

ε_{eL} is the effective dielectric constant of the substrate,

h is the height of substrate,

λ_0 is the wavelength in free space,

S is the separation between the edges of the patches

L_{ef} is the length of the patch taking into consideration fringing fields

R_0 is the resistance of free space

R_T is the input resistance of the isolated patch

ε_{eL} is the effective constant expressed as a function of the length of the patch

A second method of coupling evaluation considers the same expression as above with the substitution of ε_{eL} by ε_r. This method is referred to as Volume Equivalence Theorem combined with Green's Function.

$$C_{pe} = 20\log\left\{\frac{25R_0\varepsilon_{eL}^2}{2\pi^5(\varepsilon_r-1)}\frac{h\lambda_0^2}{SL^2}\frac{1}{R_T}\times[1+\frac{1}{hS\varepsilon_r}(\frac{\lambda_0}{2\pi})^2]\cos^2(\frac{\pi}{2\sqrt{\varepsilon_r}})\right\} - 40\log[\frac{1}{2}(\sqrt{\frac{R_T}{50}}+\sqrt{\frac{50}{R_T}})] \qquad 5.25$$

A third empirical formula has the following form:

$$C_{pe} = 20\log(qR_E) - 40\log[\frac{3}{2}(\frac{\lambda_0}{\pi L_{ef}}+\frac{\pi L_{ef}}{6\lambda_0})^2] \qquad 5.26$$

where q is a factor which is equal to:

$$q = \exp(\frac{2\pi h \varepsilon_{eL}}{\lambda_0}) \qquad 5.27$$

For an array of 2 rectangular patch elements, placed on substrate with ε_r=2.55, the above formulas were tested and compared to measured results. Fig. 5.15 includes all the described methods of coupling estimation together with measurements. The coupling coefficient has been expressed in terms of the distance S between the two radiating elements.

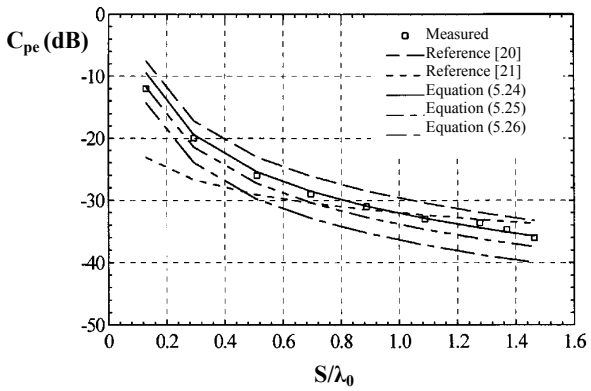

Figure 5.15: Coupling as a function of distance between radiating elements.

Measured results converge with Equation 5.24 for all values of distance S.

5.4 COUPLING MEASUREMENTS

Relay Stations (RS) are network element devices, designed to fill holes in the Base Station (BS) coverage. They receive, enhance and then retransmit the signal after digital processing [26]. The antenna system is critical to the operation of the Relay Station (RS). It aims to connect RS with BS realizing the backhaul connection and RS with user

subscribers, realizing the access link. Relays can be used in many wireless networks. The present study refers to a WiMAX wireless network in the range of 3.3 to 3.8 GHz.

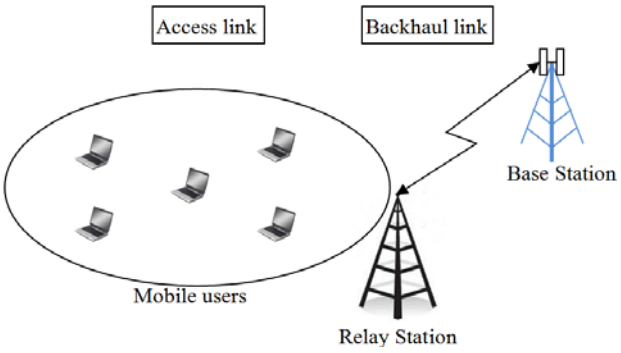

Figure 5.16: Relay Station operation.

Fig. 5.16 summarizes the operation of an antenna system showing that Relay Station can be an intermediate link between Base Station and end user. Such a topology can ensure high quality of data transmission using an antenna system that can efficiently receive and transmit information.

Many antennas have been proposed for use in the WiMAX frequency range, such as U and C slot antennas [27], [28], U-shaped patches [29], and PIFA [30]. Another important issue associated with the antenna, is coupling. Coupling is a phenomenon that expresses the level of interaction between radiation elements. It is necessary to maintain coupling as low as possible to prevent distortion of the transmitted signal. Several studies have been carried out, investigating methods to predict and evaluate mutual coupling [31] [34]. Also special attention has been given to mutual coupling reduction, by placing resonators between radiating elements [35] or by using planar EBG structures [36], [37].

In the text that follows, two simple, low cost microstrip antennas, based on microstrip technology, one for the access link and one for backhaul link are designed and presented. These antennas are compared to commercial ones and their features are outlined. The two proposed antennas are positioned together and are examined in terms of coupling. Experimental and simulated results of S_{21} are presented and compared. A clear relation between coupling and the angle between the access and backhaul antenna is found. Finally a coupling comparison between the suggested and commercial antennas is performed and corresponded results are depicted.

5.4.1 Access antenna

An access antenna was simulated and fabricated and the relevant results are depicted below. Four patches (radiating elements) fed by microstrip lines are placed on FR4 substrate (ε_r=4.4, h=1.6mm). The excitation is realized by a coaxial cable which is connected to microstrip line. The simulated antenna is depicted in Fig. 5.17a, while the fabricated one can be seen in Fig. 5.17b. Access antenna's dimensions are 12.5cm×10cm. Simulations have been performed using Ansoft HFSS v.12. Measurements of S_{11} and radiation pattern have been taken in an anechoic chamber.

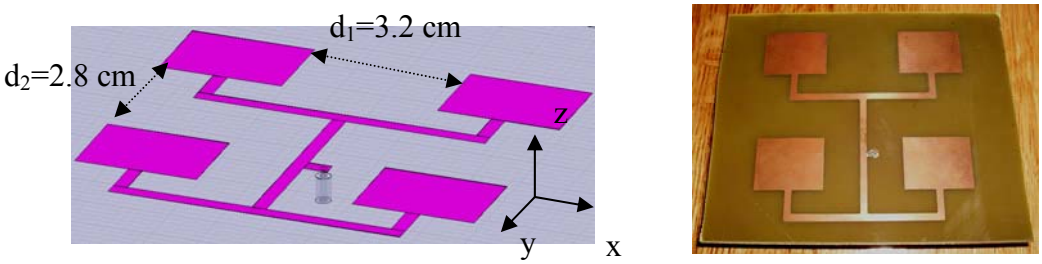

(a) (b)

Figure 5.17: Antenna geometry and measurements; (a) antenna design, (b) antenna prototype.

The S_{11} parameter as a function of frequency is depicted in Fig. 5.18.

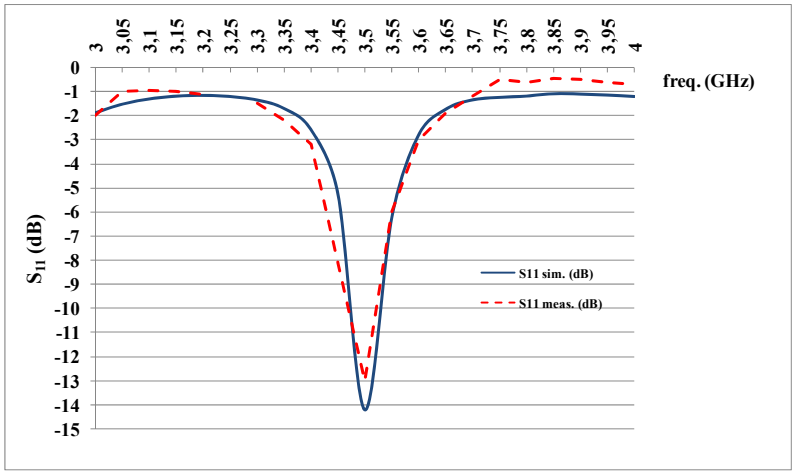

Figure 5.18: S_{11} parameter for simulated and fabricated antenna.

For the experimental estimation of S_{11}, a Vector Network Analyzer was used (Anritsu VNA MS2036A). Before measurements, calibration was performed in order to take into consideration the cable losses and increase the level of experiment accuracy. The excitation of access antenna is realized by a coaxial cable which feeds the microstrip line. In the connecting point between cable and microstrip line, losses are introduced that reduce the amount of power that enters the antenna. That is why this antenna presents narrow bandwidth [38].

Access antenna presents S_{11}= -14.3dB for 3.5GHz. The impedance bandwidth of the antenna is estimated to be 31.8MHz (S_{11}<-10dB [39]). The radiation pattern of the simulated and fabricated antenna is illustrated in Fig. 5.19a for yz plane at 3.5GHz with Half Power Beam width (HPBW) 36^{o}. The radiation pattern in xz plane is depicted in Fig. 5.19b, presenting HPBW=51^{o}. The antenna presents Gain G =7.9dB in the direction of maximum emission. Let us mention here that FR4 substrate has an increased loss

tangent (tanδ=0.02) which means low quality factor and thus increased dielectric losses. That is why the antenna gain is appeared to be less than what is expected but high enough to support the access link.

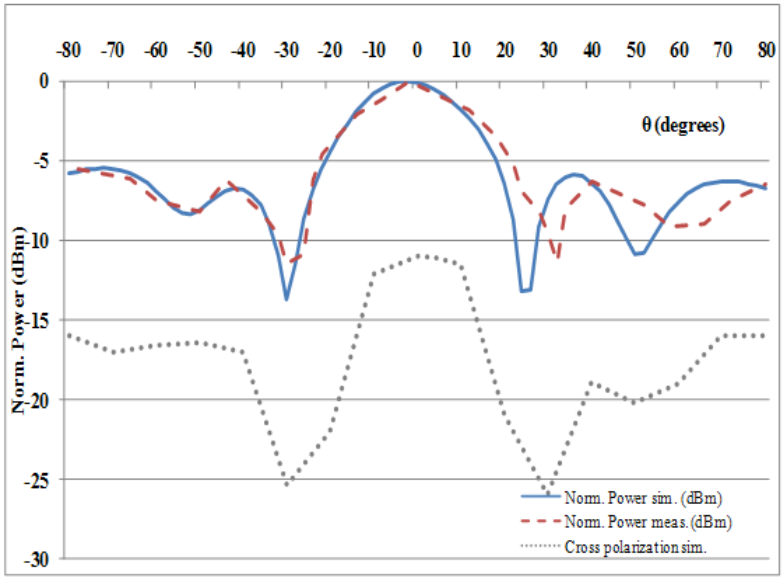

(a)

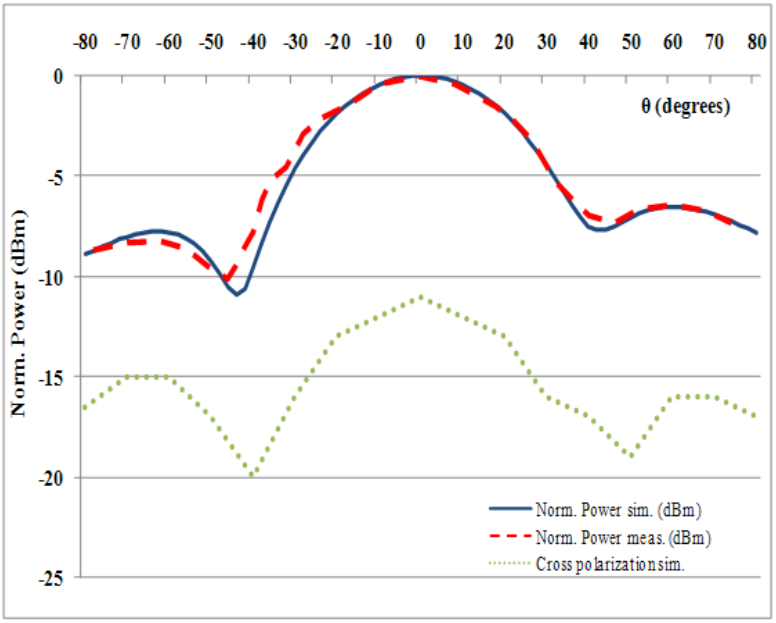

(b)

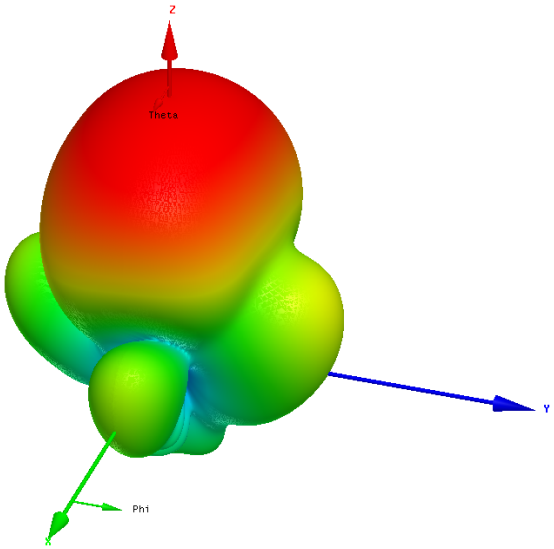

(c)

Figure 5.19: Radiation pattern of access antenna for 3.5GHz; (a) yz plane (b) xz plane (c) 3D radiation pattern.

Fig. 5.19a and 5.19b also depict the simulated cross polarization level of the access antenna. Cross polarization expresses the amount of power emitted orthogonal to the desired direction and it has to be as low as possible. Surface waves are dependent of the substrate and give rise to cross polarization. For minimizing these waves, materials with low dielectric losses could be chosen.

5.4.2 Backhaul antenna

An antenna array intended to be used for connecting the Relay with the Base Station is presented in this section. The simulated and constructed antenna can be seen in Fig. 5.20a and 5.20b, respectively. Backhaul antenna's dimensions are 25.5cm×21.5cm.

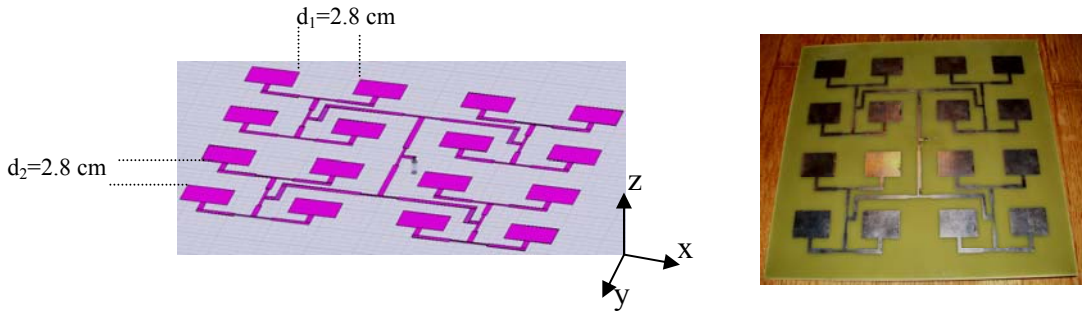

(a) (b)

Figure 5.20: Backhaul antenna geometry and measurements; (a) backhaul antenna model (b) backhaul antenna prototype.

The S_{11} parameter for the simulated and fabricated antenna is shown below (Fig. 5.21) where a slight difference is attributed to the imprecise process of construction.

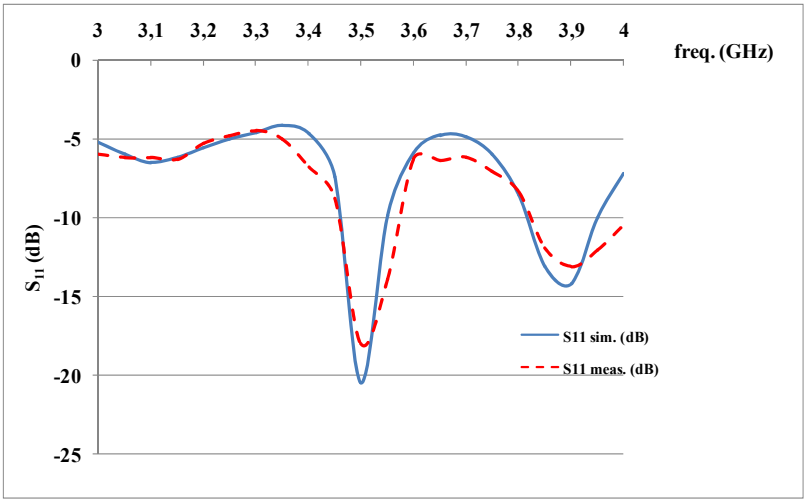

Figure 5.21: S_{11} parameter for backhaul antenna.

Backhaul antenna presents S_{11}= -17.9dB at 3.5GHz and impedance bandwidth equal to 84MHz. A second resonance frequency is appeared at 3.9GHz where S_{11}= -14.2dB. The gain of the backhaul antenna has been found 11.4dB for 3.5GHz. Gain could be greater if a substrate of lower dielectric losses was used.

The radiation pattern is presented in Fig. 5.22a and 5.22b where a narrow beam is noticed due to the increase in the number of radiation elements compared to the case of the access antenna. HPBW for yz plane has been measured 18^{o}.

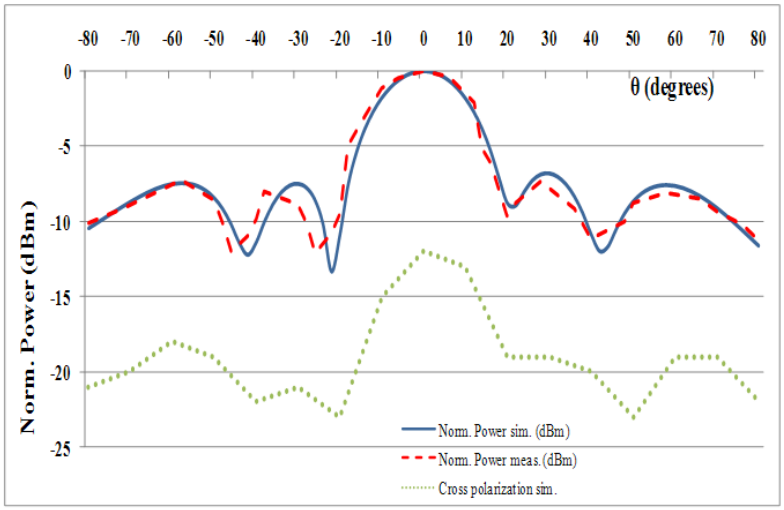

(a)

The radiation pattern in xz plane is presented in Fig. 5.22b. In this case HPBW=25.5^{o}.

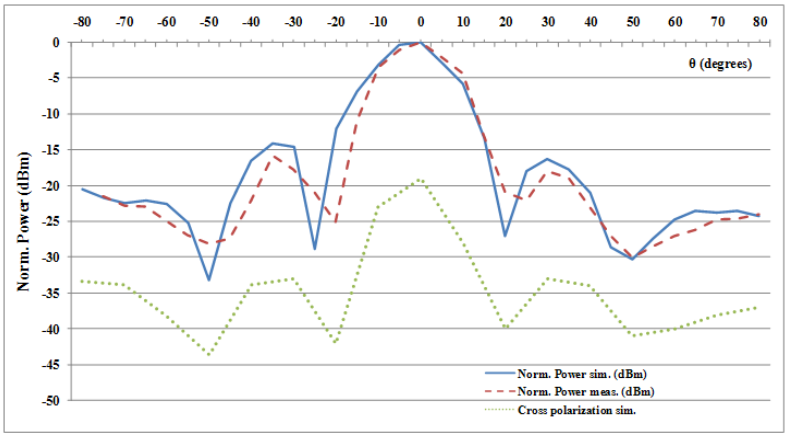

(b)

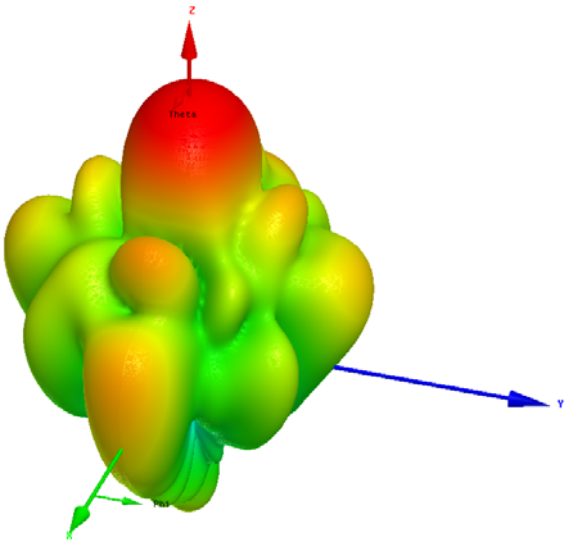

(c)

Figure 5.22: Radiation pattern of the backhaul antenna for 3.5GHz; (a) yz plane (b) xz plane (c) 3D radiation pattern (c) 3D radiation pattern.

Fig. 5.22a and 5.22b also represent the cross polarization level which is appeared to be increased due to the FR4 substrate.

Measured access and backhaul antenna characteristics are denoted in Table 5.3.

Table 5.3: Access and backhaul antenna features.

	S_{11} (dB) for 3.5GHz	Gain (dB)	HPBW (degrees) xz plane	HPBW (degrees) yz plane	Bandwidth (MHz)
Access antenna	-14.3	7.9	51	36	32
Commercial access antenna (1SKF 333808W)	-16	8	68		500
Backhaul antenna	-17.9	11.4	25.5	18	84
Commercial backhaul antenna (TSWL315177)	-18.5	18	17		400

Gain and bandwidth is increased in the case of the backhaul antenna due to the larger number of radiation elements (16 elements) compared to the access antenna (4 elements). Also Half Power Beamwidth (HPBW) is decreased in the backhaul antenna. In addition a comparison is performed between the proposed antennas and relevant commercial ones. Regarding access antenna, model 1SKF 333808W is a panel antenna presenting HPBW=68^{o}, gain 8dB and bandwidth 500MHz. The proposed access antenna gives similar gain but less HPBW and bandwidth due to FR4 substrate. Bandwidth could be enlarged by using a substrate of lower loss tangent such as Rogers RO 3006 (ε_r=6.15, tanδ=0.0025) or Rogers RT Duroid 5880 (ε_r=2.2, tanδ=0.0009). Wider bandwidth could also occur using stacked geometry including two or more substrates separated by air gaps. FR4 substrate was chosen because of its low cost and ease of fabrication. Regarding backhaul antenna, the commercial one presents enhanced bandwidth and gain. The proposed backhaul antenna uses low cost FR4 substrate which has high loss tangent that leads to limited gain, bandwidth and high side lobes. The design of access and backhaul antenna has been made maintaining low cost of fabrication and low complexity level. Both antennas can be improved in terms of gain, bandwidth by using stacked geometries and dielectrics of low losses.

Since both proposed antennas have the same resonant frequency and the Relay Station performs in the Simultaneously Transmit Receive (STR) mode, it is necessary to examine the coupling phenomenon between the antennas.

5.5 COUPLING EFFECTS STUDY

Two cases of configuration between the proposed antennas are examined. These configurations are shown in Fig. 5.23. Coupling between the two antennas in terms of S_{21} is measured using Anritsu VNA MS2036A and results are depicted below.

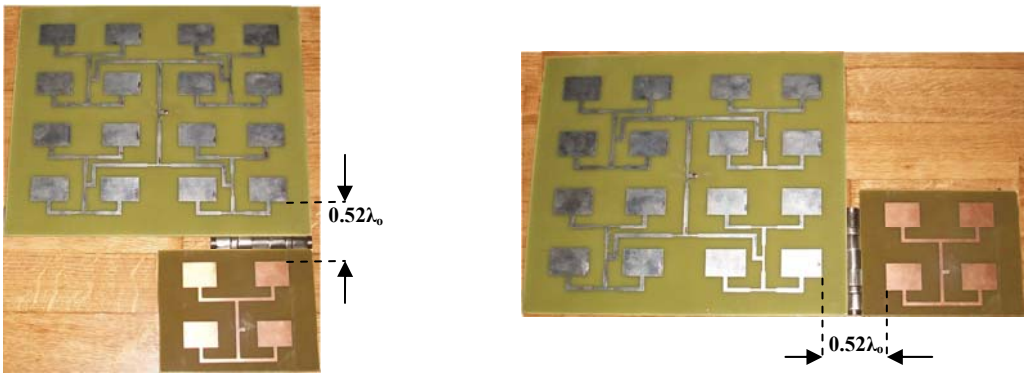

(a) (b)

Figure 5.23: Antenna arrangements under test; (a) configuration 1 (b) configuration 2.

Coupling measurements have been taken in anechoic chamber to achieve precision and validity of results. Fig. 5.24 show the experimental setup. The distance between two adjacent radiation elements of access and backhaul antennas is $0.52\lambda_o$. This distance is adequate for low mutual coupling [20] and maintaining the total size of the antenna system as small as possible.

Figure 5.24: Access and backhaul antenna setup during coupling measurements.

Study of configurations 1 and 2 due to the relative position of antennas can be consider as coupling investigation in E plane and H –plane respectively.

5.5.1 Configuration 1

In the first case (configuration 1), the two antennas are put in such a way, so that the angle between them is $\omega=180^0$ and then ω increases with a step of 10^0 and final reaches 270^0.The scheme that specifies the proposed setup can be seen in Fig. 5.25.

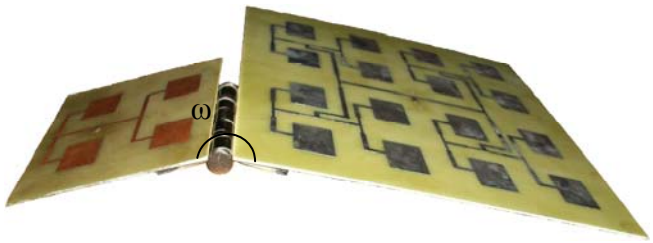

Figure 5.25: The investigated setup.

Together with the experimental measurements, simulations of S_{21} as a function of the angle ω have been carried out. Simulation and measurement of S_{21} for the case of $\omega=180^0$ is depicted in Fig. 5.26b.

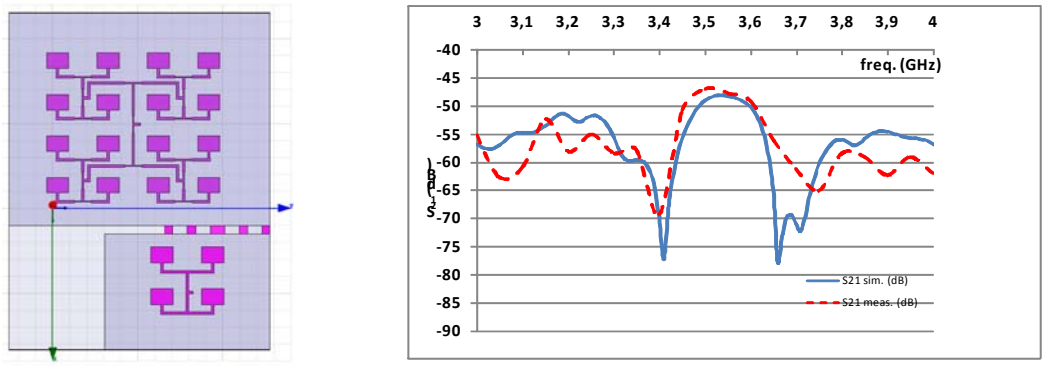

(a) (b)

Figure 5.26: S_{21} for $\omega=180^0$; (a) simulation design (b) simulation and measurement.

Fig. 5.26b shows that simulation and experimental curve of S_{21} is located below -40dB for the frequency range of 3.4 to 3.6 GHz.

For $\omega=190^0$ the experimental setup is depicted in Fig. 5.27a and the corresponded results in Fig. 5.27b.

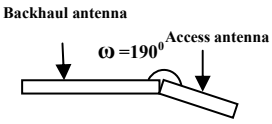

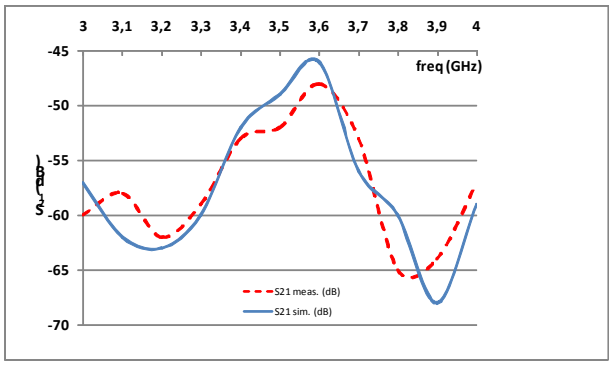

(a) (b)

Figure 5.27: S_{21} for $\omega=190^0$; (a) simulation design (b) simulation and measurement.

For $\omega=200^0$ the experimental setup is depicted in Fig. 5.28a and the corresponded results in Fig. 5.28b.

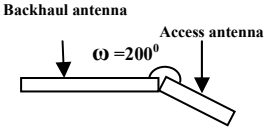

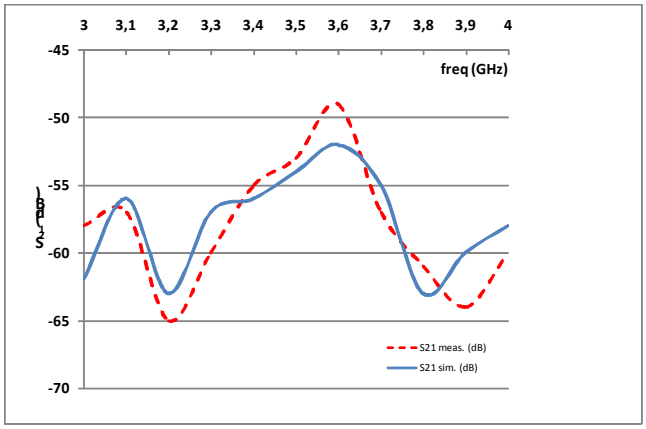

(a) (b)

Figure 5.28: S_{21} for $\omega=190^0$; (a) simulation design (b) simulation and measurement.

The experiment continues for $\omega=210^0$ till 270^0 with a step of 10^0. Coupling can change the operation frequency of an antenna and distort the radiation pattern. That is why it is necessary to maintain coupling at a low level. Coupling effect is mainly caused by space waves that end up from one antenna to another (Fig. 5.29). It is also dependent on surface waves that travel through dielectric [40]. From the analysis performed for configuration 1 it is derived that increasing the angle ω seems to reduce the density of field lines that end up from one antenna to the other thus reducing coupling effect.

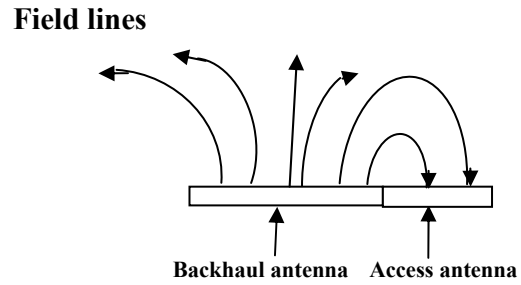

Figure 5.29: Field lines that cause coupling effect.

5.5.2 Configuration 2

In this case the access and backhaul antenna are positioned as shown in Fig. 5.30.

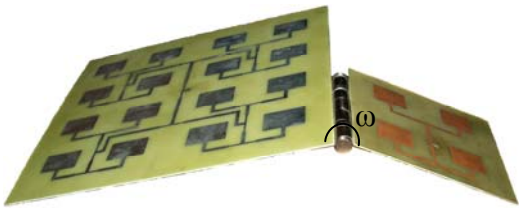

Figure 5.30: The investigated setup.

Together with the experimental measurements, simulations of S_{21} against angle ω for configuration 2 have been performed. The case of $\omega=180^0$ is depicted in Fig. 5.31a.

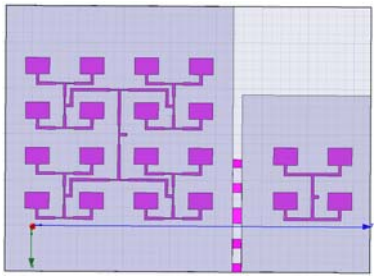

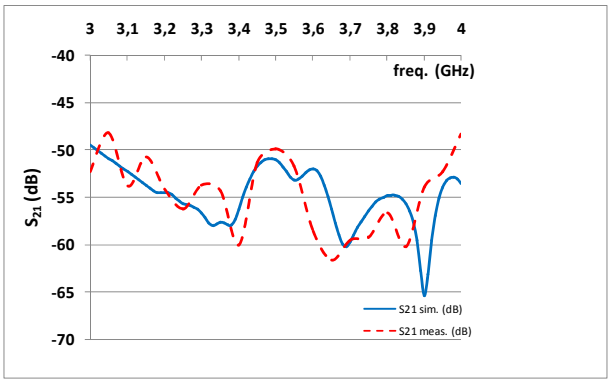

(a) (b)

Figure 5.31: S_{21} for $\omega=180^0$; (a) simulation design (b) simulation and measurement.

Fig. 5.31b represents the simulation and experimental curve for S_{21}. Coupling is at an acceptable level (S_{21}<-40dB) for the frequency range 3.4 to 3.6GHz.

For $\omega=190^0$, the corresponded results can be seen in Fig. 5.32b.

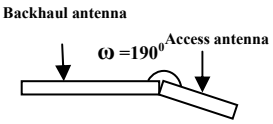

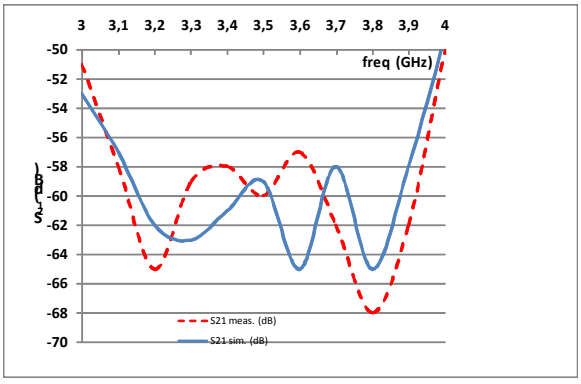

(a) (b)

Figure 5.32: S_{21} for $\omega=190^0$; (a) simulation design (b) simulation and measurement.

For ω=200^0 the experimental setup is depicted in Fig. 5.33a and the corresponded results in Fig. 5.33b.

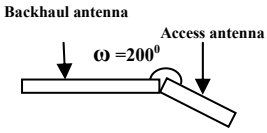

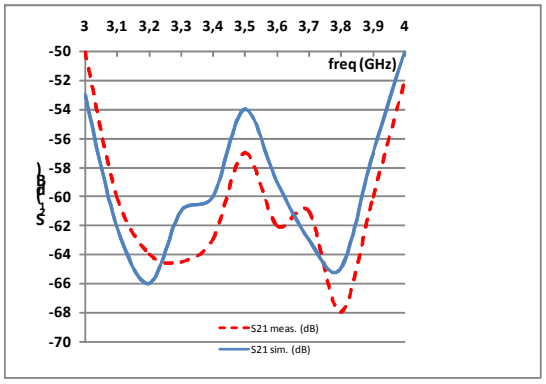

(a) (b)

Figure 5.33: S_{21} for ω=200^0; (a) simulation design (b) simulation and measurement.

The experiment continues for ω=210^0 up to 270^0 with a step of 10^0.

In configuration 2 the coupling effect is weaker compared to configuration 1 as it produces S_{21} that varies from -48 dB to -68dB.

5.6 RESULTS

In the tables that follow, the maximum value of experimental S_{21} is denoted in the frequency range of 3.4GHz to 3.6GHz, for each value of angle ω.

Table 6.4: S_{21} variation for configuration 1.

Configuration 1	**ω (degrees)**	**S_{21} max(dB)**
	180	-47,67
	190	-46,84
	200	-49,15
	210	-50,46
	220	-50,3
	230	-50,56
	240	-50,83

	250	-54,94
	260	-54,92
	270	-53,94

The maximum value of S_{21} as a function of the angle ω is depicted in Fig. 6.34.

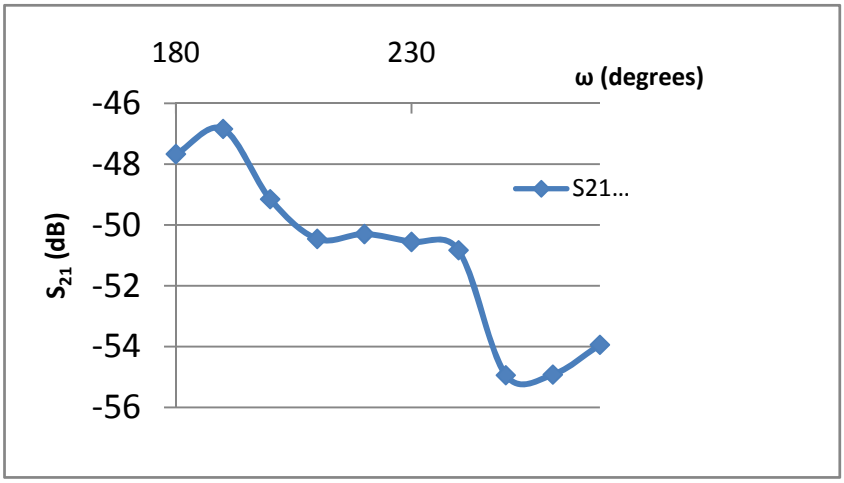

Figure 5.34: S_{21} as a function of angle ω for configuration 1.

The table for configuration 2 follows together with the corresponded S_{21} diagram.

Table 6.5: S_{21} variation for configuration 2.

Configuration 2	**ω (degrees)**	**S_{21} max(dB)**
	180	-55,56
	190	-54,7
	200	-57,34
	210	-61,01
	220	-60,26
	230	-58,36
	240	-59,1
	250	-63,02
	260	-65,35
	270	-60,68

The maximum value of S_{21} as a function of the angle ω is depicted in Fig. 5.35.

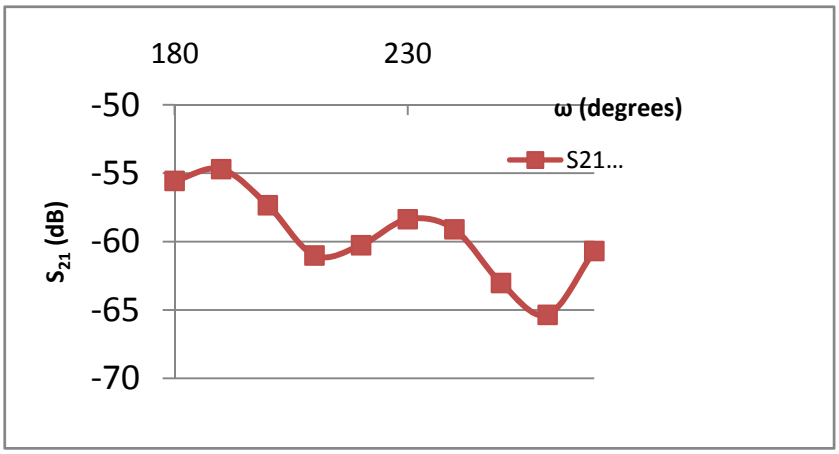

Figure 5.35: S_{21} as a function of angle ω for configuration 2.

Both configurations 1 and 2 provide a low level of coupling (S_{21} < -40dB). Coupling appears to decrease non linearly while ω increases. Configuration 2 is more acceptable because S_{21} takes values lower than 50dB for all angles of ω. The best case is occurred for configuration 2 at ω=260deg where S_{21}= -65.35dB.

A comparison in terms of coupling between the proposed antennas and the commercial ones presented in table 6.3 has also been performed. Both commercial and proposed antennas have been measured in terms of coupling for ω=270^{o}. The Relay set up including the suggested access and backhaul antenna can be seen in Fig. 5.36.

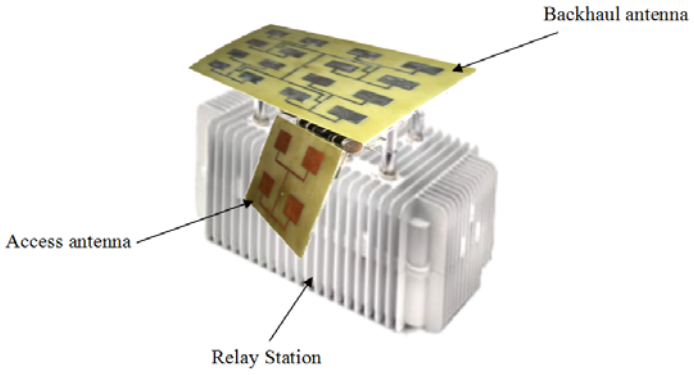

Figure 5.36: Relay Station with the proposed antennas.

Fig. 5.37 shows coupling variations for commercial antennas and the proposed ones for configurations 1 and 2 at ω=270°.

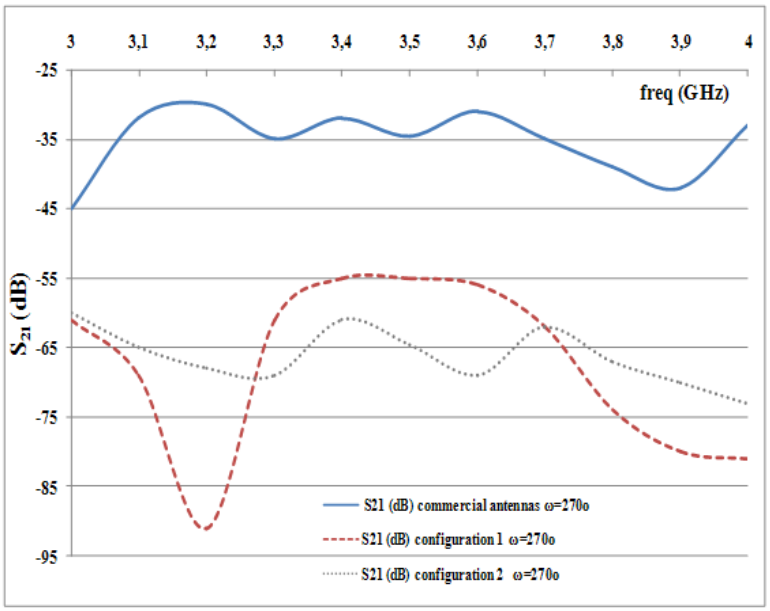

Figure 5.37: Coupling comparison.

As it is noticed from the above figure, the commercial antennas provide S_{21} from -30dB to -45dB, the configuration 1 from -55dB to -91dB and configuration 2 from -61 to -73dB. Thus configuration 2 proves to be the best setup for the frequency range of interest.

5.7 CONCLUSIONS

Concluding the preceded work, chapter 5 handled the issue of antenna coupling. For this reason coupling was defined in terms of Scattering (S), Impedance (Z) and voltage (V) parameters. Onwards some methods and techniques for reducing the interaction between antenna elements were presented and commented, including EBG and DGS

designs. Empirical formulas regarding coupling estimation in terms of the size and geometry of the antennas were also mentioned in order to clarify the relation between coupling and the antenna's dimensions. The aforementioned analysis was used as the basis for proposing two new antenna configurations for reducing coupling. More precisely, two new designs of access and backhaul antennas were presented utilizing lost cost FR4 substrate. These two new designs, operating in the same frequency, were put into two configurations that were tested in terms of S_{21} parameter. Results showed S_{21}< -45dB in all tested cases, proving the efficiency of the proposed configurations.

5.8 REFERENCES

[1] J. P. Daniel, "Mutual coupling between antennas for emission or reception Application to passive and active dipoles", IEEE Transactions on Antennas and Propagation, vol.22, no.2, pp. 347-349, March 1974.

[2] P. Bhartia, I. Bahl, R. Garg, A. Ittipiboon, "Microstrip Antenna Design Handbook", Artech House Publishers, November 2000.

[3] C. A. Balanis, "Antenna Theory Analysis and Design", John Wiley and Sons, 2nd Edition, 1997.

[4] E. H. Newman, J. H. Richmond, B.W. Kwan, "Mutual Impedance Computation Between Microstrip Antennas", IEEE Transactions on Microwave Theory and Techniques, vol. 31, no. 11, pp. 941-945, November 1983.

[5] H. Steyskal, J.S. Herd, "Mutual coupling compensation in small array antennas", IEEE Transactions on Antennas and Propagation, vol. 38, no. 12, pp.1971-1975, December 1990.

[6] M. Kuipers, "Mutual coupling computation and effects in phased array microstrip antennas", 48th IEEE Vehicular Technology Conference, vol. 2, pp.1181-1185 vol. 2, 18-21 May 1998.

[7] R.F. Harrington, “Field Computations by Moment Methods”, Macmillian, New York, 1968.

[8] R. P. Jedlicka, M. P. Toe and K. R. Carver, “Measured mutual coupling between microstrip antennas”, IEEE Transactions on Antennas and Propagation, vol. AP 29, pp. 147-149, January 1981.

[9] E. Penard and J. P. Daniel, “Mutual coupling between microstrip antennas”, Electrononics Letters, vol. 18, no. 14, pp. 605-607, 1982.

[10] C. Terret, S. Assailly, K. Mahdjoubi, M. Edimo, “Mutual coupling between stacked square microstrip antennas fed on their diagonal”, IEEE Transactions on Antennas and Propagation, vol. 39, no. 7, pp. 1049-1051, July 1991.

[11] D. M. Pozar, “Input impedance and mutual coupling of rectangular microstrip antennas”, IEEE Transactions on Antennas and Propagation, vol. AP 30, pp. 1191-1196, November 1982.

[12] M. Sonkki, E. Antonino Daviu, M. Ferrando Bataller, E. Salonen, “Optimal dimensions of two microstrip patch antennas for low mutual coupling at 5.8 GHz”, 3rd European Conference on Antennas and Propagation, pp. 3515-3518, 23-27 March 2009.

[13] V. Pynttari, R. Makinen, J. Heikkinen, M. Kivikoski, “Microstrip antenna arrays on thin substrates with electromagnetic band gap structures”, First European Conference on Antennas and Propagation, pp. 1-5, 6 10 November 2006.

[14] J. Liang, H Y.D. Yang, “Radiation Characteristics of a Microstrip Patch Over an Electromagnetic Bandgap Surface”, IEEE Transactions on Antennas and Propagation, vol. 55, no. 6, pp. 1691-1697, June 2007.

[15] F. Yang, Y. Samii, “Microstrip antennas integrated with electromagnetic band gap (EBG) structures: a low mutual coupling design for array applications”, IEEE Transactions on Antennas and Propagation, vol. 51, no. 10, pp. 2936-2946, October 2003.

[16] E. Iglesias, O. Teruel and L. Sanchez, “Mutual Coupling Reduction in Patch Antenna Arrays by Using a Planar EBG Structure and a Multilayer Dielectric Substrate”, IEEE Transaction on Antennas and Propagation, vol. 56, issue 6, pp. 1648-1655, June 2008.

[17] M. Dorigo and T. Stutzle, “Ant Colony Optimization”, The MIT Press, 2004.

[18] F. Caminita, S. Costanzo, G. Di Massa, S. Maci, G. Mauriello, I. Venneri, G. Guarnieri, "A shorted interlocked strip EBG Surface integrated in patch arrays", IEEE International Symposium Society on Antennas and Propagation, pp.1-4, 1-5 June 2009.

[19] D. Ahn, J. S. Park, C. S. Kim, J. Kim, Y. Qian, and T. Itoh, "A design of the low pass filter using the novel microstrip defected ground structure," IEEE Transactions on Microwave Theory Technology, vol. 49, pp. 86-93, January 2001.

[20] M. Salehi, A. Motevasselian, A. Tavakoli, T. Heidari, "Mutual Coupling Reduction of Microstrip Antennas using Defected Ground Structure", 10th IEEE Singapore International Conference on Communication systems, pp.1-5, October 2006.

[21] E. H. Van Lil and A. R. Van de Capelle, "Transmission Line Model for Mutual Coupling between Microstrip Antennas", IEEE Transactions on Antennas and Propagation, vol. AP 32, pp. 816-821, 1984.

[22] C. M. Krowne, ''Dielectric and Width Effect on H Plane and E Plane Coupling Between Rectangular Microstrip Antennas,'' IEEE Transactions on Antennas and Propagation, vol. AP 31, pp. 39-47, 1983.

[23] G. Dubost, ''Mutual Impedance and Coupling Coefficient Between Two Patches Expressed Through Analytical Forms,'' Electronics Letters, vol. 21, pp. 1099 1101, 1985.

[24] G. Dubost, ''Influence of Surface Wave Upon Efficiency and Mutual Coupling Between Rectangular Microstrip Antennas,'' IEEE Antennas and Propagation Symponium, Dallas, pp. 660-663, 1990.

[25] K. Mehmet, "Techniques for the computation of the mutual coupling between two rectangular microstrip antenna elements with thick substrates", Microwave and Optical Technology Letters, Wiley Subscription Services, pp. 169-176, 1997.

[26] I. Georgas, I. Petropoulos, K. Voudouris, P. Tsiakas, N. Athanasopoulos, M. V. H Cohen, B. Cyzs, G. Agapiou, and A. Rigas, "Relay vs Repeater Architectures in WiMAX", 6th Internatiohal ICST conference on mobile multimedia communications MOBEMEDIA, Lisbon Portugal, 6-8 September 2010.

[27] H.F. AbuTarboush, H. S. Al Raweshidy, R. Nilavalan, "Triple band double U slots patch antenna for WiMAX mobile applications", 14th Asia Pacific Conference on Communications, pp.1-3, 14-16 October 2008.

[28] B. Tlili, “Design of double C slot microstrip patch antenna for WiMax application”, IEEE International Symposium on Antennas and Propagation, pp.1-4, 11-17 July 2010.

[29] K. Wong, H. Tung, “An inverted U shaped patch antenna for compact operation”, IEEE Transactions on Antennas and Propagation, vol. 51, no. 7, pp. 1647- 1648, July 2003.

[30] H. F. AbuTarboush, R. Nilavalan, H.S. Al Raweshidy, D. Budimir, “Design of planar inverted F antennas (PIFA) for multiband wireless applications”, International Conference on Electromagnetics in Advanced Applications, pp.78-81, 14-18 September 2009.

[31] S. Wang, L. Guo, X. Chen, C. G. Parini,J. McCormick, “Analysis of mutual coupling in broadband arrays”, IEEE International Symposium on Antennas and Propagation, pp. 1-4, 5-11 July 2008.

[32] H. M. Hizan, A. H. Awang, “Investigation of mutual coupling effect between five element arrays of half cylindrical DRAs”, International Conference on new Techniques in Pharmaceutical and Biomedical Research, pp. 233-238, 5-7 September 2005.

[33] Z. Qi, L. Ya, W. Peng, X. Jun, X. Min, H. Min, “An Accurate Mutual Coupling Calculation For Microstrip Antennas For Impedance Mismatching”, 7th International Symposium on Antennas, Propagation & EM Theory, pp. 1-4, 26-29 October 2006.

[34] M. Wang, Z. Shen, “Nulling of Antenna Arrays Including the Mutual Coupling Effect”, Vehicular Technology Conference, 2008.

[35] L. Minz, R. Garg, “Reduction of mutual coupling between closely spaced PIFAs”, Electronics Letters, vol. 46, no. 6, pp. 392-394, March 2010.

[36] E. Iglesias, O. Teruel, L. Sanchez, “Mutual Coupling Reduction in Patch Antenna Arrays by Using a Planar EBG Structure and a Multilayer Dielectric Substrate”, IEEE Transactions on Antennas and Propagation, vol. 56, no. 6, pp. 1648-1655, June 2008.

[37] F. Caminita, S. Costanzo, G. Di Massa, G. Guarnieri, S. Maci, G. Mauriello, I. Venneri, “Reduction of Patch Antenna Coupling by Using a Compact EBG Formed by Shorted Strips With Interlocked Branch Stubs”, IEEE Antennas and Wireless Propagation Letters, vol. 8, pp. 811-814, 2009.

[38] G. Kumar and K.P. Ray, “Broadband Microstrip Antennas”, Artech House, Inc, 2003.

[39] P. Mahesh Abegaonkar, K. Aditya, A. Basu, S. K. Koul, “Parametric Study of a Parasitically fed Broadband Monopole Patch Antenna”, First International Conference on Industrial and Information Systems, pp. 450-453, 8-11 August 2006.

[40] R. Jedlicka, M. Poe, K. Carver, “Measured mutual coupling between microstrip antennas”, IEEE Transactions on Antennas and Propagation, vol. 29, no. 1, pp. 147-149, January 1981.

CHAPTER 6

CONCLUSIONS AND SUGGESTIONS FOR FURTHER WORK

6.1 CONCLUSIONS

Relay Stations (RS) are network devices used under a 4G network, such as mobile WiMAX or LTE, to extend network's coverage and throughput [1]. Relays are adaptive, small size and low cost devices which can be mounted on buildings, light poles, even in moving vehicles, to provide high quality signal and connectivity [2].

In this thesis, a novel antenna system was designed, fabricated and tested to be incorporated with a Relay Station, to provide links with the Base Station (backhaul link) and with end users (access link). The antenna system comprises two radiation modules: A single antenna element, based on microstrip technology [3] for access link realization and an antenna array, based on the same technology for backhaul link realization. Both radiation module specifications are compatible with the IEEE 802.16j air interface protocol. In addition the antenna array is capable of pointing its main lobe of radiation to the direction of Base Station, presenting at the same time low side lobe levels for gain maximization and null at the direction of interference. The beam forming feature is realized utilizing a proper circuit including two 1:8 Wilkinson power dividers [4], attenuator and phase shifter chips.

A Relay Station should have beam steering abilities in order to communicate with the Base Station regardless of the RS backhaul antenna orientation or the Relay Station's position. In this way, the beam forming feature adds flexibility during the RS installation process. Beam steering is achieved controlling the amplitude and phase excitation current of each radiation element. The control of two parameters (amplitude and phase) significantly increases the degrees of freedom giving the ability to steer the main lobe of radiation almost anywhere. Beam forming is achieved utilizing Least Mean Square (LMS) algorithm [5] which efficiently evaluates the amplitude and phase of all excitation currents, obtaining the required radiation pattern.

Furthermore the coupling phenomenon [6] of two new designs of access and backhaul antenna was measured and depicted in relevant figures. In the case where both access and backhaul antennas operate in the same frequency, the interaction between them can significantly distort their radiation patterns and cause signal degradation. For that reason two new configurations between access and backhaul antennas were investigated and coupling coefficient was derived and commented. The antenna orientation that provides the lowest coupling is highlighted and preferred.

The antenna system designed and fabricated in this thesis is based on microstrip technology. Thus in chapters 1, the main concepts of microstrip patch antennas were discussed. The patch antenna configuration was outlined together with feeding techniques references and some basic models for deriving electric and magnetic field expressions. Patch antennas provide narrow bandwidth due to their configuration and surface waves excitation [7]. In order to provide a radiation element with a bandwidth wide enough based on IEEE802.16j specification, an extensive literature review was

performed on bandwidth enhancement techniques. These techniques include stacked geometry utilization [8], fractal shaped patches [9], parasitic elements introduction [10], inhomogeneous substrates [11], H shaped [12], U slot [13], E-shaped patch [14].

The designed antenna system presented in this thesis comprises an array of high gain, directivity and enhanced bandwidth for backhaul link realization. Thus in chapter 1, the main principles of arrays and phased arrays [15] were presented. Concepts such as the directivity of a linear array, the total radiated power, gain, EIRP and total radiated field were clearly stated. The phased array architecture was depicted and described as the combination of many radiation elements with a proper circuit of power division and signal excitation control in order to provide the required radiation pattern. Furthermore the Array Factor term (AF) was expressed and described in terms of inter-element distance and angle of received signal with a reference on grating lobe prevention [16]. Onwards power dividers were presented and investigated in relation to input and output power and S parameters. The section of advances in planar arrays followed, included several techniques and configurations for bandwidth maximization, methods for low mutual coupling between radiation elements and surface wave suppression. Also some special cases of arrays including RF PIN diodes, switches and capacitors for beam forming applications were mentioned and described. In the final section of chapter 1, the total electric field of an M×N planar array was expressed in terms of element pattern, excitation and inter element spacing. The expressions of phase difference between adjacent radiation elements for main lobe or null occurrence at specific angle direction (θ, φ) were proved and denoted [17].

The antenna system proposed in this thesis is going to be integrated with a Relay Station (RS). For that reason in chapter 2 Relay Stations were defined and described in terms of usage scenarios and RF front end structure [18]. Its advantages were outlined and included throughput increase, coverage extension, low cost of fabrication and mobility support [19]. Applications of RS were clearly mentioned and supported by relevant schemes, comprising fixed and mobile RS state. A categorization of RS was performed depending on the usage scenarios and network requirements. In addition RS architecture was depicted and described, giving special attention to the RF front end schematic. The latter was simulated using ADS2009, including transmission and reception RF chain, showing the components utilized with figures where necessary. Transmission RF chain simulation comprises OFDM spectrum and time domain representations, where efficient and proper operation of RS were proved. The reception RF chain description followed showing RSS and SNR parameters for several modulation schemes.

Beam forming is necessary for the designed phased array in order to steer the main lobe of radiation to the direction of Base Station, produce suppressed low side lobe levels for gain maximization and nulls at the direction of interference. Thus in chapters 3, the main concepts of beam forming technique were outlined in terms of circuits and algorithms. Basically a beam forming module includes a power divider circuit and a beam steering algorithm [17]. The power divider circuit is responsible for power division/distribution to transmission lines connected to radiation elements, with attenuator and phase shifter chips incorporated. In addition an algorithm applied by a control unit defined specific amplitudes and phases to the excitation currents. Onwards some types of power divider circuits were investigated and described in terms of S parameters and characteristic impedances [16]. Furthermore special attention was given

to the imbalance phenomena caused by phase shifters. A matrix was proposed to overcome such problems and results were depicted and commented. Chapter 3 ended with a beam forming algorithm reference including Least Mean Square Algorithm (LMS) [20] and Constant Modulus Algorithm (CMA) [21], performing a comparison between them. Also two common Direction of Arrival Estimation (DOA) Algorithms were presented and could be used in collaboration with beam forming algorithm to provide a full adaptive and smart antenna array.

In chapter 4, the new design of antenna system in terms of the access antenna and backhaul phased array was fully described and analyzed. The access antenna was designed, simulated and fabricated, presenting S_{11}= -43.62dB for 3.4GHz, bandwidth 520MHz or 15.2% and gain 10dB. A comparison has been performed between the access antenna with the IEEE802.16j specifications, proving that the proposed one provides higher gain, wider bandwidth but HPBW in yz plane is 8^0 lesser. Moreover the backhaul phased array was designed and tested, presenting gain 21.2dB, bandwidth 424MHz and HPBW around 14^0 in both planes. The proposed phased array has dimensions 32.6×30cm and was also compared with a similar commercial one, showing higher gain, almost the same HPBW and about 80MHz lesser bandwidth. Both presented antennas comply with the IEEE802.16j specifications in terms of gain, bandwidth and HPBW and thus can be utilized as part of a Relay based wireless network. Let us mention that both access and backhaul antennas have the same structure which is an advantage that may simplify and accelerate the antenna fabrication process. In addition the planar geometry of both access and backhaul antenna make it easy to be mounted on the RS surface and thus reduce the RS volume and facilitate the RS installation procedure. Chapter 4 continued with the presentation and analysis of a new

design of beam forming circuit. The last comprises two 1:8 Wilkinson power dividers, including attenuator and phase shifter chips for amplitude/phase assignment. A two substrate Wilkinson power divider configuration was chosen to decrease the circuit's dimensions in order to be incorporated within the RS. The 1:8 Wilkinson power divider has dimensions 21.2×21.8cm and presented S_{11}= -27.112dB for 3.38GHz with 700MHz bandwidth from 3.3GHz to 4GHz. The specific measurement has been derived considering 0dB attenuation and 0^0 phase for excitation currents.

Onwards a beam forming scenario was implemented using field equations derived from literature [15]. A set of requirements were defined demanding maximum in (θ_m, φ_m), null at (θ_n, φ_n) and SLL<-10dB. The algorithm was activated and gave two 4×4 matrices of amplitudes and phases. Although amplitude and phase take quantized values based on the datasheets of the utilized chips [22], [23], a good agreement between reference signal and radiation pattern is achieved (78.13% convergence). In addition the phased array was tested considering three scenarios. For each scenario, three curves were derived. The first corresponded to LMS algorithm considering a rectangle patch with no mutual coupling, the second one to the simulation of the phased array and the third one to the measurement of the array. In all scenarios the three curves show good agreement in terms of maximum occurrence, null and side lobe levels. Any other pattern difference is due to beam forming circuit losses and errors because of the attenuator and phase shifter chip operation (imbalance phenomena). In general the LMS algorithm seems to operate efficiently and satisfactorily for the considered scenarios. The experimental radiation pattern did not seem to be significantly affected by circuit losses and imbalances and meets the beam forming requirements. In conclusion the proposed phased array effectively steers radiation pattern and meets the IEEE802.16j air interface

specifications and thus can be utilized for backhaul link realization in a RS based wireless network. Let us mention here that access and backhaul antenna operates in the same frequency band which is very beneficial for network operators due to the high cost of frequency spectrum.

Antennas placed close to each other, operating at the same time and in the same frequency produce distorted radiation pattern due to their interaction. The interaction between radiation elements is called coupling and affects the operation of a system including two or more antennas. In chapter 5, coupling phenomenon was defined and expressed in terms of S parameters [24]. The total electric field of a linear array was written as a function of the isolated element pattern plus the element pattern due to coupling, showing in this way the coupling effect in the array pattern. The analysis of chapter 5 was continued, mentioning the relation between surface waves and mutual coupling [25] and proposing methods of reduction based on literature. Several EBG and DGS structures have been proposed for minimizing the interaction between adjacent antennas and some empirical coupling formulas were denoted and compared.

Continuing with chapter 5, coupling analysis and measurements were performed to evaluate and minimize the antennas interaction. If the RS operates in STR mode then the coupling phenomenon between access and backhaul antenna becomes significant and needs to be minimized. Two new low cost and easy to fabricate designs of access and backhaul antenna were presented and tested in terms of coupling. The new access

antenna presented S_{11}= -14.3dB for 3.5GHz, bandwidth 32MHz, gain 7.9dB with HPBW equal to 36^0 and 51^0 in yz and xz plane respectively. Furthermore the new backhaul link array presented S_{11}= -17.9dB for 3.5GHz with bandwidth 84MHz and a second resonant frequency at 3.9GHz (S_{11}= -14.17dB). The gain of the array is 11.4dB for 3.5GHz and HPBW is equal to 18^0 and 25.5^0 in yz and xz planes respectively. Both antennas have limited bandwidth and especially the backhaul one presents inadequate gain due to high loss substrate (FR4 epoxy, ε_r=4.4, tanδ=0.018) utilized by both antennas. Regarding coupling the antennas were put together in two configurations and S_{21} parameter was measured. The results provided low coupling (S_{21}< -40dB) and the best case was in configuration 2 for angle $\omega=260^0$ (S_{21}= -65.35dB). The experiments showed that the examined configurations presented low level of antenna interaction and can be used in real environments. Finally S_{21} parameter for the frequency range from 3GHz to 4GHz for two commercial antennas with angle $\omega=270^0$ between them were measured and compared to configurations 1 and 2 for the same angle. The comparison showed that configuration 2 proved to be the best one due to the lowest values of S_{21} it provided.

6.2 SUGGESTIONS FOR FURTHER WORK

This work could be extended for further research regarding the following topics:

- The dimensions of the proposed phased array are 32.6×30cm while the RS size is 33×24×12cm. It is clear that the phased array cannot be inserted in the

RS box due to larger size. Further work could be done to provide a new modified design of the phased array with reduced size which could be incorporated within the RS device. In this way the total volume of RS with the antenna system would be decreased and the RS installation process would be facilitated.

- Coupling measurements of the E-shaped access and backhaul antenna could be performed to define the level of interaction between them, for the configurations described in section 6.6. If significant coupling is occurred, then some techniques for coupling reduction could be implemented such as EBG of DGS structure introduction.

- LMS algorithm provided satisfactory results for a variety of theta (θ) angles but maintaining phi (φ) equal to zero. A wider range of phi (φ) angles could be examined and investigate how close is the resulted radiation pattern with the reference signal. The limits of LMS algorithms could be studied by the introduction of two or three nulls with a specific HPBW angle for the main lobe and side lobe suppression below -20dB.

- LMS algorithm was chosen because of low complexity and quick convergence. Other beam forming algorithm could be tested such as RLS and CMA and a comparison could be performed regarding the level and time of convergence.

- The analysis in chapter 4 assumes that the direction of RS and the interference are known. In the case where these two directions are not known, a DOA algorithm is needed to scan the area for the desired signal and interferences and then a beam forming algorithm is applied for proper shaping radiation pattern. So a step forward could be the combination of DOA and beam forming algorithm to produce a fully adaptive and smart antenna system.

- Regarding coupling measurements presented in section 5.6, although the configurations provided satisfactory results, the antennas have narrow bandwidth and less gain. These antenna designs could be improved by utilizing a substrate of lower tanδ, maybe some Rogers RO material and adding a second substrate of lower dielectric constant. In this way the bandwidth and gain could grow.

- The antenna system presented in this thesis refers to a fixed, STR Relay Station. The work could be continued and examine the case of a mobile STR Relay Station where a fully adaptive antenna system is required.

- Both E-shaped antenna and array could be tested in real environment in terms of RSS and SNR to examine their performances in the presence of obstacles.

- The access antenna includes one radiation element. The substitution of the single element by a phased array for access link realization could be also studied. The introduction of many radiation elements could enhance gain

while a beam forming algorithm would provide a broad main lobe focused on high populated areas. MIMO techniques could be investigated for access link improvement.

6.3 REFERENCES

[1] K. Voudouris, N. Athanasopoulos, P. Tsiakas, A. Meir, G. Agapiou, "Relay Extends WiMAX Service", Microwaves & RF, vol. 50, no.1, pp. 68-75, 2011.

[2] N. Athanasopoulos, P. Tsiakas, K. Voudouris, I. Georgas, G. Agapiou, "Multi hop Relay in Next Generation Wireless Broadband Access Networks An Overview", 2nd International ICST Conference on Mobile Lightweight Wireless Systems, Barcelona, Spain, May 2010.

[3] D. M. Pozar, "Microstrip antennas", Proceedings of the IEEE, vol. 80, no. 1, pp. 79 91, January 1992.

[4] A. Sawicki, K. Sachse, G. Jaworski, P. Kabacik, "Comparison of planar antenna feed networks with Wilkinson and coupled line power dividers", 12th International Conference on Microwaves and Radar, vol. 2, pp. 423-427, May 1998.

[5] E.M. Al Ardi, R. M. Shubair, M. E. Al Mualla, "Performance evaluation of the LMS adaptive beam forming algorithm used in smart antenna systems", IEEE 46th Midwest Symposium on Circuits and Systems, vol. 1, pp. 432-435, December 2003.

[6] M. Sonkki, E. Antonino Daviu, M. Ferrando Bataller, E. Salonen, "Optimal dimensions of two microstrip patch antennas for low mutual coupling at 5.8 GHz", 3rd European Conference on Antennas and Propagation, pp. 3515 – 3518, March 2009.

[7] A. K. Bhattacharyya, "Characteristics of space and surface waves in a multilayered structure [microstrip antennas]", IEEE Transactions on Antennas and Propagation, vol. 38, no. 8, pp. 1231 – 1238, August 1990.

[8] S. Shekhawat, P. Sekra, D. Bhatnagar, V. K. Saxena, J. S. Saini, "Stacked Arrangement of Rectangular Microstrip Patches for Circularly Polarized Broadband Performance", IEEE Antennas and Wireless Propagation Letters, vol. 9, pp. 910-913, 2010.

[9] Y. B. Thakare, “Design of fractal patch antenna for size and radar cross section reduction”, IET Microwaves, Antennas & Propagation, vol. 4, no. 2, pp. 175-181, February 2010.

[10] Sang Hyuk Wi, Yong Shik Lee, Jong Gwan Yook, “Wideband Microstrip Patch Antenna With U Shaped Parasitic Elements”, IEEE Transactions on Antennas and Propagation, vol. 55, no. 4, pp. 1196 – 1199, April 2007.

[11] G. Kristensson, P. Waller, A. Derneryd, “Radiation efficiency and surface waves for patch antennas on inhomogeneous substrates”, Microwaves, Antennas and Propagation, IEE Proceedings, vol. 150, no. 6, pp. 477 – 483, December 2003.

[12] K. L. Chung, “A Wideband Circularly Polarized H Shaped Patch Antenna”, IEEE Transactions on Antennas and Propagation, vol. 58, no. 10, pp. 3379 – 3383, October 2010.

[13] Kai Fang Lee, S.L.S. Yang, A.A. Kishk, Kwai Man Luk, “The Versatile U Slot Patch Antenna”, IEEE Antennas and Propagation Magazine, vol. 52, no. 1, pp. 71-88, February 2010.

[14] A. Khidre, Kai Fang Lee, Fan Yang, A. Eisherbeni, “Wideband Circularly Polarized E Shaped Patch Antenna for Wireless Applications [Wireless Corner]”, IEEE Antennas and Propagation Magazine, vol. 52, no. 5, pp. 219 – 229, October 2010.

[15] A. J. Fenn, “Adaptive Antennas and Phased Arrays for Radar and Communications”, Artech House Publishers, January 2008.

[16] Robert C. Hansen, “Phased Array Antennas”, Wiley Interscience 2nd edition, December 2009.

[17] C. A. Balanis, “Antenna Theory: Analysis and Design”, Wiley Interscience 3rd edition, April 2005.

[18] N. Athanasopoulos, P. Tsiakas, K. Voudouris, D. Manor, A. Mor, G. Agapiou, “An IEEE802.16j Prototype Relay Station Architecture”, IEEE MELECON Conference, pp. 1247-1252, Valetta, Malta, April 2010.

[19] V. Genc, S. Murphy, Y. Yu, J. Murphy, “IEEE 802.16j Relay based Wireless Access Networks: An Overview”, IEEE Wireless Communications Magazine Special Issue on Recent Advances and Evolution of WLAN and WMAN Standards, 2008.

[20] Y. Qun, C. Xiang, Y. Xu, X. Xiao, “Performance of LMS algorithm in smart antenna”, (ICMMT), International Conference on Microwave and Millimeter Wave Technology, pp.1372-1375, May 2010.

[21] D. Li, Yunjian Wang, “Study of Smart Antenna Beamformer Based on Constant Modulus Algorithm”, Fourth International Conference on Information and Computing, pp.178-180, April 2011.

[22] Hittite HMC648LP6, Hittite Microwave Corporation, Chelmsford, MA, 2008. Link: http://www.hittite.com/content/documents/data_sheet/hmc648lp6.pdf

[23] Hittite HMC629LP4, Hittite Microwave Corporation, Chelmsford, MA, 2008. Link: http://www.hittite.com/content/documents/data_sheet/hmc629lp4.pdf

[24] Z. Sipus, S. Skokic, M. Bosiljevac, N. Burum, “Study of Mutual Coupling Between Circular Stacked Patch Antennas on a Sphere”, IEEE Transactions on Antennas and Propagation, vol. 56, no. 7, pp. 1834 – 1844, July 2008.

[25] M. A. Khayat, J. T. Williams, D.R. Jackson, S.A. Long, “Mutual coupling between reduced surface wave microstrip antennas”, IEEE Transactions on Antennas and Propagation, vol. 48, no. 10, pp. 1581 – 1593, October 2000.

LIST OF AUTHOR'S PUBLICATIONS

JOURNAL ARTICLES:

[1] **I. Petropoulos**, K. Voudouris, R.A. ABD Alhameed, S.M.R. Jones, and N. Athanasopoulos, "A Novel Design of Microstrip Arrays for Relay Based Wireless Network", International Journal of Antennas and Propagation, vol. 2011.

[2] K. Voudouris, N. Athanasopoulos, A. Meir, D. Manor, P. Tsiakas, I. Georgas, **I. Petropoulos**, G. Agapiou, "2×2 Switch Matrix for WiMAX Relay Station Applications", IEEE Microwave and Wireless Components Letters, vol. 21, no. 8, pp. 424-426, August 2011.

[3] **I. Petropoulos**, Nikos Athanasopoulos, Konstantinos Voudouris, Raed A Abd Alhameed, Steve M R Jones, "Phased Array Antenna Receives 4G Networks", Microwaves and RF, issue November 2012.

CONFERENCES

[1] I. Georgas, **I. Petropoulos**, K. Voudouris, P. Tsiakas, N. Athanasopoulos, M. V. H. Cohen, B. Cyzs, G. Agapiou, A. Rigas, "Relay vs. Repeater Architectures in WiMAX" 6th International ICST conference on mobile multimedia communications, Lisbon, Portugal, September 2010.

[2] N. Athanasopoulos, **I. Petropoulos**, K Voudouris, "2x2 Switch Matrix for a prototype WiMAX Relay Station", International Conference on Electromagnetics in Advanced Applications, Torino, Italy September 2011.

[3] N. Athanasopoulos, **I. Petropoulos**, K Voudouris, "A Phased Array Unit for Adaptive Backhauling in WiMAX Relay Networks", International Conference on Electromagnetic in Advanced Applications, Torino, Italy, September 2011.

SAMPLES OF AUTHOR'S PUBLICATIONS

A Novel Design of Microstrip Arrays for Relay Based Wireless Network

Ioannis Petropoulos[1,2], Konstantinos Voudouris[1], Raed A Abd Alhameed[2], Steve M R Jones[2], Nikos Athanasopoulos[1]
[1]Department of Electronics, Technological Educational Institute of Athens (TEI), Ag. Spyridonos, 12210, Athens, Greece
[2]School of Engineering Design and Technology, Bradford University, Richmond Road, Bradford, BD7 1DP
ipetro@teiath.gr, kvoud@teiath.gr, r.a.a.abd@bradford.ac.uk, S.M.R.Jones@bradford.ac.uk, nathan@teiath.gr

Abstract

A Relay Station (RS) is a smart transceiver used under a 4G wireless network in order to extend network's coverage and capacity. It uses an antenna system that includes an antenna for connecting the Relay with the end users (access link) and the RS with the Base Station (backhaul link). In this paper a 7.9 dBi access and 11.4 dBi backhaul antenna are presented for the frequency range of 3.3 to 3.8 GHz. The antennas are simulated and fabricated and relevant measured results in terms of return loss and radiation pattern are presented and analyzed. Considering that the planes of those two antennas are positioned in an angle ω (omega), two antenna configuration geometries are tested in terms of coupling. The experimental results of S_{21} for several values of the angle ω show that the interaction between the radiating elements is dependent on their relative position. Simulated and experimental results are in good agreement, showing coupling typically less than 40 dB. A comparison in terms of coupling between the proposed antennas and commercial ones proves that the suggested antennas provide 10 dB lower coupling.

1. Introduction

Relay Stations (RS) are network element devices, designed to fill holes in the Base Station (BS) coverage. They receive, enhance and then retransmit the signal after digital processing [1]. The antenna system is critical to the operation of the Relay Station (RS). It aims to connect RS with BS realizing the backhaul connection and RS with user subscribers, realizing the access link. Relays can be used in many wireless networks. The present study refers to a WiMAX wireless network in the range of 3.3 to 3.8 GHz.

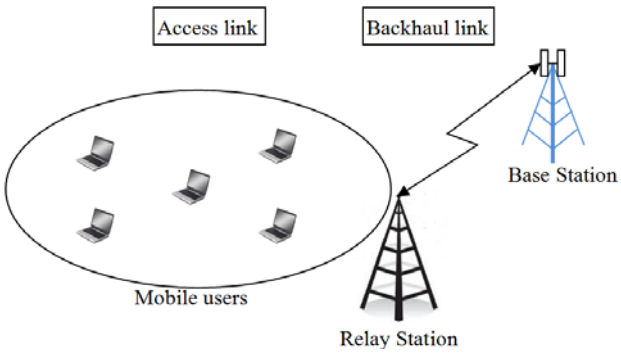

Figure 1: Relay Station operation

Figure 1 summarizes the operation of an antenna system showing that Relay Station can be an intermediate link between Base Station and end user. Such a topology can ensure high quality of data transmission using an antenna system that can efficiently receive and transmit information.

Many antennas have been proposed for use in the WiMAX frequency range, such as U and C slot antennas [2], [3], U-shaped patches [4], and PIFA [5]. Another important issue associated with the antenna, is coupling. Coupling is a phenomenon that expresses the level of interaction between radiation elements. It is necessary to maintain coupling as low as possible to prevent distortion of the transmitted signal. Several studies have been carried out, investigating methods to predict and evaluate mutual coupling [6] [9]. Also special attention has been given to mutual coupling reduction, by placing resonators between radiating elements [10] or by using planar EBG structures [11], [12].

In this paper, two simple, low cost planar antennas are presented, based on microstrip technology, one for the access link and one for backhaul link. These antennas are compared to commercial ones and their features are outlined. The two proposed antennas are positioned together and are examined in terms of coupling. Experimental and simulated results of S_{21} are presented and compared. A clear relation between coupling and the angle between the access and backhaul antenna is found. Finally a coupling comparison between the suggested and commercial antennas is performed and corresponded results are depicted.

2. Access antenna

An access antenna was simulated and fabricated and the relevant results are depicted below. Four patches (radiating elements) fed by microstrip lines are placed on FR4 substrate (ε_r=4.4, h=1.6mm). The excitation is realized by a coaxial cable which is connected to microstrip line. The simulated antenna is depicted in Figure 2a, while the fabricated one can be seen in Figure 2b. Access antenna's dimensions are 12.5cm×10cm. Simulations have been performed using Ansoft HFSS v.12. Measurements of Return Loss (S_{11}) and radiation pattern have been taken in an anechoic chamber.

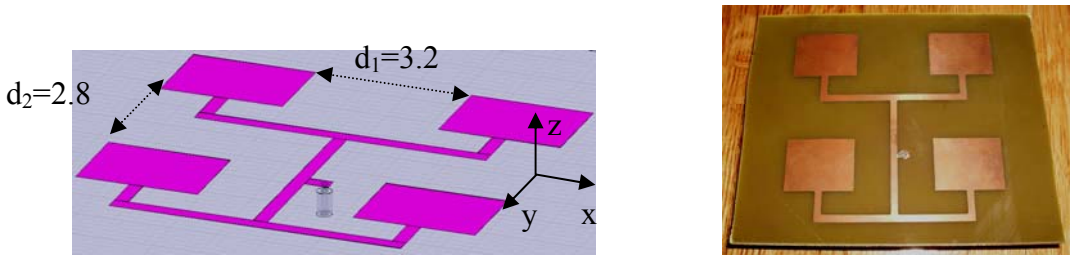

(a) (b)

Figure 2: Antenna geometry and measurements; (a) Antenna model, (b) Antenna prototype

The S_{11} parameter as a function of frequency is depicted below.

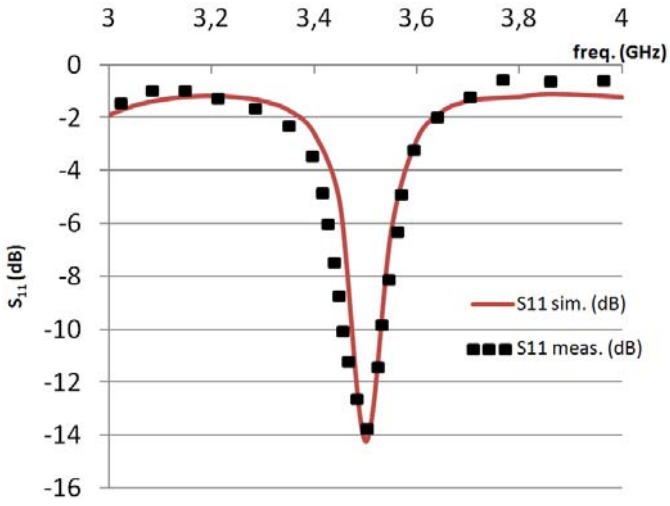

Figure 3: S_{11} parameter for simulated and fabricated antenna.

For the experimental estimation of S_{11}, a Vector Network Analyzer was used (Anritsu VNA MS2036A). Before measurements, calibration was performed in order to take into consideration the cable losses and increase the level of experiment accuracy. The excitation of access and backhaul antenna is realized by a coaxial cable which feeds the microstrip line. In the connecting point between cable and microstrip line, losses are introduced that reduce the amount of power that enters the antenna. That is why this antenna presents narrow bandwidth [13].

Access antenna presents S_{11}= -14.23dB for 3.5GHz. The impedance bandwidth of the antenna is estimated to be 31.8MHz (S_{11}<-10dB [14]). The radiation pattern of the simulated and fabricated antenna is illustrated in Figure 4a for yz plane at 3.5GHz. Half Power Beamwidth (HPBW) is 35.96^o. The antenna presents Gain G =7.94dBi in the direction of maximum emission. Let us mention here that FR4 substrate has an increased loss tangent (tanδ=0.02) which means low quality factor and thus increased dielectric losses. That is why the antenna gain is appeared to be less than what is expected but high enough to support the access link.

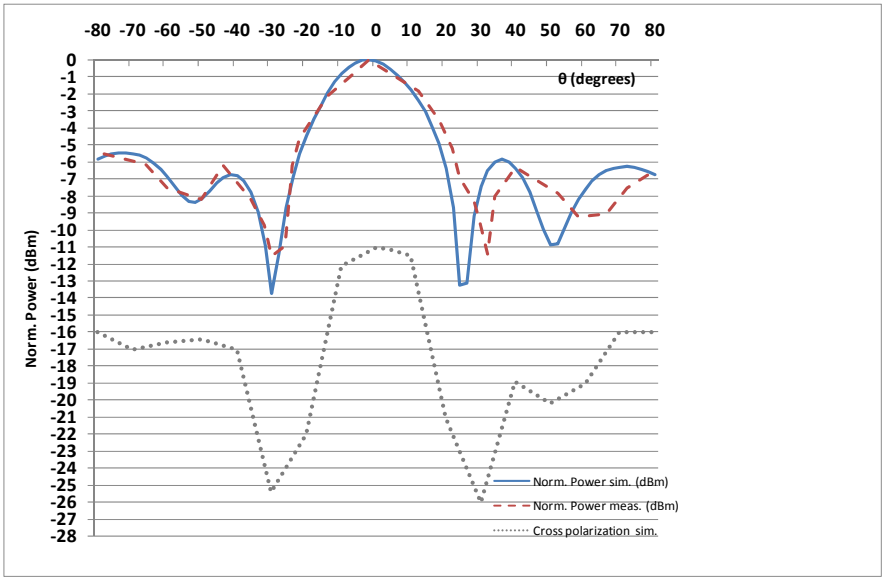

Figure 4a: Radiation pattern of access antenna in yz plane for 3.5GHz

The radiation pattern in xz plane is depicted in Figure 4b, presenting HPBW=51.07^{o}.

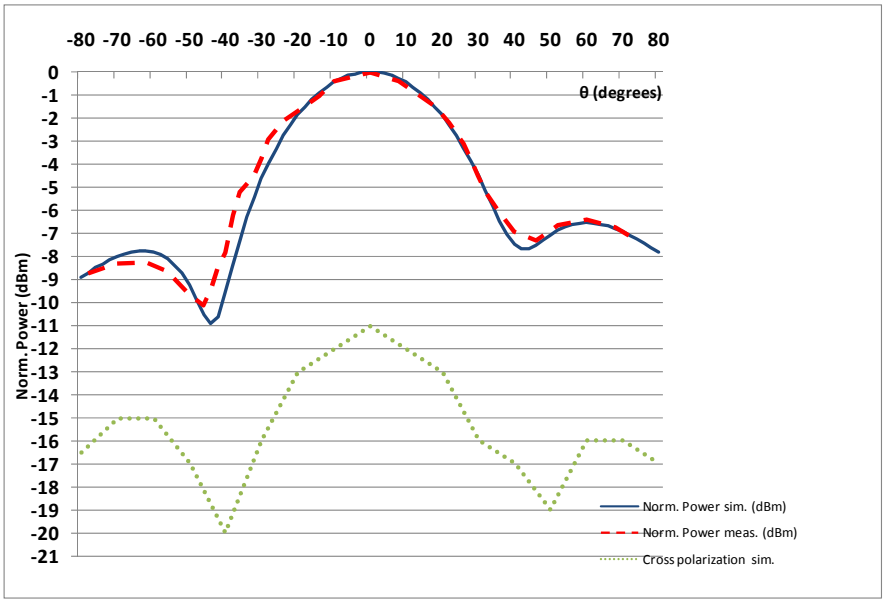

Figure 4b: Radiation pattern of access antenna in xz plane for 3.5 GHz

Figures 4a and 4b also depict the simulated cross polarization level of the access antenna. Cross polarization expresses the amount of power emitted orthogonal to the desired direction and it has to be as low as possible. Surface waves are dependent of the substrate and give rise to cross polarization. For minimizing these waves, materials with low dielectric losses could be chosen.

3. Backhaul antenna

An antenna array intended to be used for connecting the Relay with the Base Station is presented in this section. The simulated and constructed antenna can be seen in Figures 5a and 5b, respectively. Backhaul antenna's dimensions are 25.5cm×21.5cm. Figure 5c shows the radiation pattern measurements of backhaul antenna taken in an anechoic chamber.

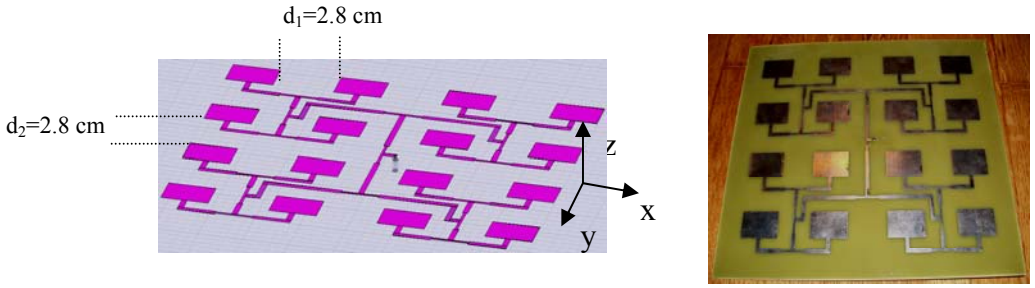

(a) (b)

Figure 5: Backhaul antenna geometry and measurements (a) Backhaul antenna model (b) Backhaul antenna prototype

The S_{11} parameter for the simulated and fabricated antenna is shown below (Fig. 6) where a slight difference is attributed to the imprecise process of construction.

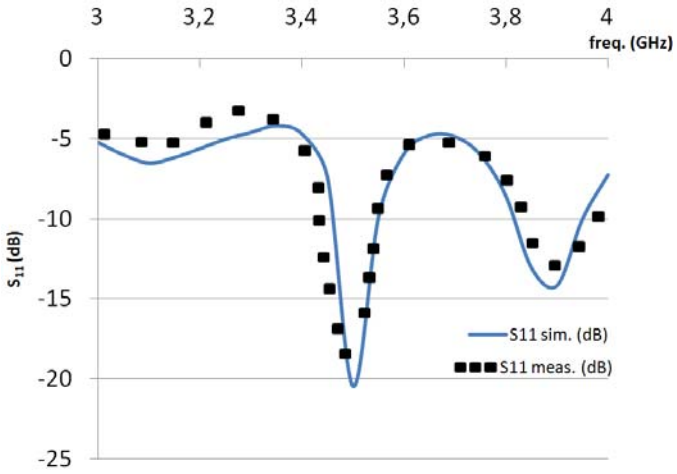

Figure 6: S_{11} parameter for backhaul antenna

Backhaul antenna presents S_{11}= -17.88dB at 3.5GHz and impedance bandwidth equal to 83.9MHz. A second resonance frequency is appeared at 3.9GHz where S_{11}=-14.17dB. The gain of the backhaul antenna has been found 11.4dBi for 3.5GHz. Gain could be greater if a substrate of lower dielectric losses was used.

The radiation pattern is presented in Figure 7a where a narrow beam is noticed due to the increase in the number of radiation elements compared to the case of the access antenna. HPBW has been measured 18.2^{o}.

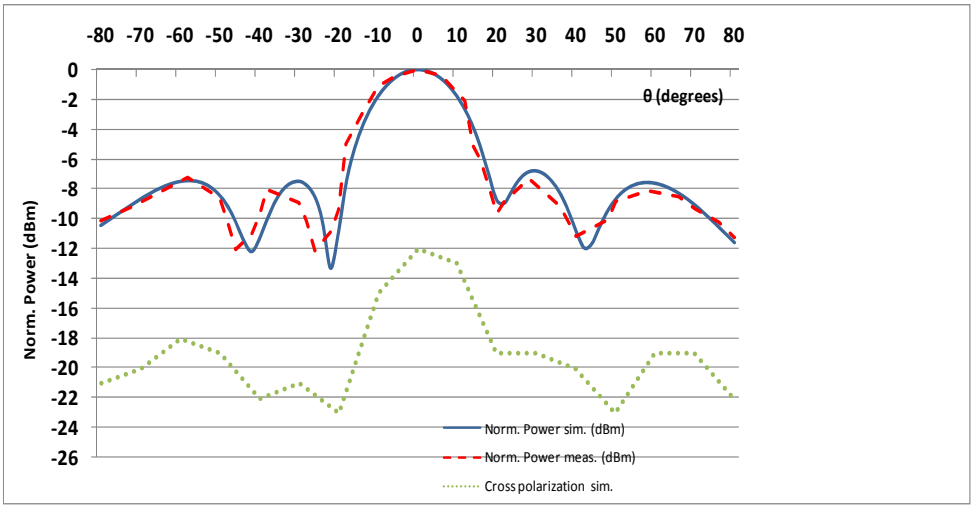

Figure 7a: Radiation pattern of backhaul antenna in yz plane for 3.5GHz

The radiation pattern in xz plane is presented in Figure 7b. In this case HPBW=25.45^{o}.

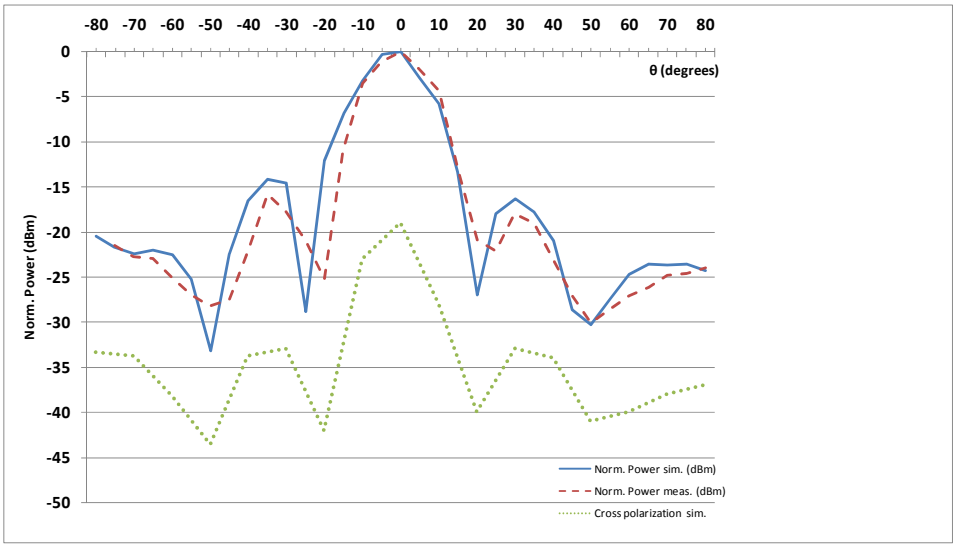

Figure 7b: Radiation pattern of backhaul antenna in xz plane for 3.5GHz

Figures 7a and 7b also represent the cross polarization level which is appeared to be increased due to the FR4 substrate.

Measured access and backhaul antenna characteristics are denoted in Table 1.

Table 1: Access and backhaul antenna features

	S_{11} (dB) for 3.5GHz	Gain (dBi)	HPBW (degrees) xz plane	HPBW (degrees) yz plane	Bandwidth (MHz)
Access antenna	-14.23	7.9	51.07	35.96	31.8
Commercial access antenna (1SKF 333808W)	-15.08	8	68		500
Backhaul antenna	-17.88	11.4	25.45	18.20	83.9
Commercial backhaul antenna (TSWL315177)	-18.48	18	17		400

Gain and bandwidth is increased in the case of the backhaul antenna due to the larger number of radiation elements (16 elements) compared to the access antenna (4 elements). Also Half Power Beamwidth (HPBW) is decreased in the backhaul antenna. In addition a comparison is performed between the proposed antennas and relevant commercial ones. Regarding access antenna, model 1SKF 333808W is a panel antenna presenting HPBW=68^o, gain 8dBi and bandwidth 500MHz. The proposed access antenna gives similar gain but less HPBW and bandwidth due to FR4 substrate. Bandwidth could be enlarged by using a substrate of lower loss tangent such as Rogers RO 3006 (ε_r=6.15, tanδ=0.0025) or Rogers RT Duroid 5880 (ε_r=2.2, tanδ=0.0009). Wider bandwidth could also occur using stacked geometry including two or more substrates separated by air gaps. FR4 substrate was chosen because of its low cost and ease of fabrication. Regarding backhaul antenna, the commercial one presents enhanced bandwidth and gain. The proposed backhaul antenna uses low cost FR4 substrate which has high loss tangent that leads to limited gain, bandwidth and high side lobes. The design of access and backhaul antenna has been made maintaining low cost of fabrication and low complexity level. Both antennas can be improved in terms of gain and bandwidth by using stacked geometries and dielectrics of low losses.
Since both proposed antennas have the same resonant frequency and the Relay Station performs in the Simultaneously Transmit Receive (STR) mode, it is necessary to examine the coupling phenomenon between the antennas.

4. Coupling effects study

Two cases of configuration between the proposed antennas are examined. These configurations are shown in the figures that follow. Coupling between the two antennas in terms of S_{21} is measured using Anritsu VNA MS2036A and results are depicted below.

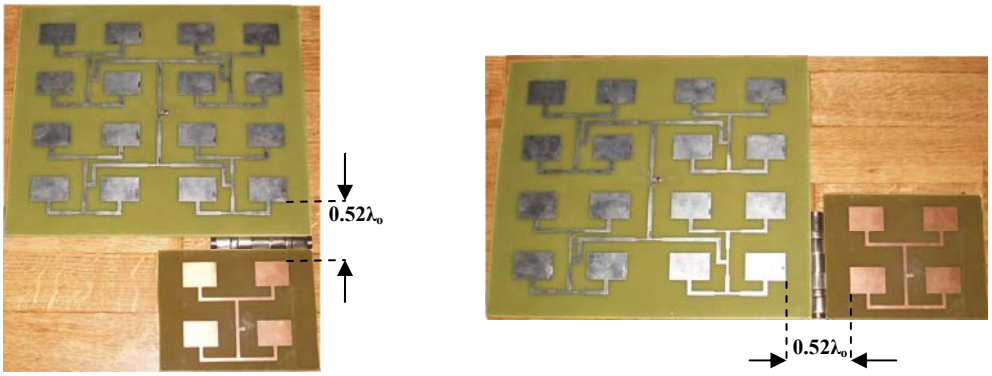

(a) (b)

Figure 8: Antenna arrangements under test; (a) Configuration 1(b) Configuration 2

Coupling measurements have been taken in anechoic chamber to achieve precision and validity of results. Figure 9a and Figure 9b show the experimental setup. The distance between two adjacent radiation elements of access and backhaul antennas is $0.52\lambda_o$. This distance is adequate for low mutual coupling [15] and maintaining the total size of the antenna system as small as possible.

(a) (b)

Figure 9: Access and backhaul antenna setup during coupling measurements

Study of configurations 1 and 2 due to the relative position of antennas can be consider as coupling investigation in E-plane and H –plane respectively.

4.1 Configuration 1

In the first case (configuration 1), the two antennas are put in such a way, so that the angle between them is $\omega=180^0$ and then ω increases with a step of 10^0 and final reaches 270^0.The scheme that specifies the proposed setup can be seen in Figure 10.

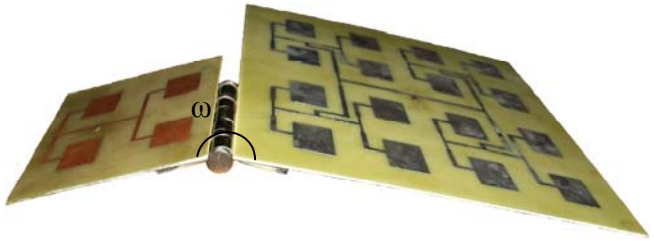

Figure 10: The investigated setup

Together with the experimental measurements, simulations of S_{21} as a function of the angle ω have been carried out. Simulation and measurement of S_{21} for the case of $\omega=180^0$ is depicted in Figure 11b.

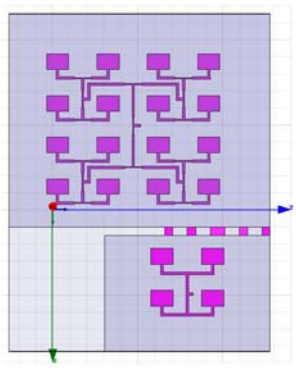

Figure 11a: Simulation of access and backhaul antenna system for configuration 1 ($\omega=180^0$)

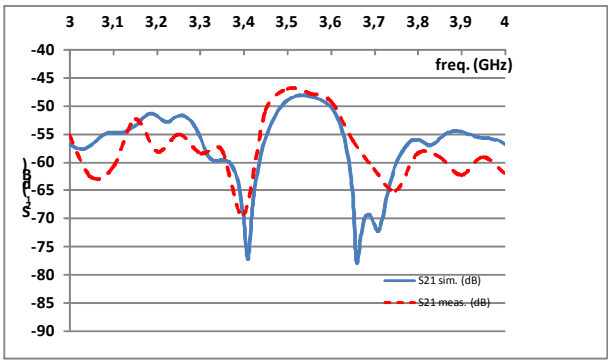

Figure 11b: Simulation and experiment S_{21} for $\omega=180^0$

Figure 11b shows that simulation and experimental curve of S_{21} is located below -40dB for the frequency range of 3.4 to 3.6 GHz.

For $\omega=190^0$ the experimental setup is depicted in Figure 12a and the corresponded results in Figure 12b.

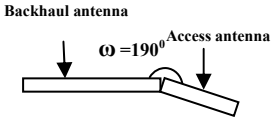

Figure 12a: Configuration for $\omega=190^0$

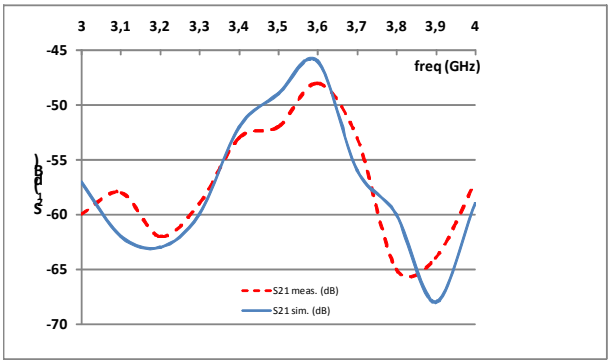

Figure 12b: S_{21} for $\omega=190^0$

For $\omega=200^0$ the experimental setup is depicted in Figure 13a and the corresponded results in Figure 13b.

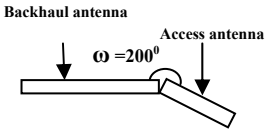

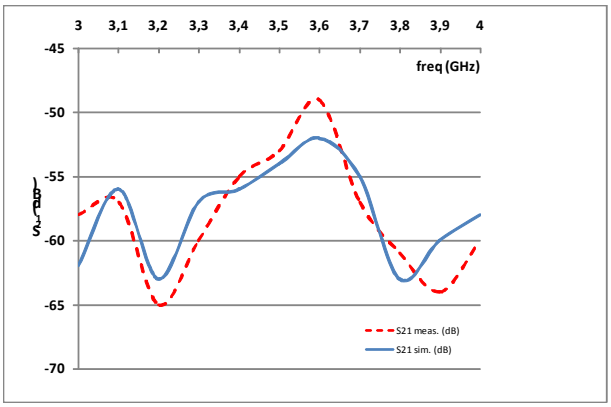

Figure 13a: Configuration for ω=200⁰

Figure 13b: S_{21} for ω=200⁰

The experiment continues for ω=210⁰ till 270⁰ with a step of 10⁰. Coupling can change the operation frequency of an antenna and distort the radiation pattern. That is why it is necessary to maintain it at a low level. Coupling effect is mainly caused by space waves that end up from one antenna to another (Fig. 14). It is also dependent on surface waves that travel through dielectric [15]. From the analysis performed for configuration 1 it is derived that increasing the angle ω seems to reduce the density of field lines that end up from one antenna to the other thus reducing coupling effect.

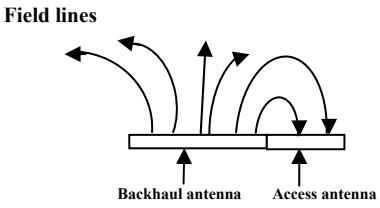

Figure 14: Field lines that cause coupling effect

4.2 Configuration 2

In this case the access and backhaul antenna are positioned as shown in Figure 15.

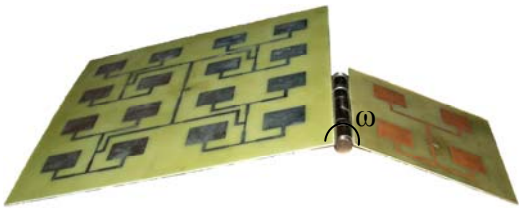

Figure 15: The investigated setup

Together with the experimental measurements, simulations of S_{21} against angle ω for configuration 2 have been performed. The case of ω=180⁰ is depicted in Figure 16b.

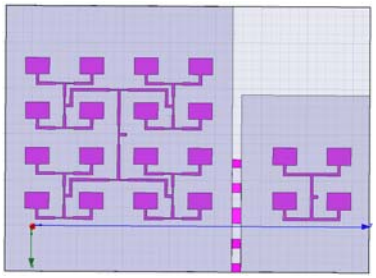

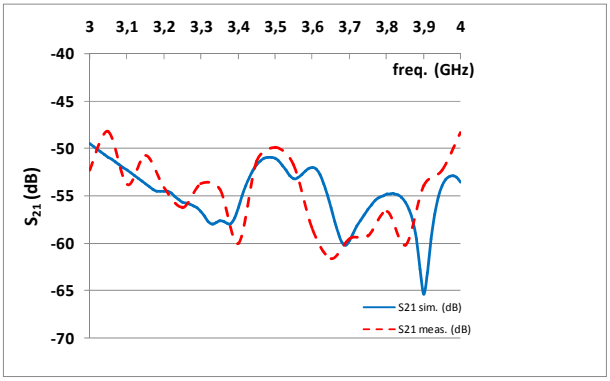

Figure 16a: Simulation of access and backhaul antenna for configuration 2 ($\omega = 180^0$)

Figure 16b: Simulation and experiment S_{21} $\omega=180^0$

Figure 16b represents the simulation and experimental curve for S_{21}. Coupling is at an acceptable level (<-40dB) for the frequency range 3.4 to 3.6GHz.

For $\omega=190^0$, the corresponded results can be seen in Figure 17b.

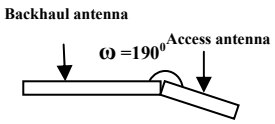

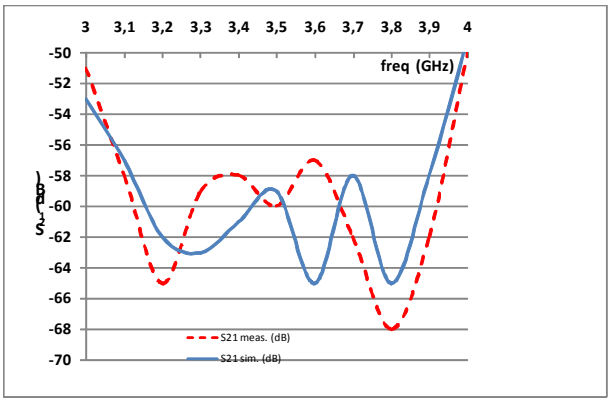

Figure 17a: Configuration for $\omega=190^0$

Figure 17b: S_{21} for $\omega=190^0$

For $\omega=200^0$ the experimental setup is depicted in Figure 18a and the corresponded results in Figure 18b.

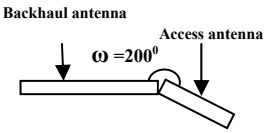

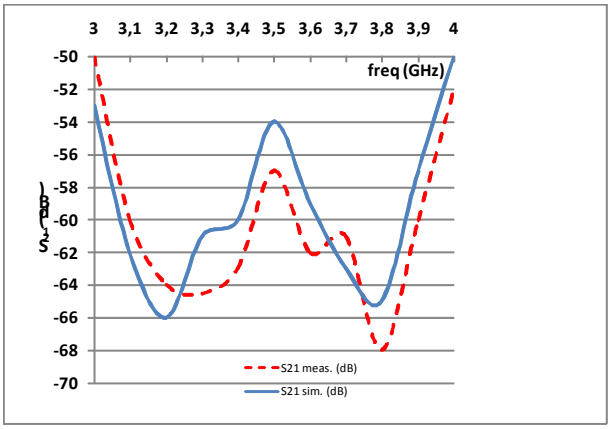

Figure 18a: Configuration for ω=200⁰

Figure 18b: S_{21} for ω=200⁰

The experiment continues for ω=210⁰ up to 270⁰ with a step of 10⁰.

In configuration 2 the coupling effect is weaker compared to configuration 1 as it produces S_{21} that varies from -48 dB to -68dB.

5. Results

In the tables that follow, the maximum value of experimental S_{21} is denoted in the frequency range of 3.4GHz to 3.6GHz, for each value of angle ω.

Table 2: S_{21} variation for configuration 1

Configuration 1	ω (degrees)	S_{21} max(dB)
	180	-47,67
	190	-46,84
	200	-49,15
	210	-50,46
	220	-50,3
	230	-50,56
	240	-50,83
	250	-54,94
	260	-54,92
	270	-53,94

The maximum value of S_{21} as a function of the angle ω is depicted in Figure 19.

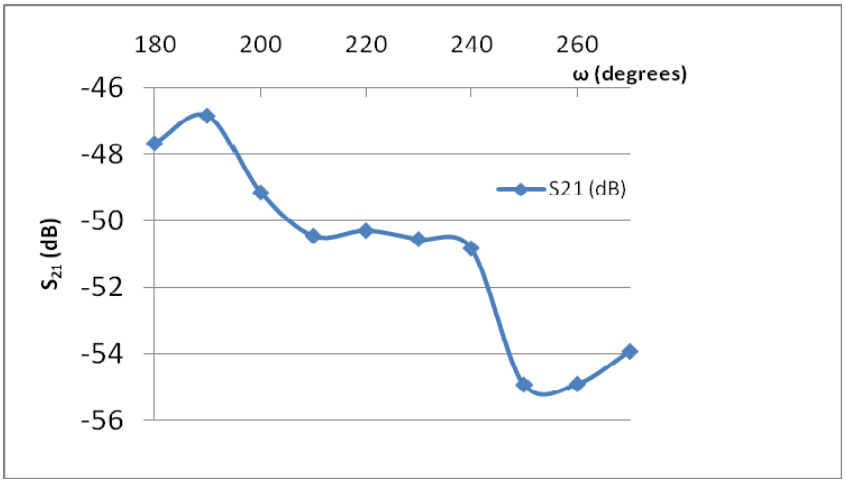

Figure 19: S_{21} as a function of angle ω for configuration 1

The table for configuration 2 follows together with the corresponded S_{21} diagram.

Table 3: S_{21} variation for configuration 2

Configuration 2	ω (degrees)	S_{21} max(dB)
	180	-55,56
	190	-54,7
	200	-57,34
	210	-61,01
	220	-60,26
	230	-58,36
	240	-59,1
	250	-63,02
	260	-65,35
	270	-60,68

The maximum value of S_{21} as a function of the angle ω is depicted in Figure 20.

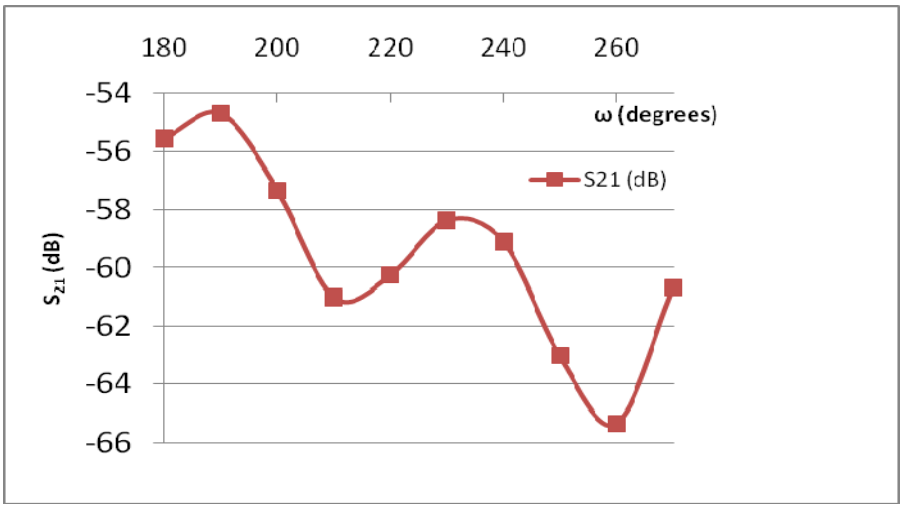

Figure 20: S_{21} as a function of angle ω for configuration 2

Both configurations 1 and 2 provide a low level of coupling (S_{21} <-40dB). Coupling appears to decrease non linearly while ω increases. Configuration 2 is more acceptable because S_{21} takes values lower than -50dB for all angles of ω. The simulated coupling results provide some confidence that the levels will remain low between the angles at which measurements were performed.

A comparison in terms of coupling between the proposed antennas and the commercial ones presented in table 1 has also been performed. Both commercial and proposed antennas have been measured in terms of coupling for ω=270°. The Relay set up including the suggested access and backhaul antenna can be seen in Figure 21.

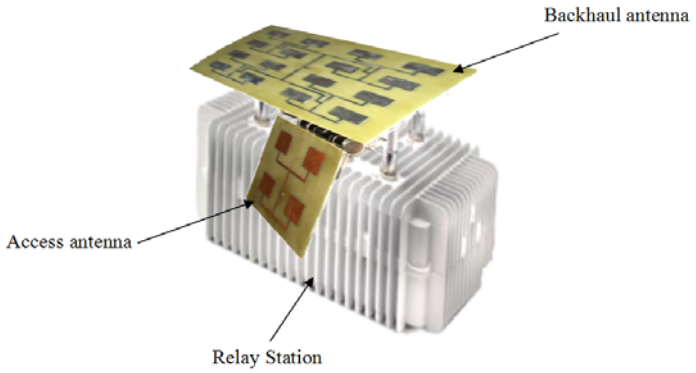

Figure 21: Relay Station with the proposed antennas

Figure 22 shows coupling variations for commercial antennas and the proposed ones for configurations 1 and 2 at ω=270°.

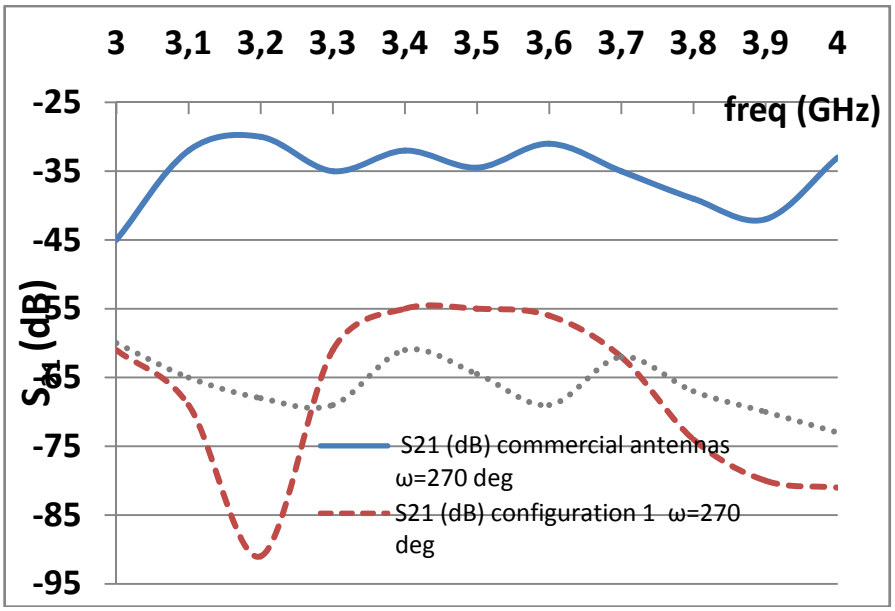

Figure 22: Coupling comparison

It is clear that both proposed configurations give lower values of S_{21} compared to the commercial antennas proving the efficiency and competence of the suggested setup.

6. Conclusions

This paper describes the design, simulation and testing of two microstrip antennas (access and backhaul). Antenna characteristics in terms of gain, bandwidth and beam width (HPBW) in xz and yz plane are approximately 8dBi, 32 MHz, 51° and 36° for the access antenna and 11.4 dBi, 84 MHz, 25.5° and 18° for the backhaul antenna respectively. S_{11} parameters and radiation pattern in xz and yz plane level for simulated and fabricated antennas were presented. The comparison between measured and simulated results shows good agreement. Access and backhaul antennas were put alongside and their interaction is investigated. Two configurations are presented for which measured and simulated S_{21} are given. Coupling (S_{21}) is investigated against the angle between the antenna planes for the two configurations. Maximum values of S_{21} against ω were presented for the frequency range of 3.4 to 3.6 GHz in which the antennas operate. Coupling is typically below -40 dB. Diagrams of S_{21} against ω show that coupling decreases with angle increase. Measurements and simulations show that the presented antennas could be used in both configurations under a Relay based network as they present an acceptably low level of interaction for all values of ω. The comparison between the proposed patch antennas and the commercial ones prove that the suggested antennas provide 10 dB lower coupling providing low interaction and high isolation.

Acknowledgements

The present work has been performed in the scope of REWIND ("RElay based WIreless Network and StandarD") European Research Project and has been supported by the Commission of the European Communities – Information Society and Media

Directorate General (FP7, ICT The Network of the Future, Grant Agreement No.216751).

References

[1] Iraklis Georgas, Ioannis Petropoulos, Konstantinos Voudouris, Panagiotis Tsiakas, Nikos Athanasopoulos, Mikael V. H Cohen, Baruch Cyzs, George Agapiou, and Andreas Rigas, "Relay vs. Repeater Architectures in WiMAX", 6th Internatiohal ICST conference on mobile multimedia communications MOBEMEDIA, Lisbon Portugal, 6-8 September 2010.

[2] AbuTarboush, H.F. Al Raweshidy, H.S. Nilavalan, R., "Triple band double U slots patch antenna for WiMAX mobile applications", 14th Asia Pacific Conference on Communications, pp.1-3, 14 16 October 2008.

[3] Tlili, B., "Design of double C slot microstrip patch antenna for WiMax application", IEEE Antennas and Propagation Society International Symposium, pp.1-4, 11-17 July 2010.

[4] Kin Lu Wong, Hao Chun Tung, "An inverted U shaped patch antenna for compact operation", IEEE Transactions on Antennas and Propagation, vol.51, no.7, pp. 1647-1648, July 2003.

[5] AbuTarboush H.F., Nilavalan R., Al Raweshidy H.S., Budimir, D., "Design of planar inverted F antennas (PIFA) for multiband wireless applications", International Conference on Electromagnetics in Advanced Applications, pp.78-81, 14-18 September 2009.

[6] Wang S., Guo L., Chen X., Parini C.G., McCormick J., "Analysis of mutual coupling in broadband arrays", Antennas and Propagation Society International Symposium, pp.1-4, 5-11 July 2008.

[7] Hizan H.M., Awang A.H., "Investigation of mutual coupling effect between five element arrays of half cylindrical DRAs", Sensors and the International Conference on new Techniques in Pharmaceutical and Biomedical Research, pp. 233-238, 5-7 September 2005.

[8] Zhou Qi, Lei Zhen ya, Wang Peng, Xie Yong jun, Xiang Min, He Min, "An Accurate Mutual Coupling Calculation For Microstrip Antennas For Impedance Mismatching", 7th International Symposium on Antennas, Propagation & EM Theory, pp.1-4, 26-29 October 2006.

[9] Min Wang, Zhongxiang Shen, "Nulling of Antenna Arrays Including the Mutual Coupling Effect", Vehicular Technology Conference, Spring 2008.

[10] Minz L., Garg R., "Reduction of mutual coupling between closely spaced PIFAs", Electronics Letters, vol.46, no.6, pp.392-394, March 2010.

[11] Rajo Iglesias E., Quevedo Teruel O., Inclan Sanchez L., “Mutual Coupling Reduction in Patch Antenna Arrays by Using a Planar EBG Structure and a Multilayer Dielectric Substrate”, IEEE Transactions on Antennas and Propagation, vol.56, no.6, pp.1648-1655, June 2008.

[12] Caminita F., Costanzo S., Di Massa G., Guarnieri G., Maci S., Mauriello G., Venneri I., “Reduction of Patch Antenna Coupling by Using a Compact EBG Formed by Shorted Strips With Interlocked Branch Stubs”, IEEE Antennas and Wireless Propagation Letters, vol.8, pp.811-814, 2009.

[13] Kumar, G. and Ray, K.P., “Broadband Microstrip Antennas”, Artech House, Inc, 2003.

[14] Abegaonkar Mahesh P, Aditya V. Krishna, Basu Ananjan, Koul Shiban K, “Parametric Study of a Parasitically fed Broadband Monopole Patch Antenna”, First International Conference on Industrial and Information Systems, pp.450-453, 8-11 August 2006.

[15] Jedlicka R., Poe M., Carver K., “Measured mutual coupling between microstrip antennas”, IEEE Transactions on Antennas and Propagation, vol.29, no.1, pp. 147-149, January 1981.

Phased Array Antenna Receives 4G Networks

Ioannis Petropoulos[1,2], Nikos Athanasopoulos[1], Konstantinos Voudouris[1], Raed A Abd Alhameed[2], Steve M R Jones[2]

[1]Department of Electronics, Technological Educational Institute of Athens (TEI), Ag. Spyridonos, 12210 Athens, Greece,
e mail: http://www.teiath.gr/stef/electronics/index.php?lang=en
[2]School of Engineering, Design and Technology, University of Bradford, Richmond Road, Bradford BD7 1DP, UK,
e mail: http://www.edt.brad.ac.uk/home/

Abstract
Relay Stations are devices that increase throughput and capacity of a wireless network. They communicate with Base Station (backhaul link) as well as end users (access link). For backhaul link, Relays are equipped with special beam steering arrays. This work presents a phased array with beam steering features that is designed and fabricated for backhaul link realization in a 4G Relay based wireless network. The proposed phased array operates at 3.42 GHz, providing 21.17dBi gain and 424MHz bandwidth. The phased array comprises modified E shaped patch elements and a beam forming circuit for power division and signal processing. Least Mean Square algorithm (LMS) is applied to provide steerable main lobe, nulls at predefined directions and side lobes suppression below desirable levels. LMS algorithm controls both amplitudes and phases of antenna elements excitation currents. Several simulations of beam forming scenarios show efficient operation of LMS algorithm.

Keywords: Relay Stations, phased array, beam forming, LMS algorithm

I. Introduction

Phased arrays are widely used in wireless networks from Base Stations to steer radiation to desired directions where end users stand and place nulls in direction of interference [1], [2]. Many beamforming algorithms have been proposed and studied in literature for beam steering realization such as Least Mean Square Algorithm (LMS), Constant Modulus Algorithm (CMA) and Recursive Least Square Algorithm (RLS) [3], [4]. These algorithms provide different convergence time and complexity level. Moreover, many antenna shapes and configurations have been proposed for achieving bandwidth and gain enhancement [7], [8].

In this paper a phased array is designed, simulated and fabricated to be incorporated in a prototype WiMAX Relay Station [9] in order to establish backhaul link, which is the link between Relay Station and its super ordinate Base Station.

The proposed phased array includes a 4×4 microstrip modified E shaped patch array [10] based on stacked geometry [11]. In addition a beam forming circuit is designed and fabricated for power division, signal processing and array excitation. LMS algorithm is used to properly assign phases and amplitudes to each radiation element and thus steer the main lobe of radiation to the direction of a Base Station. MathCAD v.14 is used to generate LMS algorithm. When phases and amplitudes are obtained, they are introduced in simulated and fabricated phased array. The simulation and experimental radiation pattern is derived, depicted and commented. Figure 1 shows the application of the proposed phased array design.

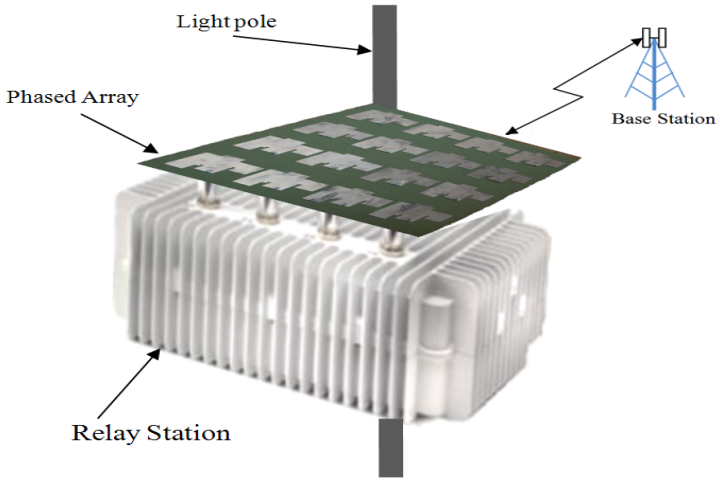

Figure 1: Proposed phased array configuration

In section II, the array design is analyzed in terms of configuration, scattering parameter S_{11} and radiation pattern. The proposed setup is compared to a similar commercial antenna in order to prove the efficiency of the designed one. In section III the beam forming module is described in terms of structure. Simulated and experimental S_{11} is derived, depicted and commented. In section IV the beam forming algorithm (LMS) is applied using MathCADv.14, requiring specific radiation pattern characteristics and obtaining values of phase and amplitude current excitations. These values are assigned to the radiation elements of the array and the radiation pattern is steered properly. Several beam forming scenarios are considered and relevant simulated and experimental radiation patterns are obtained and commented. Section V includes all conclusions from the analysis that has proceeded.

II. Antenna array

The 4×4 antenna array comprises modified E Shaped radiation elements with dimensions denoted in figure 2.

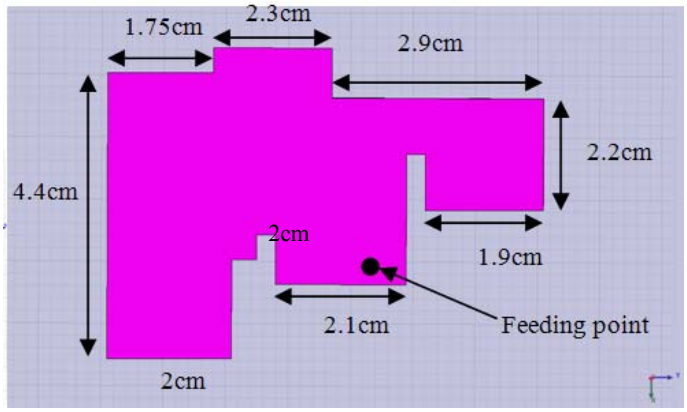

Figure 2: E shape antenna scheme

The modified E-shaped elements are placed on foam substrate (ε_r=1) with height h=0.5cm. Foam substrate is then placed on Rogers RO 3006 (ε_r=6.15) with thickness h=1.28mm. Rogers RO 3006 substrate is then mounted on ground plane of 35μm

copper. Modified E-shaped elements are coaxially fed. The structure of the proposed array is depicted in figure 3.

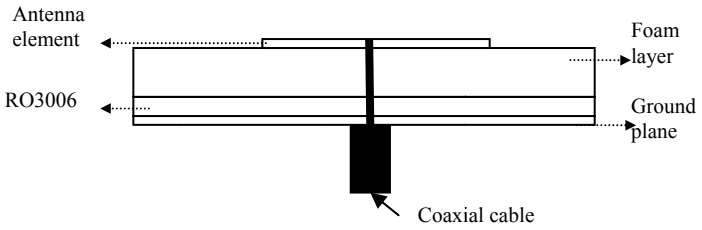

Figure 3: Cross section of phased array structure

Figure 4(a) depicts the simulated phased array indicating its dimensions and figure 4(b) shows the fabricated one.

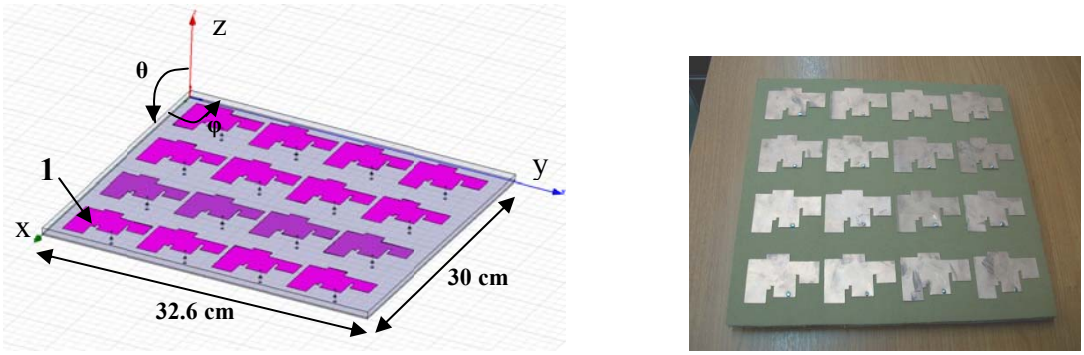

(a) **(b)**

Figure 4: (a) Simulated 4×4 Phased array (b) Fabricated 4×4 Phased array

The modified E shaped radiation elements and the usage of two substrates (Rogers RO and foam layer) are utilized for enhanced bandwidth and gain [10]. In figure 5, the edge to edge distance between two elements is denoted. The center to center distance between two adjacent elements is $0.8\lambda_0$, where λ_0 is the free space wavelength. This value has been chosen in order to produce a radiation pattern with low side lobe levels and for grating lobes prevention [12].

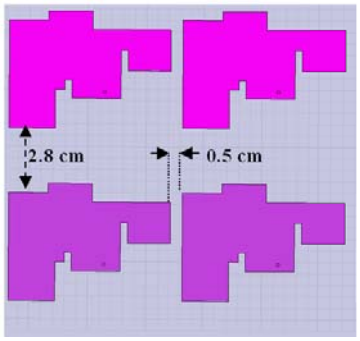

Figure 5: Inter element spacing

In figure 6, simulation and measurement curve of scattering parameter S_{11} of element "1" shown in figure 4(a) is depicted. For the experimental S_{11} measurement of element "1", all other elements have been terminated using 50Ω impedances for eliminating mutual coupling effect.

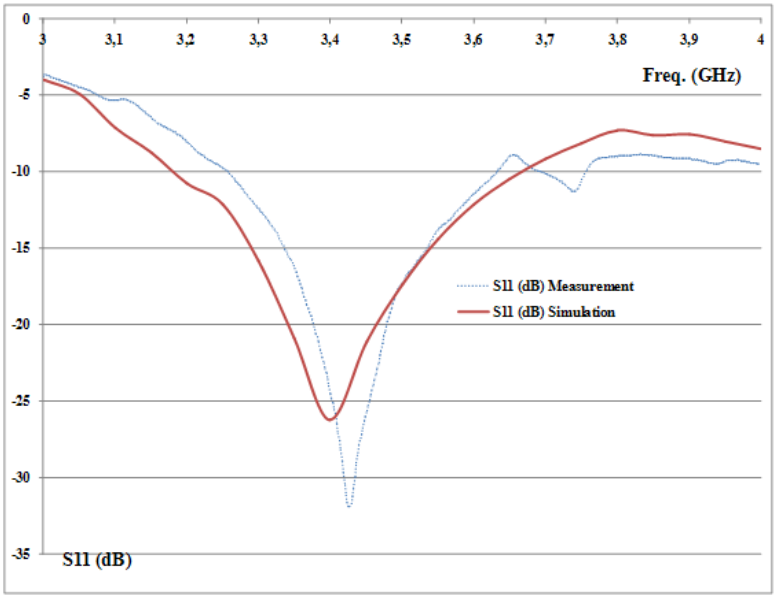

Figure 6: S_{11} simulation and measurement for E shape antenna

Both curves of figure 6 are in good agreement proving that the proposed antenna operates at 3.418GHz with a bandwidth of 424MHz (S_{11}<-10dB) or 12.4%. S_{11} measurements have been obtained using the Anritsu MS2036A VNA instrument.
Simulation and experimental radiation pattern of the 16 element array is shown in figure 7.

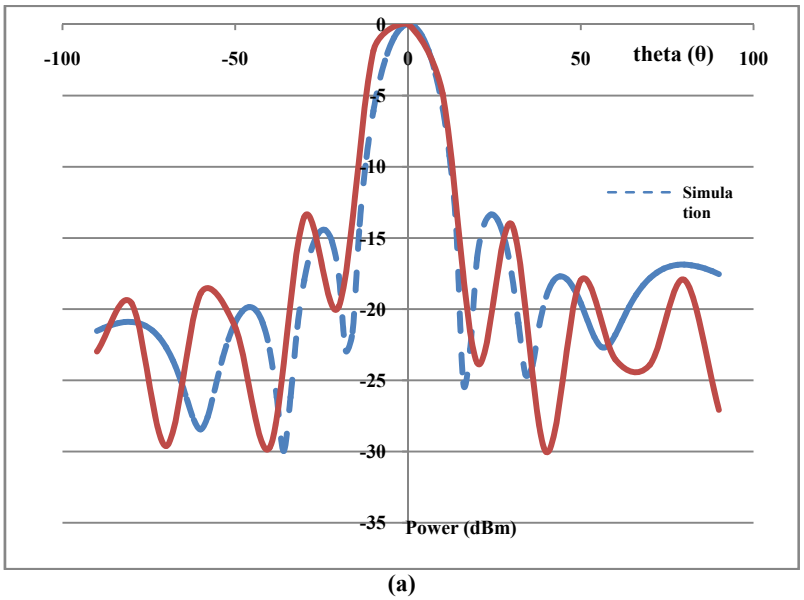

(a)

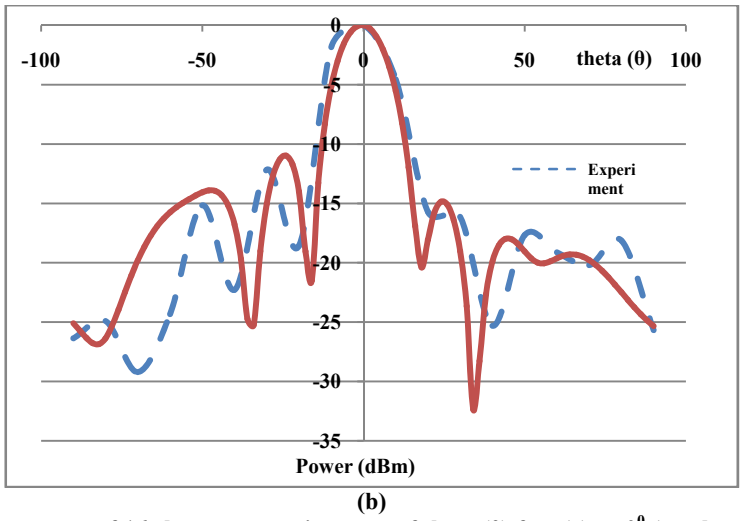

Figure 7: Radiation pattern of 16 element array in terms of theta (θ) for: (a) $\varphi=0^0$ (xz plane) and (b) $\varphi=90^0$ (yz plane)

Angle theta and xyz planes are denoted in figure 4a. Measurements have been performed in anechoic chamber.

The currents that excite each radiation element have the same amplitude and phase. The produced pattern presents a main lobe at θ=0deg and side lobes lower than 10dBi. The radiation patterns depicted in figure 7 are obtained for the frequency of 3.418GHz. The characteristics of the proposed array together with the properties of a commercial antenna operating at 3.5GHz are denoted in table 1.

Table 1: Proposed 16 element array and commercial backhaul antenna

Antenna model	Gain (dBi)	HPBW yz plane (deg)	HPBW xz plane (deg)	Bandwidth (MHz)
4×4 phased array	21.17	14.44	14.25	424
Commercial backhaul antenna Rfwel (TSWL315177)	18	15	15	500

The proposed array presents enhanced gain and low Half Power Beam width (HPBW) proved to be suitable for point to point communication. The designed array satisfies the requirements of the IEEE802.16j protocol for WiMAX and can be used for backhaul link realization between the Relay Station and the Base Station.

III. Beam forming module

Beam forming module is a two substrate planar circuit that includes two 1:8 power dividers. The proposed circuit has been designed and simulated in ADS2009 and then fabricated. The circuit has the following form:

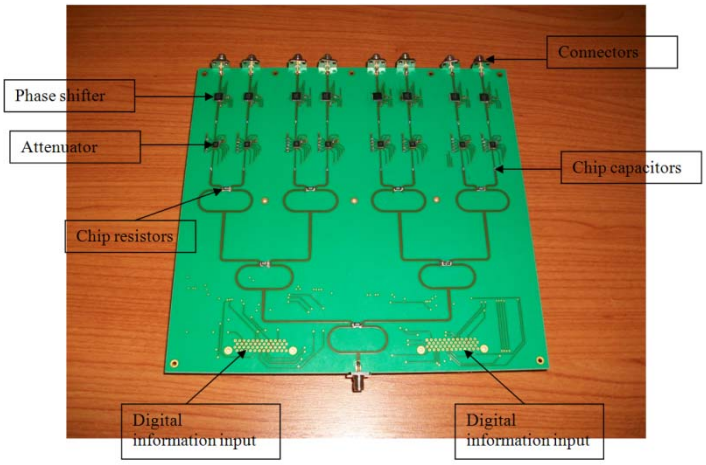

(a)

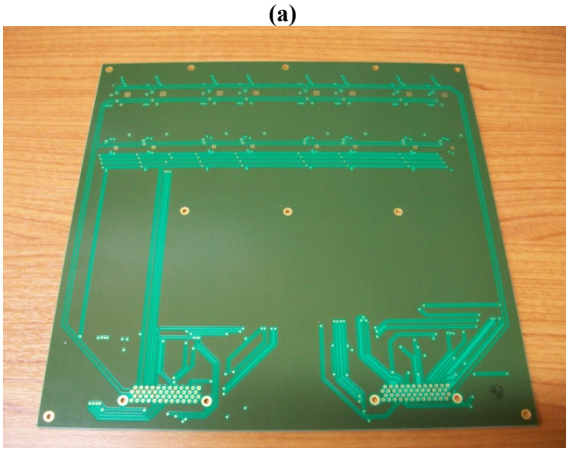

(b)

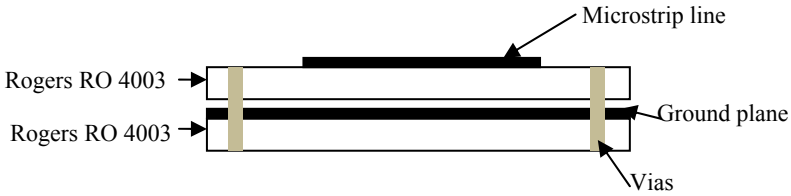

(c)

Figure 8: Beam forming unit (a) Top view (b) bottom view (c) cross section

The circuit includes Wilkinson power dividers [13], chip resistors 100Ω and capacitors, commercial digital attenuators (HITTITE HMC629LP4) and digital phase shifters (HITTITE HMC648LP6). The microstrip line circuit is placed on Rogers RO4003 substrate (ε_r=3.55, h=0.508mm). A second Rogers RO4003 substrate is placed beneath the first, on the top side of which the ground plane is positioned. Amplitudes and phases of each radiation element enter the circuit from digital information inputs and are assigned to specific attenuators and phase shifters respectively. Figure 8c depicts the cross section of the proposed beam forming circuit where both substrates are hold with vias. The microstrip line length on the top of the circuit is integer multiple of λ_0 (f_0=3.5GHz) while the width is defined using the formula in [14]. Layout of the beam forming design can be seen in figure 9.

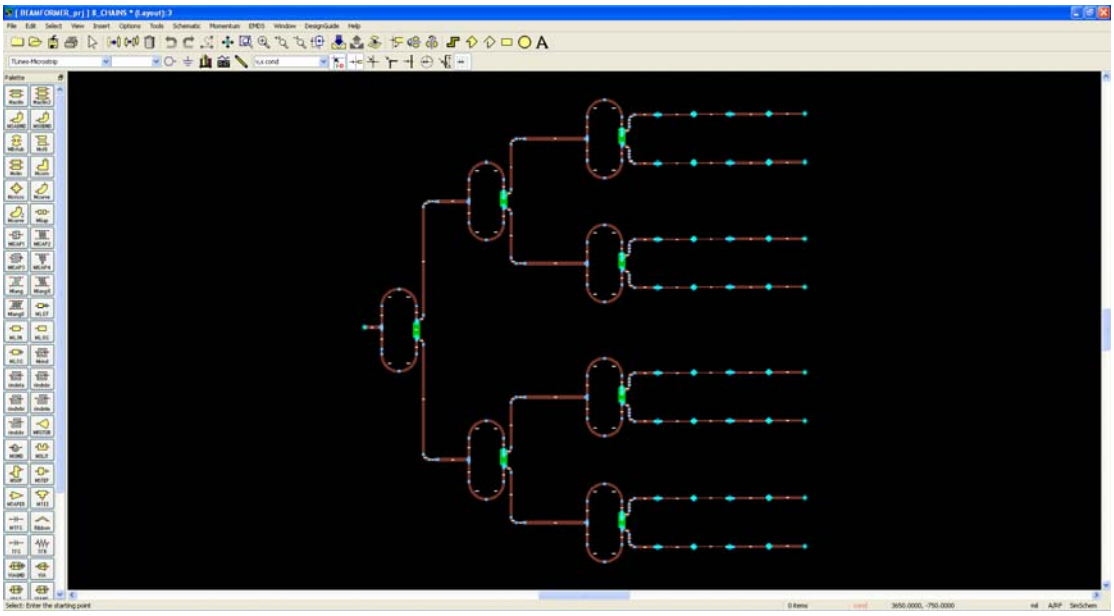

Figure 9: Layout of the beam forming module

S_{11} parameter of the simulated and fabricated beam forming circuit is depicted in figure 10.

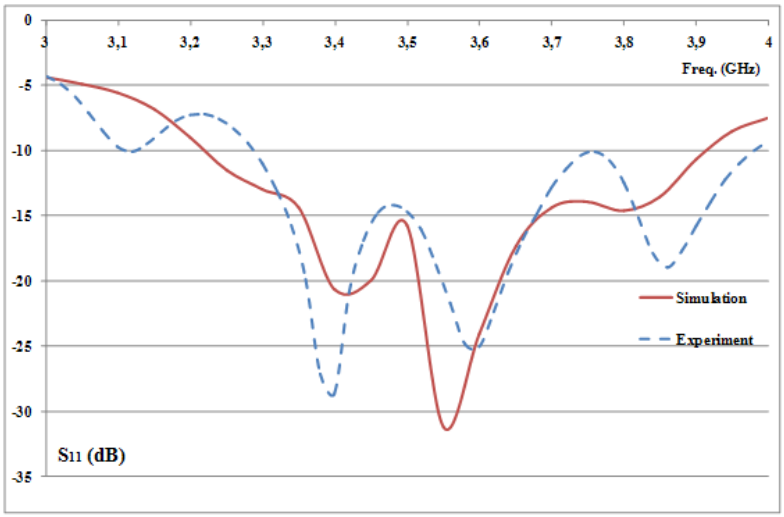

Figure 10: S_{11} of 1:8 Wilkinson power divider

Measurements of S_{11} parameter have been carried out using Anritsu MS2036A VNA. The designed beam forming circuit operates from 3.3GHz to 4GHz frequency range presenting 700MHz bandwidth (S_{11}<-10dB). The minimum experimental value of S_{11} is -27,112dB for 3.38GHz. The simulated and experimental curves depicted in figure 10 are in good agreement. Their differences are caused due to ohmic, dielectric and conductor losses and microstrip line coupling. The designed beam forming circuit presents adequate bandwidth that covers the frequency band of the array presented in the previous section. Thus the array and the beam forming circuit can be efficiently combined. Total phased array configuration including the array together with the beam forming circuit is depicted in figure 11.

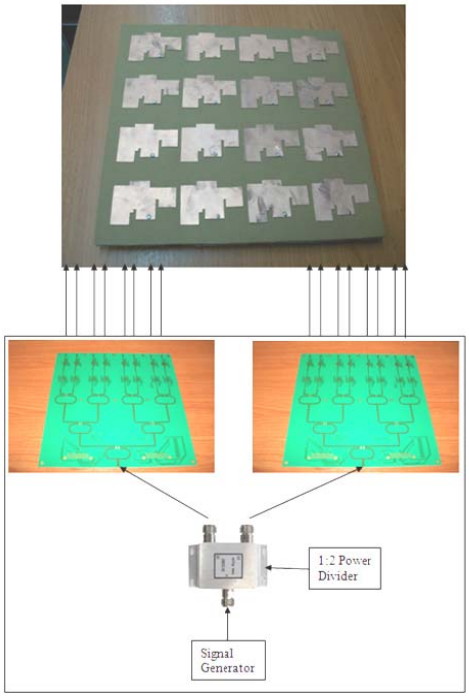

Figure 11: Phased array configuration

Signal is generated by Agilent Signal Generator (MXG N5182A) and is guided to a commercial 1:2 power divider (model PD 18/2 SMA R, DC 18GHz) which splits the signal into two equal outputs. Then these signals are forwarded to the designed beam forming module. There the signal is further divided into 16 microstrip lines which feed each one of the 16 array elements. Along these lines, commercial phase shifters and attenuators are positioned to give radiation pattern the desired form. The beam forming circuit and the array are connected through SMA cables. In addition the power divider is connected to the beam forming circuit via SMA cables. All experimental results have been derived in anechoic chamber.

IV. LMS algorithm

Radiation pattern of the array described in section II can be shaped accordingly using LMS algorithm [15]. LMS algorithm is a gradient based algorithm which performs iterative operations in order to minimize the mean square error between the array output and a reference signal.

The algorithm operates using MathCAD v.14. First a set of requirements is defined regarding radiation pattern shape. Then algorithm is executed giving amplitude and phase of each patch element that realizes the required radiation pattern. Three scenarios of beam forming have been considered.

a. Maximum at (-18^0,0^0), null at (34^0, 0^0) and Side Lobe level SLL<-10dB.

Amplitude and phase take specific quantized values [17], [18] which are:

α= [0, -3, -6, -9, -12, -15,-18, -21, -24, -27, -30, -33, -36, -39, -42, -45] in dB and

β= [0, 5.625, 11.250… 354.375] in deg with angle step of 5.625^0

The algorithm gives the following results in terms of amplitude and phase:

$$\alpha = \begin{bmatrix} -6 & 0 & 0 & 0 \\ -3 & -6 & -6 & -6 \\ -6 & -6 & -6 & -3 \\ 0 & 0 & 0 & -6 \end{bmatrix} \text{ in dB} \qquad (4a)$$

$$\beta = \begin{bmatrix} 298.2 & 275.73 & 298.2 & 191.8 \\ 258.82 & 16.85 & 135 & 140.67 \\ 90 & 163.14 & 315.05 & 208.2 \\ 123.76 & 0 & 326.35 & 315.05 \end{bmatrix} \text{ in deg} \qquad (4b)$$

The above results are assigned in each radiation element in simulation and experimental setup. Figure 12 depicts radiation pattern of the simulated and fabricated phased array.

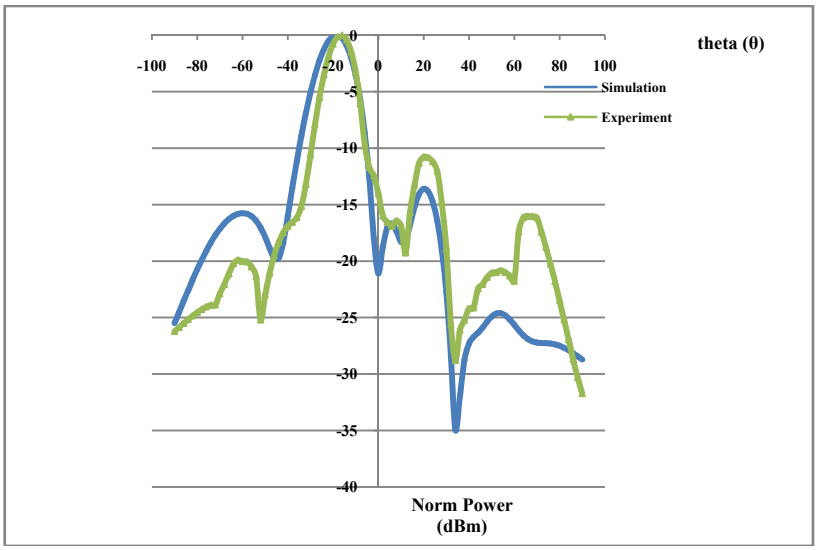

Figure 12: Simulation and experimental radiation pattern for scenario (a)

Figure 12 shows that scenario requirements are met. Side lobe levels on both curves are below -10dB. Angle of null is 34^0 while angle of maximum is -18^0. The two curves depicted in figure 12 are in good agreement. The experimental curve comprises ohmic, dielectric and conductor losses, line coupling and imbalance phenomena of attenuators and phase shifters. Imbalance phenomena are relevant to errors in attenuation and phase assignment to excitation currents due to circuit losses. In spite of these imbalances and losses the radiation pattern has the desired form and approximates the simulated curve sufficiently.

b. Maximum at $(22,0^0)$, null at $(80^0, 0^0)$ and Side Lobe level SLL<-10dB.

For scenario (b) the same procedure as above has been performed. LMS algorithm gives the following results:

$$\alpha = \begin{bmatrix} -3 & 0 & 0 & 0 \\ -6 & -6 & -6 & -3 \\ -6 & -6 & -6 & -6 \\ 0 & 0 & 0 & -3 \end{bmatrix} \text{ in dB} \qquad (5a)$$

$$\beta = \begin{bmatrix} 236.2 & 264.3 & 179.9 & 118.0 \\ 33.7 & 168.7 & 112.4 & 354.3 \\ 112.4 & 337.4 & 309.3 & 78.7 \\ 0 & 286.4 & 213.7 & 241.7 \end{bmatrix} \text{ in deg} \qquad (5b)$$

Relevant curves are depicted in figure 13.

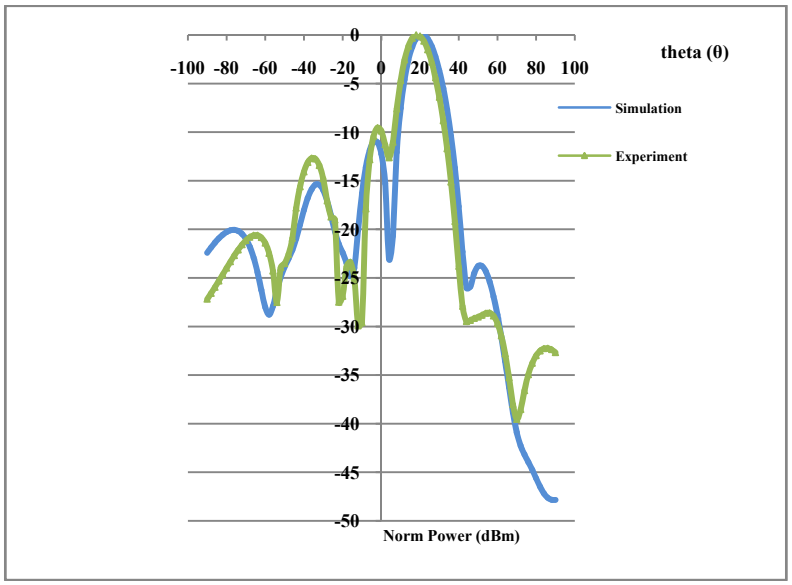

Figure 13: Simulation and experimental radiation pattern for scenario (b)

Blue line of figure 13 meets the specified requirements set by scenario (b) except from maximum of main lobe. The simulation curve presents $\theta_{max}=20^0$.
The experimental line presents maximum at $\theta_{max}=18^0$. This 4^0 deviation from the scenario requirements may be caused by losses in power divider and cable losses.

c. Maximum at (-24,0^0), null at (20^0, 0^0) and Side Lobe level SLL<-10dB.
For scenario (c) the LMS algorithm gives the following results:

$$\alpha = \begin{bmatrix} -12 & 0 & 0 & 0 \\ -3 & 0 & 0 & 0 \\ 0 & 0 & 0 & -3 \\ 0 & 0 & 0 & -12 \end{bmatrix} \text{ in dB} \qquad (6a)$$

$$\beta = \begin{bmatrix} 315.05 & 303.8 & 236.35 & 270.05 \\ 129.3 & 11.25 & 118.14 & 219.43 \\ 129.38 & 151.91 & 112.52 & 174.43 \\ 0 & 354.48 & 354.48 & 337.58 \end{bmatrix} \text{ in deg} \qquad (6b)$$

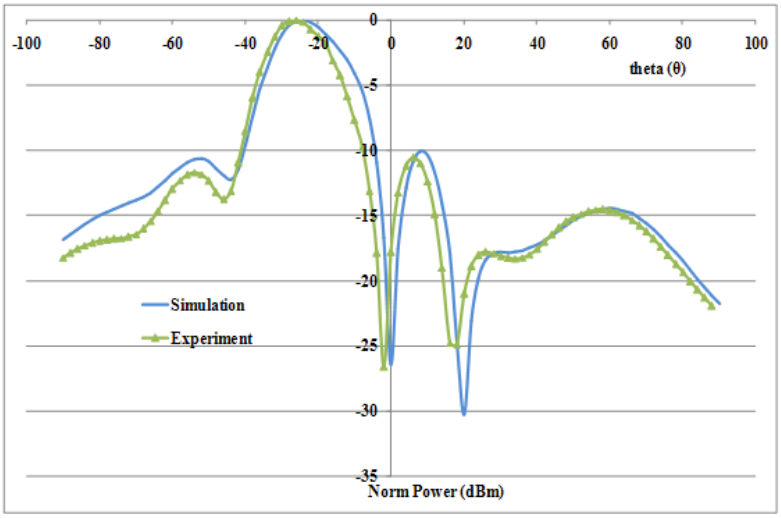

Figure 16: Simulation and experimental radiation pattern for scenario (c)

In this case the curves produced by simulation and experiment satisfy the requirements set by scenario (c). Blue and green lines coincide at high degree. The differences between simulation and experiment are probably caused because of losses in power distribution on beam forming circuit.

V. Conclusions

A phased array antenna system for connecting a Relay Station to a Base Station suitable for 4G networks at the frequency of 3.5GHz is designed and presented. The proposed system comprises two modules: The antenna array for transmit/receive data and a beam forming module for proper power division and weight (amplitude/phase) assignment. The array module is a 4×4 microstrip modified E shaped patch array of 21.17dBi Gain, 424MHz bandwidth based on stacked geometry. It is designed and simulated using electromagnetic simulator HFSSv.11. The proposed array is compared to a commercial one intended for similar use. Comparison proves the efficiency of the proposed array as it offers increased gain and narrower beam width. The beam forming module includes two 1:8 Wilkinson power dividers comprising chip resistors and capacitors, attenuators and phase shifters. Simulation set up on ADS2009 and measurement of scattering parameter S_{11} of the beam forming circuit are performed, showing good agreement. The circuit operates from 3.3GHz to 4GHz. Least Mean Square (LMS) algorithm using MathCAD v.14 is used for obtaining amplitudes and phases that give desired characteristics to radiation pattern. Three scenarios are defined. LMS algorithm is applied for each scenario and two 4×4 matrices of amplitude and phase are obtained. The values of amplitude and phase are introduced in simulated and experimental setup. Radiation patterns are extracted. The difference between simulation and experiment curve is caused by beam forming circuit losses and amplitude and phase imbalances.

References

[1] Lal C. Godara, "Application of Antenna Arrays to Mobile Communications, Proceeding of the IEEE, vol. 85, no. 8, pp. 1195-1234, August 1997.

[2] Salvatore Bellofiore, Jeffrey Foutz, Constantine A. Balanis, and Andreas S. Spanias, “Smart Antenna System for Mobile Communication Networks Part 2: Beamforming and Network Throughput” IEEE Antenna's and Propagation Magazine, vol. 44, no. 4, August 2002.

[3] Das, S., “Smart antenna design for wireless communication using adaptive beam forming approach”, IEEE Region 10 Conference, pp.1-5, 19-21 November 2008.

[4] Reeta Gaokar, Dr. Alice Cheeran, “Performance Analysis of Beamforming Algorithms”, International Journal of Electronics & Communication Technology, vol. 2 Issue 1, 2011.

[5] Chen Y.H., Jun Horng Chen, Peng Chia Hsien, Dau Chyrh Chang, Jung Hao Huang, “Performance evaluation of mobile WiMAX beam forming network implemented by RF digital step attenuators”, 14th European Wireless Conference, 2008, pp.1-6, 22-25 June 2008.

[6] J. M. Samhan; R. M. Shubair; M. A. Al Qutayri, "Design and Implementation of an Adaptive Smart Antenna System," Innovations in Information Technology, pp.1-4, November 2006.

[7] Kainan Zhao, Fei Liu, Wenhua Chen, Zhenghe Feng, “Bandwidth enhanced of a planar switched parasitic array antenna”, International Conference on Microwave and Millimeter Wave Technology, pp.1129-1131, 8-11 May 2010.

[8] Qinjiang Rao, Denidini T.A., “Electromagnetically coupling fed broadband low profile microstrip antenna array”, IEEE Antennas and Propagation Society International Symposium, vol., no., pp.893-896, 9-15 June 2007.

[9] Genc V., Murphy S., Yu Y., Murphy J. “IEEE 802.16j Relay based Wireless Access Netowrks: An Overview”, IEEE Wireless Communications Magazine Special Issue on Recent Advances and Evolution of WLAN and WMAN Standards, (2008).

[10] Pedra A.C.O., Bulla G., Serafin P., Fernandez C.R., Monser G., de Salles A.A.A., “Bandwidth and size optimization of a wide band E shaped patch antenna”, Microwave and Optoelectronics Conference, pp.422-426, October 2007.

[11] Yoharaaj D., Azmir Raja Syamsul, Ismail Alyani, “A New Approach for Bandwidth Enhancement Technique in Microstrip Antenna for Wireless Applications”, RF and Microwave Conference, pp.205-209, September 2006.

[12] Jedlicka R., Poe M., Carver K., “Measured mutual coupling between microstrip antennas”, IEEE Transactions on Antennas and Propagation, vol.29, no.1, pp. 147-149, January 1981.

[13] E. J. Wilkinson, “An N way hybrid power divider," IRE Trans. Microwave Theory Tech, vol. 8, pp. 116-118, January 1960.

[14] E.O. Hammerstad, “Equations for microstrip circuit design”, in Proc. 5th European Micro. Conf., Hamburg, pp. 268-272, Sept. 1975.

[15] Yang Qun, Cao Xiang yu; Yao Xu, Xu Xiao fei, “Performance of LMS algorithm in smart antenna”, International Conference on Microwave and Millimeter Wave Technology, pp.1372-1375, 8 11 May 2010.

[16] Balanis, C.A., “Antenna Theory: Analysis and Design”, John Wiley & Sons, Inc, 1997.

[17] Hittite HMC629LP4, Hittite Microwave Corporation, Chelmsford, MA, 2008.

[18] Hittite HMC648LP6, Hittite Microwave Corporation, Chelmsford, MA, 2008.